UCLouvain

AGRO LOUVAIN

Faculté des bioingénieurs

Evaluating traffic policies on NO_2 pollution in Brussels:

Impact of the Low Emission Zone and the Good Move Plan, 2022-2035

Authors : Mégane Pourtois & Clément Thiry

Supervisors : Patrick Bogaert, Axel Briffault

Reviewers : Emmanuel Hanert, Olivier Brasseur

Academic year : 2023 - 2024

Bioengineering in Environmental Sciences and Technologies

Acknowledgments

We extend our heartfelt thanks to Professor Bogaert, our assessor; Axel Briffault, our mentor; and Olivier Brasseur, who together formed a formidable trio, providing robust support every Thursday at noon and beyond. Professor Bogaert offered essential guidance in drafting this master's thesis, Axel helped us navigate the complexities of SIRANE and offered essential support, and Olivier Brasseur deepened our understanding of the complex topic of air pollution. We also want to express our gratitude to François Goor for his time spent explaining the emission projections crucial for this thesis, and to the computer wizard Thomas De Maet, without whom our simulations would still be running until the end of the LEZ. Additionally, we are grateful to Professor Hanert for agreeing to read and review this master's thesis.

Special thanks to DeepL, Elicit, ChatGPT, and LitMap, as well as the Master's Thesis Seminar on AI, for their indispensable assistance.

Kudos to our gang for all those breaks, during which any semblance of coherent thought were as absent as Brussels's adherence to WHO NO_2 standards.

Of course a huge shout-out to Mr. Soulhac, the god of SIRANE, whose articles made everything else we read seem like child's play.

Clément's personal acknowledgments
First of all, my sincere thanks to my father for his meticulous comments and meticulous proofreading. His support and wise counsel have been a great help to me throughout this work.

A special thank you to Mégane, my compass who kept me on track and steered me away from unnecessary detours. Her patience and knack for keeping things on point were absolutely crucial for the success of this research

Mégane's personal acknowledgments
A personal note of gratitude to my mom, who influenced this master's thesis as much as Euro 5 diesel vehicles impact air pollution in Brussels—subtly yet notably. Thanks to my dad, who generously lent his wife (yes, my mom) during crucial times throughout this master's thesis. Thanks to my brother for teaching me the fine art of crafting acknowledgments. A shout-out to Joachim (and his cat) for the motivation he provided (and his cat). And last but certainly not least, thanks to Clément. The number of misunderstandings between us rivaled the number of bugs in SIRANE, but we were truly complementary, lifting each other up from the beginning to the end. I truly admire his perseverance in finding solutions.

Finally, thank you for reading this far—rest assured, the rest of this master's thesis will fly by in less time than it takes for a simulation on SIRANE geo8. So if you have endured this introduction, you are more than equipped to breeze through the upcoming pages... probably.

Contents

List of Acronyms

A0 Highway.

A1 Metropolitan road.

A2 Main road.

A3 Inter-district road.

A4 District collector.

A5 District road.

BASE "Historical trends", withoout regional policy measures.

BCR Brussels-Capital Region.

CFD Computational Fluid Dynamics.

CNG Compressed Natural Gas.

CO carbon monoxide.

COPERT Computer Programme to Calculate Emissions from Road Transport.

EU European Union.

FAC2 Fraction of predictions within a factor of two observations.

FAIRMODE Forum for Air Quality Modelling in Europe.

FB Fractional bias.

IRM Royal Meteorological Institute.

LEZ Low Emission Zone.

LPG Liquefied Petroleum Gas.

MG Geometric mean bias.

MQI$_h$ Hourly Modeling Quality Indicator.

MQI$_y$ Yearly Modeling Quality Indicator.

MQO Modeling Quality Objective.

NAD Normalized absolute difference.

NECD National Emissions Ceilings Directive.

NEDC New European Driving Cycle.

NMSE Normalized mean square error.

NO nitrogen monoxide.

NO_2 nitrogen dioxide.

NOx nitrogen oxides.

O3 ozone.

PACE Brussels Air Climate Energy Plan.

PM particulate matter, covering PM2.5 and PM10.

PM10 particulate matter less than 10 µm in diameter.

PM2.5 particulate matter less than 2.5 µm in diameter.

RDE Real Driving Emissions test.

SO_2 sulfur dioxide.

veh-km vehicle kilometers.

VG Geometric variance.

WAM "With additional measures": in the traffic sector, covers BASE scenario, the Low Emission Zone, and the Good Move plan.

WEM "With existing measures": in the traffic sector, covers BASE scenario and the Low Emission Zone.

WHO World Health Organization.

WLTP Worldwide Harmonized Light Vehicles Test Procedure.

List of Figures

List of Tables

1 Introduction

Air pollution is an increasingly pressing issue, with multiple causes leading to significant impacts on human society. In this introductory Section, the context that shapes the objectives of this master's thesis will be explored. Several topics will be addressed, including the impacts of air pollution on the environment and human health (Section 1.1), European limits and World Health Organization (WHO) recommendations (Section 1.2), and pollution trends in Brussels (Section 1.3). The nitrogen oxides (NOx) air pollutants will then be explored in detail (Section 1.4), examining nitrogen dioxide (NO_2) concentrations (Section 1.5) and NOx emissions (Section 1.6), with a focus on their trends, sources, and the legal framework in the Brussels-Capital Region (BCR).

1.1 Impacts of air pollution

Air pollution stems from elevated concentrations of various pollutants, which are broadly defined as " any substance present in ambient air and likely to have harmful effects on human health and/or the environment as a whole " [21]. This critical issue for society implicates health, environmental and economic concerns.

Air pollution is increasingly linked to numerous health issues, including respiratory and nervous system complications, cardiovascular diseases, cancer, birth defects, and neurodegenerative conditions [22, 23, 24, 25]. Beyond its effects on morbidity, air pollution significantly impacts mortality. It is ranked as the primary environmental risk factor contributing to premature mortality, not only globally but also in Belgium, rivaling smoking and poor dietary practices [26]. In 2019, outdoor air pollution was estimated to be responsible for approximately 4.2 million premature deaths worldwide [27]. The situation is alarming; as of 2019, 99% of the global population resided in regions where air quality failed to meet the WHO guidelines [27].

Air pollution also adversely affects the environment, causing acid deposits that degrades water quality, disrupts ecosystems, and directly impacts fauna and flora [28]. Furthermore, these acid deposits affect crops and degrade buildings and cultural architecture. All these consequences come with substantial economic burdens. More stringent air quality regulations could be justified purely on economic grounds, as the direct economic benefits of air pollution control far exceed the abatement costs, even without considering the significant health benefits [29].

1.2 EU limits and WHO recommendations for air pollution

To mitigate these consequences, efforts are underway to tackle air pollution through regulatory measures. European directives 2004/107/CE [30] and 2008/50/CE [21] have established distinct legal thresholds for major pollutants, including nitrogen dioxide (NO_2), particulate matter less than 10 µm in diameter (PM10) and particulate matter less than 2.5 µm in diameter (PM2.5), ozone (O3), carbon monoxide (CO), sulfur dioxide (SO_2), lead, and benzene. These directives also prescribe specific measurement methods for those pollutants' concentration [21, 30]. Initially, these legal limit values

were formulated based on the WHO's 2005 health recommendations, while taking socioeconomic conditions into account. In 2021, the WHO revised its recommendation values downward due to recent studies indicating health impacts at levels below the previous recommendations [31].

While the current air quality standards in the EU do not align with the stricter recommendations of the WHO, there are ongoing efforts to review and potentially strengthen these standards. The European Green Deal, as outlined in its zero-pollution action plan by the European Commission in 2022, proposes a revision of the ambient air quality directives [32]. Under this initiative, the EU plans to implement stringent air quality standards by 2030, aiming notably to decrease the premature deaths caused by air pollution by more than 55% [33]. Consequently, pollutants that currently comply with the EU values may still face challenges meeting the future and generally stricter EU standards for 2030.

Furthermore, there is a long-term perspective beyond 2030 aimed at aligning EU air quality standards with the WHO's 2021 guidelines, contributing to the "zero pollution" vision by 2050 [33].

1.3 Air pollution trends

While air quality remains a critical issue in the EU, there is a positive trend across Europe globally since 2005 [23]. According to Brussels Environment [1], this improvement is primarily attributed to the implementation of emission reduction measures and the adoption of advanced technologies. Notably, the transition from diesel to gasoline-powered vehicles is believed to have played a significant role in this positive trend (Section 1.6.3).

Focusing on the BCR, as of 2020, the region has consistently met the current EU limit values for all regulated air pollutants. SO_2, CO, lead, and benzene have even respected the stricter WHO recommendations. As a result, these specific pollutants are considered non-problematic in terms of their compliance with both EU and WHO standards [1].

However, challenges persist in Brussels regarding PM2.5, PM10, O3, and NO_2, as they meet current EU thresholds but do not fully comply with WHO health recommendations. PM10 and PM2.5 concentrations have demonstrated a declining trend in BCR, Belgium, and across northwestern Europe. Despite this positive trend, particulate matter, covering PM2.5 and PM10 (PM) remains a significant concern due to its important impact on air quality and human health [1].

Ozone levels remained stable until 2016 but have since shown a slight increase in BCR. This rise is attributed to the transport of ozone precursors at the hemispheric level [1]. However, peak ozone levels have decreased thanks to local emissions reduction efforts in BCR, Belgium, and northwestern Europe [1].

NO_2, which is the primary focus of this master's thesis, presents a multifaceted challenge. Firstly, NO_2 acts as a precursor to ozone formation, as detailed in Section 1.4.3, and has the potential to contribute to the formation of PM. Thus, NO_2 exacerbates the air quality issues associated with the two other problematic pollutants, ozone, and PM. Secondly, NO_2 concentrations partially fail to align

with WHO recommendations.

1.4 Presentation of NOx

It is important to understand the dual nature of nitrogen oxides when examining their characteristics. While NOx plays a crucial role in atmospheric chemistry and ecological cycles, it also poses significant challenges due to its impact on air quality and human health. The following sections will explore the chemical identity, sources, and implications of these potent atmospheric constituents.

1.4.1 Definition of NOx

Nitrogen oxides, commonly known as NOx, are a group of chemical compounds consisting mainly of nitrogen monoxide (NO) and NO_2. The emission of nitrogen oxides results from the reaction of atmospheric nitrogen with oxygen during combustion processes through high-temperature oxidation. NOx present in the atmosphere originate from various sources, including natural ones (wildfires, lightning, volcanic eruptions, etc.) but predominantly from human activities, presented in Section 1.5 [34].

The emission ratio between NO and NO_2 is about 90/10, indicating that the majority of emissions are in the form of NO [35]. However, NO has a relatively short lifespan in the atmosphere (ranging from one to five seconds), being rapidly oxidized into a thermodynamically more stable compound, NO_2 [36]. This stability allows NO_2 to be transported by air over long distances.

1.4.2 Physical and chemical properties

In its physical state, NO exists as a colorless and odorless gas with a linear chemical structure and a molecular weight of 30 g/mol. NO, possessing one unpaired electron, falls into the category of free radicals, sometimes denoted in chemical notation as $^{\bullet}NO$ [37]. In biological systems, NO serves as a signaling molecule across various functions, including those within the nervous, cardiac, and immune systems.

NO_2 manifests as a gas with a brownish to reddish hue and is characterized by its sharp, pungent odor [38]. With a bent chemical structure, NO_2 possesses a molecular weight of 46 g/mol. The distinctive color of NO_2 stems from its absorption of light within the visible region of the electromagnetic spectrum, particularly at wavelengths of 400-500 nm.

1.4.3 Reactions and conditions of NOx formation

The primary reaction showed in is the formation equation of NO, involving the interaction between O_2 and N_2, two common components of the atmosphere [39]. The reaction occurs during the combustion process and is temperature-dependent, increasing drastically at higher temperatures.

$$\frac{1}{2}O_2 + \frac{1}{2}N_2 \rightarrow NO \tag{1}$$

In eq. (2), NO rapidly transforms into NO_2 in the presence of O3. From this point, in an environment with low levels of volatile organic compounds, a photostationary state is established where the three reactions below are in equilibrium. In the atmosphere, solar irradiation triggers ($h\nu$) the formation of oxygen radicals from NO_2, as depicted in eq. (3). This oxygen radical reacts with the present oxygen to form ozone (eq. (4)), completing the cycle [39]. Nitrogen oxides are recognized as precursors to stratospheric ozone.

$$NO + O_3 \rightarrow NO_2 + O_2 \tag{2}$$

$$NO_2 + h\nu \rightarrow NO + O^{\bullet} \tag{3}$$

$$O^{\bullet} + O_2 \rightarrow O_3 \tag{4}$$

In metropolitan areas, the increase in NO concentration, attributable to various human activities, accelerates the decomposition of ozone in accordance with eq. (2). This effect is such that rural areas often exhibit ozone pollution levels higher than those observed in urban zones due to the lower emissions of NO in rural areas.

1.4.4 Health and environmental impacts of NOx

The impacts of NOx on human health are primarily manifested through harmful effects on the respiratory system. Although the levels of NO in the air are generally too low to be considered toxic [40], NO_2, the other major component of NOx, acts as a potent oxidant and is particularly irritating to the respiratory tract [40].

During acute exposure to NO_2, individuals may experience eye and throat irritation, as well as a deterioration in lung function. Over the long term, continuous exposure to NO_2 can cause irreversible damage to the bronchioles, leading to their deformation and obstruction [41]. The segments of the population most vulnerable to the adverse effects of NOx include children, individuals suffering from chronic respiratory disorders such as asthma, cardiovascular diseases, diabetes, lung cancer, as well as the elderly. Inhalation of NO_2 is associated with an increased risk of lung infections, attributable to a decreased response capability of the immune system [42][43]. In 2018, 54,000 premature deaths in the EU were attributable to NO_2 [44]. Moreover, NO_2 can lead to acid rain through eq. 5, degrading soil and water [45] and disturbing fauna and flora [46].

$$2NO_2 + H_2O \rightarrow HNO_3 + HNO_2 \tag{5}$$

1.5 NO_2 concentrations in the BCR

Due to the serious health risks from short-term and long-term exposure to NO_2, international organizations have set concentrations limits. For the purposes of this master's thesis, it is important to examine how the BCR fits within these limits now and in the future, looking at the trends in NO_2 levels and comparing them to other locations.

1.5.1 Legal framework, monitoring and trends

Given the negative consequences of both acute and long-term exposure to NO_2, both the EU and the WHO have established legal frameworks and guidelines – as discussed in Section 1.2 – for the maximum concentration of NO_2, setting hourly, daily (WHO only), and annual limits. Furthermore, the EU has recently revised its air quality standards, aiming to tighten current limits that need to be respected starting in 2030, as explained in Section 1.5.1[1]. These standards are listed in Table 1. Considering both WHO guidelines and current EU regulations, an hourly maximum NO_2 value of 200 µg/m³ has been set by both entities, with the EU permitting up to 18 exceedances per year. This limit is consistently adhered to in BCR. However, the WHO's daily average value of 25 µg/m³, which permits 4 exceedances per year, is frequently exceeded at all monitoring stations. Some stations have exceeded this limit for more than 300 days in a year [1]. This could also raise concerns for the future EU daily limit value for NO_2, which needs to be respected starting in 2030.

Table 1: Comparison of NO_2 Maximum Limit Values set by the EU (legally binding) currently and by 2030, and by the WHO (recommendation), for one hour, one day, and for the annual average. The number of authorized overruns is also specified where applicable. Source: [15].

	Current EU Limit Values	**New EU Limit values (by 2030)**	**WHO Values (defined in 2021)**
Hour	200 µg/m³, (18 exceedances/year)	200 µg/m³, (3 exceedances/year)	200 µg/m³
Day	-	50 µg/m³, (18 exceedances/year)	25 µg/m³, (4 exceedances/year)
Year	40 µg/m³	20 µg/m³	10 µg/m³

Turning to the average annual limit value, the EU mandates a threshold of 40 µg/m³ for NO_2, whereas the WHO recommends a more stringent limit of 10 µg/m³. The EU limit values have been in force since 2010, and in 2013 many locations of BCR still consistently exceeded the EU annual average limit value for NO_2, as shown in Figure 1. However, concentrations have steadily decreased, paralleling trends observed in northwestern Europe. Since 2020, BCR has been consistently adhering to the EU limit everywhere in the region. Notably, from 2018 to 2022, NO_2 concentrations decreased by an average of 10% annually. It should be noted that there was an abnormal decline of 25% in NO_2 concentrations in 2020, attributed to COVID-related confinement measures. Subsequently, in 2021, the concentrations logically increased, but still ended up lower than in 2019, the pre-COVID period.

In 2022, all monitoring stations in the BCR met the EU average annual NO_2 norm, although just barely for one of the 12 measurement stations. However, none of the monitoring stations recorded an annual concentration below 10 µg/m³, not even in the least polluted areas of Brussels. Achieving this stringent recommendation is challenging, given that even rural stations estimating background European concentrations already report a mean concentration of 5 µg/m³. Additionally, the upcoming

[1]The legislation was approved by both the Parliament and the Council. The final step, a formal signature from the Council, is still pending but is expected to be a procedural formality.

revised EU directive on ambient air quality will likely set the annual NO_2 concentration limit at 20 µg/m³, which must be met across all areas in Brussels by 2030 [15], as shown in Table 1. In 2022, 9 of the 12 monitoring stations failed to meet the proposed stricter limit, as seen in Appendix A. Brussels will therefore face significant challenges in meeting these more stringent air quality objectives. Section 5.7 will assess whether or not it will meet these targets, based on projections.

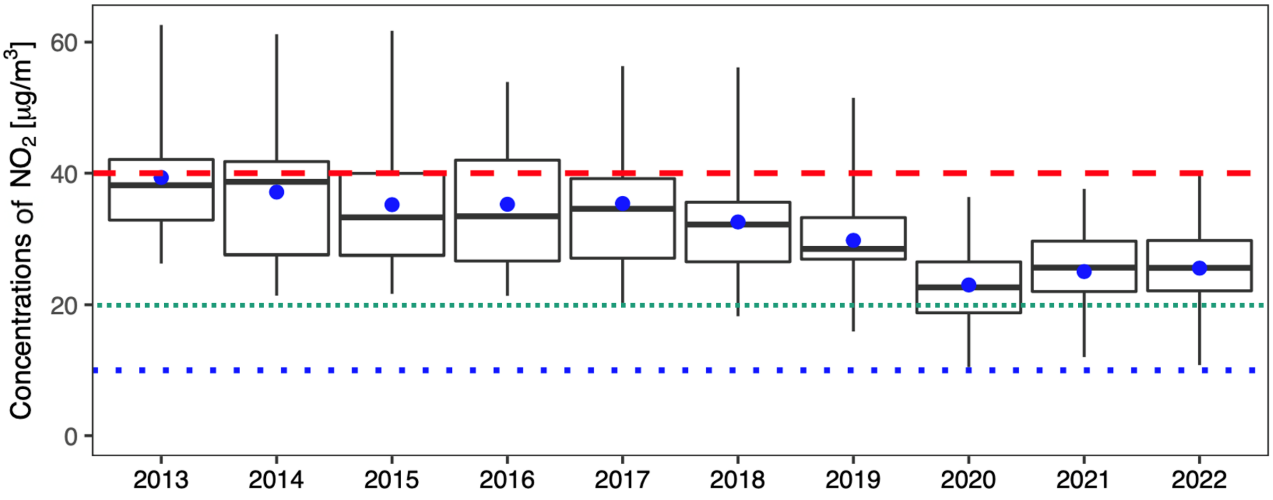

Figure 1: Average annual NO_2 concentrations from all stations for the Brussels-Capital Region over the last ten years [µg/m³]. The red dotted line indicates the currently required European annual limit value of 40 µg/m³, the green dotted line indicates the coming required European annual limit value of 20 µg/m³ and the WHO's recommended annual value of 10 µg/m³ is indicated by the blue dotted line. Source: [1]

1.5.2 Comparison to other locations

Compared to four other Belgian urban areas—Antwerp, Charleroi, Ghent, and Liège—Brussels ranks above the average, in second place of the most air polluted town following Antwerp, yet all cities exhibit a similar downward trend [35].

Additionally, Brussels exhibits a similar average annual concentration range compared to other West European capitals including Madrid, Lisbon, Paris, Berlin, Amsterdam, and Rome. In 2018, approximately 40% of the measuring points in these cities registered levels between 10 to 25 µg/m³, while over 50% reported concentrations within the range of 25 to 40 µg/m³ [47]. This data underscores the shared challenge among these capitals in adhering to potential stricter air quality standards.

Transitioning to a global perspective, the adverse health effects of NO_2 pollution exhibit a sharp contrast between urban and rural areas, with urban centers, particularly in high-income countries, facing significantly higher impacts. In 2019, an estimated 1.85 million new pediatric asthma cases globally were linked to NO_2 exposure, with two-thirds occurring in urban areas, where NO_2 levels are over twice those in rural settings [43]. Despite comprising only 14% of the global urban pediatric population, high-income countries' cities [2] accounted for 28% of these urban asthma cases. This disparity highlights the concentrated impact of NO_2 in urban areas, particularly within high-income regions.

[2] Australia, High-income Asia Pacific, High-income North America, Southern Latin America, and Western Europe.

1.5.3 Sources and contributions

Given that this problem affects a large number of European cities, it is worth examining the sources that contribute to NO_2 concentrations in Brussels. On an annual average basis, 43% of the measured NO_2 concentration is attributable to the city's traffic emissions, while 10% of the concentration corresponds to urban background pollution (measured in the city, far from direct emissions) [48]. Furthermore, 35% of the concentration is associated with external contributions to the BCR, encompassing transregional contributions. As discussed in Section 1.4.1, NO_2 molecules are characterized by their stability, enabling them to be transported over long distances. Consequently, to reduce the concentration of NO_2 in Brussels and align more closely with the WHO's recommendations, it is necessary to implement measures at the local level within Brussels as well as to undertake actions at both national and European levels. Some of these regional and European measures are detailed in Section 3.1.

1.6 NOx emissions in the BCR

As NO_2 concentrations originate from NOx emissions, it is important to analyze the legal framework and emission sources of NOx within BCR.

1.6.1 Legal framework

While European legislation focuses only on NO_2 levels in terms of concentrations, the European legal framework governing emissions, detailed below, addresses NOx (both NO_2 and NO) as a whole. The National Emissions Ceilings Directive (NECD) (2001/81/EC) mandated member states to achieve maximum national emission ceilings for specific atmospheric pollutants, with targets set to begin from 2010. Belgium failed to meet the prescribed NOx emission ceiling (176 kt/year [49]) until 2015. However, it was able to obtain an adjustment for NOx emissions within the road transport sector, since non-compliance was attributed to unforeseen changes in the emission inventory [50]. These changes include the underperformance of certain Euro vehicle emission standards, notably for diesel vehicles, discussed in Section 3.1.1. Subsequently, the revised NECD (2016/2284) introduced more stringent national emission ceilings requirements for atmospheric pollutants, with new targets set in 2020 and further reductions by 2030, based on the total emissions from the reference year of 2005. In alignment with this directive, Belgium has commited to reduce its NOx emissions by 41% by 2020 and by 59% by 2030, relative to the 2005 emission levels [51].

Furthermore, an ordinance divides these emission reductions into absolute targets (in kt/year) for the three regions. The BCR has thus committed to reducing its emissions to not exceed 4.4 kt by 2020 and 3.4 kt by 2030 for NOx. The region successfully met the NOx emission targets for 2020, with a recorded emission of 3.4 kt [52].

1.6.2 Sources and contributions

In terms of NOx emissions in BCR, in 2021, road transport was the leading source, contributing 54%, with over half stemming from passenger cars, light duty vehicles (LDV) and heavy duty vehicles (HDV) and buses each accounting for a quarter of the sector's emissions. Combustion in residential and tertiary buildings is the next significant source, comprising 32% of emissions (18% from residential and 13% from tertiary buildings). Public energy production (electricity and heat) was responsible for 9%, industry for 4%, and railways for 1% of emissions [53]. This distribution is illustrated in Figure 2.

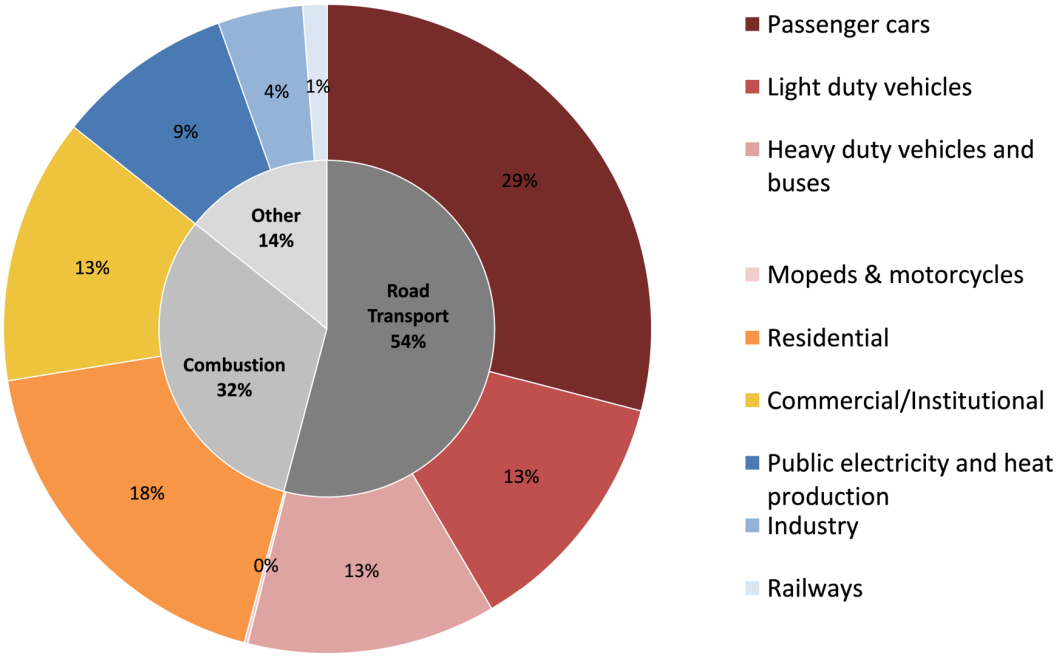

Figure 2: Source of NOx emissions in the BCR in 2021. Data source: Inventaire des émissions de polluants air LRTAP de la Région de Bruxelles-Capitale (1990-2021, soumission 2023).

Emissions of NOx in the Brussels region have significantly and consistently decreased over the past few decades. Between 1990 and 2021, NOx emissions experienced a significant reduction of 67% [35]. The reduction in NOx emissions can be attributed to various influencing factors. In the road transport sector in particular, the progress made in engine efficiency thanks to the specific directives imposed by the EU concerning emission standards for various categories of vehicle (known as Euro standards, as explained in Section 3.1.1), and the widespread adoption of catalytic converters in new vehicles since 1993, have played a decisive role [35]. Furthermore, improvements in building insulation and heating system performance, as well as the introduction of a "DeNOx" system at the Neder-Over-Heembeek waste incineration plant in 2006, have collectively contributed to the observed drop in NOx emissions [35].

Over time, the sources of emissions have shifted as well, as illustrated in Figure 3. In the building sector, a reduction in emissions related to the consumption of heating oil was observed: it accounted for 31% of NOx emissions in the building sector in 2005, decreasing to 13% by 2021 (Figure 3a). Conversely, natural gas accounted for 84% of the sector's emissions in 2021. For the transport sector,

the relative contributions remained stable, with 89% attributed to diesel and 11% to gasoline (Figure 3b) [52].

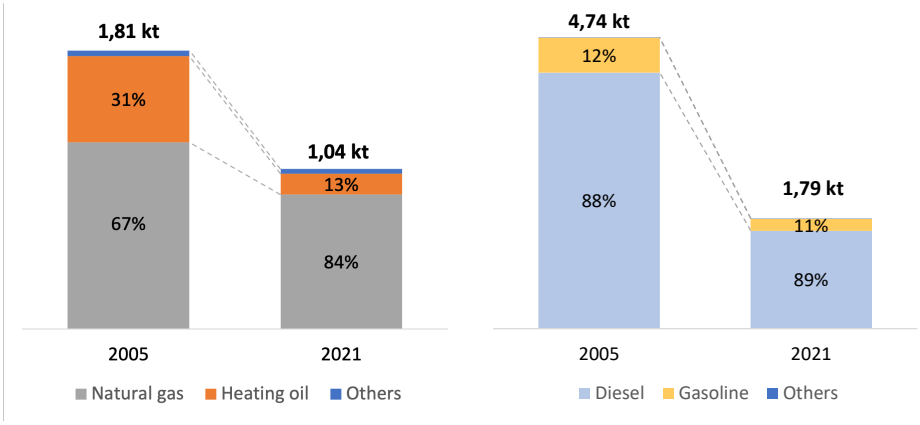

(a) NOx emissions in the building sector **(b)** NOx emissions in the transport sector

Figure 3: Sectoral trends in NOx emissions in BCR (2005-2021)
Data source: Bruxelles Environnement

1.6.3 Traffic composition in Brussels

With road transport responsible for 54% of regional NOx emissions, the composition of Brussels' traffic represents an important lever of action for reducing emissions.

In terms of vehicle categories, the traffic composition in 2022 is as follows [2]:

- Passenger cars: 87%
- Vans: 10.5%
- Heavy duty vehicles: 1%
- Buses and coaches: 0.4%
- Two-wheelers, tricycles, and quadricycles: 0.4%

In terms of fuel type, there is a trend of transitioning from diesel to gasoline or hybrid engines, as well as to electric vehicles. Regarding cars (Figure 4): since the establishment of the LEZ (cfr. Section 3.1.2) in 2018, the proportion of diesel vehicles has nearly halved (from 62.4% to 34.6%). Gasoline engines have seen a reverse trend (from 37.3% to 62.9%). The share of electric vehicles is experiencing growth, although they still constitute a small fraction of vehicles on the road (1.3% in early 2022 to 2.4% in mid-2023). In 2022, hybrid vehicles on average accounted for 9.4% of the total number of passenger cars (with 7.8% being petrol hybrids and 1.6% diesel hybrids). Regarding vans, the proportion of diesel is still predominantly high, with petrol or Compressed Natural Gas (CNG)/Liquefied Petroleum Gas (LPG) vans only making up 6% of the fleet. Electric vans are emerging in the market but represent less than 1% of the fleet.

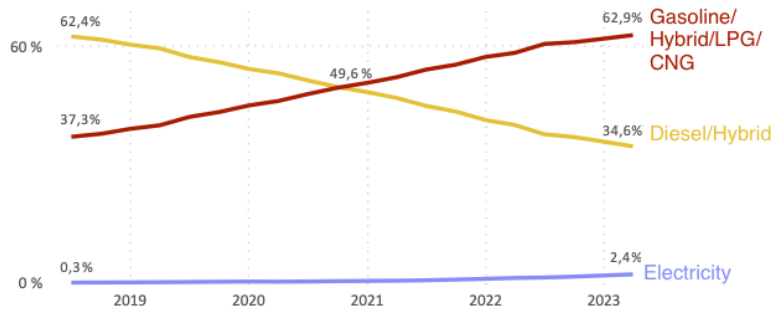

Figure 4: Evolution of the composition of passenger cars in Brussels by fuel type from 2018 to 2023. Adjusted from: [2]

1.6.4 Link between NOx emissions and NO_2 concentrations

While the EU sets legal limits for NOx emissions (see Section 1.6), it only sets concentration limits for NO_2 (see Section 1.5.1). However, reducing NOx emissions does not necessarily lead to a proportional reduction in NO_2 concentrations. Firstly, Section 1.4.1 highlights that NO_2 can travel long distances, resulting in about 35% of NO_2 levels in the BCR stemming from external sources. Therefore, meeting NO_2 concentration limits in the BCR also depends on controlling emissions from other regions and continents.

Secondly, the concentration of NO_2 is primarily influenced by total NOx emissions, but it is also secondarily affected by the ratio of directly emitted NO_2 (as a primary pollutant) to the total NOx emitted. This ratio, which is known as the NO_2/NOx emissions ratio, increased until 2009 (not only in BCR, but in all Belgian agglomerations, as well as in Germany, the Netherlands and London) [35]. The ratio is due firstly to the proportion of diesel in the fleet, diesel emitting relatively more NO_2, secondly to oxidizing catalysts from vehicles, and thirdly to particulate filters on trucks, which indirectly increase NO_2 emissions [35].

2 Objectives

This master's thesis investigates the effectiveness of two major transport policy interventions on reducing NO_2 concentrations in Brussels between 2022 and 2035. The interventions are:

1. **The Low Emission Zone (LEZ)**: Progressively restricting access to the most polluting vehicles in a phased approach, implemented from 2018 to 2035. Further details are provided in Section 3.1.2.

2. **The regional mobility plan Good Move**: This master's thesis focuses only on a specific ambition of Good Move, which aims for a 24% reduction in passenger car kilometers by 2030, alongside a shift in traffic from local roads to major roadways. Details of Good Move are explained in Section 3.1.3.

For this purpose, the SIRANE dispersion model is used to assess spatially distributed NO_2 concentrations, using traffic NOx emissions projections as inputs for the model. Three scenarios are analyzed: BASE (historical trend), WEM (With Existing Measures) , and WAM (With Additional Measures). The BASE scenario represents a baseline where no policy measures are implemented. The WEM scenario involves the enactment of the LEZ, while the WAM scenario combines both the LEZ and the Good Move plan.

This master's thesis will follow several lines of research to meet specific objectives:

- Assess the overall reduction and temporal evolution of NO_2 concentrations from 2022 to 2035 of each policy measure, identifying pivotal years where policy measures exert the most significant effects. This analysis includes both absolute and relative reductions due to each policy measure.

- Examine the impact of each policy measure on NO_2 concentrations specifically by road hierarchy, detailing which road types are most affected.

- Identify the types of vehicles banned under the LEZ that contribute most significantly to reducing NO_2 concentrations.

- Determine whether the implemented strategies will enable Brussels to meet the EU's future regulatory annual, daily and hourly, NO_2 concentration standards by 2030.

3 State of the art

This Section will first examine the policy measures implemented to reduce NOx emissions in the BCR, thereby decreasing NO_2 concentrations (Section 3.1). Next, it will outline the methods used to measure NO_2 levels and describe the monitoring infrastructure in place in the BCR (Section 3.2). Finally, the Section will discuss various air pollution dispersion models, which offer detailed spatial representation and forecasts pollutant dispersion, highlighting their characteristics and application scales (Section 3.3).

3.1 Political measures aiming to impact NO_2 concentrations in the BCR

Several policy measures have been implemented to enhance air quality, particularly to comply with the NECD directive on NOx emissions (refer to Section 1.6.1) and the EU thresholds for NO_2 concentration as outlined in the Ambient Air Quality Directive (refer to Section 1.5.1). Among these various policy measures, the most significant ones are highlighted in this Section. At the European level, the focus is on the European Emission Standards for vehicles. At regional level, the most notable plans are the LEZ, the Good Move regional mobility plan and the Brussels Air Climate Energy Plan (PACE), detailed hereafter.

3.1.1 European emission standards and testing flaws

The European Emission Standards establish exhaust NOx emission limits for new vehicles sold within the EU to mitigate air pollution. Initiated with Euro 1 in 1992, which mandated the adoption of three-way catalysts to notably convert NOx into nitrogen, these standards have progressively tightened emission rules for manufacturers up to Euro 6d in 2020 [54].

Despite the intent to decrease air pollution, the reduction in NOx emissions has not met NECD legal ceiling in Belgium until 2015, as discussed in Section 1.6.1. This discrepancy was partly due to the testing procedure, particularly for diesel vehicles, and in urban environments. This testing procedure, called New European Driving Cycle (NEDC), was created in the 1970s and adjusted in the 1990s, when vehicles were lighter and less powerful than contemporary models. Nowadays, this test fails to accurately simulate real driving conditions, leading to vehicles surpassing emission limits in real-world conditions [54]. In addition, both diesel and gasoline vehicles emit more NOx emissions in urban areas compared to highways, posing a significant public health concern due to increased exposure in densely populated areas [55]. Furthermore, diesel vehicles, which already have less stringent emission standards, are the ones exceeding them the most [55]. In Europe, a significant portion of the vehicle fleet comprises diesel cars [3], a trend largely driven by the efforts of national governments to reduce carbon emissions from the transportation sector. Diesel vehicles, known for their greater fuel efficiency compared to gasoline-powered cars, are associated with lower carbon dioxide emissions. Consequently, EU countries have promoted the acquisition of diesel cars through fiscal incentives, including tax reductions on diesel fuel, aligning with broader environmental objectives [57].

[3] 42% for passenger cars and over 90% for buses and light, medium and heavy commercial vehicles in EU, 2021 [56]

To address the underestimation of the NEDC testing procedure, a new laboratory test, the Worldwide Harmonized Light Vehicles Test Procedure (WLTP), [4] has been replacing the NEDC for all new vehicles since 2019 (Euro 6c), offering a more accurate representation of real-world driving conditions [54]. Complementing the WLTP, the Real Driving Emissions test (RDE) has been implemented for light vehicles (Euro 6d-TEMP and Euro 6d). Unlike the WLTP, which is conducted in a controlled laboratory setting, the RDE is an on-road test that captures emissions under actual driving conditions, though it does not yet cover all highly polluting driving scenarios. As shown in Figure 5, vehicles which were not evaluated using RDE testing have been recorded emitting NOx at levels exceeding several times the regulatory limits (especially diesel vehicles meeting Euro 4, 5 and 6 standards). Conversely, vehicles that fulfill the more recent Euro 6d-TEMP and Euro 6d standards, and therefore undergo RDE testing, exhibit NOx emissions that are substantially lower [3]. Furthermore, the new Euro 7 standard, entered into force in May 2024 [58], maintains the same NOx emission standards as Euro 6d, with the exception of buses and trucks. These vehicles must reduce their emissions by 2028 to comply with Euro 7 requirements.

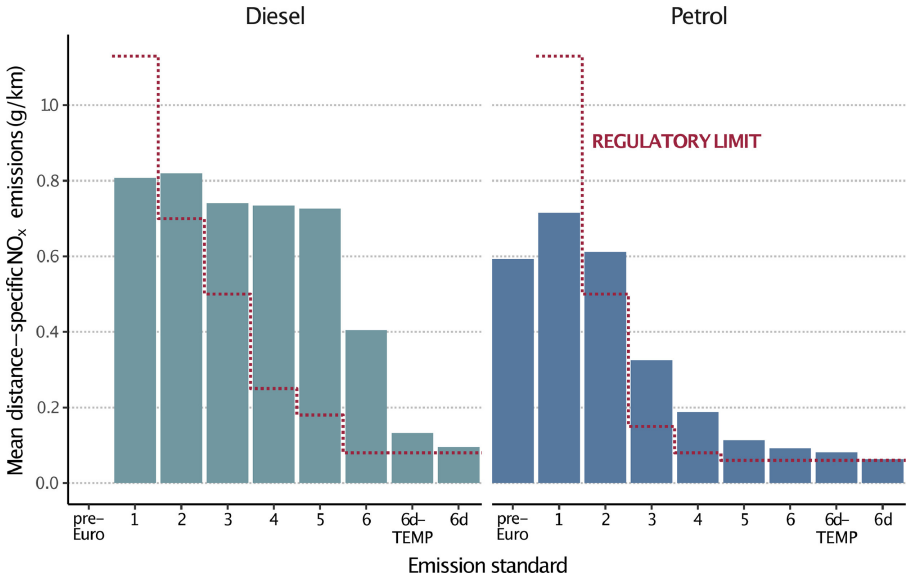

Figure 5: Average NOx emissions per distance unit from passenger vehicles observed across four European cities (Brussels, Krakow, London, and Paris) during the period 2017-2020. The thresholds for laboratory type-approval emission standards are marked in red. Source: [3]

3.1.2 LEZ

The LEZ aims at progressively banning the most polluting vehicles based on their fuel type and Euro standard. Its objective is to accelerate the renewal of the vehicle fleet, thereby achieving a reduction in emissions sooner than would have been possible without such measures. Thus, while fleet emissions will eventually align with levels that would have been reached without the LEZ, the policy ensures that emission reductions are realized earlier, contributing to improve air quality in the short or medium term, and simultaneously meet the EU's new NO_2 limit by 2030.

[4] For passenger cars and LCV only. For heavier vehicles, the new test procedures are World Harmonized Stationary Cycle (WHSC) and the World Harmonized Transient Cycle (WHTC) since Euro VI

Initiated in 2018, the Brussels LEZ encompasses all 19 municipalities within the region, covering an area of 161 km². Enforcement of the driving bans is facilitated through the use of automatic number plate recognition cameras, which operate continuously throughout the year [59].

In 2024, diesel and hybrid diesel light vehicles and buses up to Euro 4/IV standard, as well as petrol/hybrid/LPG/CNG vehicles up to Euro 1/I standard, are prohibited. Access is currently permitted for all heavy vehicles, as they typically experience delays regarding bans compared to lighter vehicles. The 2025–2036 timetable, as illustrated in Appendix B, includes important milestones such as a ban on diesel/hybrid diesel vehicles by 2030, and a ban on all thermal vehicles (including petrol, LPG, CNG, hybrid) by 2035 (with the exception of coaches and heavy-duty vehicles) [2].

Assessing the LEZ's effect on air quality is challenging due to various confounding factors. These include meteorological conditions, the number of vehicle kilometers, the evolving composition of the vehicle fleet, especially near the monitoring stations, economic factors and the other policy measures [16]. Although over 250 cities in Europe have implemented LEZ policies, there is a scarcity of high-quality studies that quantify their impact on air quality. A review on the effectiveness of LEZ's in improving urban air quality across European cities was conducted in 2015 [16]. Impact evaluations based on modeling studies are not considered as they have been overly optimistic. This is primarily due to uncertainties in the emission factors, which failed to accurately represent real driving conditions, particularly for NOx as seen in Section 3.1.1. Monitoring studies, on the other hand, have generally not accounted sufficiently for confounding factors, especially meteorological conditions, but are still reported in Table 2.

Table 2 summarizes the studies included in the literature review of [16] and their results on the effects of LEZ's on NOx and/or NO_2 levels. No significant impact of LEZ's on NO_2 or NOx concentrations has been observed, with the exception of Germany, where a slight impact was noted. [16] argue that little or no effect from the past LEZ's is not so surprising, given the evidence that actual NOx emissions per vehicle-kilometer have not decreased substantially for diesel vehicles with the introduction of Euro emission standards up to Euro 5 (see Figure 5), and the Euro 6 was not introduced at that time. Unfortunately, there are very few recent studies that evaluate LEZs enforcing the Euro 6 standard. Further supporting this, a more recent literature review ([60]) concurs with [16]'s conclusions. A notable exception is a study of a LEZ in central London, enforced since 2019, which includes Euro 6/VI standards for all diesel vehicles [61]. This study is not included in Table 2 because it was not covered by the literature review conducted by [16]. This scenario, similar to what is anticipated for Brussels by 2025, showed that after three years, the mean roadside NO_2 concentrations in central London were 35 µg/m³ or 44% lower than what would have been expected without the LEZ. This improvement was also observed beyond the LEZ's boundaries, indicating that when LEZs incorporate strict standards such as Euro 6, they can significantly enhance urban air quality. The findings of this study are discussed and compared with the results of this master's thesis in Section 6.5.
In addition, the effectiveness of LEZ's varies significantly based on several factors, including the size of the area covered, the level of policy stringency and the exemptions allowed. Most LEZ's in the study did not encompass entire cities but were limited to city centers, unlike Brussels. Furthermore,

Germany stood out as the only country that included passenger cars in its LEZ's and where a measurable reduction in NOx and NO_2 emissions was reported. Brussels, which was not included in this study, also includes passenger cars in its LEZ.

Table 2: Summary of the reduction in long-term concentrations of NOx and NO_2 attributable to LEZ's, as identified from monitoring data in the literature review of [16].

City	NOx	NO_2	Notes	Reference
Amsterdam, The Hague, Den Bosch, Tilburg, Utrecht	No effect	No effect	Comparison before and after LEZ	Boogaard et al., 2012 [62]
Copenhagen	No effect		Comparison before and after LEZ	Jensen et al., 2011 [63]
London	No effect		Simple comparison of data from sites in and outside LEZ.	Ellison et al., 2013 [64]
London	3-7% from traffic contribution	No effect	Detailed filtering of data to remove confounding factors	Barrett, 2014 [16]
17 German cities with LEZ's		Up to 4%	Matched quadruplets for before and after LEZ and within LEZ and at reference stations (Stage 1 of LEZ)	Morfeld et al., 2014 [65]
Berlin		8%	Comparison between 2007 (no LEZ) and 2012	Lutz, 2013 [16]

In Brussels, a theoretical assessment of the LEZ impact was conducted prior to its implementation in the BCR in 2018 [5] [66]. It was estimated that the NOx emissions from road transport would decrease by $\sim$ 32% by 2020 with the LEZ (compared to 30% without the LEZ) and 66% by 2025 (as opposed to 47% without), relative to the emission levels of 2015 [66].

When modeling the potential impact of the LEZ, it is important to consider that some parameters can mitigate the effects of the LEZ. There are some vehicles in breach of the LEZ, those that have paid a daypass, or those benefiting from derogations [6]. However, these cases represent only a minor fraction of overall traffic. In 2023, only 0.8% of vehicles were in violation, 0.1% of traffic was made up of vehicles benefiting from an exemption, and an even smaller percentage represented daypasses, although their number is increasing [2].

Six years after the implementation of the LEZ, the first results are starting to appear. Assuming constant mileage, the total NOx emissions from the circulating fleet have experienced an almost linear reduction from 2018 to 2022 since the implementation of the LEZ. Specifically, there was a reduction of 31% in NOx emissions between 2018 to 2022, while this reduction was estimated to be

[5] This estimation operates under the assumption that the mobility choices of Brussels' inhabitants remain unchanged, and that 25% of the vehicles that would be banned under the LEZ regulations continue to operate within the region due to exemptions, day passes, and violations.

[6] including priority vehicles, oldtimer cars over 30 years old, vehicles for people with reduced mobility (PMR)

achieved by 2020 for the theoretical assessment, which was therefore too optimistic [2]. In addition, between 2018 and 2022, NOx emissions from passenger cars were reduced by 44%, compared to only 10% for vans. This disparity could be attributed to the slower transition from diesel to petrol or electric vehicles for vans compared to cars. As of 2022, diesel vans still constituted 93% of the total vans in circulation. However it remains challenging to isolate the impact of the LEZ from various confounding factors.

In 2023, a simulation using the SIRANE model (explained in Section 4.1) was conducted as part of a project by the Université Catholique de Louvain to compare NO_2 concentrations in 2018 with those in 2022, exclusively by modifying the vehicle fleet composition to isolate the impact of the LEZ [2]. Results are presented in Figure 6. Particularly on major high-traffic roads, NO_2 concentrations decreased by up to approximately 30% between June 2018 and October 2022.

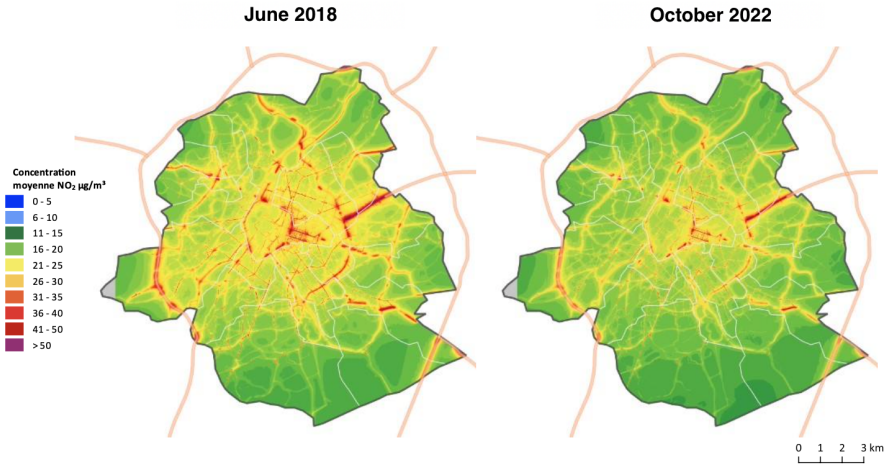

Figure 6: Evolution of average NO_2 concentration in BCR (2018-2022). Source: [2]

Furthermore, the reduction in NOx emissions related to traffic through the LEZ is likely to continue until 2035, according to Figure 7. This Figure illustrates the estimated share of total NOx emissions for passenger cars operating in Brussels during Autumn 2020, categorized by emission standards and fuel type [4]. It shows that diesel vehicles under the Euro 4, 5, and 6 standards, permitted within the LEZ in 2020 yet not subjected to pre-RDE testing, accounted for over three-quarters of NOx emissions. Meanwhile, as of October 2020, these vehicles constituted only 49% of the passenger car fleet in Brussels [67]. Diesel Euro 4 cars accounted for only 12% of the passenger vehicles surveyed in the study. However, they were estimated to produce 26% of the total NOx emissions. Euro 5 diesel vehicles also exhibit a similar overrepresentation in NOx emissions, as they share the same emission factor as Euro 4 diesel, as shown in Figure 5. This clarifies why the positive impact of the LEZ is anticipated to increase from 2020 to 2025. In Autumn 2020, Euro 6d vehicles constituted a minor fraction of the emissions since they had only recently been introduced. Their prevalence in Brussels' vehicle fleet and their contribution to total emissions are expected to increase gradually until the introduction of Euro 7 [4]. However, significant changes in NOx emissions are not anticipated compared to Euro 6d, as detailed in Section 3.1.1, where it is explained that Euro 7 and Euro 6d have similar NOx emissions standards, except for buses and trucks.

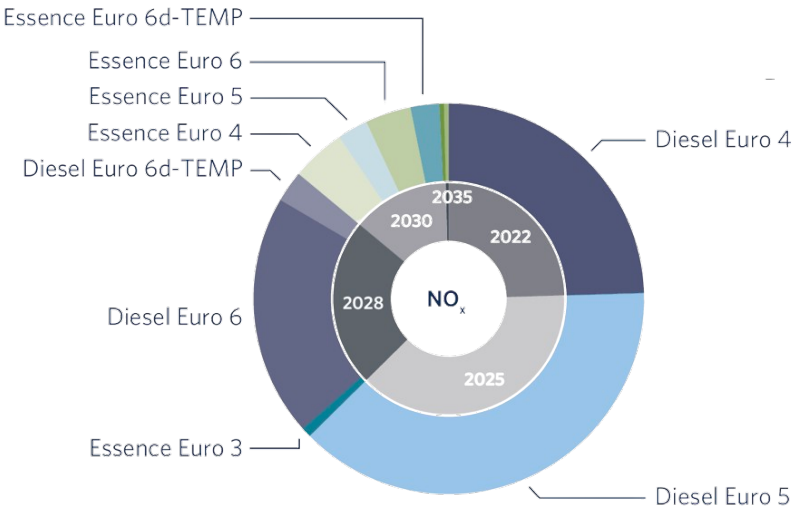

Figure 7: Estimated share of total NOx emissions from passenger cars operating in Brussels in the autumn of 2020 by emissions standard and fuel type. The inner ring breaks down total emissions by the year in which vehicle groups will be subject to LEZ restrictions. Source: [4].

3.1.3 Good Move : regional mobility plan

The "Good Move Plan" is a regional mobility plan for Brussels, covering the years 2020-2030 [68]. It began in 2016 as a collaborative process involving a wide range of stakeholders from Brussels and Belgium, both public and private, as well as associations. The plan aims to transform mobility in Brussels. Given that NO_2 is primarily emitted by road transport, the plan is expected to have an impact on the pollutant's concentration and spatial distribution. The goal is to create a safer, more pleasant city, improving the living environment for the citizens of Brussels notably thanks to a better air quality, while supporting the socio-economic growth of the city. A key goal is to eliminate fatal accidents on the roads. To this end, one significant achievement under the Good Move plan is the designation of Brussels as a 'City 30' starting in 2021, which sets a general speed limit of 30 km/h throughout the city's streets.

Another key ambition of Good Move is to create "Low Traffic Neighborhoods" in the capital, prioritizing quality of life. This involves more public and green spaces and fewer personal motor vehicles, by promoting alternative transport modes. To achieve this, the city's traffic plan needs to change, as illustrated in Figure 8. The road network for motor vehicles is categorized in three levels: PLUS, CONFORT, and QUARTIER [68]. PLUS roads are major metropolitan routes, CONFORT roads supplement the network, and QUARTIER roads are within calm neighborhoods. The circulation plan is based on a "cascading diversion" principle, directing motor traffic towards PLUS and CONFORT roads, while QUARTIER roads are reserved for local traffic. There is also a specific network for heavy vehicles, based on the same categories, to manage supply routes in Brussels.

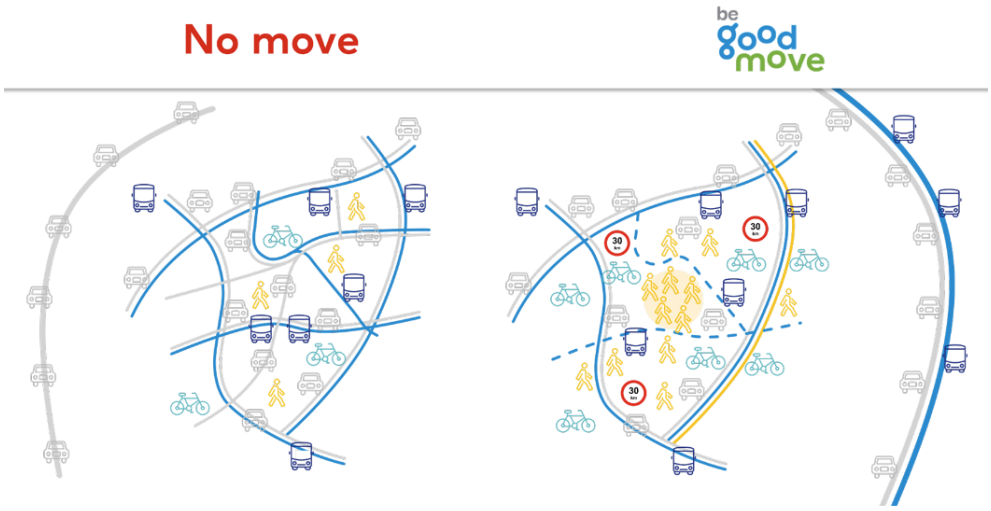

Figure 8: Comparative visualization of a Brussels neighborhood traffic flow: On the left, the "No Move" scenario depicts the neighborhood as permeable to traffic with challenging accessibility for all. On the right, the implementation of the Good Move strategy portrays a tranquil neighborhood where transit traffic is redirected to main axes, and alternative modes of transportation are promoted. Source: [5]

The updated regional mobility plan marks an 85% increase in roads classified as 'local' compared to its predecessor, signifying a substantial portion of the network is now categorized as QUARTIER. These are streets with limited through traffic, potentially leading to congestion on PLUS and CONFORT roads. To alleviate potential congestion on these major roads, the Good Move plan emphasizes a simultaneous push towards a modal shift, reducing the total number of kilometers traveled by passenger cars by 24%. [68]. It intends to reduce the reliance on personal cars and to make alternative modes of transport (like walking, cycling, and public transport) more attractive. The plan encourages parking outside public roads and promotes shared and electric cars as well.

Brussels Mobility has identified 50 potential Low Traffic Neighborhood zones (1 to 2.5 km^2 each) to be established by 2030, with five new zones each year at the suggestion of municipalities [69]. After a neighborhood is chosen to become a Low Traffic Neighborhood, a detailed assessment leads to new traffic plans, which kick-start public space improvements and traffic changes. Although the plan envisioned the creation of five new Low Traffic Neighborhood per year, aiming for 20 by 2024, there are currently only 18 [70]. Of these, six are fully developed neighborhoods, while two are on hold due to protests from local residents. In addition, only two projects were proposed in 2023 and 2024 respectively, far from the five annual projects planned.

3.1.4 PACE

The PACE [71] is a regional plan containing a set of actions, with objectives extending through 2045 which find their legal basis in Brussels Air Climate Energy Code. In addition, the content of this PACE feeds into the Brussels contribution to the national plan, the National Climate Energy Plan, the new version of which will be updated in mid-2024. Some of the actions and objectives relate more specifically to air quality, climate or energy, but several are cross-cutting, as the three issues are

interlinked. The plan gives priority to the two main sources of NOx emissions in the region, transport and combustion in residential and tertiary buildings.

In the transport and mobility sector, the PACE supports the acceleration of the Good Move plan and the implementation of the "Low Emission Mobility" roadmap, aiming to phase out thermal vehicles in the BCR by 2035. Additional measures include expanding electric vehicle charging infrastructure in alignment with the "Electrify.brussels" plan and enhancing the Regional Sustainable Development Plan (PRDD) efforts to promote a "short-distance city" concept, thereby reducing transportation needs.

In the framework of the PACE, efforts to reduce NOx emissions in the buildings sector include the gradual phase-out of coal and oil heating, along with reductions in wood heating. However, there are no concrete actions yet for phasing out natural gas, which accounted for 84% of NOx emissions in this sector, as discussed in Section 1.6.2. Moreover, due to considerable inertia within the buildings sector, the effects of these actions will take longer to materialize compared to those in the transport sector [12].

An ambitious and important objectives of PACE in terms of air quality is to bring the concentration thresholds for all atmospheric pollutants in line with WHO recommendations. To achieve this, one of the actions is to advocate at national and European level the alignment of European standards with the WHO's recommended guide values. This objective is necessary to target the 35% of NO_2 concentration attributable to an external contribution, as seen in Section 1.5.3.

Finally, a pivotal ambition of the PACE that aligns with the scope of this master's thesis is the enhancement of the air quality modeling and mapping tool, and its accessibility to both the public and European authorities. This initiative is critical as it enables the ex ante evaluation of the alignment between PACE's measures and objectives with the European and regional concentrations and emissions of air pollutants. In an era where ambitious emissions reductions and air quality improvements are increasingly sought, accurately assessing the impact of measures is essential. Every potential incremental gain in this context can contribute significantly to the objectives. Such enhanced modeling tools are necessary for policymakers and the EU, facilitating the verification of whether set objectives are on track to meet expectations.

3.2 NOx concentration measurement methods

As described in Section 1.5.1, the EU has set hourly and annual ceilings for NO_2 concentrations. To facilitate the collection of comparable data among member states, standard measurement methods have been implemented. For the measurement of NO_2 and NOx, the European standard EN 14211 from 2005 identifies chemiluminescence as the reference method [72].

3.2.1 Chemiluminescence

Chemiluminescence, a measurement method specific to NO, involves a chemical process where the energy released during a reaction is emitted as light. For NOx, the initial chemical reaction involves

an excess of ozone reacting with NO, leading to the formation of electrically excited NO_2 (eq. 6). As NO_2 returns to its ground state, radiation ($h\nu$) is emitted (eq. 7). The intensity of this light is directly proportional to the concentration of NO in the sample [73].

To determine the concentration of NO_2, it must first be reduced to NO, making the chemiluminescence method an indirect measurement approach. The concentration of NO_2 is then deduced by calculating the difference between the total concentrations of NOx and NO. The concentration range of this method extends from 1 to 500 ppm.

$$NO + O_3 \rightarrow NO_2^* + O_2 \tag{6}$$

$$NO_2^* \rightarrow NO_2 + h\nu \tag{7}$$

The chemiluminescence method has numerous advantages, including excellent selectivity and sensitivity, making it particularly suited for continuous environmental monitoring. This technique demonstrates remarkable sensitivity, with a detection limit close to one $\mu g/m^3$, and enables the acquisition of almost instantaneous data, thanks to a temporal resolution of less than an hour. This ability to quickly provide crucial information to the public is a significant benefit. However, its deployment is constrained by economic considerations, such as high initial costs and significant operational expenses, which are potential obstacles to its widespread adoption [74].

It is also important to note that the presence of certain nitrogen compounds in the atmosphere (HNO_3, organic nitrates, Polyacrylonitrile (PAN), etc.) can cause interference by reacting through reduction with the molybdenum oxide catalyst, leading to an overestimation of NO_2 concentrations [75]. This interaction can lead to significant errors in the quantification of NO_2, particularly in rural or remote areas [76][77].

In the BCR, a telemetry measurement network is operational and managed by Brussels Environment [6]. This network consists of 12 measurement stations where various pollutants are assessed. The location of the various stations in Brussels is depicted in Figure 9.

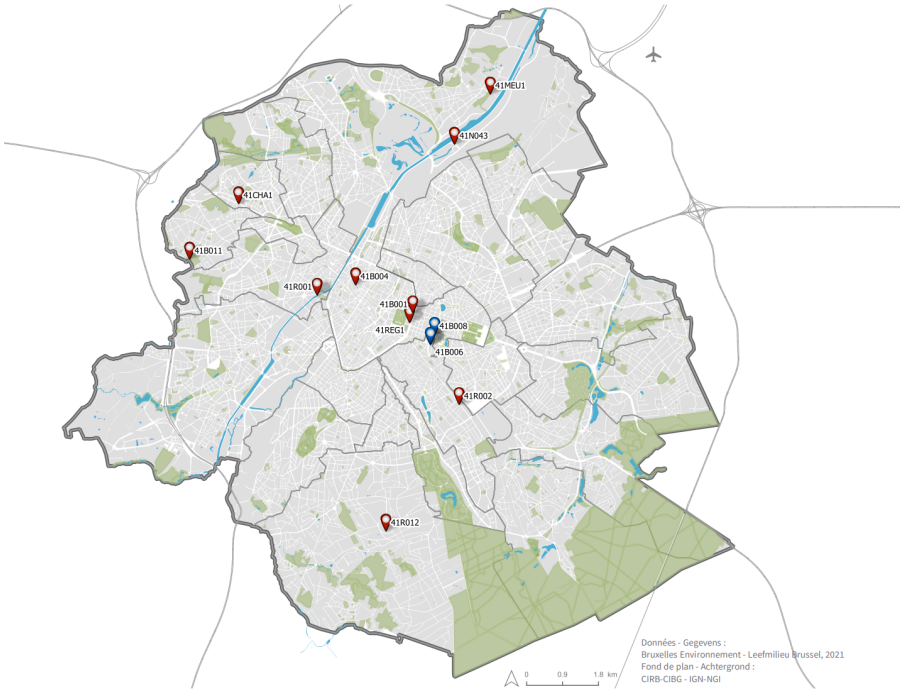

Figure 9: Map of telemetry network measurement stations in BCR. Stations 41B006 and 41B008, highlighted in blue, are not managed by Brussels Environment. Source : [6]

In addition, there are two stations (41B006 and 41B008) managed by a private company working for the European Parliament. The locations of the different stations have been strategically chosen to cover various urban environments. Table 3 categorizes the stations according to their respective environments.

Table 3: Environment surrounding air quality monitoring stations in Brussels. Source: [6]

Station environment	**Stations**
Urban with very low traffic influence	41R012 - Uccle 41B011 - Berchem-Sainte-Agathe
Urban with low traffic influence	41MEU1 - Neder-Over-Heembeek 41B006 - European Parliament
Urban with moderate traffic influence	41R001 - Molenbeek-Saint-Jean 41B004 - Sainte-Catherine
Urban with high traffic influence	41R002 - Ixelles 41CHA1 - Ganshoren 41B008 - Belliard 41B001 - Arts-Loi
Urban with very high traffic influence	41REG1 - Regent
Industrial with moderate traffic influence	41N043 - Avant-Port

Since 2020, there have been changes in the number and location of stations. Following the relocation of the Brussels Environment Air Laboratory, the Woluwe-Saint-Lambert station, which was situated in an environment with moderate traffic influence, was removed. However, in 2021 and 2022, two

new stations were added in environments with high traffic influence, named Ganshoren and Regent. The locations of the different stations have been strategically chosen to ensure adequate coverage as required under the European Directive 2008/50/EC (Ambient Air Quality Directive).

3.3 NO_2 concentration modeling: approaches and methods

Modeling of NO_2 concentrations is essential in atmospheric science, playing a crucial role in environmental assessments and public health policy. While measurement stations provide precise NO_2 concentrations, modeling offers detailed spatial representation and forecasts pollutant dispersion. In this master's thesis, the SIRANE model will be used, detailed in Section 4.1. For comprehensive understanding, this section explores other atmospheric dispersion models. A classification of these models based on structural design and application scale is presented. The operating principles of box models, Gaussian models, and Lagrangian models will be reviewed in Section 4.1 of the SIRANE model.

3.3.1 Atmospheric dispersion model

Atmospheric dispersion models serve as essential tools for predicting pollutant concentrations from emission sources. These models facilitate the analysis of pollutants' movement and their physical and chemical transformations within the atmosphere [78]. Models can be classified based on their application scale or structural design, with the application scale related to the model's resolution. The geographical interest area's size dictates the resolution's specificity. Table 4 outlines an ascending scale hierarchy of models [17].

Table 4: Classification of atmospheric chemical transport models by spatial scale and typical resolution. Source : [17]

Model	Typical domain scale	Typical resolution
Microscale	200 x 200 x 100 m	5 m
Mesoscale (urban)	100 x 100 x 5 km	2 km
Regional	1000 x 1000 x 10 km	36 km
Synoptic (continental)	3000 x 3000 x 20 km	80 km
Global	65,000 x 65,000 x 2000 km	4° x 5°

The accuracy of the results is highly dependent on the model selection. Over recent decades, a variety of atmospheric models have emerged, with distinct operational frameworks. The subsequent discussion in this Section will focus on five types of atmospheric model structures as proposed by J.B. Johnson [79], highlighting their respective advantages and limitations.

3.3.1.1 Box models [Scale $\sim$ <1km]

In the early stages of pollutant modeling, box models emerged as the simplest and initial approach, as represented in Figure 10. These models are founded on the principle that emission sources distribute pollutants uniformly across a defined volume or "box," with the atmosphere itself acting as this box

and allowing for the calculation of an average concentration [80]. The simplicity of box models facilitates the inclusion of more complex chemical processes within the simulation [79]. Moreover, they require relatively minimal computational resources, enabling the rapid completion of simulations.

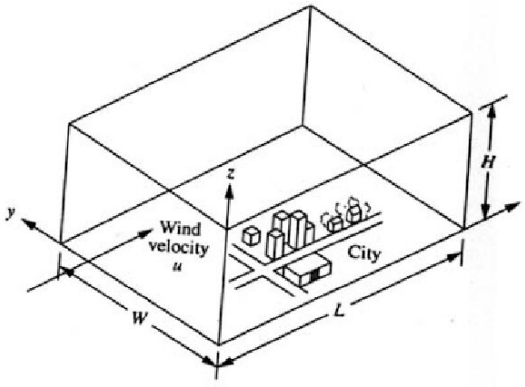

Figure 10: Fixed box model of a rectangular city with 'W','L' and 'H' denoting Width, Length and Height dimensions. Source : [7]

However, the basic nature of box models often leads to a compromise in precision, as they tend to overestimate pollutant concentrations [80] [81]. Due to these limitations, box models have largely fallen out of common usage, except in specific scenarios such as indoor environment simulations.

3.3.1.2 Eulerian models [Scale $\sim$ 10-1000 km]

Eulerian models operate by segmenting the study area into a fixed grid of cells, both horizontally and vertically. Atmospheric variables such as wind speed, wind direction, turbulence, and pollution sources are defined within this grid and assumed to remain constant over time for each grid point. Concentrations of various pollutants are computed at each time step within each cell by solving the advection-reaction-diffusion equation in a fixed coordinate space. This equation encapsulates three pivotal processes:

(i) advection, the wind-driven transport of pollutants

(ii) reaction, the chemical transformations pollutants undergo

(iii) diffusion, the spread of pollutants from areas of higher to lower concentration,

mirroring atmospheric mixing

One of the key advantages of Eulerian models is their straightforward applicability in 3D simulations. They tend to deliver superior performance compared to other types of models, such as box models or Lagrangian models, due to their comprehensive incorporation of chemical and physical processes and pollutant transport mechanisms [79]. However, they can quickly become computationally demanding, leading to prolonged simulation times.

3.3.1.3 Gaussian models [Scale $\sim$ 1-100 km]

Gaussian models assume that plume dispersion arises from pollutant diffusion, as shown in Figure 11. These models hypothesize that pollutant concentrations follow a Gaussian distribution both horizontally and vertically. Pollutants are emitted continuously, forming an ongoing plume along the wind direction (x-axis), and spreading over time across the y and z axes. The x-axis represents the plume's downstream advancement from the source, with pollutant concentration decreasing with distance due to atmospheric dispersion. Gaussian models assume constant emission rates and meteorological conditions, no chemical transformations, and wind speeds of at least 1 m/s [79].

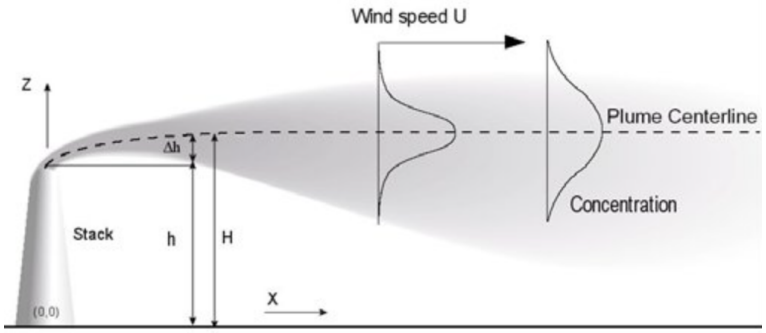

Figure 11: Representation of a gaussian plume model emanating from a stack. The diagram illustrates the plume centerline with wind speed 'U' influencing the plume's dispersion. The stack height is denoted by 'h', while Δh represents the effective plume rise above the stack height, resulting in a total height 'H'. Source : [8]

The appeal of this model type lies in its calculation method. Instead of solving differential equations at each receptor point, Gaussian models aim to compute the plume's Gaussian distribution equation. This approach results in significantly rapid and computationally light calculations [9]. However, Gaussian models tend to underperform in conditions of low wind speed or when three-dimensional diffusion is significant—scenarios often linked with stable stratified atmospheres or low-level inversions, which are critical in real-world atmospheric dispersion issues.

3.3.1.4 Lagrangian models [Scale $\sim$ 1-1000 km]

In the field of atmospheric pollutant dispersion modeling, Lagrangian models present a sophisticated approach that diverges from traditional Eulerian methodologies. Unlike the latter, which employs deterministic partial differential equations to simulate concentration fields, Lagrangian models utilize stochastic ordinary differential equations [82]. This methodology approximates the solution to the dispersion equation by focusing on the positional vectors of pollutants, which are conceptualized as either "particles" or "puffs." This shift in perspective enables a more dynamic and accurate representation of how pollutants disperse in the atmosphere [83].

"Puff" models are a specific subtype of Lagrangian models, simulating pollutant dispersion through the periodic emission of pollutant "puffs" from a source, as depicted in Figure 12. The Gaussian puff model is especially illustrative of this category, assuming that each "puff" follows a Gaussian distribution as it moves and expands under the influence of wind. These three-dimensional elements expand in all directions (x, y, and z) over time, moving away from their source of emission [79].

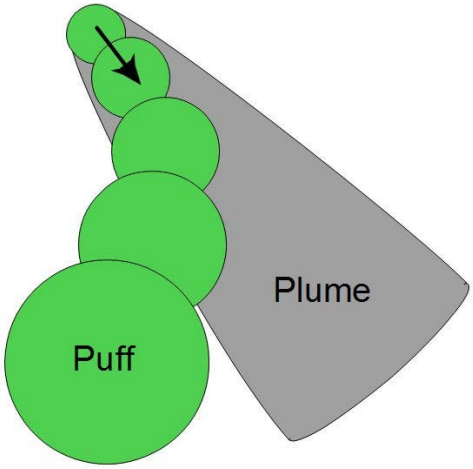

Figure 12: Schematic depiction of gaussian plume and puff models. While puff models also predict gaussian dispersion, they incorporate the ability to account for spatial and temporal variations in wind conditions. Source : [9]

Trajectory models, another subset of Lagrangian models, focus on the stochastic simulation of individual pollution particle trajectories. Unlike "puff" models, which conceptualize pollutants as collective bursts, trajectory models track each particle independently [9]. This method allows for a more detailed examination of the combined effects of advection, buoyancy, and turbulence on particle movement.

3.3.1.5 Computational fluid dynamics models (CFD) [Scale $\sim$ <1-10 km]

Computational Fluid Dynamics (CFD) models are grounded in solving the Navier-Stokes equations, which articulate the movement of fluids through the principles of mass, momentum, and energy conservation. CFD models are particularly suited for high-resolution simulations within complex urban environments, featuring intricate building geometries. This fine-scale resolution is a significant advantage over Lagrangian/Eulerian models, which may provide too coarse a resolution for detailed pollutant transport analysis. CFD applications have predominantly been implemented for industrial sites and urban street canyons, where unique air circulation patterns exist [84] [85]. However, two primary drawbacks of CFD models can be identified. Firstly, the application scale is constrained by the significant computational power required. Secondly, the reliability and relevance of CFD results tend to decrease as the scale of application widens [9].

3.3.2 Model selection based on application scale

In the multifaceted arena of atmospheric dispersion modeling, the optimal selection of a model is contingent upon the application's spatial scale and specific needs. The matrix provided by [9], depicted in the accompanying Table 5, succinctly encapsulates recommended modeling strategies across a range of scales and practical scenarios. CFD models, renowned for their detailed flow and dispersion simulations, are favored for complex terrains and urban microenvironments, especially where intricate interactions with structures or topographical features are critical. Within the proximity of the source less than one kilometer, CFD models are indispensable for short-term, high-resolution studies in street

canyons and areas where the landscape's nuances dominate dispersion patterns.

Table 5: Recommended strategies for assorted scales and applications in atmospheric dispersion analysis. Source : [9]

Application	< 1 km	1–10 km	10–100 km	100–1000 km
Online risk management (short runtime is important)	–	Gaussian	Puff	Eulerian
Complex terrain	CFD	Lagrangian	Lagrangian	Eulerian
Reactive materials	CFD	Eulerian	Eulerian	Eulerian
Source-receptor sensitivity	CFD	Lagrangian	Lagrangian	Lagrangian
Long-term average loads	–	Gaussian	Gaussian	Eulerian
Free atmosphere dispersion (volcanoes)	–	Lagrangian	Lagrangian	Lagrangian
Convective boundary layer	(CFD)	Lagrangian	Eulerian	Eulerian
Stable boundary layer	CFD	Lagrangian	Eulerian	Eulerian
Urban areas, street canyon	CFD	CFD	Eulerian	Eulerian

As the scale expands from one to ten kilometers, Gaussian models are deemed appropriate for online risk management due to their swift computational performance, whereas Lagrangian models are preferred for their detailed particle-tracking capabilities in scenarios like complex terrains and source-receptor sensitivity analyses. For even broader scales, ranging from ten to one hundred kilometers, puff models are employed to capture the episodic release of pollutants, providing a balance between computational demand and the need to address temporal and spatial variations in wind fields. At the grandest scales of one hundred to one thousand kilometers, Eulerian models reign supreme, offering a more generalized and computationally manageable approach suitable for long-term and regional-scale assessments, thus highlighting the pragmatic approach that model selection is less about seeking an elusive perfect model and more about matching the model to the task's specific demands.

4 Materials and methods

In order to achieve the objectives of this master's thesis several steps are required. First, a description and analysis of the pollutant dispersion model SIRANE will be conducted (Section 4.1, 4.2, 4.3). Next, before running simulation projections, a road refinement process will be carried out to more accurately allocate traffic emissions among different types of roads (Section 4.4). Calibration will then be conducted to align the modeled NO_2 concentrations, derived from the 2022 NOx inventory emissions data, with NO_2 concentration measurements from monitoring stations (Section 4.5). After this preparatory work, simulations will be launched using emission projections from Brussels Environment as input for SIRANE, in order to produce NO_2 concentration projections up to 2035 (Section 4.6). Then, the methodology for accounting for future meteorological variability and its influence on concentrations will be explained (Section 4.7). Finally, the process of converting SIRANE outputs into concentration data for each street segment will be detailed (Section 4.8). Figure 13 summarizes the work conducted in this master's thesis.

The various code used in this master's thesis were written in Spyder 5.2.2 with Python 3.9. It is available on GitHub: Click here to access the GitHub.

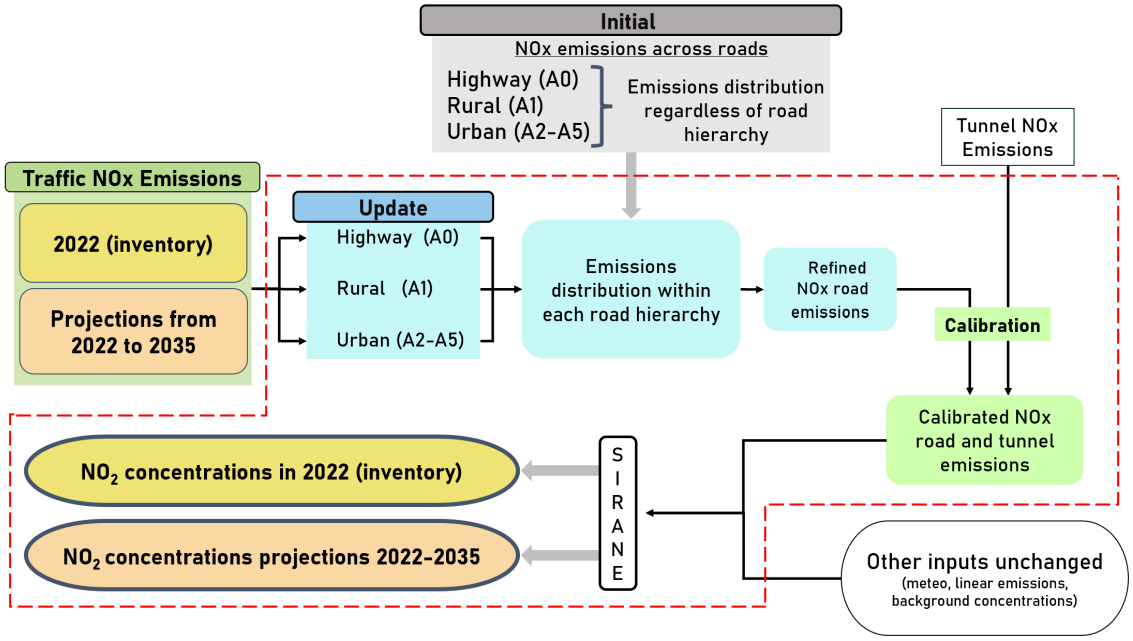

Figure 13: Methodology of this master's thesis. The dashed red line indicates the scope covered, separating it from external data that were provided. The blue text zones are the road refinement process, the green zones are the calibration process, and NO_2 concentrations are obtained from NOx emissions data using SIRANE.

4.1 SIRANE : street network and transport mechanisms

Among the various scales of pollution dispersion models described in the Section 3.3, it is the district scale (scale $\sim$ 1-10 km) that has received comparatively minimal attention in research to date. Modeling at the district scale presents significant challenges, primarily due to urban structures that alter atmospheric flow—such as the creation of intense shear layers above the urban canopy—and

the variable and intermittent nature of emission sources, including those from traffic, heating, and industrial activities. Despite these challenges, it is precisely the district scale that is the most suitable for the creation of pollutant maps in urban areas, and helping decision makers [11].

Within the district scale, CFD models are available, as discussed in Section 3.3.1.5, but they require too high a computational cost for operational purposes for the size of Brussels. Among models that use a more simplified approach to urban geometry and pollutant transfer processes, ADMS-Urban, a Gaussian model which is explained in Section 3.3.1.3, and SIRANE are notable. What sets SIRANE apart is its innovative approach that incorporates the street box model, explained in Section 3.3.1.1, and divides the flow into two distinct components: the external atmospheric flow and the urban canopy sub-flow, explained below. By employing this methodology, SIRANE can map the average concentrations of a range of pollutants (NO, NO_2, PM10, PM2.5, O3) for each street segment, providing updates on an hourly basis.

Unless otherwise noted, Sections 4.1.1 to 4.2.1 are entirely based on [11], the only research paper by the author that thoroughly explains the functioning of SIRANE. SIRANE employs a box model approach for the urban canopy, conceptualizing the street network as interconnected segments, as shown in Figure 15. Each segment is treated as a discrete "box" within which a balance of pollutant fluxes is computed. This calculation encompasses the influx, efflux, and emission of pollutants. Each box is conceptualized as a cavity with a defined length (L), width (W), and height (H), alongside an aerodynamic roughness parameter, and a distributed release of pollutants denoted by the mass rate (Q_S).

4.1.1 Transport mechanisms

In order to model pollutant dispersion, SIRANE accounts for three transport mechanisms within the canopy, illustrated in Figure 15:

1. **Convective mass transfer along the street:** The flow along a street is three-dimensional, characterized by helicoidal streamlines [86]. However, for SIRANE, only the mean advective flux at the upstream and downstream edges of the street is significant, as illustrated in Figure 15b. This is because the model averages concentrations along street segments. This transport is characterized by the spatially averaged velocity parallel to the street axis, U_{street}, which is proportional to the component of the external wind parallel to the street axis, as well as the length, width, and height of the street [87].

2. **Convective transport at street intersections:** This transport mechanism is essential in redistributing pollutants between streets and in exchanges with the atmosphere. It is a complex process influenced by multiple parameters. First, an initial estimate of the horizontal airflow responsible for air transfer between streets is required, as illustrated in Figure 14, accounting for the influence of wind and the non-uniformity of incoming concentration profiles [10]. Then, a vertical airflow is added, which emerges due to pressure differences or flow volume imbalances between downstream and upstream streets, showed in Figure 15a.

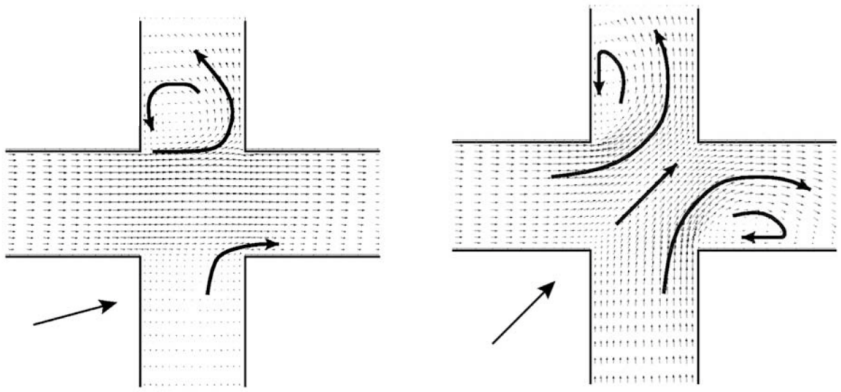

(a) Wind direction of 15° **(b)** Wind direction of 45°

Figure 14: Velocity field at $z = H/2$ within a street intersection, depending on the wind direction. The wind direction is indicated by the arrow in the lower-left corner. Source: [10]

3. **Turbulent transfer across the interface between the street and the overlying atmospheric boundary layer:** This will be examined in Section 4.1.4, and is illustrated in Figure 15d.

4.1.2 Concentration fluxes for each street

The average concentration of each street segment is calculated at each hourly time step, taking into account several pollutant fluxes for the mass balance of each box, described in Figure 16 as follows :

$$\underbrace{Q_s + Q_I + Q_{\text{part},H}}_{\text{Fluxes in}} = \underbrace{Q_{H,\text{turb}} + HWU_{\text{street}}C_{\text{street}} + Q_{\text{part},gr} + Q_{\text{wash}}}_{\text{Fluxes out}} \tag{8}$$

where Q $[g \cdot s^{-1}]$ represents the flux of pollutants, with each component defined as follows:

- Q_S $[g \cdot s^{-1}]$: Emission within the street.
- Q_I $[g \cdot s^{-1}]$: Flux by the mean flow along the street axis, entering at the upwind intersection. This flux accounts for wind direction and its standard deviation to include effects of turbulent mixing.
- $Q_{\text{part},H}$ $[g \cdot s^{-1}]$: Sedimentation of solid particles from the street-atmosphere interface. This flux is neglected in the model.
- $HWU_{\text{street}}C_{\text{street}}$ $[g \cdot s^{-1}]$: Flux by the mean flow leaving at the downstream edge, where H [m] is the street height, W [m] is the street width, U_{street} [m s^{-1}] is the averaged wind velocity along the street axis, and C_{street} [g m^{-3}] is the spatially averaged concentration in street canyons.
- $Q_{H,\text{turb}}$ $[g \cdot s^{-1}]$: Exchange through turbulent diffusion at the street-atmosphere interface.
- $Q_{\text{part},gr}$ $[g \cdot s^{-1}]$: Deposition flux of solid particles towards the ground (re-suspension is included in Q_S).
- Q_{wash} $[g \cdot s^{-1}]$: Removal of air pollutants by wet deposition, depending on precipitation and pollutant type.

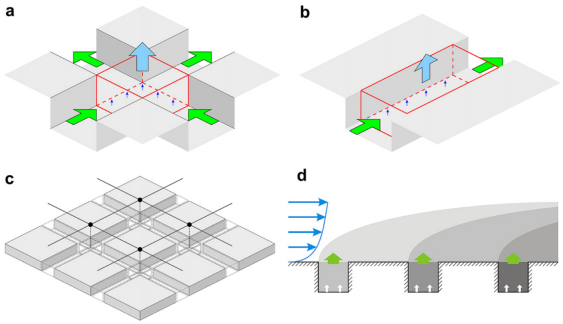

Figure 15: The different components of the SIRANE model, where the big green and blue arrows are fluxes inside the urban canopy and between the urban canopy and atmosphere, respectively. (a) Fluxes at a street intersection. (b) Box model for each street, with the overall flux balance. (c) Network of streets used by SIRANE. (d) Gaussian plume model for roof-level transport. The blue arrows represent the vertical profile of the wind. Source: [11]

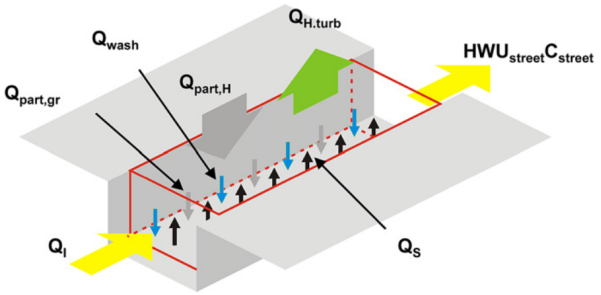

Figure 16: Air fluxes balance within a street canyon. The different terms are explained in eq. 4. Q_I, Q_S, $Q_{\text{part},H}$ and sometimes $Q_{H,\text{turb}}$, represented by the yellow arrow, small black arrows, grey arrow, and green arrow respectively, are the only fluxes that introduce air pollutants into the street. Source: [11]

4.1.3 Chemical reactions modeling

Most chemical transformations in the atmosphere take place over longer periods than the typical district-scale dispersion of pollutants, which often lasts only tens of minutes. Nevertheless, the chemical reactions involving NOx and ozone (see Section 1.4.3) occur rapidly enough to significantly alter pollutant concentrations within an hour.

In the first step, SIRANE simulates the dispersion of NOx as if they were passive pollutants. In a second step, SIRANE's chemical model estimates NO, NO_2 and O3 concentrations based on the resulting NOx concentration field and on the background concentrations of NO, NO_2 and O3, following equation :

$$\frac{J_{NO_2}}{k} = \frac{[NO][O_3]}{[NO_2]} \tag{9}$$

where J_{NO_2} [h^{-1}] is the rate of NO_2 photolysis (explained in eq. 3), k [µg/m³/h] is the rate of NO reaction with O3 (eq. 2), and [NO], [O_3] and [NO_2] are the concentrations of NO, O_3 and NO_2 respectively [µg/m³]. Consequently, SIRANE assumes that pollutants reach a photostationary state (constant concentration) at each hourly time step.

4.1.4 Flow and dispersion above the roof level

The 'external flow module' uses simplified data on urban geometry compared to the urban canopy module, modeling the collective impact of the urban canopy on the atmospheric boundary layer's flow, as shown in Figure 17. It only uses an aerodynamic roughness length and a displacement height representative of the district, derived from empirical models, used to simulate the mean velocity and temperature profiles.

This methodology is particularly effective for modeling districts characterized by high building density, where these parameters are uniform. However, it is not suitable for application in areas with sparse building density, where the urban geometry significantly differs.

Pollutants within the urban atmospheric boundary layer originate from elevated sources, such as stacks, or are released within the urban canopy. The latter are modeled as a collection of point sources at the roof level, with their intensity denoted as $Q_{H,\text{turb}}$ in eq. 8. $Q_{H,\text{turb}}$ can be positive, indicating a pollutant flux from the streets to the atmosphere, or negative, reflecting a downward flux from the atmosphere to the street canyons. The exchange of pollutants between the street and atmosphere through turbulence is dynamic and intermittent, described by the mean concentration within and above the street, the street dimensions, and an exchange velocity (u_d), proportional to the standard deviation of vertical velocity at the roof level.

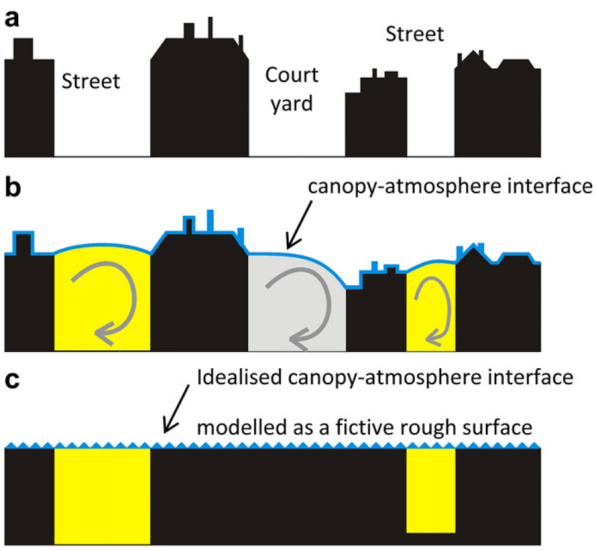

Figure 17: Description of the urban geometry in the SIRANE model. a) Real geometry.
b) Geometry within the urban canopy. Yellow-shaded regions represent areas modeled as a street network, while grey-shaded regions are not included in the street network model.
c) Geometry for dispersion in the overlying atmosphere, where the entire city is seen as a surface with a roughness parameter. Interactions with streets are limited to canyon streets shown in yellow. Source: [11]

Above roof level, the dispersion of pollutants is captured using a Gaussian plume model, described in Section 3.3.1.3. This approach enables the calculation of pollutant distribution and concentration as influenced by wind movement, either within the urban canopy or above it.

4.1.5 Computational approach

Given that the concentration of pollutants within a street is influenced by conditions in adjacent streets, it becomes imperative to address this interdependency by solving a system of linear equations. The unknowns in this system are the spatially averaged concentrations in each street within the computational domain. To this end, an iterative method is used within the computational domain. Furthermore, SIRANE has addressed the computational challenges of simulating air pollutant dispersion in areas with dense street networks in its new version (SIRANE 2.0) by adopting a new algorithm [88]. This algorithm differentiates the pollutant sources based on their proximity to receptors, treating nearby emissions individually with Gaussian puffs within a 1.5 km x 1.5 km buffer zone. Emissions from sources outside this buffer are aggregated into larger surface sources measuring 300 m x 300 m. This approach reduces the computational load by simplifying the calculations for distant sources while maintaining detailed modeling for those closer to the receptor, striking a balance between computational efficiency and accuracy in air quality simulation.

4.2 SIRANE : analysis

4.2.1 Simplifications and limitations

SIRANE's simplified approach towards urban geometry and pollutant transfer processes is a trade-off aimed at balancing the computational efficiency. Given this context, several key simplifications and their implications for the model's performance and applicability are highlighted:

- **Topography scale:** SIRANE assumes an external flow over a flat surface, with uniformly distributed buildings parameters. This assumption restricts the model's domain application primarily to districts situated on flat or nearly flat terrain. Furthermore, SIRANE disregards the presence of a roughness sub-layer above the roof level, applying vertical velocity and temperature profiles across the entire boundary layer down to the roof level.
- **Building geometry details:** SIRANE does not consider detailed building features such as doors, chimneys, and balconies. Instead, their effects are represented through uniformly distributed wall roughness at the building scale within the urban canopy module. While these details impact local-scale dynamics, compiling such detailed information is impractical. Consequently, pollutants are assumed to be uniformly mixed within the street volume, and SIRANE outputs an average pollutant concentration for the entire street canyon volume and for street intersections, treated as nodes.
- **Low-wind conditions:** SIRANE assumes steady conditions for each hour, striking a balance between the timescales of atmospheric turbulence (ranging from a few seconds to minutes) and the changes in weather conditions (lasting up to days). In the previous version of SIRANE, the model estimated concentrations independently of the previous timestep, thus not accounting for pollutants emitted earlier. This method revealed its limitations under calm wind conditions lasting several hours, potentially leading to significant pollutant accumulation in urban areas, which SIRANE fails to capture. To improve this simplification, SIRANE 2.0 now uses a Gaussian puff model, as explained in Section 3.3.1.4. The model integrates emissions from previous hours into large grid cells (1 km by 1 km) [88].
- **Sparse density of buildings:** The SIRANE model is well-suited for districts with high building density but is less applicable to areas with sparse building density, such as squares, parks, and rivers. In such regions, where flow patterns are more complex, the flow is treated as part of the atmospheric flow. In Brussels, a notably green city, this limitation could raise concerns for the various forests and parks. However, pollution levels are generally not as concerning in these areas.

4.2.2 Parameterization and validation

Parametrization studies ([89, 90, 91, 92, 93] as cited in [93]) have been conducted using wind tunnel experiments to investigate the three primary mechanisms of transport: the advection of pollutants along street axes, the exchange at street intersections, and the exchange of pollutants at roof level.

Furthermore, two field measurement validation studies of the model were conducted in Lyon, providing empirical support for the model's efficacy in real-world conditions. Both studies conducted the validation of the model with statistical performance criteria, as proposed by Chang and Hanna, discussed in Section 4.5.2.

The first validation took place within a distinct district of Lyon, France, over a period of two weeks [94]. The findings indicated that the overall performance of the model is satisfactory, with the exception of NO concentrations. It was recommended that the SIRANE model should incorporate new photochemical models to enhance the prediction accuracy for NO concentrations. Among the six pollutants analyzed, the model exhibited the highest performance accuracy in predicting NO_2 concentrations.

A wider validation study [88] spanned a year (2008) and encompassed the entire urban area of Lyon, focusing on NO_2 concentrations. The study concluded that the model's performance in capturing both the temporal and spatial variability of NO_2 concentrations was generally good. Nevertheless, a consistent tendency for SIRANE to underestimate pollutant concentrations was noted, particularly at monitoring stations situated near heavily congested traffic routes. The study stated that a possible explanation could be the underestimation of emission factors by the software "COPERT", as discussed in Section 3.1.1, because COPERT is linked to European emission standards (see Section 4.3.5.1). SIRANE also exhibited reduced accuracy where measurement stations are positioned in areas characterized by complex air flows, displaying a systematic bias influenced by wind direction [88].

A comparative analysis assessed the predictive accuracy of SIRANE against a large-eddy simulation model known for its high-resolution capabilities [95]. This analysis corroborated the findings of the first validation study: SIRANE effectively identifies the main trends in street level average NOx concentrations. Nonetheless, it demonstrates systematic biases dependent on the assumption of photostationarity for chemical reactions.

4.2.3 Sensitivity analysis

A sensitivity analysis was carried out to identify the influence of input parameters on SIRANE outputs [94]. It also assesses the impact of uncertainties in these parameters on model performance. Changes were recorded across three outputs: modifications in direct NOx concentrations ($C_{NO_{x,dir}}$), overall NOx concentrations (C_{NOx}, incorporating both direct emissions and background concentrations), and overall NO_2 concentrations (C_{NO_2}). The alterations in C_{NOx} were consistently and significantly smaller compared to $C_{NO_{x,dir}}$, underscoring the critical role of background concentration which, within the context of this study, contributed on average 56% to NOx (leaving $C_{NO_{x,dir}}$ responsible for the remaining 44%). The changes in C_{NO_2} were smaller than those in NOx, reflective of its nature as mostly a secondary pollutant, largely due to chemical transformations seen in Section 1.4.3.

The analysis highlighted emission rates and wind velocity as the parameters with the greatest impact. Concerning emission rates, factors that influence these emissions—including traffic fluxes, vehicular fleet composition, and to a lesser extent, the NO_2 emission rate factor— consequently also affect significantly the model's output. It is interesting to notice that a 50% adjustment in traffic flows

resulted in a more than 50% modification in $C_{NOx,dir}$. This phenomenon is attributed to the fact that variations in traffic flow also alter the speed of vehicles.

The study also highlighted the substantial influence of the month on concentration levels: for instance, compared to July, January exhibited an increase in $C_{NOx,dir}$ of 43%. This variation is notably due to meteorological conditions. Unstable atmospheric conditions, common in summer due to intense solar heating, promote vertical mixing, which effectively disperses pollutants, potentially leading to lower ground-level concentrations. Conversely, stable conditions, typical of colder months, limit vertical movement, resulting in diminished dispersion and, consequently, potentially higher ground-level pollutant concentrations. This dynamic illustrates how temperature differences influence atmospheric stability and, by extension, pollutant dispersion.

4.3 SIRANE : required data and data sources

An overview of the essential input data and models required for calculating pollutant concentrations in the SIRANE framework is provided in Figure 18.

First, the street network of Brussels, as detailed in Section 4.3.1, provides information on the circulation of pollutants, such as whether the circulation is open or in canyon mode. The background NO_2 concentration is applied across the entire area, calculated at the Uccle station (see Section 4.3.2). This is important as it provides information on areas not influenced by traffic. Additionally, meteorological data, discussed in Section 4.3.3, are essential for understanding pollutant dispersion and reaction rates. General parameters used for the SIRANE model are briefly discussed in Section 4.3.4. Lastly, SIRANE accounts for various types of emissions—linear, point source, and surface—detailed in Section 4.3.5, including traffic emissions from the MuSti and COPERT models.

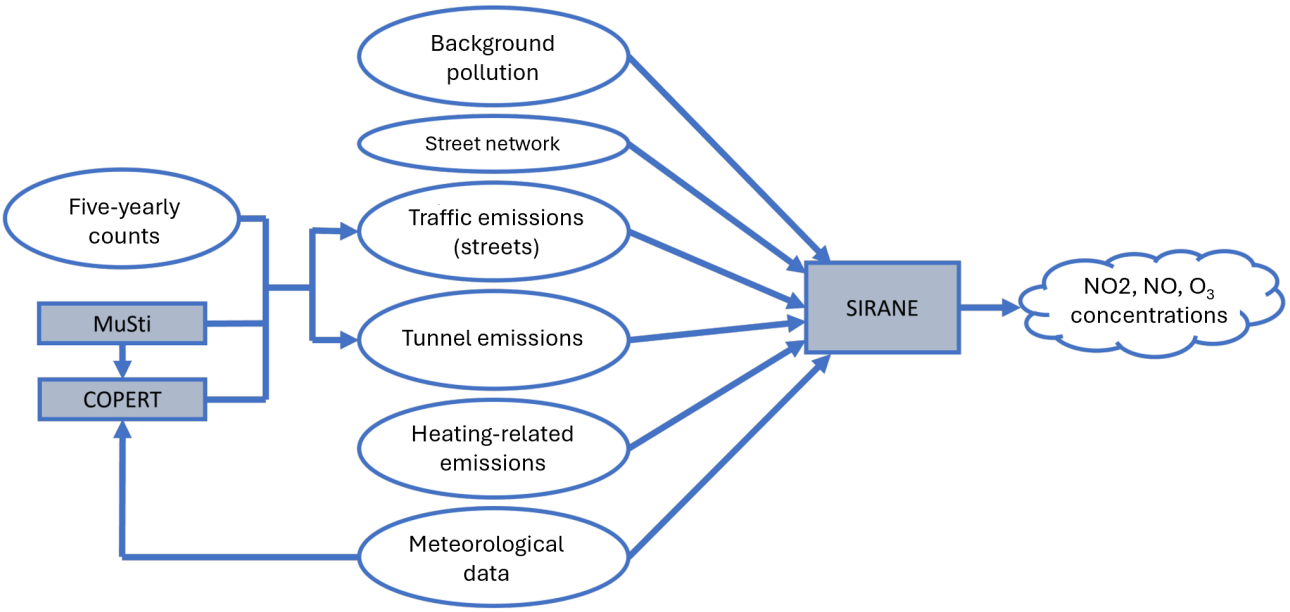

Figure 18: Integrated data input framework for MuSti, COPERT and SIRANE models: This diagram represents the complete structure of input data required by the MuSti, COPERT and SIRANE models to assess and simulate air quality and traffic emissions. The models are represented by rectangles and the data by ovals.

4.3.1 Street network input

The building-scale characteristics, specifically buildings' size, spacing, and orientation, crucially influence dispersion patterns at the district scale. Users must provide SIRANE with a street network adapted to its requirements. The street network is divided into segments, not necessarily the entire street if it is not straight, as SIRANE conceptualizes segments as a series of boxes. Since SIRANE is designed for street canyons, building-scale characteristics are necessary to distinguish street canyon environments from open terrains. The street aspect ratio (Width/Height) differentiates open terrain (Width/Height > 3) from street canyons (Width/Height < 3). Geographic Information System (GIS) data, combined with numerical methods, provides this building-scale information to SIRANE. Additionally, to address discrepancies between street and traffic networks—important for emissions estimates—a numerical tool maps traffic emissions to the nearest SIRANE street segment. For Brussels, the street network was provided as part of a project to model black carbon concentrations and was adapted by Axel Briffault [96].

4.3.2 Background concentrations data

Background pollution refers to levels typical for a region, unaffected by local traffic. The Uccle station is considered to provide these background concentrations, as it is located away from local traffic emissions, and primarily upwind of the BCR.

4.3.3 Meteorological data

Meteorological data are provided by the Royal Meteorological Institute (IRM) for the Uccle station. This data includes wind speed, wind direction relative to North, air temperature, precipitation, and solar radiation. During the 2022 simulation runs, errors were reported in the "Meteo" file containing this information. After investigation, a lack of data for certain hours of the year 2022 was detected. To address this shortfall, for each missing hour it was decided to calculate the difference in value between the same hour of the previous day and the hour before that of the previous day. This value difference was then applied to the missing hours to maintain proportionality among the meteorological measures. This methodology was chosen because the variability in the difference between two consecutive hours across two different days is assumed to be less than the variability in temperature at the same hour across two different consecutive days.

4.3.4 General parameters

The following parameters, characteristic of the study site (in this case Brussels), are also required as input data for SIRANE:

a) **Aerodynamic roughness**: This parameter measures how buildings slow airflow, influencing the vertical profile of mean velocity.

b) **Displacement height**: This is the height above ground level at which buildings displace the main flow of air, modifying the vertical velocity profiles of the urban atmosphere.

c) **Albedo**: This indicates the amount of sunlight reflected by surfaces, influencing air and ground heat.

d) **Emissivity**: This indicates the extent to which surfaces release heat.

e) **Priestley-Taylor coefficient**: This measures the moisture available for evaporation.

All these parameters must be entered both for the study site (the BCR) and for the meteorological measurement site. For the study site, the parameters were set to the default values used in the SIRANE model. For the meteorological measurements, the data were provided by the IRM. For information, their values are shown in Appendix D.

4.3.5 Emissions

For pollutant emissions, SIRANE categorizes them into three distinct types:

- Linear emissions: This category includes emissions from local, urban streets, and highways. The variability of these emissions depends on vehicle speeds, fuel types, and vehicle emission standards.
- Point Source Emissions: This category is used to represent highly localized sources of pollution such as industrial chimneys, incinerators, and, most notably, numerous tunnels in the capital city. The primary source of emissions from these tunnels is vehicular traffic.
- Surface emissions: This category encompasses emissions not originating from vehicular traffic, excluding those from the previous categories. In order of importance by sector, these emissions include combustion processes mainly related to heating in residential and tertiary sectors. This is followed by electricity generation and various industrial combustion processes.

For the calculation of traffic emissions on roads and in tunnels, traffic counting campaigns are organized every five years. In addition, two models (MuSti and COPERT) are used to complete the emission calculations, which are detailed in the following two sub-sections.

4.3.5.1 COPERT and MuSti

COPERT, or the COmputer Programme to calculate Emissions from Road Transport, is essential for generating precise emissions inventories prior to usage. This software is internationally recognized and predominantly utilized within European methodology to prepare emissions inventories for transport at local, regional (like Brussels), and national scales [97]. Notably, it is employed by 22 out of the 27 EU countries. During the integration of SIRANE for Brussels in 2018, version 5.4 of COPERT was employed. The software has been updated to version 5.7.3, which will be used for subsequent calculations. This version includes modifications in various areas such as updates to the emission factors for different pollutants, including NOx, alongside resolutions of software bugs and recalibrated coefficients for different driving phases. These different versions further extend the vehicle categories, with a focus on Euro 6 standards and the introduction of a specific category for battery-electric passenger cars [98].

COPERT's operation is based on a database of emission factors specific to automobile traffic, enabling traffic data to be transformed into estimated quantities of pollutants. This process is summarized in the following equation:

$$E = A \times EF \tag{10}$$

where :

- E [g] is the pollutant quantity expressed in mass over a given period. The time period generally used is the year.
- A [vehicle.km] is the activity of vehicles, indicated by the distance traveled per vehicle category.
- EF [g/km] is the unit emission factor, expressed in grams per kilometer.

COPERT consequently uses an extensive set of emission factors, with a unique emission factor assigned to each pollutant type and vehicle category. Various input parameters are required, including fleet composition, current emission standards, variety of fuel types used and total vehicle mileage [99] [100]. The MuSti traffic model was used to provide the mileage covered by the different vehicles represented by A in the eq. 10.

Moreover, the model incorporates data on fuel evaporation informed by fuel specifications and current meteorological conditions. Traffic activity also plays a significant role in the inputs, categorized by the classification of roadways, the level of vehicular congestion, traffic flow volume, and observed travel speeds.

In the emissions calculation process, COPERT further distinguishes emissions into three distinct types:

- Hot emissions : emissions released by vehicles when operating at optimal temperatures.
- Cold Start emissions : emissions discharged when vehicles start up and have not yet reached optimal operating temperatures. COPERT applies a higher emission factor during this phase.
- Non-Exhaust emissions : These account for fuel evaporation, tire wear, and brake wear and are primarily considered in the calculation of PM.

The results display annual emissions of various pollutants (NO, NO_2, PM10, PM2.5) for each vehicle type, categorized into five groups:"Urban Off Peak", "Urban Peak", "Rural", "Highway", and "Total," with the latter representing the aggregate of the previous categories.

4.4 Road refinement

Although COPERT provides annual NOx emissions data for a wide range of vehicle types, fuels, Euro norms, and vehicle sizes, a systematic method to allocate these emissions to specific road segments is needed. MuSti software has been designed for this attribution process. Its function is to model traffic patterns in the Brussels region, calculating the annual distance traveled on each road segment. In

MuSti, vehicles are classified into five categories: "Light vehicles", "Utility vehicles", "Construction truck", “Transport truck” and “Buses”. Given the large number of vehicle categories in COPERT, the many classes were consolidated into the five categories used in MuSti, as shown in Table 6.

Table 6: Association between MuSti classes and COPERT vehicle categories

Classes type in MuSti	**Category in COPERT**
Light vehicle	Passenger cars L-category[1]
Utility vehicle	Light commercial vehicles
Construction truck	Heavy duty trucks[2] (Rigid)
Transport truck	Heavy duty trucks[3] (Articulated)
Buses	Buses

With MuSti providing mileage for the 5 classes of vehicules and COPERT providing annual emission data for pollutants including NO, NO_2, PM10, and PM25 for each vehicle type, these annual emissions can now be distributed among all street segments. This data can then be used as input by SIRANE. To achieve this, up until now, emissions assigned to a segment were solely based on its mileage given by MuSti, as indicated by the following equation:

$$e_{i,\text{veh,poll}} = \frac{10^6}{365 \times 24 \times 3600} \cdot \frac{E_{\text{veh,poll}} \cdot m_{i,\text{veh}}}{m_{\text{veh}}} \tag{11}$$

where:

- $e_{i,\text{veh,poll}}$ [g/s] is the emission rate for road segment i, vehicle type veh, and pollutant poll.
- $E_{\text{veh,poll}}$ [t/year] represents total annual emissions for the region by vehicle type and pollutant given by COPERT.
- $m_{i,\text{veh}}$ and m_{veh} [veh.km] are the vehicle-kilometers on segment i and across the region for the year, respectively, given by MuSti.

However, the distribution of emissions is not solely dependent on mileage; it also varies with the type of road, which affects driving style and speed, and thus influences emissions. To refine the segment emissions based on not only their mileage but also road type, both MuSti and COPERT provide certain data. MuSti has classified different segments into road hierarchies: Highway (A0), Metropolitan road (A1), Main road (A2), Inter-district road (A3), District collector (A4) ans District road (A5).

Regarding COPERT, annual emissions per vehicle category are provided for two distinct road types: "Highway" (corresponding to A0) and "Rural" (corresponding to A1). Subsequently, emissions from

[1] L-Category : motorcycles, mopeds, micro-car, Quad & ATVs
[2] Heavy Duty Trucks (Rigid) : > 3.5 t, Rigid <= 7.5 t, Rigid 7.5 - 12 t, ..., Rigid > 32 t
[3] Heavy Duty Trucks (Articulated) : Articulated 14-20 t, Articulated 20-28, ..., Articulated 50-60 t

these two categories were deducted from the total calculations, leaving only the emissions attributed to road types A2 to A5. Thus, the equation becomes:

$$e_{i,\text{veh,poll}} = \frac{10^6}{365 \times 24 \times 3600} \cdot \frac{E_{\text{road type,veh,poll}} \cdot m_{i,\text{veh}}}{m_{\text{veh}}} \tag{12}$$

where $i \in$ road type corresponding to $E_{\text{road type,veh,poll}}$ (e.g., A0, A1, or A2-A5).

The remaining emissions must now be allocated for the hierarchies from A2 to A5. A distribution coefficient is recalculated for each vehicle class to determine the usage level among the road hierarchies, presented in Table 7. These proportions for each vehicle class from A2 to A5 will be used by simple multiplication to allocate the remainder of COPERT emissions.

Table 7: Proportion of different vehicle classes according to the number of vehicle.kilometers travelled in segments A2 to A5

	Distribution by vehicle class [%]				
	Light vehicle	Utility vehicle	Construction truck	Transport truck	Buses
A2	0.23	0.22	0.23	0.24	0.25
A3	0.38	0.35	0.4	0.39	0.40
A4	0.10	0.12	0.12	0.11	0.11
A5	0.29	0.32	0.25	0.26	0.25

During the implementation of the emission distribution changes between COPERT and MuSti, the file containing the road network hierarchy was found to be invalid for 662 out of 19,508 segments. Due to the small number of affected segments and the fact that the overwhelming majority of these segments did not belong to either A0 or A1 categories, these 662 road segments were classified under hierarchy A5 for simplification, following a visual verification using ArcGIS software. The Figure E.1 provides a spatial representation of the different hierarchies used, illustrating that a significant majority of the road segments are classified under hierarchy A5.

4.5 Calibration of SIRANE for the year 2022

To operate SIRANE, a significant amount of input data is required. Each of these necessary data sets carries varying degrees of uncertainty, sometimes substantial, particularly the MuSti and COPERT traffic models. Quantifying the model's uncertainty is, therefore, quite challenging. Hence, calibration is essential, relying on recorded measurements for various pollutants at the 12 stations comprising the telemetry network.

4.5.1 Calibration methodology

In this context, calibrating the model for the year 2022 involves applying one coefficient to NO traffic emissions and a different coefficient to NO_2 traffic emissions, so that the resulting NO_2 concentrations are closer to those observed at monitoring stations. These two coefficients are constant in time and space and are applied to both linear traffic emissions and point source emissions (the tunnels), while surface emissions remain unchanged. The calibration is performed by trial and error. For each

simulation of SIRANE, the coefficients for NO and NO_2 emissions are adjusted, and the resulting hourly NO_2 concentrations are compared with measurements from monitoring stations. While SIRANE also provides modeled NO concentrations, and measurement stations record these as well, the variability is high and SIRANE is not as effective at predicting NO concentrations, as explained in Section 4.2.2. Therefore, this variability and lack of accuracy make it unsuitable to use SIRANE's NO concentration data in addition to NO_2 concentrations for calibration purposes. The simulations continue until the statistical indicator values meet the acceptance criteria presented in Section 4.5.2.

In the first step, to avoid excessive computational costs, the calibration is performed only for January. This month experiences the highest and most variable emissions throughout the day due to very low temperatures affecting NO_2 dispersion and the time required for vehicles to reach full efficiency (see Section 4.2.3). Specifically, COPERT categorizes emissions by operating conditions between "Cold" and "Hot" start, leading to a longer duration of "Cold" start emissions in January, resulting in higher emissions during this period.

In the second step, once the modeled concentrations were sufficiently close to reality, the same procedure was applied to June, a month with less variation in concentrations due to more stable meteorological conditions (temperature, rainfall, etc.). Finally, a simulation of 2022 was conducted to validate the calibration over the entire year.

4.5.2 Validation of SIRANE calibration

In air quality modeling, achieving a perfect model is unattainable because of the influence of unpredictable atmospheric processes. However, it is crucial to closely approximate reality by comparing the model's results with actual observations to determine when the calibration coefficients make the model acceptable. This comparison ensures the model's predictions are reliable. Chang & Hanna [101] suggest a two-step process for evaluating models. First, they recommend looking at the data in visual ways, like using scatter plots, plots comparing predictions with observations over time or space, and others, to get a qualitative understanding. Then, for a quantitative analysis, they advise using specific statistical measures. These include:

– Fractional bias (FB)

$$FB = \frac{(\overline{C_o} - \overline{C_p})}{0.5(\overline{C_o} + \overline{C_p})} \tag{13}$$

– Normalized mean square error (NMSE)

$$NMSE = \frac{(C_o - C_p)^2}{\overline{C_o}\,\overline{C_p}} \tag{14}$$

– Geometric mean bias (MG)
$$MG = \exp\left(\ln\overline{C_o} - \ln\overline{C_p}\right) \tag{15}$$

– Geometric variance (VG)

$$VG = \exp\left(\left[\ln C_o - \ln C_p\right]^2\right) \tag{16}$$

– Normalized absolute difference (NAD)

$$NAD = \frac{\overline{|C_o - C_p|}}{\overline{C_o} + \overline{C_p}} \tag{17}$$

– Fraction of predictions within a factor of two of observations (FAC2)

$$\text{FAC2} = \text{fraction of data that satisfy: } 0.5 \leq \frac{C_p}{C_o} \leq 2.0 \tag{18}$$

An ideal model would be characterized by values of MG, VG, and FAC2 equaling 1, and FB, NMSE, and NAD equaling 0.

Chang et al. have established realistic acceptance criteria for these statistical indicators dedicated to dispersion models in rural environments [101]. These criteria were then adapted to urban environments as shown in Table 8 [18]. Taking into account the reduced performance of urban models compared with rural models, due among other things to building-induced variability, the criteria are less stringent in urban environments.

Table 8: Acceptance criteria for rural and urban dispersion models. Data source: [18]

Indicator	**Rural**	**Urban**
$\|FB\|$	≤ 0.3	≤ 0.67
NMSE	≤ 3	≤ 6
FAC2	≥ 0.5	≥ 0.3
NAD	≤ 0.3	≤ 0.5

To consider a model acceptable, it must meet at least half of the performance criteria at a minimum of half the measurement stations. It is crucial to use various measures to evaluate a model, as no single metric can cover all aspects. FB and MG focus on systematic errors, meaning that a model can be out of phase with observations but still achieve good results if the errors cancel out. On the other hand, NMSE and VG consider both systematic and random errors, with NMSE and VG being more sensitive to extreme values. FAC2 is probably the more robust measure, as it is less affected by outliers, offering a balanced approach to model evaluation. If concentrations vary by several orders of magnitude, it is advisable to use MG and VG because of their logarithmic scale, which makes it possible to handle large variations. However, these measurements can be distorted by very low values and do not work for zero values. For concentrations whose orders of magnitude do not vary considerably, FB and NMSE are more suitable, since they are linear measurements [101]. In Brussels in 2022, the NO_2 concentrations recorded by the monitoring station did not vary significantly in magnitude, reaching up to 143 µg/m³. Therefore, FB and NMSE will be used for evaluation, rather than MG and VG.

Chang and Hanna acknowledged that the acceptance criteria for the proposed rural and urban models are somewhat arbitrary, but that a more valid and widely recognized set has yet to emerge.

In the context of European Air Quality Directives, the Forum for Air Quality Modelling in Europe (FAIRMODE) community proposes a minimum level of quality that a model needs to achieve for

policy use [19]. This level is called the Modeling Quality Objective (MQO). The MQO is based on a statistical indicator: the Modeling Quality Indicator (MQI_y), as mathematically described in eq. 20. The MQI quantifies the discrepancy between measurements and modeling results, normalized by the measurement uncertainty (eq. 19) and a scaling factor. For each of the twelve measurement stations involved, one MQI value is computed. To meet the MQO, 90% of these stations must have an MQI of one or less. Given that there are twelve MQI values, the 90th percentile of all MQI values is obtained by interpolating between them, as shown in eq. 21. The values of various parameters utilized in the calculation of MQI_y are presented in Table 9.

$$U(\overline{O}) = U_r(RV)\sqrt{\frac{(1-\alpha^2)\overline{O}^2}{N_p} + \frac{\alpha^2 RV^2}{N_{np}}} \tag{19}$$

Where $U(\overline{O})$ $[\mu g/m^3]$ is the measurement uncertainty of the annual average observed concentration of the pollutant $\overline{O}$ $[\mu g/m^3]$, $U_r(RV)$ [-] is the relative uncertainty associated with a reference value RV $[\mu g/m^3]$, α [-] is the fraction of the uncertainty that is independent of the measured concentration O, and N_p [-] and N_{np} [-] are coefficients that account for the compensation of errors due to random noise and other factors.

$$MQI_y = \frac{|\overline{O} - \overline{M}|}{\beta U(\overline{O})} \tag{20}$$

Where MQI_y is the Modeling Quality Indicator [-], $\overline{M}$ $[\mu g/m^3]$ is the annual average modeled concentration of the pollutant, and β is the scaling factor set arbitrarily at 2, implying that the allowed deviation between modeled and measured concentrations is twice the measurement uncertainty.

$$MQI_{90th} = MQI(S_{90}) + [MQI(S_{90}+1) - MQI(S_{90})] \cdot \text{dist} \quad \text{and MQO is fulfilled when } MQI_{90th} \leq 1 \tag{21}$$

where $S_{90} = \text{integer}(N \cdot 0.9)$ [-] and $\text{dist} = N \cdot 0.9 - \text{integer}(N \cdot 0.9)$ [-]. This method interpolates between sorted MQI values, where S_{90} is the index at the 90th percentile and dist accounts for the fractional part of the index, and N [-] is the number of measuring stations,.

Table 9: Values of the parameters proposed for the calculation of MQI_y, for NO_2. Source: [19]

Parameter	β [-]	$U_r(RV)$ [-]	RV $[\mu g/m^3]$	α [-]	N_p [-]	N_{np} [-]
Value	2	0.24	200	0.2	5.2	5.5

While eqs. 19 and 20 apply to yearly averages, MQO can also be validated for hourly time steps using different equations where MQI_y becomes MQI_h (detailed in Appendix F). Fulfilling MQO for yearly averages does not guarantee compliance on an hourly basis, and vice versa. Although this master's thesis focuses on yearly averages, calibration has been performed for both durations since it will also support Lucas Petit's master's thesis, which involves hourly data.

4.6 Projection of emissions

To estimate NO_2 concentration projections based on selected policies over the years, this master's thesis uses NOx emission projections from Brussels Environment, specifically traffic emissions. This section first contextualizes traffic emissions within other sectors 4.6.1, then describes the methodology behind the traffic emission projections 4.6.2. This helps in understanding and discussing the concentration results in relation to the emissions and their assumptions.

4.6.1 Projection of emissions from all sectors

Bruxelles Environnement has developed projections based on three primary scenarios regarding the evolution of NOx emissions [12]. These include the "Historical trends", withoout regional policy measures (BASE) scenario, based on historical trends, the "With existing measures": in the traffic sector, covers BASE scenario and the Low Emission Zone (WEM) scenario incorporating policies adopted before 2020, and the "With additional measures": in the traffic sector, covers BASE scenario, the Low Emission Zone, and the Good Move plan (WAM) scenario, which includes policies introduced post-2020. These three scenarios receive particular attention in the traffic sector within this master's thesis and will all be explained in Section 4.6.2. Figure 19 shows the WEM projections by NOx emission source [10]. The same projections for WAM can be found on Appendix G, showing similar trends.

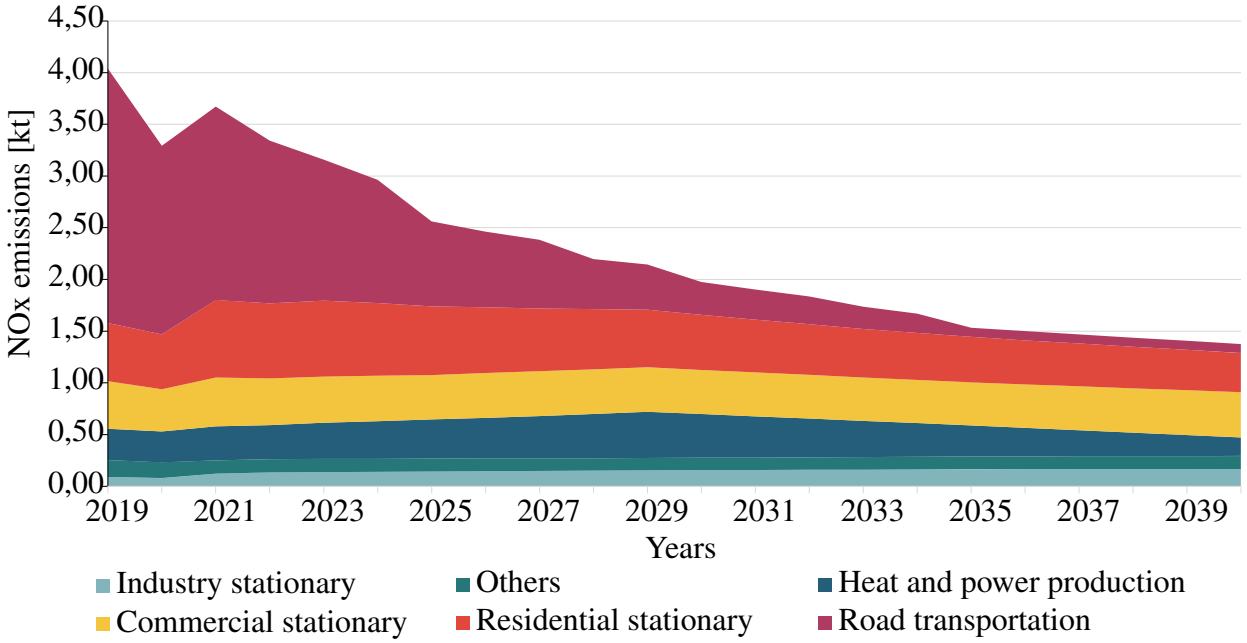

Figure 19: NOx emissions projection by sector for the WEM scenario. Source: [12]

The transport sector, the predominant source of emissions in the baseline year of 2019, shows the most significant and consistent reductions—96% under the WEM scenario and 97% under the WAM scenario by the year 2040. In contrast, the other major sectors—heat and power production, commercial, residential, and industrial combustion—show more moderate changes. As explained in Section

[10] No data have been provided for the BASE scenario

3.1.4, these changes take longer due to the inertia in the buildings sector. In some years, all four sectors even show slight emission increases under the WEM scenario, with the heat and power and industrial sectors also rising in the WAM scenario.

For the purposes of this master's thesis, projections of spatial NO_2 concentrations consider only projections in NO and NO_2 emissions from the traffic sector. Furthermore, all other projection inputs for SIRANE, including meteorological data, linear emissions (all other sectors than road transportation outlined in Figure 19) and background pollution levels, are identical to those taken for 2022. This consistency ensures reliable comparisons across different years and scenarios and helps isolate the impact of traffic policy measures. However, another objective of this master's thesis is to assess whether Brussels will meet the EU's 2030 standards for NO_2 concentrations. A limitation of these projections is their exclusion of emissions from sectors other than traffic.

However, as previously mentioned, the decrease projected for other sectors are relatively minor compared to those for the transport sector. Moreover, when combined, emissions from these sectors show a consistent decrease from the 2022 projections—which serve as the baseline for concentration projections. This approach of keeping other emissions constant instead of recognizing their overall decline effectively assumes a worst-case scenario. Therefore, if the projections conclude that Brussels will comply with the EU's 2030 NO_2 standards, the actual concentrations could potentially be even lower when considering the decreasing emissions from these sectors.

It is also worth noting that no uncertainty analysis has been conducted for any of these projections due to the complexity of the task. However, the margin of uncertainty is likely to be large [12].

4.6.2 Methodology for projecting traffic emissions

Below, and detailed in Table 10, a summary of the characteristics of the three scenarios concerning the traffic sector is presented:

- **Projection BASE** (= Historical trend): This scenario assumes a continuation of the current trend in the evolution of the vehicle fleet, based on historical trends in the vehicle fleet's composition. This does not take into account any additional NOx reduction policy measures, therefore excluding LEZ and Good Move.
- **Projection WEM** (= with existing measures): This scenario builds on the BASE scenario, incorporating changes in the fleet composition based on the LEZ schedule, explained in Section 3.1.2.
- **Projection WAM** (= with additional measures): Building on the WEM scenario, this scenario integrates the impact of Good Move transport's demand ambitions. Unlike the BASE and WEM scenarios, which follow a "No Move" evolution—presuming trends in vehicle kilometers until 2030 and a subsequent trend toward 2035—the WAM scenario anticipates a 24% reduction in kilometers traveled by light-duty vehicles and a 10% reduction in freight transport by 2030.

Table 10: Summary of the differences between BASE, WEM, and WAM scenarios for the traffic sector. Source: [20]

	BASE	**WEM**	**WAM**
Vehicle fleet composition	Historical trend	BASE + LEZ calendar	BASE + LEZ calendar
Transport demand (see Table 11)	Historical trend	Historical trend	Good Move ambitions

Concerning methodology, traffic emissions were calculated based on projections of the vehicle fleet and transport demand. Subsequently, NOx emissions were computed using COPERT 5.6.1. The methodology for these projections is based on the following two formulas for each vehicle category [20]:

$$Stock_t = \frac{\text{Transport Demand}_t}{\text{Average Annual Mileage}_{t_{\text{start}}}} \tag{22}$$

$$Stock_t = Stock_{t-1} - \text{Scrappage}_t + \text{New Vehicles}_t \tag{23}$$

Where:

- Stock_t [veh] is the total number of vehicles in the fleet at year t.
- $\text{Transport Demand}_t$ [veh · km/year] is the total distance traveled by all vehicles in the fleet during year t.
- $\text{Average Annual Mileage}_{t_{\text{start}}}$ [km/year] is the average distance that a vehicle travels in one year, calculated based on the data from the baseline year 2019, assumed constant.
- Scrappage_t [veh] is the number of vehicles removed from the fleet in year t.
- New Vehicles_t [veh] is the number of vehicles added to the fleet in year t.

In the WEM scenario, the implementation of the LEZ results in increased scrappage, due to the removal of vehicles that do not conform to LEZ standards as well as older vehicles. This has an impact on both the influx of new vehicles and the overall vehicle stock. The WAM scenario, in addition to incorporating the LEZ, anticipates a reduced transport demand, as triggered by the Good Move plan. Using COPERT, which incorporates the composition of the vehicle fleet and the number of vehicle kilometers for each category (along with other parameters needed to operate COPERT), the annual NO and NO_2 emission projections can then be calculated.

To implement these formulas, various inputs are necessary, presented below [20, 12].

Starting point: Stock and mileage from the year 2019 are used as baselines, based on the emission inventory and MuSti data. The stock accounts for commuter and foreign vehicles, and it is assumed that mileage remains constant over time and across all scenarios.

Transport demand projections: For the BASE and WEM scenarios, projections are based on historical data compiled by the Federal Planning Bureau and MuSti. For the WAM scenario, the ambitions

of the Good Move policy aim to reduce transport demand by 24% for cars and 10% for freight transport. Changes in transport demand for various vehicle types during key years are presented in Table 11. For intervening years, linear regression is used to estimate values.

Table 11: Changes in vehicle-kilometers from 2018 to 2040 by vehicle type and scenario. Source: [20]

Vehicle type	2018-2030 BASE & WEM	2018-2030 WAM	2030-2040 BASE & WEM & WAM
Car	-3.8%	-24.0%	0%
Coach	0%	0%	0%
HDV	2.1%	-5.6%	0%
LDV	-3.5%	-10.8%	0%

Survival curves: The survival curves determine the historical scrappage rate for each vehicle age [20].

Redistribution of remaining vehicle kilometers (veh-km): The remaining veh-km from the transport demand that surviving vehicles do not cover is replaced by pre-owned vehicles, and by new vehicles [11] [20, 12]. For pre-owned vehicles, the redistribution of veh-km is based on the distribution of vehicles in circulation for the respective year. Regarding new vehicles that replace those scrapped, the replacement is modeled using the newest vehicle model from the latest Euro standard included in COPERT. Consequently, this methodology adopts a conservative approach by not accounting for future standards not yet included in the used version of COPERT. Therefore, the most recent Euro norm considered for light vehicles is Euro 6d; Euro 7 is not included. This progressive change in the vehicle fleet aligns with a study [13] that details fuel usage projections, ensuring that the proportions of different fuel types match those outlined in the study.

Projections of fuel types: The fuel projections incorporate various scenarios, elaborated step-by-step, in which the anticipated effect of each measure is cumulatively added to the preceding scenario [13, 102]. These are represented for passenger cars in Figure 20 and for other vehicle types in Appendix H.

The initial scenario, corresponding to the BASE scenario (Figure 20a), is a theoretical forecast based on current figures and relies on the Bass model—a scientific forecasting model for the S-curve evolution typical of new technology adoption. In this case, it includes an S-curve for electric vehicles and a reversed S-curve for diesel and gasoline vehicles. Subsequently, the price parity effect is considered (Figure 20b). This is the effect of the cost of electric vehicles falling to the cost of combustion engine vehicles. This influences consumers' purchasing decisions. Further, the impact of the 2030 ban of LEZ on diesel cars (Figure 20c) and the subsequent 2035 ban on all combustion engine cars (Figure 20d) are included. For company cars, the study also considers the annual reduction in tax benefits for non-electric vehicles. The WEM and WAM scenarios incorporate all cumulative effects for the fuel types projections, represented for passenger cars in Figure 20d.

[11] The repartition between pre-owned and new vehicles has not been provided

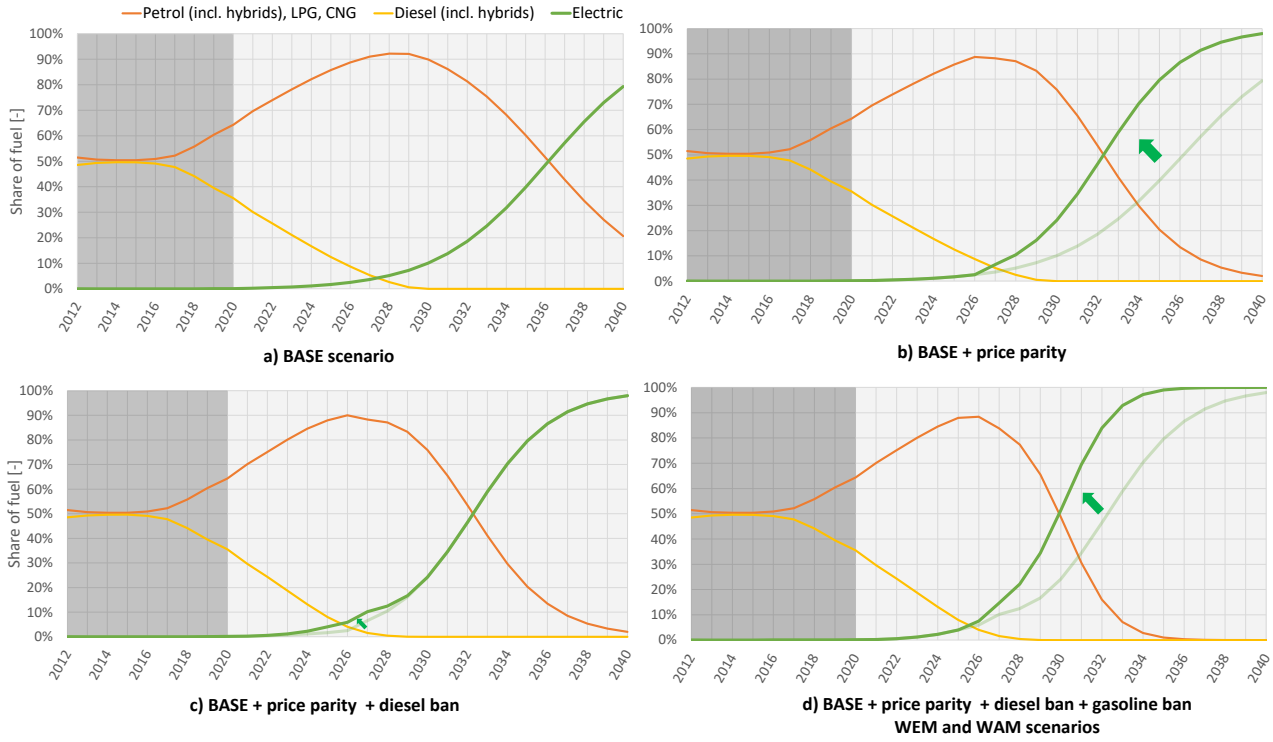

Figure 20: Share of fuels in passenger cars across various scenarios. The light green curve represents outcomes from the preceding scenario, while the green arrow indicates the impact introduced by the additional measure of the described scenario. The dark grey area is historical data, and the light grey area represents projections. Source : [13]

Effects of the LEZ: For the WEM and WAM scenarios, the impact of LEZ vehicle bans is accounted for, including people's anticipation of changing their cars prior to the ban [12]. The fuel type projections mentioned above, which incorporate the diesel and gasoline bans, are used, while the remainder of the methodology remains unchanged. Moreover, not all vehicles comply with LEZ regulations due to day-passes, exemptions, or non-conformity; the latter accounting for 0.8% of vehicles in 2022 [103]. It is hypothesized that non-compliance affects constantly 5% of the fleet [12].

Using the vehicle fleet composition and the number of veh-km per category (along with additional parameters such as speed limits), annual NO and NO_2 emission projections can then be calculated. The results of these projected emissions are presented and illustrated in Section 5.4.

4.7 Impact of meteorological variability on EU NO_2 threshold compliance

The choice to calibrate the year 2022 was based on the availability of the most recent data, and the meteorological conditions from 2022 were used for all simulations to enable comparisons. In 2022, Belgium recorded its second warmest and driest year, following 2020, based on the IRM. Despite these extreme conditions, wind speeds remained consistent with the historical average.

In addition to comparison between scenarios and years, it is pertinent to consider meteorological variability when assessing the likelihood of exceeding the EU's annual average NO_2 concentration threshold of 20 µg/m³ by 2030. The threshold must be respected, taking into account these fluctua-

tions. Studies focusing on the Netherlands [104] and Europe [105] indicate that deviations in NO_2 concentrations due to meteorological variability are normally distributed with a standard deviation of 5%. Employing eq. 24 representing a normal distribution, the derived values are presented in Table 12.

$$Z = \frac{X - \mu}{\sigma} \tag{24}$$

where Z [-] is the Z-score; X is the annual threshold not to be exceeded [µg/m³], µ is the mean annual NO_2 concentration in the distribution [µg/m³], and σ is its standard deviation [µg/m³].

Table 12: Probability that EU 2030 threshold of 20 µg/m³ annual NO_2 concentration will not be exceeded, for various target NO_2 concentrations and taking into account meteorological variability

NO_2 concentration [µg/m³]	**Probability**
20 (limit value)	50%
19.5	69%
19	85%
18	99%

Thus, the Table 12 shows that it is "likely" (> 66% chance according to IPCC terminology) to meet the EU 2030 annual NO_2 threshold of 20 µg/m³ by targeting a concentration of 19.5 µg/m³, taking meteorological fluctuations into account. Therefore, Brussels should target a 19.5 µg/m³ NO_2 annual concentration.

Furthermore, meteorological conditions are evolving due to climate change. Projections indicate increases in temperatures, precipitation levels, westerly winds during winter and early spring (which transport relatively cleaner air from the Atlantic), and sunlight during spring and summer [106]. Climate change is also expected to lead to more frequent occurrences of heavy precipitation and drought episodes. However, historical data up to 2007 have not shown significant effects of climate change on the annual average concentrations of NO_2 [104].

Therefore, to account for meteorological variability, locations where future air quality standards may be exceeded are now identified by recording exceedances at 19.5 µg/m³ instead of the 2030 EU annual average threshold of 20 µg/m³.

4.8 Processing SIRANE outputs

The simulations for the three scenarios were conducted for the years 2022, 2025, 2027, 2028, 2030, 2033, and 2035, with most of these years marking key phases of the LEZ banning process. Moreover, the year 2030 is interesting because it marks the point when the EU thresholds come into force. Analysis beyond 2035 will not be conducted, as there is negligible change in NOx emissions between 2035 and 2040. After the simulation, SIRANE produces raster maps as outputs. These maps are used for visualization and must be processed to obtain concentration data in a tabular format, providing insights into the concentration levels for each street.

Buffer application and zonal statistics

A 2-meter buffer was applied to a vector dataset containing the street segments, creating a buffered zone of 2 meters on either side of each street's axis, resulting in a 4-meter-wide buffer zone. The Zonal Statistics tool was then applied to calculate the mean concentration of the raster pixels within the buffered zones corresponding to the streets.

The 2-meter buffer distance was chosen arbitrarily but ensures that most street segments, which are more than 4 meters wide, are adequately represented. If, for example, the median width of the street segments (18 meters) was used, it would mean that half of the street segments are narrower, and the mean concentration of these segments would be greatly underestimated. This underestimation would occur because the calculation would include raster pixels at rooftop levels, which generally have lower pollution levels than street level, to meet the 18-meter width requirement. In this context, segments narrower than 4 meters account for only 0.35% of all segments. Conversely, for the 99.65% of street segments that are wider than 4 meters, the raster pixels at the street's edges are excluded from the calculations. This exclusion leads to a possible overestimation of the average concentration for these street segments, as only the central part of the street is considered.

Tunnel correction

When visualizing the different maps, it became clear that concentrations near the point sources (the tunnels) were excessively high. In the preparatory work by Axel Briffault, the tunnel concentrations were estimated on the basis of theoretical concepts only. Empirically, this tends to overestimate the concentration, and this overestimation is too significant for the various projections made. Therefore, all roads intersecting the plume at the tunnel exits were removed from the tabular data as they were considered irrelevant. This removal may lead to an underestimation in the calculation of the total concentration for Brussels.

After this adjustment, the overall concentration of the Region for each scenario and year was calculated. This was done by averaging the mean concentration of each street segment and weighting it by their length. The overall concentration for each road hierarchy was also calculated similarly, as there might be discrepancies between them that need to be highlighted. To analyze how the future norm will be respected, the lengths of street segments exceeding a mean annual concentration of 19.5 $\mu g/m^3$ (accounting for meteorological variability as discussed in Section 4.7) were summed. This total length of exceedance of the future EU annual concentration threshold was also categorized by road hierarchy.

5 Results

The following section presents the results obtained to address the various objectives of this master's thesis. Initially, variations in emissions and concentrations across different road hierarchies due to road refinement are presented (Section 5.1). After the calibration, the modelled NO_2 concentrations for 2022 are compared with measurements from various stations, and the model's validity is assessed (Section 5.2). A comparison of 2022 NO_2 concentrations derived from NOx emission scenarios and inventory emissions is then conducted to evaluate the relevance of the projections (Section 5.3). The estimated NO_2 concentrations for the BASE, WEM and WAM scenarios up to 2035 are presented next, quantifying the impacts of the LEZ and Good Move policies (Section 5.4). These impacts are further analyzed and broken down by road hierarchy (Section 5.5). The maps of Brussels for 2028, a year with significant impacts from the LEZ and Good Move policies, will be presented in Section 5.6. Finally, compliance with the EU 2030 NO_2 thresholds is assessed for the three scenarios (Section 5.7).

To quantify the impacts of the LEZ and Good Move scenarios, the effects are measured in terms of absolute concentration differences in µg/m³ between the BASE and WEM scenarios, and between the WAM and WEM scenarios, as well as in relative differences compared to the BASE scenario, in percentage. To accurately calculate the relative differences, the background concentration of 10.80 µg/m³ is subtracted from the simulation results. This subtraction isolates the portion of NO_2 concentration that can be directly influenced by local policy measures affecting the Brussels region, since the background concentration remains unchanged over the years. This approach ensures that the analysis specifically accounts for the impact of local measures, highlighting the concentration changes directly attributable to the city's policies. For clarity in the Results and Discussion sections, terms such as "relative reduction" or "relative change" will refer to this subtraction of the regional background concentration.

5.1 Road refining

As explained in Section 4.4, various changes in the distribution of emissions across road hierarchies between COPERT and MuSti have been implemented, and their impacts are presented below.

5.1.1 Changes of the distribution of NOx emissions among road hierarchies

The changes in the distribution of emissions across road hierarchies after the modifications between COPERT and MuSti in 2022 are presented in Figure 21. The direct linkage of the "Highway" and "Rural" emission categories to A0 and A1 respectively resulted in a significant decrease in emissions. The proportion of emissions for A0 decreased from 24.8% to 9%, while A1 decreased from 28.2% to 15%. In contrast, urban roads experienced an increase in emissions due to the reassignment of urban emissions from COPERT. For information, the new distribution of the NOx emissions by road hierarchy is shown in Appendix I. A3 now holds the leading position, rising significantly to 30% of the total emissions. It is followed by A2 and A5, each contributing 19% to the total emissions, then A1, A0, and A4.

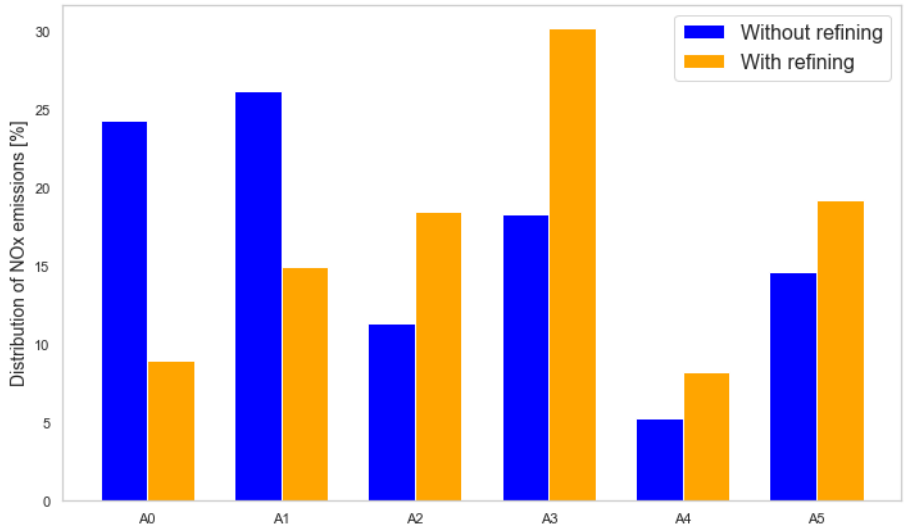

Figure 21: Impact of road refinement on NOx emissions distribution across the road hierarchy of MuSti in 2022.
A0 : Highway A1 : Rural A2-A5 : Urban road

The Figure 22 presents the contribution of each vehicle type to the emissions within each road hierarchy. In terms of proportion, all road hierarchies exhibit the highest NOx emissions from light vehicles, with A0 having the highest contribution. The A1 hierarchy shows the largest proportion of emissions from utility vehicles. For the bus category, the A2-A5 hierarchies have the greatest share of their emissions from this vehicle type. Finally, when combining the two types of heavy trucks, A0 shows the highest emission contribution from this category of vehicles.

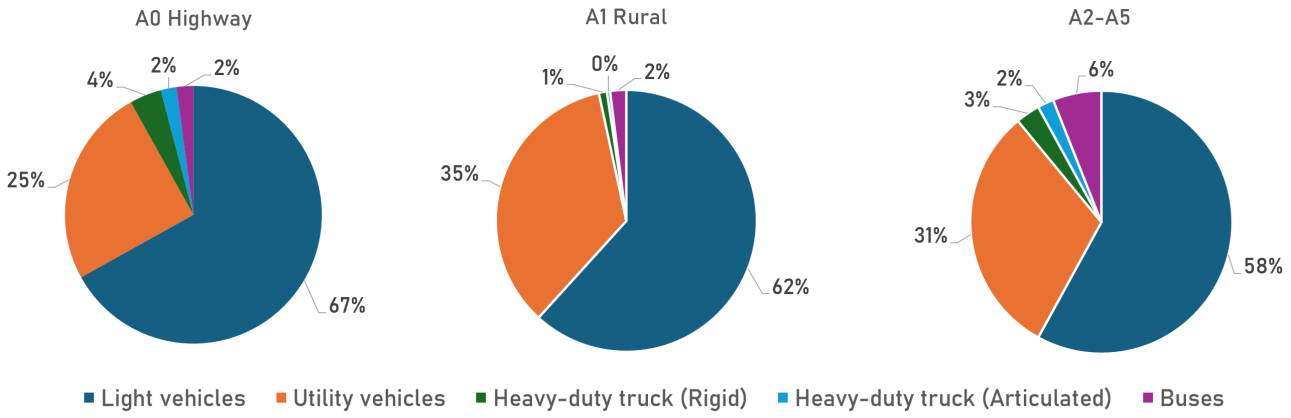

Figure 22: Distribution of NOx emissions by vehicle type in the different road hierarchies in 2022

5.1.2 Changes of the distribution of NO_2 concentrations among road hierarchies

Using the output data provided by SIRANE at the end of a simulation, it is possible to spatially project the annual average NO_2 concentration in Brussels, as illustrated in Figure 23. This map is the result of road data refinement and calibration performed for 2022. Outside the urban center, concentrations are lower, approaching background levels, particularly visible in the south within the Soignes Forest. The average concentrations in 2022 for each road type are presented in Table 13, along with a comparison without road refinement. Concentrations for highways (A0) and rural (A1) roads have lowered by

18.38 and 2.55 µg/m³, respectively. Inversely, A2-A5 hierarchies have increased overall, in ascending order: A5 < A4 < A2 < A3.

Table 13: Impact of refinement changes on the average NO_2 concentration for each type of road in 2022. The "Relative change" category calculates the percentage change by first subtracting the background concentration

	A0	A1	A2	A3	A4	A5
Without refinement [µg/m³]	48.35	24.01	21.69	19.73	19.07	16.40
With refinement [µg/m³]	29.97	21.46	24.76	22.54	21.02	16.98
Relative change [%]	-48.94	-19.28	28.15	31.44	23.55	10.35

The 'Relative change' category summarizes the average impact of these changes, while Figure 24 visually represents these changes spatially. The decrease in concentration for highways was particularly significant, shown in dark blue, while A1 experienced a lighter decrease, depicted in light gray and light blue. However, road refinement increased the NO_2 concentration of A2-A5 roads. Changes due to road refinement are therefore similar for NOx emissions and NO_2 concentrations. Classifying the hierarchies based on the relative changes in emissions distribution, the order from most to least impacted is A0, A3, A2, A4, A1, and A5.

In summary, the road refinement resulted in a significant decrease in NOx emissions for A0 and A1 roads in 2022. In contrast, urban roads, experienced an increase in NOx emissions, particularly A3 now holding the leading position, followed by A2 and A5. Similarly, concerning NO_2 concentrations, the road refinement led to a marked decrease for A0 (very significantly) and A1. Conversely, the other roads (A2-A5) experienced an increase in NO_2 concentrations, with A0 maintaining its leading position, followed by A2 and A3.

5.2 Validation of model calibration

As detailed in Section 4.5.1, a calibration of NOx emissions was carried out for the 2022 NOx emissions inventory. Through this process, coefficients of 1 for NO_2 emissions and 0.75 for NO emissions were determined. Therefore, all NO emissions from traffic and tunnels, both from the 2022 inventory and projection emissions, will be multiplied by 0.75 to account for traffic emission biases. Here, a qualitative and quantitative analysis of this calibration is presented.

5.2.1 Qualitative analysis

Figure 25 compares the NO_2 concentrations, after road refinement and calibration, from the model with the measurements obtained at all 12 stations, presenting the average weekly profile for the year. Additionally, for more information on the calibration results, see Figure J.1 for a density histogram and Figure J.2 for a comparison of the ratio of modeled to measured values against a perfect model. Figure J.4 presents a comparison of measured concentrations with modeled concentrations for each

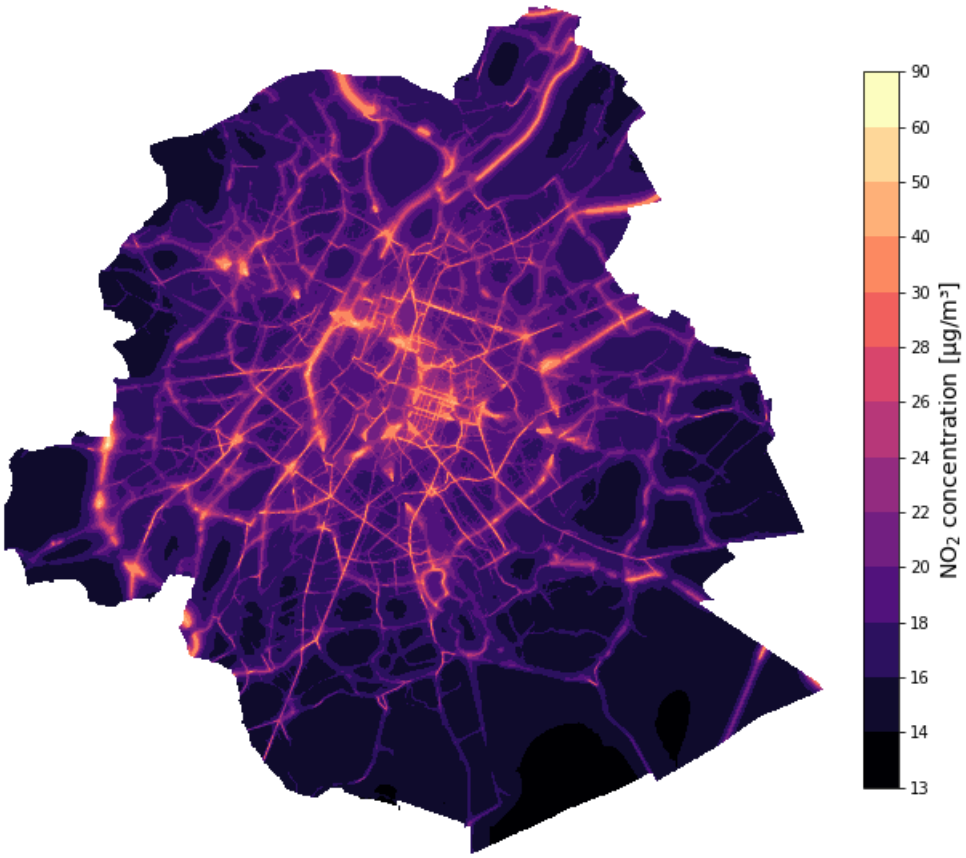

Figure 23: Annual NO_2 concentration of 2022 calibrated and with refined NOx emissions among road hierarchies

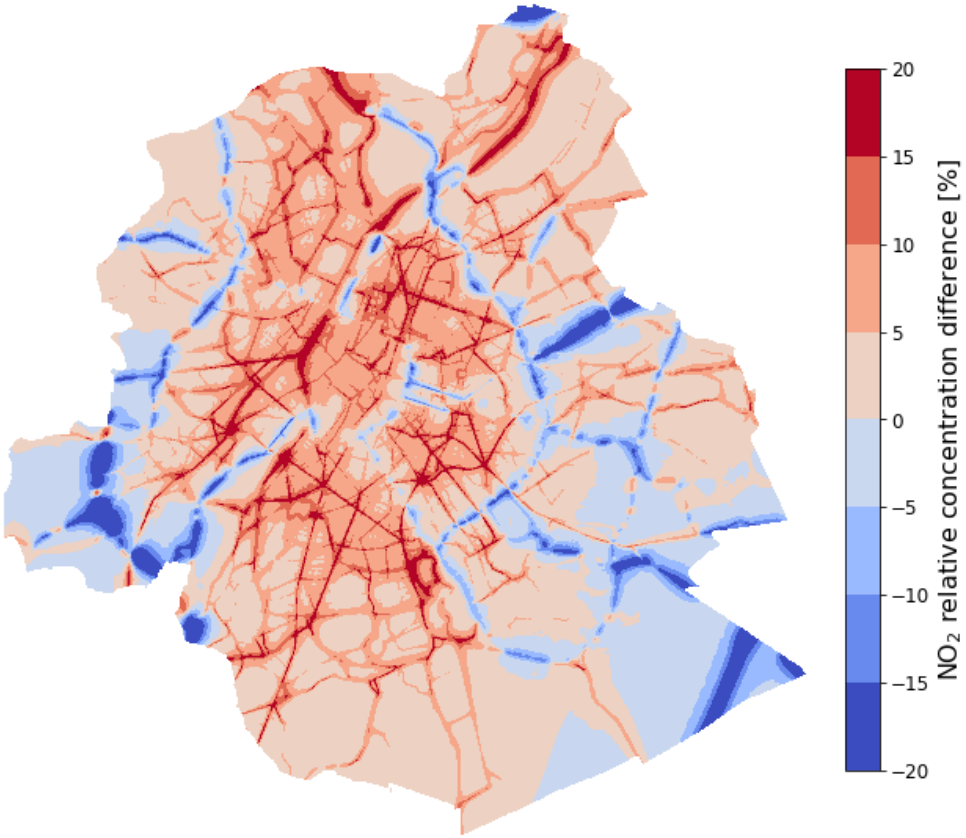

Figure 24: Changes in annual NO_2 concentrations due to road refinement between MuSti and COPERT

station. Figure J.3 contains box plots for the different stations, offering a visual representation of the distribution of predictions relative to actual measurements.

Influence of hour and day on concentrations

In Figure 25, the stations are arranged according to traffic influence, gradually increasing from the top to the bottom of the figure for simplicity. At the top of the graph, stations such as Uccle and Berchem-Sainte-Agathe show the lowest NO_2 concentrations, while the last station at the bottom right, Regent, represents a very high traffic influence.

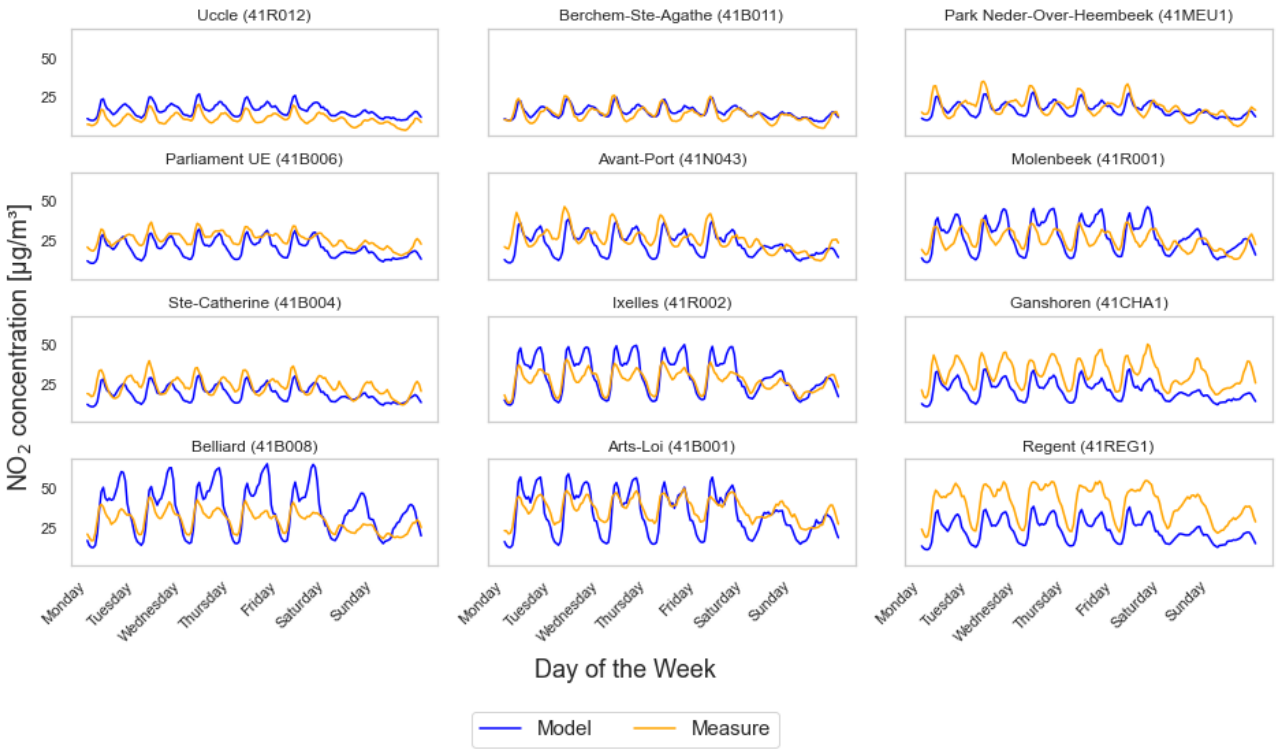

Figure 25: Average weekly profiles of NO_2 concentrations measured and modelled at the 12 stations in the measurement network in 2022
Traffic influence → Very low : Uccle, Berchem-Ste-Agathe Low : Park Neder-Over-Heembeek, Parliament UE Moderate : Avant-Port, Molenbeek, Ste-Catherine High : Ixelles, Ganshoren, Belliard, Arts-Loi Very High : Regent

This weekly average representation helps avoid the influence of random parameters such as weather conditions, construction work affecting traffic flow, etc. In the profile, two peaks in concentration are visible for each day, representing morning and afternoon rush hours. Similarly, concentrations are lower on Saturdays and Sundays compared to other weekdays due to the decrease in the number of vehicles on the road.

Overall, Figure 25 shows that after the road refinement and calibration, the modeled concentrations generally align well with measured concentrations, particularly for low traffic stations. Low-traffic stations like Uccle and Berchem-Ste-Agathe, as well as all the other stations at concentrations between 0 to 20 µg/m³, follow the measurement curve particularly well, although Uccle tends to slightly over-estimate. However, as traffic influence increases, the discrepancy between the two curves becomes more pronounced. For Regent and Ganshoren, the model consistently underestimates concentrations

in the weekly profile, while for Belliard and Ixelles, the model overestimates during high traffic periods. Arts-Loi is the high-traffic station where the peak concentrations modeled align most closely with measurements, while its lower concentrations are underestimated.

5.2.2 Quantitative analysis

The Table 14 presents the various statistical indicators used to validate modeled emissions compared to the monitoring stations measurements, as explained in Section 4.5.2. Overall, the model is assessed acceptable both for Hanna & Chang criteria and for European Commission criteria (FAIRMODE) [107] [108].

Table 14: Statistical Indicators for NO_2 Measurement Stations: FB, NMSE, FAC2, NAD, MQI_h, and MQI_y. Values not meeting the criteria are highlighted in bold red.

Stations	FB	NMSE	FAC2	NAD	MQI_h	MQI_y
Molenbeek	-0.09	0.36	0.74	0.23	0.66	0.23
Ixelles	-0.11	0.27	0.79	**0.37**	0.60	0.34
Arts-Loi	0.08	0.29	0.79	0.21	0.70	0.25
Ste-Catherine	0.22	0.33	0.83	0.20	0.51	0.49
Berchem-Ste-Agathe	-0.09	0.35	0.62	**0.33**	0.40	0.16
Uccle	**-0.43**	0.26	0.56	**0.37**	0.33	0.65
Avant-Port	0.13	0.33	0.79	0.21	0.57	0.33
Neder-Over-Heembeek	0.08	0.39	0.70	0.27	0.49	0.15
Parliament UE	0.25	0.36	0.87	0.19	0.56	0.58
Belliard	-0.22	0.46	0.73	0.24	0.89	0.72
Ganshoren	**0.42**	0.76	0.57	**0.31**	0.83	**1.05**
Regent	**0.54**	0.73	0.59	**0.300**	0.90	**1.46**

According to the Hanna & Chang criteria, all of these indicators are within the acceptance thresholds for an urban dispersion model. For the stricter rural acceptance criteria, eight indicators do not meet the specified limits, in red in FB and NAD columns. For the NMSE and FAC2 indicators, the rural criteria are met, with all stations having NMSE values below three and FAC2 values above 0.5. The FB and particularly the NAD indicators are the least adhered to.

Concerning the European Commission (FAIRMODE) indicators, MQI_h and MQI_y, the indicators show significant variations between stations. Despite two stations exceeding the limit for MQI_y, in red in MQI_y column from Table 14, the model is accepted under FAIRMODE criteria as the overall MQO is met since more than 90% of the MQI values are below 1, with an average of 0.83 for MQI_h and 0.72 for MQI_y The Regent and Ganshoren stations account for the majority of limit exceedances, with six of the ten exceedances.

In summary, the modeled concentrations—after road refinement and calibration—generally align well with the measured concentrations in areas and times of low traffic. However, they exhibit greater deviations in high-traffic areas. Additionally, the model is deemed acceptable according to both Hanna & Chang and the European Commission's statistical criteria (FAIRMODE).

5.3 Comparison of 2022 NO_2 concentrations from NOx emissions scenarios and inventory emissions

Before examining the projected concentrations for future years such as 2030 or 2035, a comparison of the baseline concentration levels of the three scenarios (BASE, WEM, WAM) against the actual concentrations recorded in 2022 was conducted. The objective of this step is to determine which scenario the year 2022 most closely resembles. Additionally, the purpose of this comparison is to observe whether the projections of NO_2 concentrations derived from NOx emissions projections that are based on the 2019 inventory data remain relevant or have become outdated. Figure 26 presents the difference between the three projection scenarios and the NO_2 concentrations measured in 2022. Table 15 shows the percentage of areas occupied by different concentration intervals for the three maps in Figure 26.

Table 15: Percentage of surface area within different concentration intervals for the three scenarios shown in Figure 26, representing the absolute difference in NO_2 concentrations between the three scenarios in 2022 and the 2022 concentrations based on inventory data.

	Surface area [%]		
Concentration interval [µg/m³]	BASE	WEM	WAM
< -0.5	0	2.74	3.81
-0.5 - -0.1	0	9.53	16.72
-0.1 - 0.1	9.08	69.30	77.56
0.1 - 0.5	56.80	18.20	1.89
> 0.5	34.12	0.22	0.02

For the BASE scenario, the entire map shows predominantly positive differences, with concentrations predominantly ranging between 0.1 and 0.5 µg/m³. This indicates more NO_2 concentration for the BASE scenario compared to the 2022 situation, specifically in the city center, while highways and rural roads have similar concentrations compared to 2022.

Similarly, comparisons to 2022 real data were made for the WEM and WAM scenarios. Overall, the concentration differences are smaller and exhibit less variation, and the WAM map is closer to reality, but with a tendency of less NO_2 concentration than the reality. In addition, there is lesser NO_2 concentration in the main roads compared to 2022 for WEM and even more for WAM, as shown in green in Figure 26. In contrary, in some A2-A5 roads, WEM particularly and WAM as well are more polluted than the reality.

In terms of surface area (Table 15), approximately 70% of the concentrations are between -0.1 and 0.1 µg/m³ for WEM and around 77% for WAM. Appendix K shows a box plot of the NO_2 concentrations

in road segments for 2022 for the BASE, WEM and WAM scenarios compared to the simulation with the real data, also supporting these results.

In summary, the BASE scenario shows higher NO_2 concentrations compared to the 2022 situation, particularly in the city center, while concentrations on highways and rural roads are similar to those in 2022. However, the concentration differences are smaller for the WEM and WAM scenarios, with the latter being even closer to reality, albeit with a tendency towards lower NO_2 concentrations than actual measurements. Additionally, NO_2 concentrations on main roads are lower in the WEM scenario and even lower in the WAM scenario compared to 2022.

5.4 Projected NOx traffic emissions and NO_2 average concentration

Based on the methodology described in Section 4.6.2, François Goor working at Bruxelles Environnment has provided emission projections for NO and NO_2 from the traffic sector under BASE, WEM and WAM scenarios [12]. Furthermore, the emissions projections have also been broken down by vehicle type, fuel type, Euro Standard, and vehicle size and are shown in Appendix L. Using these emissions, projections of average annual NO_2 concentrations—a key result of this master's thesis—were made following the methodology described in Section 4.8, for the years 2022, 2025, 2027, 2028, 2030, 2033 and 2035. These NO_2 concentration projections can thus be analyzed and compared with the NOx emissions. Then, the specific impacts of the LEZ 5.4.2 and Good Move 5.4.3 are quantified.

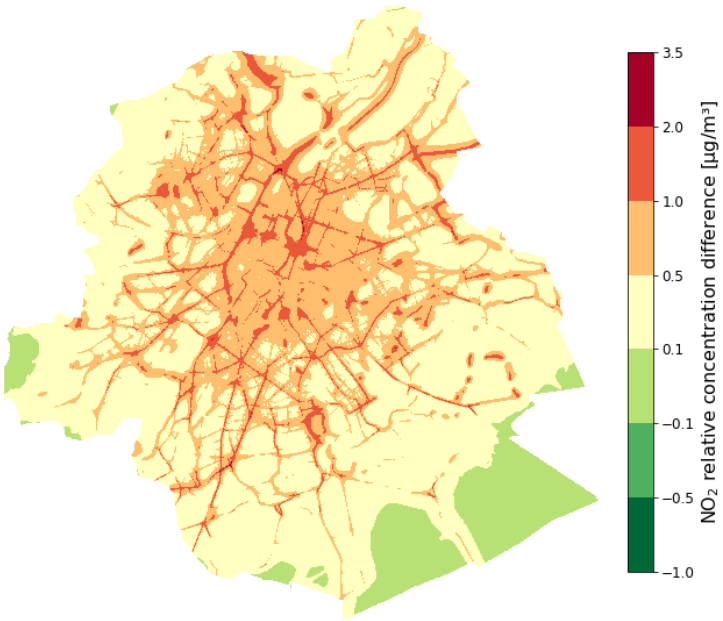

(a) Difference between BASE 2022 projection and 2022 NO_2 concentrations

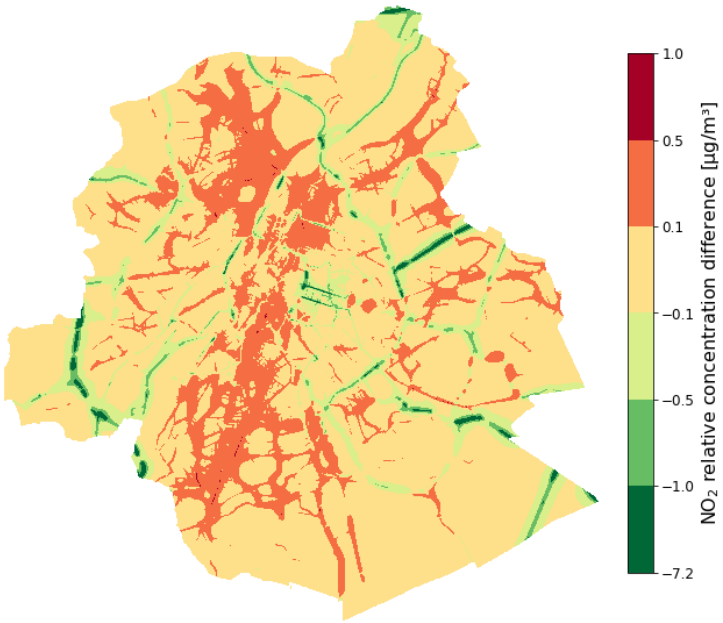

(b) Difference between WEM 2022 projection and 2022 NO_2 concentrations

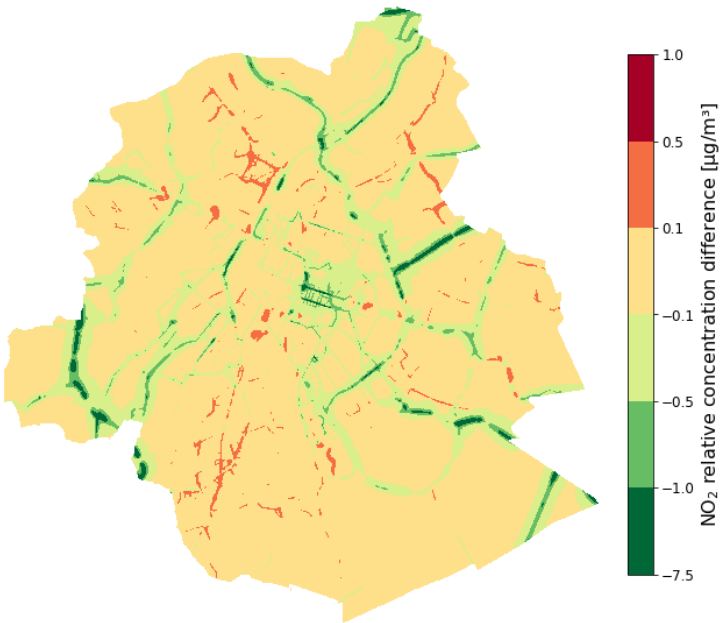

(c) Difference between WAM 2022 projection and 2022 NO_2 concentrations

Figure 26: Difference between the various projections (BASE, WEM, WAM) and the NO_2 concentrations based on inventory data for the year 2022

5.4.1 Emissions and concentration projections and overall trends

Figure 27 shows NO_2 and NO emissions projections from 2019 to 2040. Line graphs in Figure 28 project spatially averaged annual NO_2 concentrations from 2022 to 2035, derived from these emissions. Bar graphs depict the relative difference of WEM compared to BASE and the additional relative difference of WAM compared to BASE, excluding the background concentration set at 10.8 µg/m³. Raw and detailed data on emissions and concentrations are also available in Appendix M.
Despite differences in magnitude and units, the trends across the Figures 27 and 28 are very similar. In these three Figures, the BASE scenario shows a steady decrease in NOx emissions and NO_2 concentration. In contrast, under the WEM and WAM scenarios, emissions and concentration trajectories show abrupt decreases, particularly before the years 2025, 2028, 2030 and 2035.

From 2022 to 2035, NO emissions in the BASE, WEM and WAM scenarios will fall by 72%, 93% and 96% respectively, while NO_2 emissions will drop by 90%, 98% and 98% respectively. Over the same period, NO_2 concentrations are reduced by 26% for BASE and 30% for both WEM and WAM. The correspondence between NOx emissions and NO_2 concentration is clearly illustrated in Appendix N, where the curves of emissions and concentrations are plotted on the same graph. The relationship between emissions and concentrations, as derived from the emission projections data and simulations, can be quantitatively described by the following empirical model (eq. 25):

$$C_{\text{av}} = 12.693 + 0.0037 \times E_{\text{NOx}} \tag{25}$$

where C_{av} represents the average NO_2 concentration in µg/m³, and E_{NOx} represents the NOx emissions in tons. Although this is not a real equation since the units do not directly correspond, this empirical relationship provides a highly accurate fit to the data, with an R^2 value of 0.999. This relationship holds under the assumption that all other variables introduced in this master's thesis remain constant.

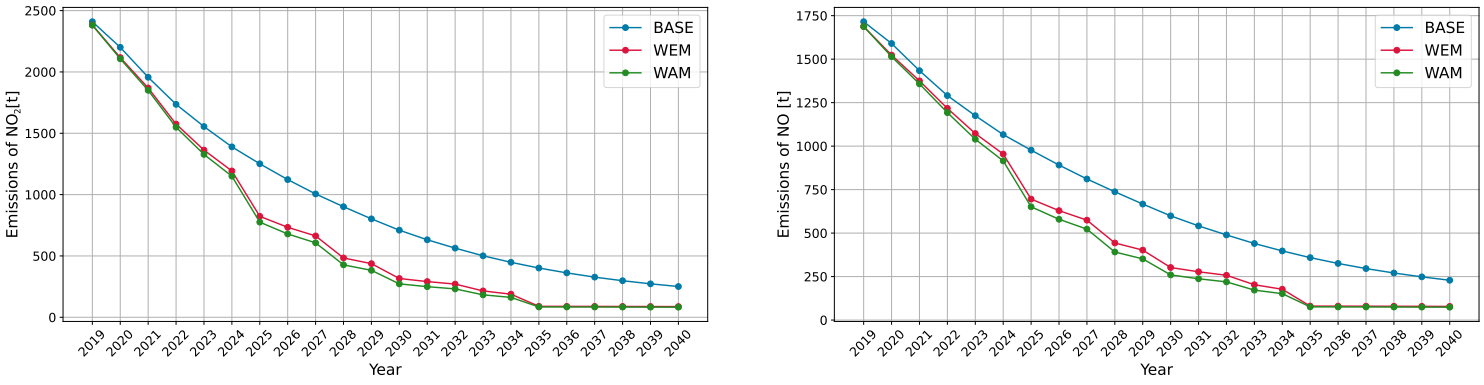

(a) NO_2 **(b)** NO

Figure 27: Annual NOx Emissions Projections in Brussels. Data source : [12]

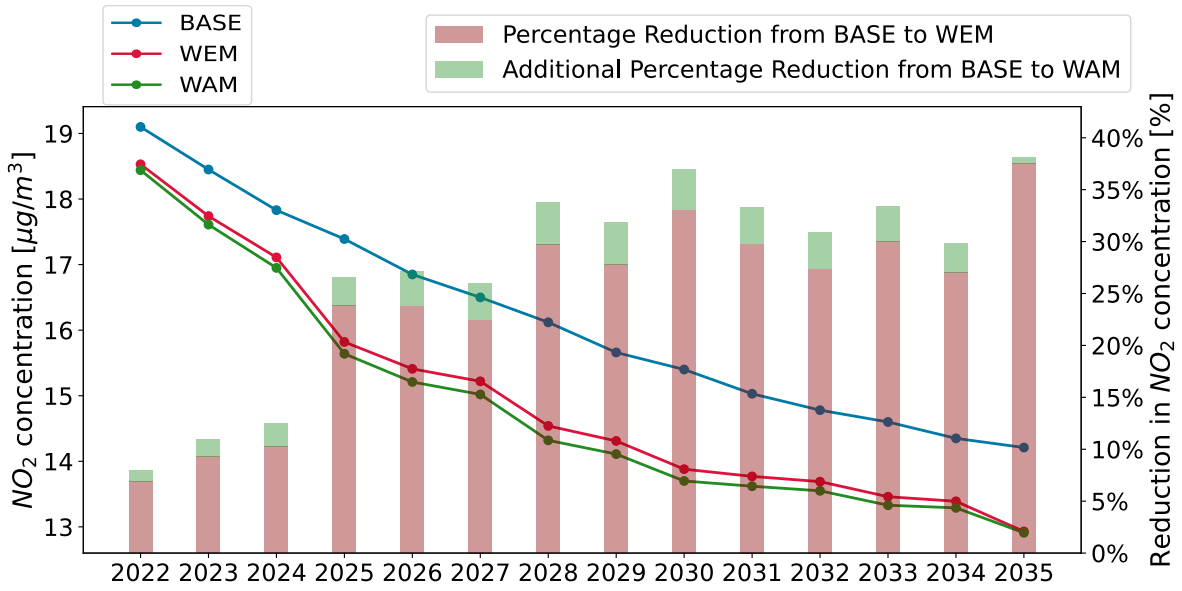

Figure 28: Projections of annual NO_2 concentrations in Brussels (2022-2035). The lines represent the projected evolution of annual NO_2 concentrations in Brussels from 2022 to 2035 for the BASE, WEM, and WAM scenarios. The red bars show the yearly relative difference in concentration between the WEM and BASE scenarios, excluding background concentration. The green bars on top represent the additional relative difference for the WAM scenario compared to BASE, also excluding background concentration.

5.4.2 LEZ effects on NO_2 concentration

Evaluating the effectiveness of policies is crucial not only at the end of their implementation but throughout their duration. The LEZ measures (covered in WEM and not in BASE scenario) aim to accelerate improvements in the vehicle fleet, achieving air quality benefits earlier than the BASE scenario. Therefore, assessing air quality improvements before 2035 and identifying key moments of policy impact is essential.

As shows Figure 28, in the BASE scenario, the decrease in NO_2 concentration slows over the years, ranging from -0.65 to -0.14 µg/m³ per year. The WEM scenario follows a similar trend but shows stronger and abrupt decreases before 2025, 2028, 2030 and 2035. Its absolute reductions range from -0.073 µg/m³ in 2034 to -1.29 µg/m³ in 2025. These abrupt decreases diminish over time, and the reductions in the intervening years are less significant than in the BASE scenario.

From 2022 to 2035, the NO_2 concentration in the WEM scenario is on average 1.18 µg/m³ lower than in the BASE scenario, ranging from 0.57 µg/m³ to 1.58 µg/m³. The smallest differences are experienced in the early years, while the largest differences occur between 2025 and 2030, particularly in 2025, 2028, and 2030. The difference then decreases, with a notable peak still observed in 2035. The relative difference of WEM compared to BASE, excluding background concentration (referred to as the "relative difference"), is shown in the red bars in Figure 28. It shows that the WEM scenario helps reduce NO_2 concentration, by 6.82% to 37.48%, with the highest effectiveness observed in 2035. Overall, this relative difference tends to increase over time. Looking at the years with the biggest jumps in relative difference compared to the previous years, 2025 shows the greatest increase with a 13% jump compared to 2024, followed by notable increases in 2035, 2028, and 2030 (in

descending order).

5.4.3 Additional Good Move mileage ambition effects on NO_2 concentration

What is noticeable when looking at the emissions and concentrations graphs in Figures 27 and 28 is the small difference between the WEM and WAM (which includes Good Move measures not covered in WEM) scenarios. On average, from 2022 to 2035, the reduction in NOx emissions from BASE to WEM is 7.9 times greater compared to the reductions from WEM to WAM. While for NO_2 concentrations, this difference is even greater, with BASE to WEM reductions being 8.6 times greater than those from WEM to WAM. Annually, the LEZ contributes to an average reduction of 1.18 µg/m³ (a 24.2% relative reduction) in NO_2 concentrations compared to the BASE scenario, while the Good Move policy adds an additional 0.15 µg/m³ (an additional 2.93% relative reduction) reduction per year on average. Annually, the LEZ reduces the concentration of NO) by an average of 1.18 µg/m³, which is a relative decrease of 24.2% compared to the BASE scenario. Additionally, the Good Move policy further lowers the NO_2 concentration by an average of 0.15 µg/m³ annually, amounting to an extra 2.93% reduction. Due to this small difference, the overall trends of decreases and differences with the BASE scenario are similar to WEM.

The absolute difference in NO_2 concentrations between WAM and WEM gradually increases, peaking at 0.22 µg/m³ in 2028, then slightly decreases. Relative to WEM, WAM shows a 1.54% reduction in concentration in 2028. The additional relative difference of WAM compared to BASE, excluding background concentration, is shown in the green bars in Figure 28. This illustrates the effectiveness of the Good Move policy, ranging from 0.63% to 4.21%, with the highest value in 2028. From 2022 to 2035, the WEM scenario consistently achieves higher effectiveness percentages compared to the WAM scenario, being 8.2 times higher on average.

In summary, the trends of NOx projected emissions and NO_2 projected concentrations are very similar. The BASE scenario shows a steady decrease. In contrast, under the WEM and WAM scenarios, emissions and concentration trajectories show abrupt decreases in 2025, 2028, 2030 and 2035. These abrupt decreases diminish over time. From 2022 to 2035, the LEZ is projected to reduce NO_2 concentrations by 1.18 µg/m³ on average compared to BASE (24.2% excluding background concentrations). Good Move's additional impact is eight times smaller than LEZ's impact, contributing a further reduction of 0.15 µg/m³ on average (amounting to an extra 2.93% reduction), with a maximum decrease in 2028.

5.5 Difference in concentration between road hierarchies

As SIRANE provides spatialised data, it is possible to analyze both the differences in NO_2 concentration and how these concentrations change over time among different road categories. Figure 29 presents the projected mean concentrations for the different road hierarchies from 2022 to 2035 under the WEM scenario. Similar graphs for the BASE and WAM scenarios can be found in Appendix O.

5.5.1 Overall trends

All road hierarchies from all three scenarios show similar trends, as discussed in Section 5.4.1: a steady decrease in concentrations over time, with the rate of decrease gradually slowing, and sharp reductions specifically for the WEM and WAM scenarios. However, the differences between road hierarchy in terms of decrease over the years and comparison with the BASE scenario can still be analyzed.

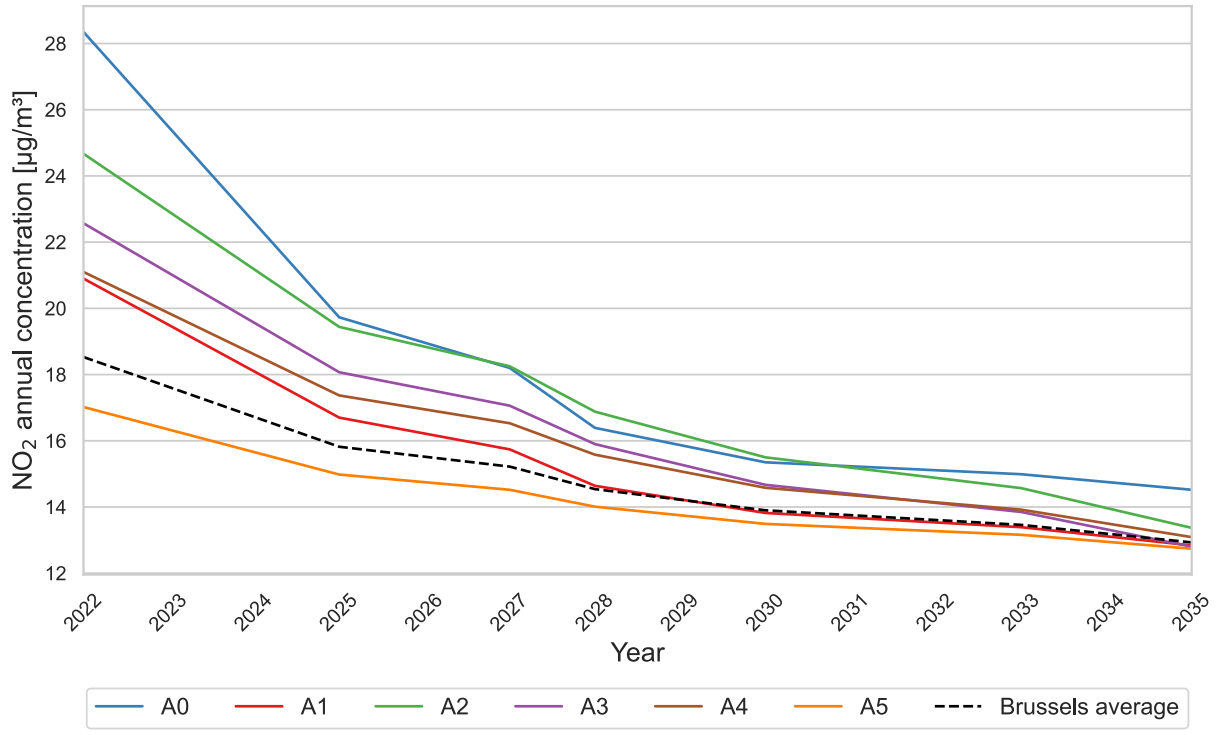

Figure 29: Projections of annual NO_2 concentrations in Brussels by road hierarchy under the WEM scenario (2022-2035).

There is a gradient in concentration across the road hierarchy from highways (A0) to local roads (A5) in 2022, the base year. Concentrations are highest on A0 roads, ranging from 28.3 to 30.1 µg/m³ depending on the scenario. Following this gradient, the lowest concentrations in 2022 are found on A5 roads, with levels between 16.9 and 17.4 µg/m³. It is worth noting that A1 roads are an exception to this pattern, with lower concentrations than A4 roads. Additionally, for all scenarios, the regional average is close to and slightly above the A5 concentrations, the hierarchy with the lowest concentration, following a similar curve throughout the years.

5.5.2 BASE scenario

In the BASE scenario, showed in Appendix O, the mean concentrations for all road hierarchies decrease and converge to between 13.7 and 16.2 µg/m³ by 2035, maintaining the same ranking of concentrations among the road types over the years. A0 roads exhibit the steepest overall decline in concentrations, with an average decrease of -1.07 µg/m³ per year. This is followed by A2, A3, and A1 roads, all of which have similar slopes with an average decrease of -0.65 µg/m³ per year. A4 and A5 roads show the least steep declines. The differences in the rates of decrease are more pronounced in the early years compared to the later years.

5.5.3 WEM scenario

The absolute and relative differences of WEM compared to BASE, excluding background concentration, averaged between 2022 and 2035, can be found by road hierarchy in Table 16. Overall, roads classified as A0 are the most impacted by the policy, with an average absolute difference of -3.18 µg/m³/year and a relative difference averaging 32.9% compared to BASE. Roads classified as A4 and A5 have the least impact in terms of both absolute and relative differences. Roads classified as A1, A2, and A3 fall between A0 and A4/A5, with their rankings varying based on absolute or relative differences.
However, there are variations over the years between the road hierarchies. From 2022 to around 2028-2029, the trends reflect the overall pattern: A0 roads show the most significant differences, with reductions approximately twice as much as other hierarchies, while A5 roads decrease by about half as much. Notably, in 2027, A0 roads become less polluted than A2 roads. After 2028-2029, roads classified as A2 to A5 continue to experience significant differences, especially in 2030 and 2035, aligning with the regional averages shown in Figure 28 (red bars). In contrast, the reduction for A0 roads diminishes significantly after 2028-2029, unlike A2 to A5. Roads classified as A1 show trends between those of A0 and A2 to A5, with a relatively consistent decrease. By 2031, A2 roads become less polluted than A0, and by 2032, A3 roads become less polluted than A4.

Table 16: Absolute and relative differences in concentration due to LEZ (WEM scenario compared to BASE scenario) and the additional absolute and relative differences due to Good Move (WAM scenario compared to BASE scenario, excluding the LEZ impact) by road hierarchy per year, averaged between 2022 and 2035.

	A0	A1	A2	A3	A4	A5	Region
LEZ absolute impact [µg/m³]	-3.18	-1.85	-2.61	-2.25	-1.83	-0.97	-1.18
Good Move absolute additional impact [µg/m³]	-0.18	-0.16	-0.32	-0.29	-0.23	-0.12	-0.15
LEZ-induced reduction (Excl. Background) [%]	32.9	31.9	30.6	32.5	28.9	23.6	24.2
Good Move reduction (Excl. Background) [%]	1.96	2.56	3.64	3.85	3.43	2.77	2.93

5.5.4 WAM scenario

Since the WAM scenario is very similar to the WEM scenario, the concentration decrease over the years follows a similar pattern, primarily driven by LEZ. The difference in concentration between WEM and WAM follows the same trend for all road hierarchies as the average concentration discussed in Section 5.4.1, slightly increasing, peaking in 2028, and then slightly decreasing.

The absolute difference of WAM compared to BASE, excluding LEZ impact per year, averaged over the time period to assess Good Move impact, is shown in Table 16. This difference is greatest for

A2, following the gradient: A2 > A3 > A4 > A0 > A1 > A5, with the maximum difference in 2028 ranging from 0.46 µg/m³ for A2 to 0.18 µg/m³ for A5.

The additional relative difference of WAM compared to BASE, averaged per year between 2022 and 2035, is also shown in Table 16 to evaluate policy effectiveness. Each road hierarchy follows the same trend as the average concentration, with additional reductions ranging from 1.96% for A0 to 3.85% for A3, following the gradient A3 > A2 > A4 > A5 > A1 > A0. Comparing this additional relative difference of Good Move to the relative difference of the LEZ for each road hierarchy shows that the impact of LEZ is 8 times larger than the impact of Good Move for A2 to A5, 12 times larger for A1, and 18 times larger for A0.

In summary, all road hierarchies exhibit similar trends over time for each scenario: a consistent decrease in NO_2 concentrations, with the rate of reduction slowing over time and more pronounced decreases observed in the WEM and WAM scenarios. In 2022, the baseline year, there is a gradient in concentration across the road hierarchy, with highways (A0) recording the highest and local roads (A5) the lowest concentrations. The reduction in concentrations over time is proportional to this gradient, both for the BASE scenario and the overall impact of the LEZ. Specifically, the LEZ has the most significant impact on A0 roads, particularly between 2022 and 2030. Additionally, the Good Move plan predominantly affects A2 and A3 roads.

5.6 Difference in NO_2 concentration between the three scenarios for 2028

In the Section 5.4, Figure 28 illustrated the evolution of NO_2 concentrations over the years, with the percentage relative reductions achieved by WEM and WAM over time. Notably, 2028 showed the highest absolute reduction both for the LEZ and for Good Move.

To quantify the spatial impact of WEM and WAM for this year, Figures 30 and 31 were created, representing the relative reduction. Again, the background concentration was subtracted before making the difference between the projections. Visually, the smallest reductions are observed on the city periphery, with increasing reductions towards the center. Mostly, the reduction is significantly more important for WEM (the LEZ) than the additional reduction of WAM (Good Move), as illustrated in Table 17, which provide data on the surface area affected by different ranges of reductions. WEM is primarily focused on the main roads, as can be seen from the maps highlighting the main arteries of Brussels, while the additional impact of WAM is more widely distributed across the region.

For WEM, reductions are mainly concentrated between 5% and 30%, impacting 90% of the surface area compared to BASE. Regarding WAM, the additional reductions are mostly between 1% and 4%, impacting more than 80% of the area. Higher reduction intervals cover a smaller proportion of the surface area, primarily corresponding to highways and tunnels. The locations of all tunnels are detailed in Figure E.3.

In summary, 2028 exhibited the most substantial absolute reduction in NO_2 concentrations for both the LEZ and Good Move initiatives. However, the reduction was significantly greater for WEM (the LEZ), particularly on the main arteries, while the additional reduction from WAM (Good Move) was smaller and more dispersed across Brussels.

Table 17: Distribution of the area occupied by different relative reduction intervals in 2028

Difference between WEM and BASE

Reduction interval [%]	Surface area [%]
0 - 5	0.98
5 - 10	10.95
10 - 15	12.38
15 - 20	23.66
20 - 25	27.00
25 - 30	16.62
30 - 40	7.89
40 - 50	0.51

Difference between WEM and WAM

Reduction interval [%]	Surface area [%]
0 - 0.5	0.00
0.5 - 1	5.67
1 - 2	14.41
2 - 3	29.34
3 - 4	35.43
4 - 5	12.56
5 - 7.5	2.60

5.7 EU 2030 compliance

In this section, compliance with the EU 2030 NO_2 concentration thresholds is evaluated for each scenario in 2030, covering annual, daily, and hourly thresholds (Section 5.7.1). To illustrate where exceedances occur, maps of NO_2 concentrations for each scenario in 2030 are presented (Section 5.7.2). The evolution of these exceedances from 2022 to 2035 by scenario is analyzed in Section 5.7.3, examining patterns across different road hierarchies and providing a detailed follow-up in Section 5.7.4. Analyzing the exceedances for the 2030 threshold in years prior to its enforcement is insightful. This approach allows to consider the possibility that the model might be overly optimistic (or pessimistic), projecting overly significant reductions in concentrations. Consequently, the actual conditions in 2030 might more closely resemble the modeled scenarios for earlier years (or later years), rather than the overly optimistic (or pessimistic) projections for 2030 itself. It is important to note that to take account of meteorological variability, the length exceeding 19.5 µg/m³ was considered to exceed the threshold as explained in Section 4.7.

5.7.1 Compliance of EU annual, daily and hourly thresholds in 2030

The Table 18 shows the proportion of street length projected to exceed the EU annual threshold in 2030, broken down by road hierarchy and scenario. In 2030, 13.3% of the street length exceeds the threshold in the BASE scenario, which decreases to 1.74% with WEM and further to 0.74% with WAM. While A0 and A2 have a higher proportion of streets exceeding the threshold in the BASE scenario, A2 and A3 dominate in the WEM and WAM scenarios. The 2022 exceedance of the current threshold of 40 µg/m³ (based on real data) is comparable to the projected overall compliance with a 20 µg/m³ threshold in the WAM scenario for 2030. The exceedance in 2022 is greater than the projected exceedance for 2030 under both WEM and WAM scenarios for A0 and A1 roads, but lower for the other hierarchies.

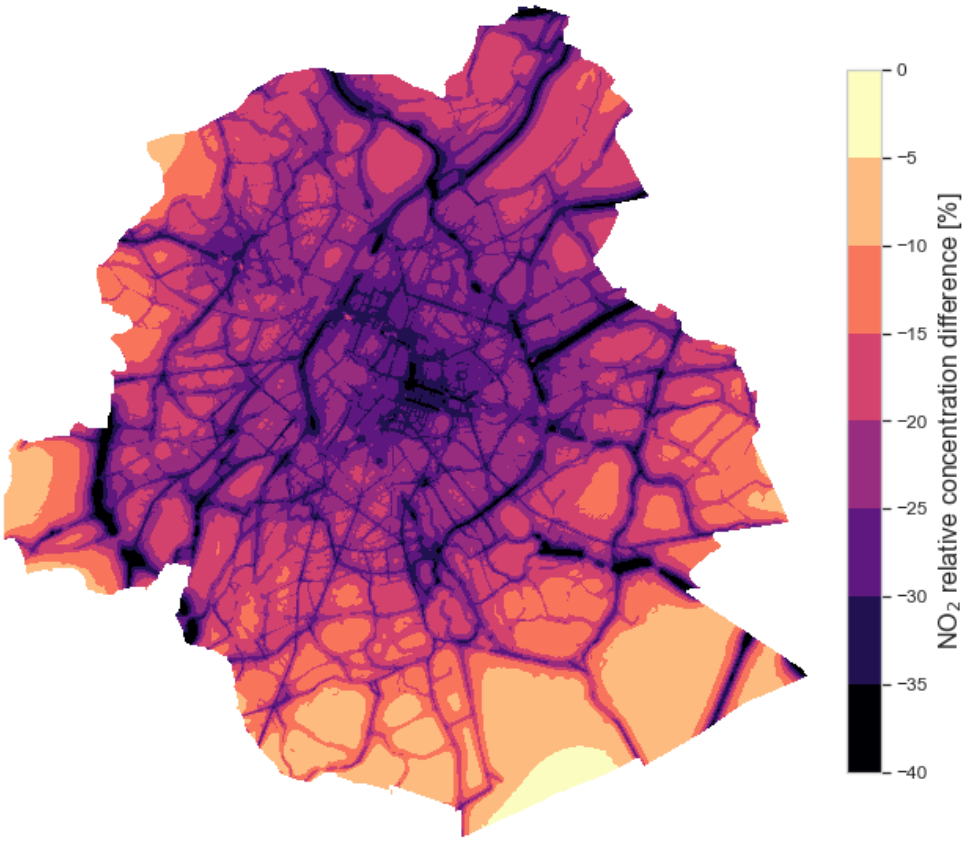

Figure 30: Percentage relative difference in NO_2 concentration between WEM and BASE scenarios for the year 2028

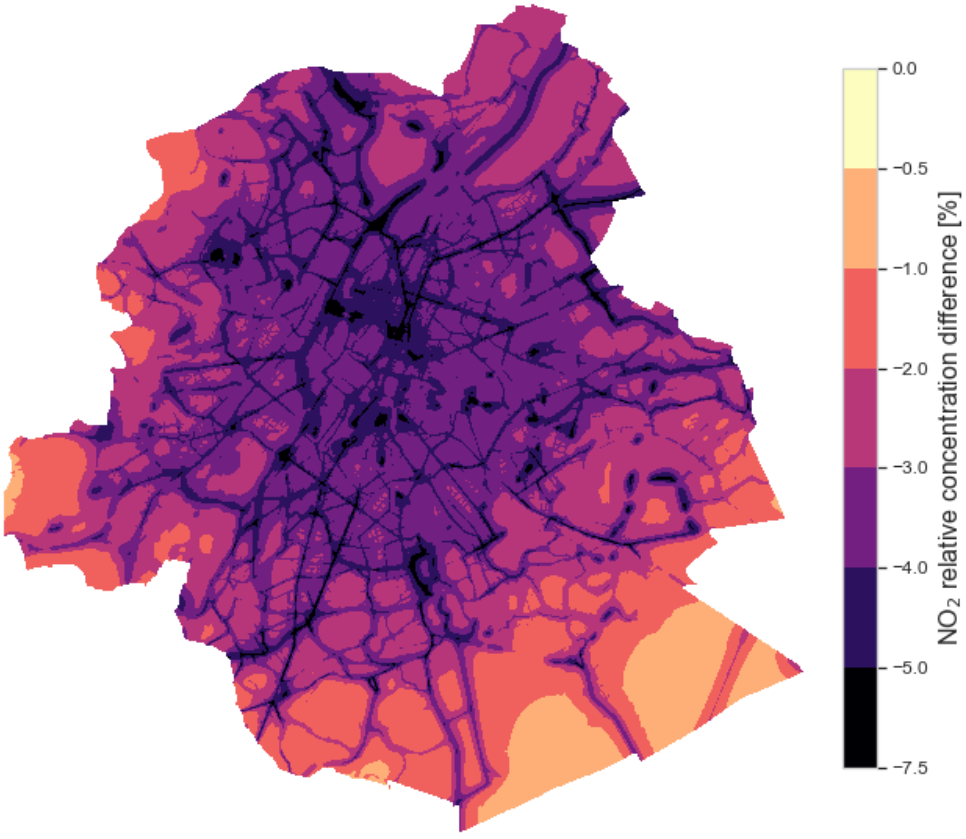

Figure 31: Relative additional impact of WAM compared with WEM using the BASE scenario as a reference for the year 2028

Table 18: Portion of street length and corresponding distances exceeding the EU annual threshold of 20 µg/m³ for BASE, WEM, WAM by road hierarchy in 2030, and 40 µg/m³ in 2022.

Portion of street length exceeding 20 µg/m³ [%]	A0	A1	A2	A3	A4	A5	Total	Distance [km]
BASE	45.2	11.7	41.3	31.3	24.6	3.2	13.3	403
WEM	0.08	0.11	6.15	8.11	1.73	0.06	1.71	52
WAM	0.08	0.00	2.44	3.73	0.57	0.03	0.74	23

Portion of street length exceeding 40 µg/m³ [%]	A0	A1	A2	A3	A4	A5	Total	Distance [km]
2022 real data	2.10	0.69	2.25	3.38	0.46	0.02	0.93	28

Analysis can also be conducted regarding the hourly and daily limits; however, no spatialized data are provided by SIRANE for these limits, only data from the 12 station measurement locations. The hourly limit value of 200 µg/m³ set by WHO and the EU for 2030[12] was respected at all stations in 2022 and is projected to be respected for all three scenarios through 2035. Regarding average daily limits, the EU will set a concentration of 50 µg/m³ in 2030[13], and the WHO sets 25 µg/m³[14]. Figure 32 shows the trend in the number of exceedance days for these values at the monitoring stations.

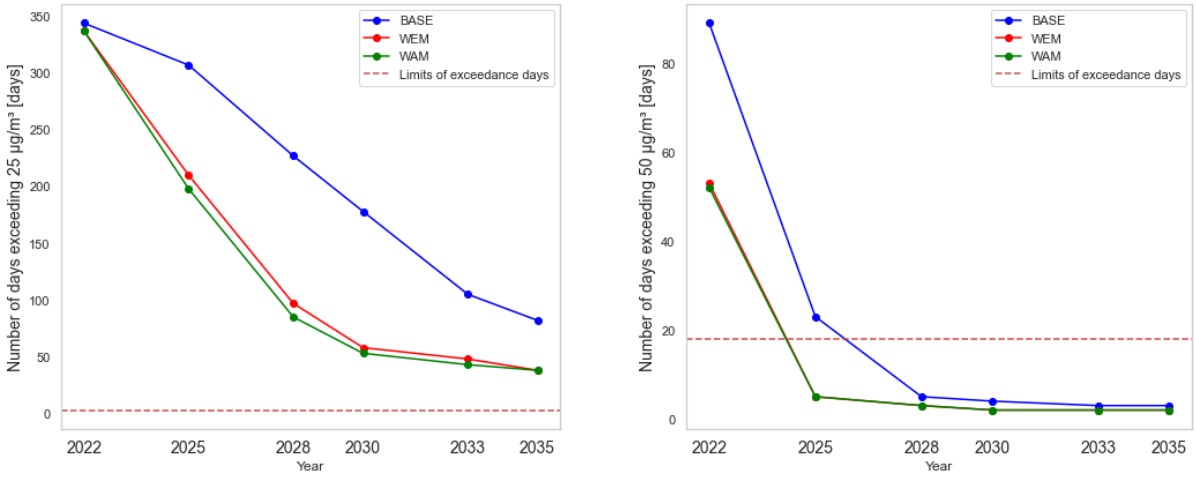

Figure 32: Evolution of the number of exceedance days for WHO and 2030 EU limits for the different scenarios over the years. a) WHO regulations B) EU regulations

For the EU limit, all three scenarios comply, with the BASE scenario showing 4 exceedances compared to 2 exceedances for both WEM and WAM. Notably, by 2025, both WEM and WAM already comply with EU regulations.

[12] with a maximum of 3 exceedances/year for the EU by 2030
[13] with a maximum of 18 exceedances/year for the EU by 2030
[14] with a maximum of 4 exceedances/year

Regarding WHO regulations, none of the scenarios meet the limit in 2030 despite a significant reduction in exceedance days. The BASE scenario shows 178 exceedance days, while WEM and WAM have 58 and 53 days, respectively, far from the four exceedances permitted.

5.7.2 Map assessment of NO_2 trends in 2030

Figure 33 illustrates the NO_2 concentration landscape in Brussels for the three projections. The concentration intervals are consistent across the maps to facilitate comparison. Visually, the WEM and WAM scenarios show similar distributions with a comparable reduction in NO_2 levels, while the BASE scenario maintains higher concentrations, still highlighting major roadways such as the pentagon.

This observation is corroborated by Table 19, which presents the percentages of areas occupied by NO_2 concentration intervals. The trend in the WEM and WAM scenarios indicates that more than 90-95% of the area would have concentrations below 16 µg/m³, with less than 1% exceeding 20 µg/m³. In contrast, the BASE scenario shows less favorable outcomes, with only 69% of the area below 16 µg/m³ and more than 3.42% exceeding the regulatory limit of 20 µg/m³. Overall, the same conclusions can be drawn as in the previous sections, with a greater adherence to the EU thresholds for 2030 observed in the WEM scenario, and an even higher compliance noted in the WAM scenario. The percentage exceeding 20 µg/m³ is lower than that shown in Section 5.7.1, Table 18, because this analysis considers the entire map of the region, including open spaces. In contrast, the percentage in Section 5.7.1 represents the percentage among streets.

Table 19: Surface representation for the 3 scenarios for each of the concentration ranges used in Figure 33. The term "Max" represents the maximum value of the maps.

	Surface area [%]		
Concentration range [µg/m³]	BASE	WEM	WAM
13 - 14	13.59	31.69	37.78
14 - 16	55.03	62.68	58.19
16 - 18	22.77	4.18	3.05
18 - 20	5.19	0.99	0.7
Max - 20	3.42	0.46	0.28

Additionally, it is noteworthy that the highest values are primarily due to tunnels, which form a cone of high concentration values, particularly visible on the WEM and WAM maps.

For additional information, the spatial evolutions of concentration maps for the three scenarios during key LEZ years (2022, 2025, 2028, 2030, 2035) aree available in Figures P.2, P.3, and P.4 for BASE, WEM and WAM respectively.

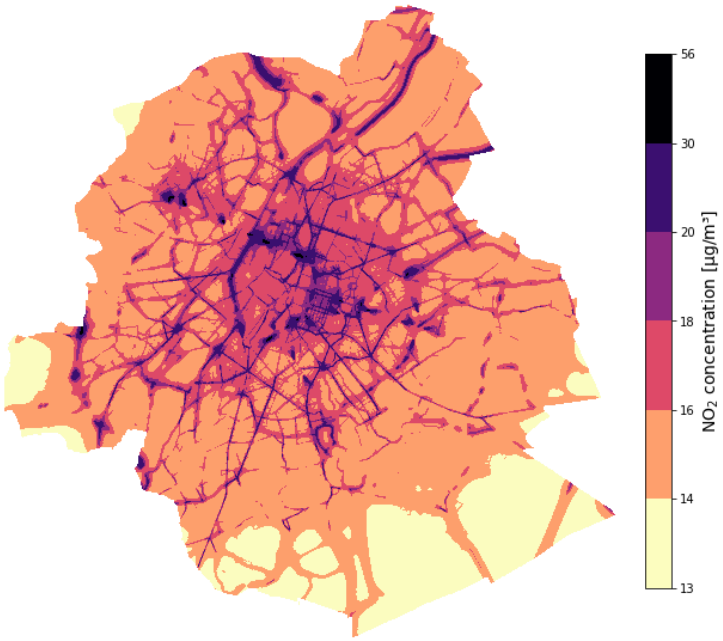

(a) 2030 BASE

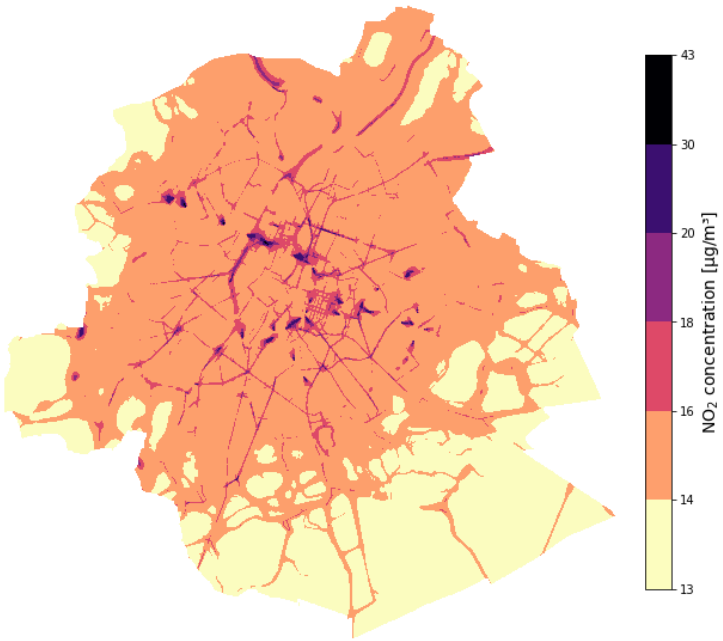

(b) 2030 WEM

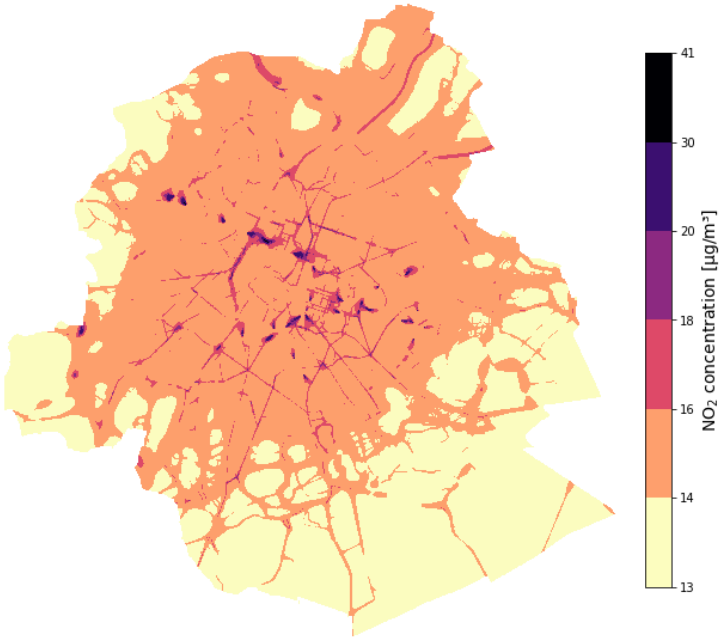

(c) 2030 WAM

Figure 33: Average annual NO_2 concentration for the different scenarios for the year 2030

5.7.3 Overall trends and comparisons between scenarios

Figure 34 shows the total street length (km) and the percentage of the total street length in Brussels that exceeds the EU 2030 threshold of 20 µg/m³ annually from 2022 to 2035. This graph is broken down by scenario and by road hierarchy. Note that the time steps are irregular, as the data come from the specific years when the simulations were conducted. Out of 3029 km of roads, in 2022, the percentages of roads exceeding the threshold are 48.4% for BASE, 43.7% for WEM, and 42.8% for WAM. The simulation with the inventory data from 2022, calibrated, indicates that 43.4% of roads exceed the future standard of 20 µg/m³, which is closer to what the WEM scenario predicted. All scenarios consistently decrease the length of roads exceeding the threshold over the years, reaching 13.3% (403 km), 1.71% (52 km), and 0.74% (22.5 km) by 2030 for BASE, WEM and WAM

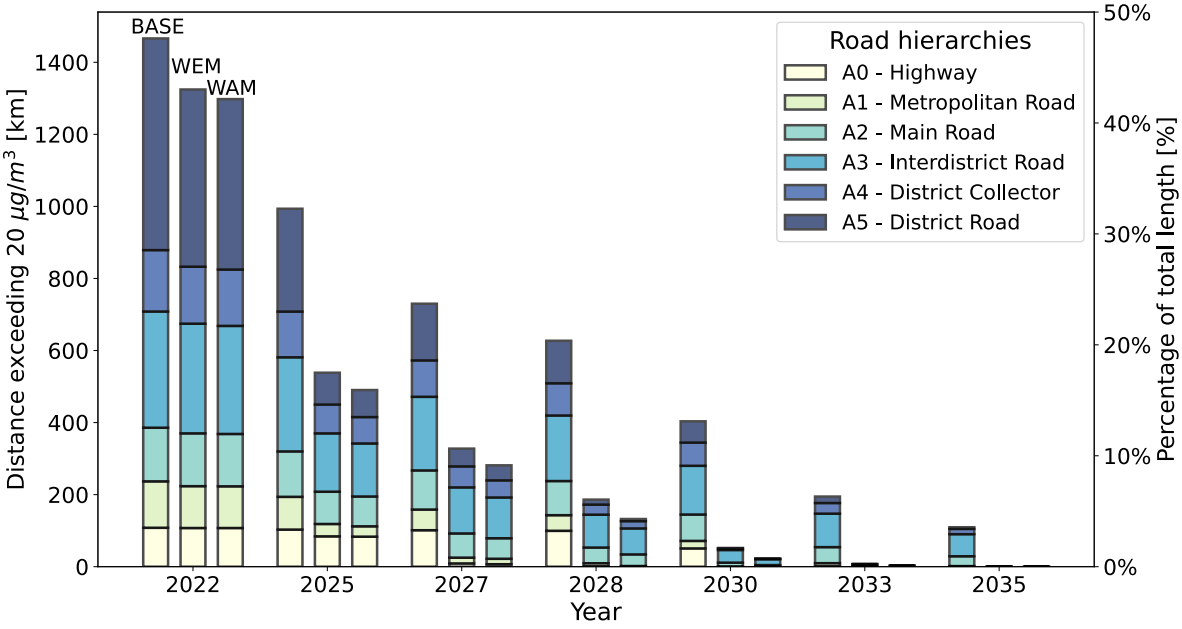

Figure 34: Street length distance and percentage of total distance exceeding the future EU threshold of 20 µg/m³ (effective from 2030), for the years simulated in SIRANE. For each year, the left bar represents the BASE scenario, the middle bar represents the WEM scenario, and the right bar represents the WAM scenario. Each bar is further broken down by the contributions of different road hierarchies.

Overall, WEM decreases much faster than BASE between 2022 and 2025 (9% per year compared to 5% per year), and then decreases less rapidly, as it has already quickly achieved low levels of exceedance. When considering the total percent of street length that exceeds the threshold in BASE and comparing it to the levels reached by WEM, the number of years by which BASE lags behind WEM increases over time. Initially, BASE is one year behind WEM. By 2030, the 13% exceedance level reached by BASE is four years behind WEM, which is expected to achieve in 2026. By 2035, BASE is six years behind, as the 4% exceedance level was attained by WEM in 2029. Therefore, the levels achieved by WEM starting in 2030 are not reached by BASE within this period. Concerning WAM, it decreases approximately at the same rate as WEM but has fewer exceedances mostly because it started with fewer exceedances in 2022. From 2026 to 2029, WAM has the greatest impact compared to WEM regarding the length of exceedance. During that period, the difference in exceedance length

between WEM and WAM is 47 km, which is 1.6% of the total street length.

5.7.4 Breakdown per road hierarchy

In 2022, the total road kilometers exceeding the threshold are primarily from A5 (37% for both WEM and WAM), followed by A3 (23% for both WEM and WAM), with the other hierarchies each representing about 10% of the total, as shown in Figure 34. Initially, A5 and A3 have the greatest share of kilometers exceeding the threshold. However, over the years, the relative proportion of A3 exceeding the threshold increases significantly, while the relative proportion of A2 also increases, but to a lesser extent. However, when analyzing the percentage of total kilometers within each road hierarchy that exceed the threshold in 2022, as illustrated in Figure 35, it can be observed that 26% of A5 kilometers exceed the threshold. This is considerably lower compared to other hierarchies, where the percentage is above 60%, reaching up to 96% for A0, as shown in Figure 35. This difference can be explained by the fact that A5 comprises the largest share of total road kilometers at 62%, followed by A3 at 14%, with A0, A1, A2, and A4 each contributing between 4% and 9%.

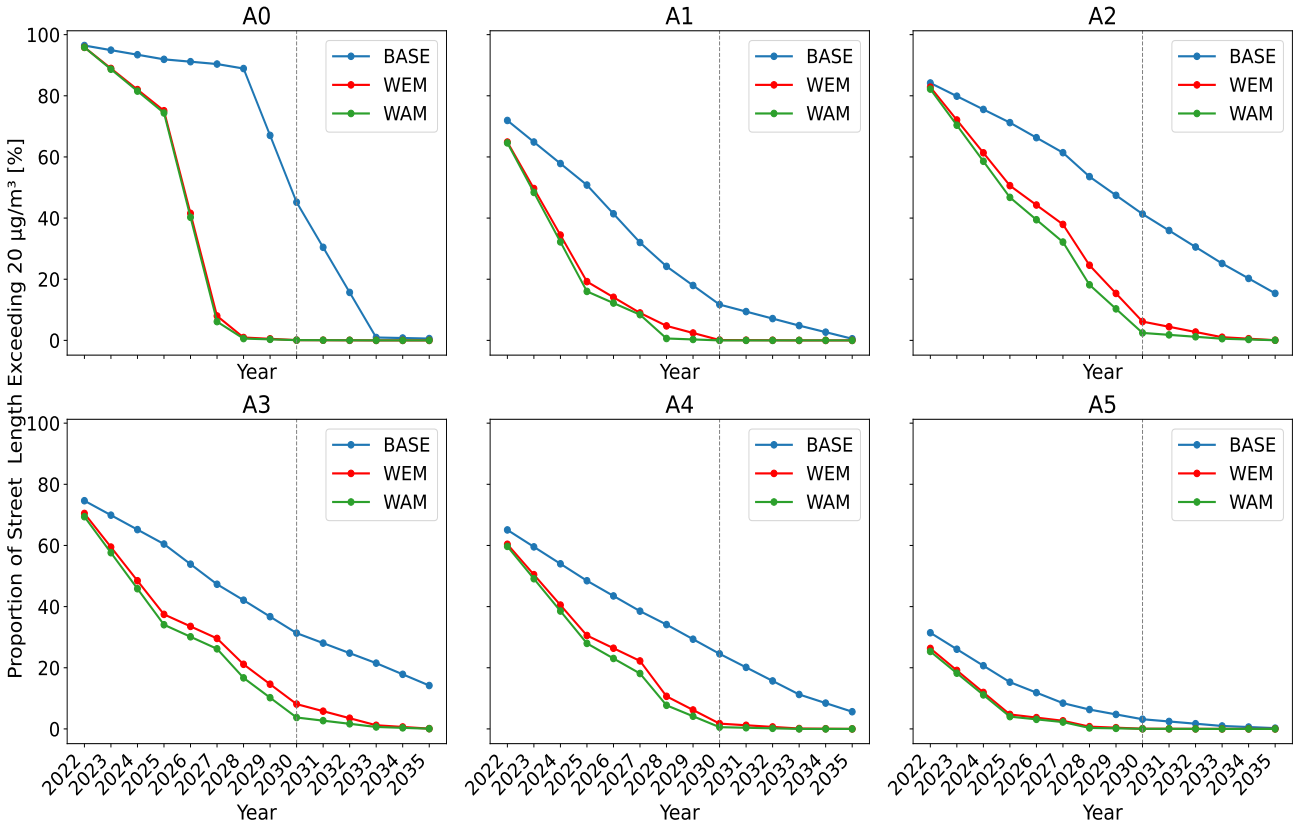

Figure 35: Proportion of street length exceeding the future EU threshold of 20 µg/m³ within each road hierarchy. The vertical line marks 2030, the year when the threshold will take effect.

For WEM and WAM, all hierarchies except A0 experience the greatest decrease between 2022 and 2025. A2, A3, and A4 also show significant decreases between 2028 and 2030. A0 has the most substantial decrease, with 67% of its roads transitioning from exceeding to not exceeding between 2025 and 2027. Between 2022 and 2025, A1 shows the greatest difference compared to BASE, with 32% of its kilometers exceeding in BASE but not in WEM. Overall, A0 shows the most significant difference between BASE and WEM, particularly between 2026 and 2030, with 40% to 88% of its kilometers exceeding in BASE but not in WEM by 2028. The gradient of the annual difference in percentage excess kilometres between BASE and WEM is the same as the gradient of the absolute difference: A0 > A2 > A3 > A1 > A4 > A5. A significantly low level of exceedance (<5%) within their road hierarchy is achieved the quickest by A5 (2025), followed by A0 (2027), A1 (2028), A4 (2029), and A2 and A3 (2030) for WEM.

Concerning WAM, the reductions in exceedances are greatest for A2, with an average between 2022 and 2035 showing that 3% of the kilometers belonging to A2 that exceed in WEM do not exceed in WAM. The gradient of reduction compared to WEM is A2 > A3 > A4 > A1 > A5/A0, with A5 and A0 both at 0.4%.

In summary, the adherence to the future EU annual NO_2 threshold of 20 µg/m³ in 2030 is generally observed in the WEM scenario, with only 1.74% exceedance, and even better in the WAM scenario, which shows a 0.74% exceedance. In contrast, the BASE scenario presents a less favorable outcome, with a 13.3% exceedance. However, none of the scenarios can meet the annual WHO limit in 2030, as the background concentration—unchanged from 2022—already exceeds this threshold. Exceedances in 2030 are predominantly observed on A3 roads across all scenarios. Analyzing the percentage of kilometers exceeded within each road hierarchy, A3 roads show the highest exceedances for both the WEM and WAM scenarios. For the BASE scenario, A0 records the greatest exceedance. A2 roads rank second in terms of exceedances for all scenarios. For average daily limits, all scenarios comply with the EU's 2030 threshold before 2030, but none meets the WHO daily limit in that year. The hourly limit value set by both WHO and the EU for 2030 is respected at all monitoring stations in 2022 and is projected to be maintained through 2035 under all three scenarios.

6 Discussion

6.1 Impact of road refining

In Section 5.1, the shift in NOx emission attribution from COPERT to MuSti significantly impacted NO_2 concentrations across different road hierarchies. Highways (A0) and rural roads (A1) saw decreases in NO_2 concentrations of 50% and 20%, respectively, while urban roads (A2 to A5) experienced a 23% increase. This change reflects the road refinement process's aim to accurately assign real emission factors to corresponding road types, indicating lower emission factors for A0 and A1 and higher ones for urban roads.

Figure 36 illustrates that NOx emissions increase at low speeds, typical of urban driving, and at high speeds, common on highways. This explains the higher emission factors assigned to the A2-A5 urban roads, which operate at 30 km/h. Additionally, the 'Cold Start' mode, which leads to higher emissions due to cooler engine temperatures, was exclusively assigned to A2-A5 roads by COPERT, under the assumption that vehicles on A0 and A1 roads maintain optimal temperatures. The emission factors for A1 roads, typically set at speeds of 50-70 km/h, can also be explained by the speed-dependent emissions factor using Figure 36. However, contrary to theoretical expectations of higher emissions on highways (A0), COPERT data shows unexpectedly lower emission factors for A0 compared to A1 for most vehicle types, a discrepancy that remains unexplained. Figure 36 also shows that the emission factor for Euro 6 vehicles remains more constant across different vehicle speeds. This suggests that as the share of Euro 6 vehicles increases in the fleet, the variability in emission factors between road hierarchies could decrease, if COPERT accounts for it.

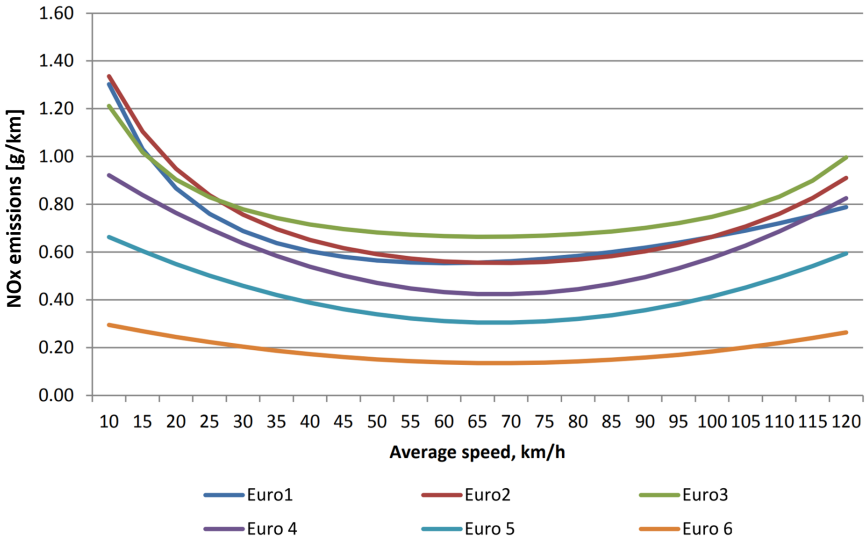

Figure 36: Evolution of the NOx emission factor as a function of speed for different Euro standards. Source : [14]

6.2 Impact of calibration

In the calibration process described in Section 4.5.1, it was determined that 2022 NO emissions from traffic and tunnels need to be adjusted by a factor of 0.75 to align with data from measurement sta-

tions, while NO_2 calibration coefficient remains unchanged. This contrasts with the previous 2018 calibration by Axel Briffault, following the same methodology, where NO and NO_2 emissions required coefficients of 2.6 and 1.4, respectively, to substantially increase the modeled NOx emissions. Therefore, while the 2018 calibration significantly elevated the emissions estimates, the 2022 adjustments moderately reduce them. Several hypotheses could explain this change, all of which are not mutually exclusive, with three main ones being considered:

- Hypothesis 1: Between 2018 and 2022, the version of COPERT used underwent significant updates, correcting bugs and emission factors, to improve its known underestimation [109] [110] (explained in Section 3.1.1), which therefore likely had a smaller impact in 2022, or it may have even led to an overestimation of emissions.
- Hypothesis 2: The calibration coefficient of 0.75, being close to 1, could simply be an adjustment to address model inaccuracies which don't perfectly reflect 2022 conditions, notably within MuSti and COPERT, rather than revealing any significant new trends or discrepancies.
- Hypothesis 3: In 2018, no road refinement was performed prior to calibration, unlike in 2022. Without road refinement, A0 and A1 roads received more NOx emissions, and A2 to A5 roads received less NOx emissions than estimated by COPERT. The model required a high adjustment coefficient due to more A2-A5 stations (8) underestimating due to no road refinement and fewer A1 stations (3) in 2018. This hypothesis only explains why the 2018 coefficient is high and therefore different from the 2022 coefficient, but it does not directly explain the 2022 coefficient.

6.2.1 Qualitative analysis

As noted in Section 5.2.1, the modeled NO_2 concentrations are closer to the measured NO_2 concentrations in areas and times of low traffic, whereas they deviate more in high-traffic areas. This could be because traffic emissions introduce greater uncertainty compared to background concentrations, particularly due to MuSti and COPERT. The validation study in Lyon discussed in Section 4.2.2 noted the same observation, with a tendency of underestimation of the model however, and made the same hypothesis about COPERT uncertainty [88]. This is likely the case for the Ixelles station, which is located in a "perfect" street canyon. This type of environment has been shown to be well modeled by SIRANE [95]. Therefore, the suspected reason for its overestimation compared to the measurements would likely be an error in quantifying emissions by MuSti and COPERT. As mentioned earlier, perhaps COPERT's corrections to address previous underestimations were overdone.

Moreover, additional different specific types of discrepancies between modeled and measured concentrations, discussed in Section 5.2.1 and showed in Figure 25, were observed for the high-traffic stations Regent, Ganshoren, Arts-Loi and Belliard, as well as the Uccle background concentration station. The hypotheses to explain these variations could go beyond the uncertainties of traffic emissions attributed to COPERT and MuSti.

The two new stations implemented in 2022, Regent and Ganshoren, show a significant underestimation by the model compared to the measured concentrations, contrary to other high-traffic stations.

The primary suspected reason is the incorrect initial positioning of the coordinates of the two stations in the SIRANE street network. The station locations, as initially set up in Axel Briffault's preparatory work, were inadvertently positioned in the model, a few meters away from the sidewalks where the monitoring stations are located. This placement put them in the middle of buildings, causing the SIRANE model to calculate concentrations as if the stations were on rooftops. This led to a significant underestimation of concentrations compared to their true positions on the sidewalks.

For the Arts-Loi station, there is an underestimation of the model for low concentrations, likely due to its complex position in terms of pollutant dispersion. The receiver is situated between the inner ring road (a wide street) and Rue de la Loi (a street canyon). Additionally, a very large building near the intersection affects air flow. All these conditions suggest that the station is an area with complex air flow, which is problematic as SIRANE has been shown to model these spaces less accurately [95] as discussed in Section 4.2.2.

For the Belliard station, the minimum concentrations modeled are similar to the measurement curve, but the daytime peaks are significantly higher. This is also likely due to the complex location of the monitoring station. It is positioned in a canyon street that opens into an open area a hundred meters further southeast, with a forest to the south and a shopping center featuring its own tunnels and complex geometry. Considering all these effects, this station can also be considered as being in a semi-open space, similar to the Arts-Loi station as discussed in Section 4.2.2.

Lastly, the model tends to overestimate concentrations at Uccle station. The main reason would be that the background concentration used for the region was calculated at the same location, leading to an overestimation because SIRANE accounts for both the concentration due to local emissions and the background concentration.

6.2.2 Quantitative analysis

Considering the explanation in the previous Section 6.2.1 regarding the two high-traffic stations Ganshoren and Regent, the decision was made to exclude them from further analysis. As a result of excluding these two stations, out of the exceedances of the Hanna and Chang statistical acceptance criteria and MQI from Section 5.2.2, only four exceedances remain across the ten exceedances obtained in Table 14. Furthermore, regarding the EU FAIRMODE criteria, none of the 10 MQIh and 10 MQIy values exceed one. The model is therefore consider ed acceptable for both statistical criteria.

For statistical evaluation, FB and NAD are interesting indicators because they are complementary. While FB accounts for systematic biases indicating the tendency of overestimation or underestimation, NAD addresses random biases that occur due to unpredictable factors in measurement and modeling processes.

For the Ixelles and Berchem-Ste-Agathe stations, the NAD does not meet the rural criteria (NAD > 0.3), indicating that predictions vary significantly from actual values at certain times, despite these errors balancing out over the long term—as reflected by their FB being close to 0, which shows no strong systematic bias. On the other hand, the Uccle station exhibits a systematic bias with a tendency to overestimate, as indicated by $|FB| < 0.3$, and a significant random bias (NAD > 0.3), likely due

to the impact of very low values and minimal changes. However, these stations' statistical indicators still conform to the urban criteria and could be considered close to other stations' results, which could explain why these differences are not apparent in various graphs.

6.3 Comparison between scenarios and real data in 2022

As discussed in Section 5.3, the three scenarios for 2022 show similarities with the simulation based on inventory data. This suggests that the emission projections remain relevant up to 2022. Secondly, the BASE scenario shows higher NO_2 concentrations than the simulation with inventory data. This latter simulation is positioned between the WEM and WAM scenarios, with a closer alignment to the WAM scenario. This observation could indicate that traffic policy measures, notably the LEZ bans on Euro 0 to Euro 4 diesel vehicles and Euro 0 to Euro 1 petrol vehicles up to 2022, and the Good Move's goals, may have achieved their projected impact.

If the WEM and WAM 2022 scenarios align well with the majority of the simulation using inventory data, a small portion of the roads, namely all the A0 and A1 roads, do not. On highways (A0) and rural roads (A1), both WEM and WAM scenarios project lower concentrations than those observed in the inventory data simulation. In contrast, the BASE scenario tends to more closely reflect reality on those roads, despite still reporting higher average concentrations than the actual data. This could be due to the projections in NOx emissions. Table 20 presents the difference in NOx emissions between the scenarios and the 2022 inventory. The WEM and WAM scenarios predict similar emissions as assessed in the inventory data for urban roads (A2-A5), but have lower emissions for highways (A0) and rural (A1) roads. This suggests that the impacts of the LEZ on these specific roads were overestimated, and an adjustment of the projections emissions may be necessary in the future.

Table 20: Percentage difference in NOx emissions between the 2022 inventory and the BASE, WEM, WAM scenarios for highway (A0), rural (A1) and urban (A2-A5) roads

	BASE [%]	WEM [%]	WAM [%]
Highway	0.15	-11.22	-11.66
Rural	0.16	-12.60	-13.01
Urban	11.75	2.20	0.25

Although the three scenarios closely match the simulation with inventory emissions from 2022, this correspondence does not guarantee their continued accuracy in the coming years. As projections extend into the future, the scenarios could diverge further due to the uncertainty accumulating over the years.

6.4 Overall NO_2 concentration decrease due to change in fleet composition (particularly diesel)

Overall, all three scenarios show a consistent decrease in the average NO_2 concentration in Brussels, decreasing between 4.9 µg/m³ to 5.6 µg/m³ between 2022 to 2035, with the rate of decrease slowing over the years, as showed in Figure 28.

In the BASE and WEM scenarios, the veh-km for each vehicle category remain almost unchanged (see Table 11), although the decrease in concentration is consistent. Therefore, the reduction in concentration is primarily due to changes in the fleet composition, either through the replacement of vehicles with electric cars, which do not emit NOx, and/or by upgrading to the latest Euro standards: Euro 6d for light vehicles and Euro VI D/E for heavy trucks and buses.

The decrease in NO_2 concentration is greatly impacted by the renewal of diesel vehicles. As seen in Figures L.6 and L.5, in 2022, diesel vehicles were responsible for about 90% of NO and almost 100% of NO_2 emissions, making diesel engines the greatest lever for action. While the Euro 6d standard does not change for gasoline engines compared to Euro 5 (except for new testing procedures discussed in Section 3.1.1), it significantly reduces emissions for diesel light vehicles (by more than half) and diesel heavy trucks and buses (by a factor of five) [111]. Additionally, only 7% of diesel engines met the latest Euro 6d/Euro VI D/E standards in 2022.

Thus, not only are diesel vehicles the largest source of NOx emissions, but a large portion of these vehicles have not yet been upgraded, presenting a significant potential for emissions reduction. Upgrading these vehicles will have a major impact on reducing NOx emissions. As the vehicle fleet becomes less polluting, achieving further reductions becomes progressively harder, explaining why the rate of decrease slows over time.

6.5 LEZ: the key years with the most impact on NO_2 concentration

Significant decreases of NO_2 concentration occur abruptly in the WEM scenario due to LEZ bans in 2025, 2028, 2030, and 2035, as shown in Figure 28.

However, as seen in Section 5.4.2, the years in which Brussels sees the biggest absolute difference in NO_2 concentration between the LEZ (WEM) and the BASE scenario do not necessarily align precisely with these ban periods. The years with the most significant absolute difference in NO_2 concentration between the BASE and WEM scenarios are each year between 2025 and 2030, including the years with no LEZ bans. This highlights the impact of LEZ ban years (2025, 2028, 2030) on NO_2 concentrations in years without bans (2026, 2027, 2029).

As the effect of the LEZ is to speed up the renewal of the vehicle fleet, WEM initially decreases NO_2 emissions rapidly. Consequently, there are the greatest differences between 2025 and 2030. After this fast decrease, it becomes harder to achieve further reductions compared to the BASE scenario, which still has more potential for reduction. Therefore, it is highly unlikely that the effect of the LEZ on NO_2 pollution will last forever, as the BASE scenario catches up at a later stage, negating the benefits of the LEZ. From this it can be concluded that delaying the implementation of the same LEZ restriction would result in a diminished positive impact. However, stricter and further restrictions could still be put in place to try reducing the last $\mu g/m^3$ of NO_2 to achieve the WHO target of 10 $\mu g/m^3$, as with ambitious target of very low concentration, even the smaller reduction count since background pollution will change less easily. Decreasing the background concentration also depends on the reduction of NO_2 levels at interregional and international levels, and therefore on the policy measures implemented at these scales.

Regarding relative reduction, on average, the LEZ removed 24% of the BASE concentration between 2022 and 2035, excluding background concentration. To identify the key years of policy effectiveness of the LEZ, the relative difference in NO_2 concentrations for each year from 2022 to 2035 was compared to the previous year. The years with the highest impact were 2025 > 2035 > 2028 > 2030, marking all years of LEZ bans. In 2025, the LEZ reduced an additional 13.5% of the BASE NO_2 concentration compared to 2024. The substantial decrease between 2022 and 2025 seems to be largely attributed to the ban of Euro 5/V diesel passenger cars, light commercial vehicles, and buses, where the portion of emissions is shown in Figures 7 for the year 2020 and in Figures L.3, L.4 for the projections up to 2040. Again, this mark the profound difference in emissions between Euro 5 and Euro 6 diesel vehicles. Finally, Table 21 shows the absolute and relative differences of NO_2 concentration compared to the previous year during the LEZ ban years, as well as the top three vehicle categories that reduced NOx emissions the most during these years.

In summary, while the most noticeable impact on NO_2 concentration compared to BASE is seen between 2025 and 2030, the LEZ achieved the greatest reductions in NO_2 concentration during each ban period, particularly in 2025 (13.52% reduction) with the ban on Euro 5/V diesel passenger cars, light commercial vehicles, and buses.

Table 21: Impact of LEZ bans on NO_2 concentration and vehicle categories reducing the most NOx emissions between the previous year and these years, written in descending order. PC stands for passenger cars, LCV for light commercial vehicles.

Year	NO_2 [µg/m³]	NO_2 [%]	Vehicle category banned
2025	1.57	13.52	Diesel Euro 5/V: PC, Buses, LCV
2028	1.58	7.22	Diesel Euro 6 a/b/c: PC, LCV; Diesel Euro 6d: PC
2030	1.52	5.23	Diesel Euro 6d: PC, LCV; Petrol Euro 6 a/b/c: PC
2035	1.28	10.44	Petrol Euro 6d: PC, LCV; Diesel Euro VI A/B/C: Buses

Comparison of estimated LEZ impacts with London and Paris

The results found on the impact of LEZ can be compared with studies conducted in London [61] (ex-post) and Paris [112](ex-ante), explained in Section 3.1.2. The London study is one of the few LEZ studies banning up to Euro 5, while Paris is a projection study of NO_2 concentrations, using a similar methodology as this master's thesis. London's LEZ from the study is similar to Brussels' 2025 WEM scenario. Three years post-implementation, London observed a 44% decrease in NO_2 levels (35 µg/m³), a stark contrast to the 9% reduction (1.6 µg/m³) forecasted for Brussels, including background concentration. Paris' LEZ, similar to Brussels' 2022 WEM scenario, anticipated a 12-17% drop (5-7 µg/m³), also significantly exceeding the overall reduction of 3% or 0.6 µg/m³ forecast for Brussels, also including background concentration. Factors contributing to the estimated lower impact of the LEZ in Brussels than in London and Paris include the following:

- **Initial NO_2 levels:** London and Paris had initial NO_2 levels 4.5 and 2-3 times higher than Brussels, respectively.
- **Timing of bans:** London and Paris implemented bans 6 and 2 years earlier, respectively.

- **Size of traffic-dense LEZs:** London's and Paris' LEZs areas are smaller—six times and two times, respectively, than Brussels, focusing efforts in densely trafficked areas, while Brussels covers high and low traffic areas.
- **Background concentration measurements and models:** While London directly measures background concentration evolution and Paris models it, this master's thesis assumes a constant background concentration for Brussels. However, it is very likely that the background concentration will decrease over time due to reductions in NOx emissions from other regions, other sectors, and the impact of reductions in NOx emissions from traffic on the background concentration. As discussed in Section 4.2.3, background concentration plays a critical role in determining overall NO_2 concentration. Excluding background concentration, Brussels shows significant reductions due to the LEZ, with a 24% reduction in 2025 (the year matching London LEZ bans) and a 7% reduction in 2022 (the year matching Paris LEZ bans).
- **Methodological variations in BASE scenarios:** London's method may overestimate BASE scenario concentrations, exaggerating LEZ effectiveness; methodological differences also vary results.

In Brussels, the impact of the LEZ on driving behavior has not been accounted for, which could potentially lead to an underestimation of its overall effectiveness on NO_2 concentration. Indeed, some individuals might prefer to change their mode of transport rather than purchase a new vehicle when their current one is banned due to LEZ regulations. A study conducted in Paris [113] suggests that approximately 1.4% of total trips might transition from vehicle use to alternative modes of transport due to the LEZ, a phenomenon particularly notable in large-scale LEZs. Parisian projections account for this behavioral shift, and in London, such changes are directly measured. Moreover, LEZs can influence the areas around their boundaries both positively and negatively. For example, in the short term, some drivers might change their itinerary to avoid entering the LEZ, which could increase the concentration of pollutants on the periphery [113]. However, the London study observed a decrease in NO_2 concentrations at the LEZ boundaries, which they attributed to reductions in traffic, changes in fleet composition in response to the LEZ, and atmospheric convection of pollutants [61]. In Brussels, the northeastern region could benefit most from the LEZ, as prevailing wind directions tend to carry pollution in that direction.

6.6 LEZ: concentrations by road hierarchy and their evolution

As shown in Section 5.5.1, and in Figure 29, there is a gradient in NO_2 concentrations across the road hierarchy in 2022, ranging from highways (A0) to local roads (A5). The concentration decreases from the BASE scenario, and the additional decrease due to the LEZ follows the same pattern, with the highest reduction on A0 and the lowest on A5. The initial concentrations and subsequent reductions due to changes in fleet composition, either from the BASE or the WEM scenario, are closely linked to traffic density. This density also follows a gradient, being highest on A0 and lowest on A5. Therefore, roads with higher traffic volumes exhibit higher initial NO_2 concentrations, and changes in fleet composition most significantly affect these roads.

A1 roads are an exception to this gradient as they have the second highest traffic density but exhibit the second lowest initial average NO_2 concentration. This could be partially attributed to the emissions density (emissions per road km) on A1 roads being lower than on A2 roads, as illustrated in Figure 37, likely because the emission factor for A1 is significantly lower than that for urban roads (A2-A5), as discussed in Section 6.1. However, A1 roads still have a higher emission density than A3 and A4, while their average concentrations remain lower than those on A3 and A4. This could be explained by the higher proportion of street canyons in urban areas (A2-A5), which trap pollutants and lead to higher concentrations. In contrast, rural roads like A1, which are more open, allow pollutants to disperse more effectively. This effect is detailed in Figure E.2, listing street canyon percentages by road hierarchy. Therefore, factors such as traffic density, emission factors, and the presence of street canyons could all play significant roles in determining NO_2 concentrations.

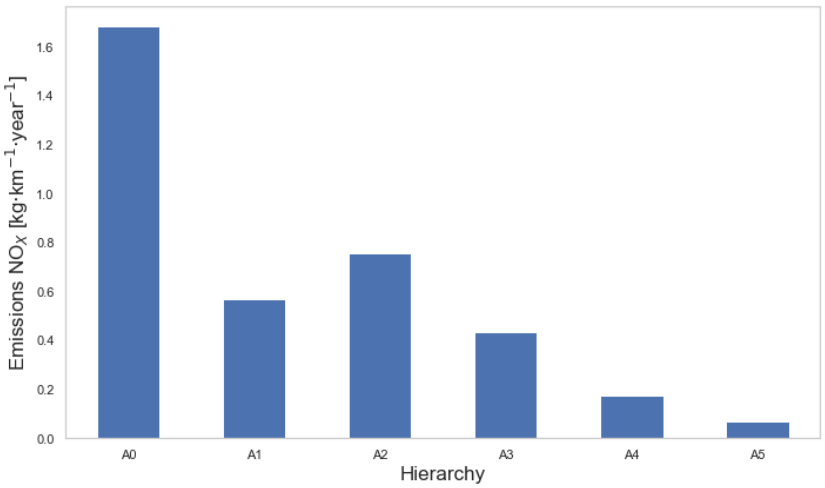

Figure 37: Total NOx emissions per kilometer between road hierarchies in 2022

Moreover, the greatest reductions occur between 2022 and 2028 for the WEM curves, especially. For A0 and A1, with a 71% and 66% relative decrease respectively, compared to an average of 58% for urban roads, along with the discussion above on the gradient in high-traffic density. This could be explained by the ratio between diesel and petrol emissions. Figure 38 presents the evolution of the diesel-to-petrol ratio for both the BASE and WEM scenarios from 2022 to 2035, separating highways, rural roads, and urban roads (A2-A5).

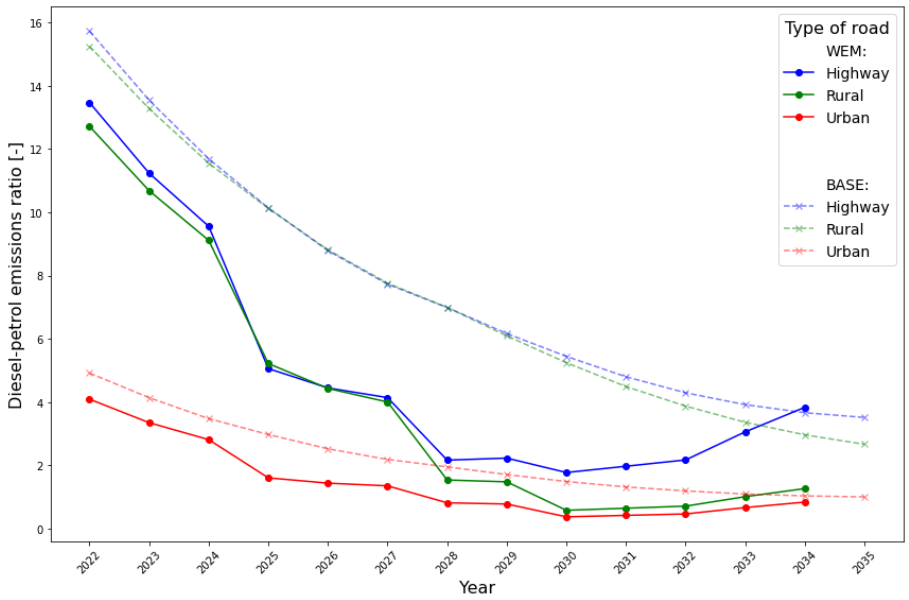

Figure 38: Evolution of the NOx emissions ratio between diesel and petrol for the WEM and BASE scenarios between 2022 and 2035

As discussed in Section 1.6.2, diesel vehicles are the most significant source of NOx emissions and are also reducing their emissions the most, especially in the early years. In both scenarios, the diesel-to-petrol ratio is much higher for highways and rural roads compared to urban roads in 2022. Therefore, the impact of reducing diesel vehicle emissions will be much more effective on highways and rural roads. After 2030, the various WEM ratios increase because diesel emissions from buses and trucks remain almost constant, while petrol emissions continue to decrease until the petrol ban in 2035. With regards to diesel buses and trucks, they will continue to be allowed after 2030, and even in 2036 for some categories, as illustrated in Appendix B. This is illustrated in Figures L.5 and L.6. The greater increase in the diesel/petrol ratio on A0 could be attributed to a higher proportion of diesel vehicles, particularly heavy trucks and buses, compared to other roads. This also explains the relatively smaller decrease in diesel use after 2030 compared to urban roads.

6.7 Good Move impacts - WAM scenario

The results in Section 5.4.3 show that Good Move's impact on NO_2 concentrations is eight times less than that of the LEZ, despite that the Good Move ambition of reducing by 24% the veh-km in passenger car is estimated very optimistic [12]. Nevertheless, this study evaluates only one of several ambitions of Good Move—the reduction of traffic. Various other Good Move ambitions partially explained in 3.1.3 could also contribute to reduce NO_2 concentrations. The most substantial impact of the WAM scenario is observed in 2028. In the initial years, the reduction in veh-km is too minor to make a significant difference, as Good Move was only initiated in 2020. Although this reduction grows over time, in later years the vehicle fleet becomes less polluting, diminishing the effect of reduced veh-km. Thus, 2028 emerges as the year most impacted by Good Move, likely due to a balance between these factors. Additionally, the LEZ policy has a proactive effect; it encourages people to purchase less polluting vehicles ahead of the ban, resulting in an earlier reduction in emissions. Conversely, citizens tend to maintain their usual driving habits until the measures imposed by Good Move forcefully restrict vehicular use. Therefore, the impact of Good Move is diminished as the vehicle

fleet becomes less emissive more rapidly.

Good Move restructuring Plan

As seen in Figure 31, Good Move has the smallest relative impact on A0 and A1 roads, in contrast to the LEZ. This outcome aligns with Good Move strategy to establish Low Traffic Neighborhoods, as detailed in Section 3.1.3. The plan involves redirecting veh-km from local roads to main roads, a shift considered in the NOx emissions calculations using COPERT. While veh-km traveled by passenger cars overall show a decrease between 2020 and 2030 in WAM scenario, the reduction is less pronounced on larger roads compared to local roads. Furthermore, the other vehicle categories experience a reduction in veh-km on local roads but an increase on A0 and A1 roads.

However, Good Move's restructuring ambition introduces a road hierarchy that slightly differs from the one used in this master's thesis [114]. In these projections, emission distribution across street segments still relies on the 2018 MuSti data, which is likely outdated for all scenarios, but particularly for the WAM scenario.

The planned restructuring by Good Move offers benefits but also potential drawbacks. Positively, local roads from A2 to A5, constituting 90% of all streets, experience reduced pollution. This decrease could benefit public health in Brussels for a large part of the bcr population, by lowering average pollution levels; however, the maximum reduction would be only 0.48 µg/m³. On the downside, channeling more traffic onto main roads could increase pollution and risk exceeding EU 2030 thresholds on these roads. These roads already bear heavy traffic; without strict adherence to Good Move's objective to cut overall veh-km, emissions may increase. Additionally, congestion might become more frequent along these axes, reducing speed and raising emission factors—as shown in Figure 36—thus further increasing the likelihood of exceeding EU limits, as explained in Section 4.2.3. Nevertheless, a key advantage of these main roads is their openness, as most are not canyon streets, which allows for quicker pollutant dispersal, as shown in Figure E.2. Furthermore, a study on low-traffic neighborhoods has demonstrated reductions in traffic volume and NO_2 levels, even on these major roads [115]. However, as mentioned in Section 3.1.3, the full implementation of Good Move remains uncertain, due for example to political pressure particularly against Low Traffic Neighborhood zones [116]. Although the plan envisioned the creation of five new Low Traffic Neighborhood each year, aiming for 20 by 2024, there are currently only 18 [70]. Of these, six are fully developed neighborhoods, while two are on hold due to protests from local residents. In addition, only two projects were proposed in 2023 and 2024 respectively, far from the five annual projects planned.

Moreover, Good Move has other ambitions that were not assessed in this master's thesis that could have positive or negative impacts. First, for the LEZ to gain acceptance and compliance from the public, a series of supportive measures are necessary [117]. These include improvements in public transport availability and connectivity between different modes of transport, as well as promoting shared mobility approaches. Such measures are integral components of the Good Move initiative's ambitions. Therefore, if these ambitions are realized effectively, they will support the acceptance of the LEZ. However, the Good Move measure of reducing the default speed limit from 50 km/h to 30 km/h might increase NO_2 concentrations on A2-A5 roads due to higher emission factors, as shown in Figure 36. For instance, a study in Dublin predicted that increased mortality from higher NO_2

levels due to reducing speed limits from 50 km/h to 30 km/h would outweigh the reduction in fatal accidents resulting from this measure [118]. However, a vehicle fleet with fewer pollutants, notably due to LEZ, could lead to reduced mortality from NO_2 pollution while still benefiting from lower accident mortality rates.

6.8 Assessing EU 2030 NO_2 compliance: hourly, daily, and annual limits

One of the objectives of this master's thesis is to determine whether the 2030 EU NO_2 concentration limits per hour, per day, and per year would be met by 2030, and under which scenario. Regarding the annual limit, the LEZ and Good Move policies demonstrate their efficacy, with only 1.71% for WEM and 0.74% for WAM of Brussels street length exceeding the limit, compared to 13.3% for the BASE scenario (see Section 5.7.1). EU regulations theoretically require the norm to be respected everywhere. However, as seen in 2022, 0.93% of street length exceeds the current threshold despite being considered compliant. This will therefore depend on the placement and number of measurement stations in the future and the strict enforcement of the regulation. It is also challenging to assess if the Good Move policy tips the balance between compliance or non-compliance: the WAM scenario is likely considered compliant as fewer streets exceed the limit than in 2022, considered respecting the current threshold, but the WEM scenario, with twice the percentage, remains low but uncertain to be compliant. Regarding the WHO annual threshold, non of the scenarios can meet it in 2030, as the background concentration–unchanged from 2022– already exceeds this threshold.

The EU currently has no daily limit, but the 2030 EU daily limit is not respected in 2022. However, it would be met by 2030 even without policy interventions. Regarding the WHO daily limit, while significant improvements are expected from 2022 to 2035, it will still fall short of the limit, with the LEZ helping to get closer compared to the BASE scenario.

Regarding the hourly limit, Brussels is already compliant with both the EU 2030 threshold and the stricter limit set by WHO and is projected to remain compliant under any scenario. Therefore, it is not a concern at the moment and is unlikely to become one in the future, regardless of policy measures.

In conclusion, by 2030, the LEZ combined with the Good Move plan (WAM), and possibly even the LEZ alone (WEM), will likely meet the annual EU 2030 threshold. Furthermore, the LEZ will approach the WHO daily recommendation, highlighting the significance of these measures. The EU 2030 hourly and daily thresholds will be met even without these policies.

For the annual limit, there might be larger exceedances on A0 and A1 roads, as WEM and WAM underestimated NO_2 concentrations on these roads, and Good Move would transfer traffic to them. Therefore, special attention is needed for these roads.

6.9 Limitations and improvements of the model

The availability of data to project a system as complex as a city's transport system is limited, which likely represents the main source of uncertainty in projecting NO_2 concentrations. These projections rely on assumptions about transport demand and changes in vehicle composition, as explained in Section 4.6.2. These factors significantly impact the results. It would be advisable to conduct periodic

reviews in future years to ensure the projections align with reality. A recent review of the VUB study, which projects fuel shares, suggests that the current assumptions regarding the rate of vehicle fleet electrification are overly optimistic [119]. This affects all three scenarios, potentially resulting in actual exceedances in 2030 that could mirror those modeled in earlier years. Firstly, if the scenarios are actually too optimistic, this suggests that even with the implementation of the WEM and WAM scenarios, Brussels may not achieve compliance with the established norms by 2030, indicating the need for additional reduction measures. Secondly, the significance and impact of the LEZ would be even more pronounced if the scenarios are deemed too optimistic. In such cases, the modeled scenarios for earlier years might align more closely with the actual conditions expected in 2030. As shown in Figure 34, these earlier years notably 2028, are projected to have more substantial impacts compared to than those modeled for 2030.

To reallocate traffic NOx emissions projections both temporally (throughout the year) and spatially (between the streets), traffic count data from 2017 and MuSti data from 2018 were used. These datasets are likely becoming outdated, particularly with the introduction of new mobility plans like the current Good Move Regional Mobility Plan. More recent datasets could be obtained from LEZ scan data or real-time data; however, access is currently restricted due to privacy concerns and high costs, respectively. Moreover, tunnel exit concentrations are estimated based on theoretical concepts, but these should be reviewed. Given the lower NO_2 concentrations expected in the future, these estimations likely significantly overestimate concentrations compared to other areas on the maps (see Appendix P).

Regarding the 2022 calibration, it appears that June and January responded differently to the calibration factor during the process of calibrating these months before the entire year, as explained in Section 4.5.1. Therefore, the model could be improved by applying a different calibration coefficient for each month. This would make sense considering that a monthly factor has been applied in the preparatory work of SIRANE by Axel Briffault and may therefore require adjustments through different monthly calibration coefficients.

Finally, due to constraints in computational time, simulations were only conducted for specific years between 2022 and 2035. Carrying out simulations for intermediate years would improve the accuracy of the projections. Despite these various uncertainties, the projections of NOx emissions used as an input appears robust as of 2022, as discussed in Section 6.3. It would be prudent to continue to compare these projections in future years to see if they have become outdated and to recalibrate them if necessary.

6.10 Further research

For future research beyond the model, it would be beneficial to develop a model for projecting background concentrations using a larger-scale model like CHIMERE (explained in Section C.2), integrated with urban background diminution calculations for each street, similar to the projections used in Paris [120].

Moreover, a main goal of this master's thesis was to evaluate the impact of traffic policies on NOx

emissions. However, incorporating projections of NOx emissions from other sectors could enhance the accuracy of projected NO_2 concentrations, despite these sectors showing smaller reductions compared to traffic (see Section 4.6.1). This would also be interesting as the relationship between NOx emissions and NO_2 concentrations is non-linear. Direct summation of emissions reductions across different sectors does not necessarily equate to a proportional decrease in NO_2 concentrations. Therefore, solely analyzing the impact of isolated policies may overestimate their effectiveness when combined together, suggesting a need for a more integrated approach to accurately assess policy impacts on air quality.

Further studies should consider conducting a health impact assessment and a cost-benefit analysis of LEZ implementations. Although the LEZ's impact on pollution reduction decreases over time, the health benefits continue to accumulate [112]. There are very few long-term studies of LEZs, but a recent study [121] has shown significant health benefits for newborns in LEZs compared with non-LEZs. This improvement in health for this specific age group alone offsets around a quarter of the cost of retrofitting older diesel vehicles initially affected by LEZs. However, accurate health impact estimation would require more comprehensive data, including spatialized health data, exposure modeling, and correlations between air pollutants and health outcomes.

The socio-economic implications of LEZs also warrant attention. Typically, lower-income individuals, who often own older vehicles affected by LEZ bans, may struggle to afford compliant new vehicles [122]. On the other hand, deprived people from Brussels generally live in areas with higher NO_2 concentrations [123, 124] and are more vulnerable to its health effects [123], so low-income people could benefit more from the LEZ. The socio-economic impact can be assessed using the spatialized results presented in this master's thesis, along with supplementary data.

To gain a more comprehensive understanding of the impacts of the LEZ and the Good Move plan on air quality, it is important to assess additional air pollutants, specifically O3 and PM (PM2.5 and PM10), since these pollutants are concerns for Brussels, as detailed in Section 1.3. The SIRANE model, which also accounts for the dispersion of these pollutants, can be used for this purpose. Among these pollutants, the objectives described in this master's thesis could be more readily extended to PM2.5, as emission projections have been made by Bruxelles Environnement, unlike for the other pollutants. This extension is especially relevant for understanding the nuances of the LEZ's impacts on air pollution, given that PM is also emitted by electric vehicles [125]. However, it should be noted that only a few monitoring stations currently measure PM2.5, so the calibration process would be less robust [126].

Regarding the Good Move plan, a more holistic approach should be adopted. While this master's thesis covers only a portion of the 50 different ambitions outlined in the plan, it is important to note that unlike the LEZ, the Good Move plan aims for a more systematic change by altering the modal share of users. Therefore, effectiveness should be measured using indicators that include health and socio-economic impacts, as recommended for LEZ, but also other metrics such as congestion levels, public transport use and improved accessibility for pedestrians and cyclists.

Although SIRANE was used following the policies decision process, it could also serve as a valuable

tool during the decision-making process. For instance, in planning urban development projects or Low Traffic Neighborhoods, various scenarios could be simulated using SIRANE. These simulations could then be analyzed with stakeholders to determine which scenario offers the most benefits.

7 Conclusion

The aim of this master's thesis was to assess the effectiveness of the LEZ and Good Move's ambition to reduce passenger car veh-km by 24% by 2030, in Brussels between 2022 and 2035 on NO_2 concentration. Firstly, as part of the efforts to model NO_2 concentrations more accurately, refinements have been made to the attribution of emissions across different road types. For urban roads, NOx emissions have been increased due to elevated emission factors associated with lower speeds and specific driving styles. Conversely, emissions on rural roads and highways have been lower, attributed to lower emission factors than average. After refinement and calibration, the SIRANE model has been validated for 2022 using statistical indicators, showing alignment with measured NO_2 concentrations, particularly in low traffic conditions. These results affirm the model's reliability and its utility for projecting NO_2 concentrations, despite discrepancies in high-traffic areas. Those are likely due to uncertainties in the COPERT and MuSti data and complex airflow locations, highlighting areas for improvement.

Three of the four objectives of this master's thesis were to assess the overall impact of policy measures over time, analyze the impact by road hierarchy, and identify the vehicle types banned by the LEZ that significantly reduce NO_2 concentrations.

The results demonstrate that while the BASE scenario predicts a gradual reduction in NO_2 concentration over the years, the LEZ significantly accelerates this decrease. From 2022 to 2035, the LEZ contributes to an average additional reduction of 1.18 µg/m³, or 24.2%, excluding background concentrations. The most notable reductions are seen between 2025 and 2030, with 2025 being the peak year of LEZ effectiveness due to the largest relative difference. This peak is primarily attributed to the ban on Euro 5/V diesel vehicles—particularly passenger cars, followed by buses, and light vehicles—which have significantly higher NOx emission factors than their upgraded Euro 6 counterparts. Diesel vehicles are the main contributors to the LEZ's impact, with the most substantial effects observed on road types that have high traffic density and a high presence of diesel vehicles.

Regarding the Good Move strategy, its impact is 8 times less than that of the LEZ, achieving an additional average NO_2 reduction of 0.15 µg/m³, or 2.93%, excluding background concentrations. Its effects are most pronounced in 2028, a year in which there are significant reductions in passenger car veh-km and sufficient NOx emissions from the car fleet to make a noticeable impact. While Good Move's approach of rerouting traffic from urban roads to main roads (A0 and A1) may risk exceeding NO_2 thresholds on these high-traffic routes by 2030, it is expected to slightly benefit the vast majority (90%) of the region's urban streets (A2-A5).

The final objective of this master's thesis is to evaluate whether Brussels will meet the EU's NO_2 concentration thresholds by 2030. The results indicate that without policy measures, 13.3% of street lengths in Brussels will exceed the annual NO_2 limit. Implementations of the LEZ and Good Move significantly enhance compliance, reducing exceedances to 1.71% and 0.74% respectively. It remains uncertain whether the LEZ alone is sufficient for compliance by 2030, or if Good Move is necessary to tip the scales. While all scenarios meet the EU's hourly and daily limits, and the hourly WHO recommendation by 2030, the WHO's annual and daily targets are not met, with the LEZ significantly

helping in approaching these targets.

The projected NO_2 concentrations for WEM and WAM in 2022 generally align well with the NO_2 concentration from the 2022 inventory data. This suggests that the projections are still applicable through 2022. Additionally, this data suggests that policy measures are partially having their anticipated effects. However, the WEM and WAM projections for NO_2 concentrations along main roads are overly optimistic.

To improve accuracy, updating traffic data from MuSti to more recent and precise datasets is recommended, along with using a monthly calibration coefficient instead of an annual one. Additionally, incorporating larger-scale models of background concentrations and other sector emissions will enhance compliance assessments with 2030 EU thresholds. The findings from this master's thesis offer valuable insights for policymakers and can serve as a foundation for conducting health and socio-economic impact assessments, aiding future urban and traffic management planning. Extending assessments to include other pollutants like PM and O3 would provide a more comprehensive view of air quality and policy effectiveness.

References

[1] BRUXELLES ENVIRONNEMENT. La qualité de l'air en région Bruxelles-Capitale. July 2023. URL: https://document.environnement.brussels/opac_css/elecfile/RAP_2022_AirQualityAnnualReport_fr.pdf.

[2] S.Dehouck, A.Gerard, S.Hollander, and J.Counet. Evaluation de la zone de basses émissions - Rapport annuel 2022. 2023. URL: https://environnement.brussels/media/14247/download?inline.

[3] E.Mulholland, J.Miller, Y.Bernard, K.Lee, and F.Rodríguez. *The role of NOx emission reductions in Euro 7/VII vehicle emission standards to reduce adverse health impacts in the EU27 through 2050*, volume 9, page 100133. 2022. URL: https://doi.org/10.1016/j.treng.2022.100133.

[4] Y.Bernard, T.Dallmann, K.Lee, I.Rintanen, and U.Tietge. Evaluation of real-word vehicle emissions in Brussels. November 2021. URL: https://theicct.org/publication/evaluation-of-real-world-vehicle-emissions-in-brussels/.

[5] Bruxelles Mobilité. Good neighbourhood. 2024. URL: https://mobilite-mobiliteit.brussels/fr/good-move/good-neighbourhood.

[6] Bruxelles Environnement. La qualité de l'air en région de Bruxelles-Capitale: Rapport annuel 2021. 2021. URL: https://document.environnement.brussels/opac_css/elecfile/RAP_2021_AirQualityAnnualReport_fr.pdf.

[7] Vahakn Kabakian. *War and Air Pollution*, pages 8–1. United Nations Development Programme, January 2006.

[8] S.Amany, M.Ayman, and A.Atef. ICFD11-EG-4006 air quality assessment of west Port-Said industrial region, Egypt. December 2013.

[9] A.Leelossy, F.Molnár, F.Izsák, Á.Havasi, I.Lagzi, and R.Mészáros. *Dispersion modeling of air pollutants in the atmosphere: a review*, volume 6, pages 257–278. 08 2014. URL: https://doi.org/10.2478/s13533-012-0188-6.

[10] L. Soulhac, V. Garbero, P. Salizzoni, P. Mejean, and R.J. Perkins. *Flow and dispersion in street intersections*, volume 43, pages 2981–2996. 2009. URL: https://doi.org/10.1016/j.atmosenv.2009.02.061.

[11] L.Soulhac, P.Salizzoni, F.-X.Cierco, and R.Perkins. *The model SIRANE for atmospheric urban pollutant dispersion; part I, presentation of the model*, volume 45, pages 7379–7395. 2011. URL: https://doi.org/10.1016/j.atmosenv.2011.07.008.

[12] F.Goor. Personal communication, March and April 2024. Personal communications on March 14, 2024, and April 26, 2024.

[13] VUB. Back and forecasting of measures. Study report, Bruxelles Environnement, 2022. Study available from Bruxelles Environnement.

[14] R.Smithers, R.Harris, and G.Hitchcock. The ecological effects of air pollution from road transport: an updated review. February 2016. URL: https://www.researchgate.net/publication/312938118_The_ecological_effects_of_air_pollution_from_road_transport_an_updated_review.

[15] European Parliament. Air pollution: parliament adopts revised law to improve air quality. April 2024. URL: https://www.europarl.europa.eu/news/en/press-room/20240419IPR20587/air-pollution-parliament-adopts-revised-law-to-improve-air-quality.

[16] C.Holman, R.Harrison, and X.Querol. *Review of the efficacy of low emission zones to improve urban air quality in European cities*, volume 111, pages 161–169. 2015. URL: https://doi.org/10.1016/j.atmosenv.2015.04.009.

[17] R. Yadav, P. Trivedi, L. K. Sahu, G. Beig, and N. Tripathi. *Air Pollution Modeling*, pages 37–55. Environmental Chemistry for a Sustainable World. Springer. ISBN 9789811534812. 2020. URL: https://doi.org/10.1007/978-981-15-3481-2_3.

[18] S.Hanna and J.Chang. *Acceptance criteria for urban dispersion model evaluation*, volume 116, pages 133–146. 2012. URL: https://doi.org/10.1007/s00703-011-0177-1.

[19] S.Janssen, P.Thunis, M.Adani, A.Piersanti, C.Carnevale, C.Cuvelier, P.Durka, E.Georgieva, C.Guerreiro, L.Malherbe, B.Maiheu, F.Meleux, A.Monteiro, A.Miranda, H.Olesen, F.Pfäfflin, J.Stocker, G.Sousa Santos, A.Stidworthy, M.Stortini, M.Trimpeneers, P.Viaene, L.Vitali, K.Vincent, and J.Wesseling. FAIRMODE guidance document on modelling quality objectives and benchmarking. (EUR 31068 EN), 2022. URL: https://fairmode.jrc.ec.europa.eu/document/fairmode/WG1/Guidance_MQO_Bench_vs3.3_20220519.pdf.

[20] STRATEC and Bruxelles Environnement. Contribution au calcul des émissions de gaz à effet de serre et de polluants affectant la qualité de l'air par le transport routier en région de Bruxelles-Capitale. April 2023.

[21] European Union. Directive 2008/50/ce of 21 may 2008 on ambient air quality and cleaner air for europe, 2008. URL: https://eur-lex.europa.eu/eli/dir/2008/50/oj.

[22] B.Brunekreef and S.T.Holgate. *Air pollution and health*, volume 360, pages 1233–1242. 2002. URL: https://doi.org/10.1016/S0140-6736(02)11274-8.

[23] European Environment Agency. Air Quality in Europe - 2022 Report, 2022. URL: https://www.eea.europa.eu/publications/air-quality-in-europe-2022/air-quality-in-europe-2022.

[24] World Health Organization. WHO global air quality guidelines: particulate matter (PM2.5 and PM10), ozone, nitrogen dioxide, sulfur dioxide and carbon monoxide. 2021. URL: https://iris.who.int/handle/10665/345329.

[25] United States Environmental Protection Agency. Integrated science assessment for oxides of nitrogen – Health criteria. Technical Report EPA/600/R-15/068, United States Environmental Protection Agency, Research Triangle Park, NC, January 2016. URL: https://www.epa.gov/isa.

[26] Health Effects Institute. State of global air 2020: special report. 2020. URL: https://www.healthdata.org/sites/default/files/files/policy_report/2021/soga-2020-report-10-26_0.pdf.

[27] World Health Organization. Fact sheet: ambient (outdoor) air quality and health. 2018. URL: https://www.who.int/en/news-room/fact-sheets/detail/ambient-(outdoor)-air-quality-and-health.

[28] Center for Science Education, UCAR. Effects of air pollution. URL: https://scied.ucar.edu/learning-zone/air-quality/effects-air-pollution.

[29] OECD. Executive summary. in the economic consequences of outdoor air pollution. 2016. URL: https://doi.org/10.1787/9789264257474-3-en.

[30] European Parliament and the Council of the European Union. *Directive 2004/107/EC of the European Parliament and of the Council of 15 December 2004 relating to arsenic, cadmium, mercury, nickel and polycyclic aromatic hydrocarbons in ambient air*, volume L 023, page 3. December 2004. URL: https://eur-lex.europa.eu/legal-content/EN/TXT/?uri=CELEX:32004L0107.

[31] World Health Organization. WHO global air quality guidelines: particulate matter (PM2.5 and PM10), ozone, nitrogen dioxide, sulfur dioxide and carbon monoxide. 2021. URL: https://iris.who.int/handle/10665/345329.

[32] European Parliament. Legislative resolution of 24 april 2024 on the proposal for a directive of the european parliament and of the council on ambient air quality and cleaner air for europe (recast). April 2024. URL: https://www.europarl.europa.eu/doceo/document/TA-9-2024-0319_EN.html#title2.

[33] European Commission. Pathway to a healthy planet for all EU action plan: 'towards zero pollution for air, water and soil', June 2021. URL: https://eur-lex.europa.eu/legal-content/EN/ALL/?uri=COM:2021:400:FIN.

[34] Wallonie Environnement Awac. Emission de NOx. . URL: https://awac.be/inventaires-demission/emission-de-nox/.

[35] J. de Villers, M. Squilbin, and P. Vanderstraeten. Oxydes d'azote (NOX). pages 1–22, 2016. URL: https://fr.scribd.com/document/602778987/Air8-rev2016.

[36] BioTechUSA France. Oxyde nitrique: propriétés et mode d'action - BioTechUSA france. URL: https://biotechusa.fr/oxyde-nitrique-proprietes-et-mode-daction/.

[37] Wikipedia. Nitric oxide. URL: https://en.wikipedia.org/w/index.php?title=Nitric_oxide&oldid=1198331831.

[38] Emwelt. Effets des NOx sur la santé et l'environnement. Accessed: 2019-06-05. URL: http://environnement.public.lu/fr/loft/air/Polluants_atmospheriques/les_oxydes_d_azote_NOx/effets-NOx.html.

[39] Y.Couture. *Guide d'estimation de la concentration de dioxyde d'azote NO_2 dans l'air ambiant lors de l'application des modèles de dispersion atmosphérique*. August 2008. URL: https://www.environnement.gouv.qc.ca/air/criteres/guide-azote-aout2008.pdf.

[40] Wallonie Environnement Awac. Oxydes d'azote - NOX. . URL: https://www.wallonair.be/fr/en-savoir-plus/les-polluants/oxydes-d-azote-nox.html.

[41] Agency for Toxic Substances and Disease Registry. Toxfaqs™ for nitrogen oxides. March 2014. URL: https://wwwn.cdc.gov/TSP/ToxFAQs/ToxFAQsDetails.aspx?faqid=396&toxid=69.

[42] Ministry For The Environment. Nitrogen dioxide. September 2021. URL: https://environment.govt.nz/facts-and-science/air/air-pollutants/nitrogen-dioxide-effects-health/.

[43] S.C. Anenberg, A. Mohegh, D.L. Goldberg, G.H. Kerr, M. Brauer, K. Burkart, P. Hystad, A. Larkin, S. Wozniak, and L. Lamsal. *Long-term trends in urban NO2 concentrations and associated paediatric asthma incidence: estimates from global datasets*, volume 6, pages 49–58. 2022. URL: https://doi.org/10.1016/S2542-5196(21)00255-2.

[44] A.González Ortiz and C.De Brito Beirao Guerreiro. Air quality in Europe — 2020 report, 2020. URL: https://doi.org/10.2800/786656.

[45] S. Witchalls. How does acid rain affect the environment. March 2022. URL: https://earth.org/how-does-acid-rain-affect-the-environment/.

[46] Effects of acid rain. March 2016. URL: https://www.epa.gov/acidrain/effects-acid-rain.

[47] Eurostat. Nitrogen dioxide concentrations in European capital cities - monthly averages, experimental statistics. October 2023. URL: https://doi.org/10.2908/ENV_AIR_NO2.

[48] Bruxelles Environnement. Synthèse état de l'environnement 2015-2016. October 2016. URL: https://document.environnement.brussels/opac_css/elecfile/RAP_SEE%20Synthese%202015-2016.

[49] European Parliament and Council of the European Union. Directive 2001/81/ec of the european parliament and of the council of 23 october 2001 on national emission ceilings for certain atmospheric pollutants. Journal Officiel des Communautés Européennes, November 2001. ELI: http://data.europa.eu/eli/dir/2001/81/oj.

[50] IRCEL-CELINE. Adjustment emission inventory report – NEC reporting 15.02.2017 & LRTAP reporting 15.02.2017. February 2017. URL: https://www.irceline.be/nl/emissies/Adjustment_Report_2017_BE.pdf.

[51] The European Parliament and The Council of The European Union. Directive (eu) 2016/2284 of the european parliament and of the council. Official Journal of the European Union, December 2016. URL: https://eur-lex.europa.eu/legal-content/EN/TXT/?uri=CELEX:02016L2284-20240206.

[52] Bruxelles Environnement. Qualité de l'air extérieur : état des lieux. October 2023. URL: https://environnement.brussels/citoyen/outils-et-donnees/etat-des-lieux-de-lenvironnement/qualite-de-lair-exterieur-etat-des-lieux.

[53] Région Bruxelles-Capitale. Inventaire des émissions de polluants air LRTAP de la Région de Bruxelles-Capitale (1990-2021, soumission 2023). 2023. URL: https://environnement.brussels/citoyen/lenvironnement-bruxelles/proteger-sa-sante/comment-evolue-la-qualite-de-lair.

[54] European Environment Agency. *Explaining road transport emissions: a non-technical guide*. Luxembourg, 2016. URL: https://doi.org/10.2800/71804.

[55] R. O'Driscoll, M. Stettler, N. Molden, T. Oxley, and H. ApSimon. *Real world CO2 and NOx emissions from 149 Euro 5 and 6 diesel, gasoline and hybrid passenger cars.*, volume 621, pages 282–290. 2018. URL: https://api.semanticscholar.org/CorpusID:3797803.

[56] European Automobile Manufacturers' Association (ACEA). Enabling factors for alternatively-powered cars and vans in the European Union. January 2023. URL: https://www.acea.auto/files/ACEA-report-vehicles-in-use-europe-2023.pdf.

[57] Charles W. Schmidt. *Beyond a one-time scandal: Europe's ongoing diesel pollution problem*, volume 124, pages A19–A22. 2016. URL: https://doi.org/10.1289/ehp.124-A19.

[58] European Parliament and the Council. Regulation (EU) 2024/1257 on type-approval of motor vehicles and engines and of systems, components and separate technical units intended for such vehicles, with respect to their emissions and battery durability (Euro 7), amending Regulation (EU) 2018/858 and repealing regulations (EC) No 715/2007 and (EC) No 595/2009, commission regulation (EU) No 582/2011, commission regulation (EU) 2017/1151, commission regulation (EU) 2017/2400 and commission implementing regulation (EU) 2022/1362. Official Journal of the European Union, April 2024. URL :http://data.europa.eu/eli/reg/2024/1257/oj.

[59] Green-Zones.eu. Low emission zone Brussels. 2022. URL: https://www.lez-belgium.be/en/low-emission-zones/brussels.

[60] T. Williamson, B. Mance, and C. Bautista. Quantifying the impact of low- and zero-emission zones: evidence review for the clean cities campaign. October 2022. URL: https://cleanc

itiescampaign.org/wp-content/uploads/2022/10/12009C_Quantifying-the-impact-of-low-and-zeroemission-zones-Evidence-Review_final.pdf.

[61] Mayor of London. Expanded ultra low emission zone – six month report including low emission zone – one year report. Report, Mayor of London, July 2022. URL : https://www.london.gov.uk/sites/default/files/expanded_ultra_low_emission_zone_six_month_report.pdf.

[62] H. Boogaard, N. A. H. Janssen, P. H. Fischer, G. P. A. Kos, E. P. Weijers, F. R. Cassee, S. C. van der Zee, J. J. de Hartog, K. Meliefste, M. Wang, B. Brunekreef, and G. Hoek. *Impact of low emission zones and local traffic policies on ambient air pollution concentrations*, volume 435-436, pages 132–140. 2012. URL: https://doi.org/10.1016/j.scitotenv.2012.06.089.

[63] S. S. Jensen, M. Ketzl, J. K. Nøjgaard, and T. Becker. What are the impacts on air quality of low emission zones in denmark? *Artikler fra Trafikdage på Aalborg Universitet*, 2011. URL: https://www.trafikdage.dk/papers_2011/31_SteenSolvangJensen.pdf.

[64] R. B. Ellison, S. P. Greaves, and D. A. Hensher. *Five years of London's low emission zone: effects on vehicle fleet composition and air quality*, volume 23, pages 25–33. 2013. URL: https://doi.org/10.1016/j.trd.2013.03.010.

[65] P. Morfeld, D. A. Groneberg, and M. F. Spallek. *Effectiveness of low emission zones: large scale analysis of changes in environmental NO2, NO and NOx concentrations in 17 German cities*, volume 9. August 2014. URL: https://doi.org/10.1371/journal.pone.0102999.

[66] Brussels Environment. Effets attendus de la zone de basses émissions sur le parc automobile et la qualité de l'air en région bruxelloise. January 2019. URL : https://www.lez.brussels/medias/lez-note-fr-vdef.pdf?context=bWFzdGVyfGRvY3VtZW50c3w4NjgwMzQ5fGFwcGxpY2F0aW9uL3BkZnxkb2N1bWVudHMvaDI5L2hjYi84ODAxNjI2NzUxMDA2LnBkZnwwNTBjZTE5YTI4NWUyNjIzYzZmNTgxZDE4YWU5NjQ0Mjg4MmQ0MDY2ZWUwYjA2Zjk1YmZjMDQ0ZTAyODFlZTFj.

[67] L.Duprez, G.Bastin, S.Dierckx, C.Banken, N.Dupont, S.Dehouck, M.Henrard, T.DE Vos, and F.Goor. Evaluation de la zone de basses émissions - Rapport 2020. Technical report, Bruxelles Environnement, 2021. URL: https://lez.brussels/medias/RAPP-2020-LEZ-FR-FINAL.pdf?context=bWFzdGVyfHBkZnwyMjkwMDg4fGFwcGxpY2F0aW9uL3BkZnxoZDIvaGNlLzg4NDIzMjg4MDEzMTAvUkFQUF8yMDIwX0xFWl9GUl9GSU5BTC5wZGZ8MDk2ZjdmZjRhODFmNzFiYTUxMGEwYTgwNDQ1OWZiOGY3OGFkNjc2YWJiODQ0YjllYTY3NTA1NTMzYzIyZDNiNA.

[68] Bruxelles Mobilité. Good Move - Plan régional de mobilité 2020-2030. 2020. URL: https://mobilite-mobiliteit.brussels/fr/good-move.

[69] Bruxelles Mobilité. Quartiers apaisés, 2021. URL: https://mobilite-mobiliteit.brussels/fr/good-move.

[70] Service Public Régional de Bruxelles - Bruxelles Mobilité. Quartiers apaisés: L'essentiel, 2024. URL: https://mobilite-mobiliteit.brussels/fr/good-move.

[71] Bruxelles Environnement. Plan régional air-climat-energie. April 2023. URL: https://document.environnement.brussels/opac_css/elecfile/PACE_FR.pdf.

[72] M.Gemmer and B.Xiao. *Air Quality Legislation and Standards in the European Union: Background, Status and Public Participation*, volume 4, pages 50–59. March 2013. URL: https://doi.org/10.3724/SP.J.1248.2013.050.

[73] J. Wang, W. Zhang, R. Cao, X. You, and H. Lai. *Analysis of Nitrogen Dioxide in Environment*, volume 07, pages 278–288. January 2016. URL: https://doi.org/10.4236/abb.2016.76026.

[74] Defra Department for Environment Food and Rural Affairs. Measurement methods and UK monitoring networks for NO2. 2004. URL: https://uk-air.defra.gov.uk/library/assets/documents/reports/aqeg/chapter4.pdf.

[75] E. Dunlea, S. Herndon, D. Nelson, R. Volkamer, F. Martini, P. Sheehy, M. Zahniser, J. Shorter, J. Wormhoudt, B. Lamb, E. Allwine, J. Gaffney, N. Marley, M. Grutter, C. Marquez C, S. Blanco, B. Cardenas, A. Retama, C. Villegas, and M. Molina. *Evaluation of nitrogen dioxide chemiluminescence monitors in a polluted urban environment*, volume 7. May 2007. URL: https://doi.org/10.5194/acp-7-2691-2007.

[76] M. Steinbacher, C. Zellweger, B. Schwarzenbach, S. Bugmann, B. Buchmann, C. Ordonez, A. Prevot, and C. Hueglin. *Nitrogen oxide measurements at rural sites in Switzerland: Bias of conventional measurement techniques*, volume 112. June 2007. URL: https://doi.org/10.1029/2006JD007971.

[77] Deliverable 3.17. updated measurement guideline for nox and vocs, 2018. URL: https://ec.europa.eu/research/participants/documents/downloadPublic?documentIds=080166e5bef908e2&appId=PPGMS.

[78] A. Leelossy, T. Mona, R. Mészáros, I. Lagzi, and Á. Havasi. *Eulerian and Lagrangian Approaches for Modelling of Air Quality*, volume 24, pages 73–85. January 2016. ISBN 978-3-319-40155-3. URL: https://doi.org/10.1007/978-3-319-40157-7_5.

[79] J. Joel. An introduction to atmospheric pollutant dispersion modelling. August 2022. URL: https://doi.org/10.3390/ecas2022-12826.

[80] F. Gronwald and S.-Y. Chang. *Evaluation of the precision and accuracy of multiple air dispersion models*, volume 6, pages 1–11. October 2018. URL: https://www.researchgate.net/publication/323153600_Evaluation_of_the_Precision_and_Accuracy_of_Multiple_Air_Dispersion_Models.

[81] B.Sportisse. *Box models versus Eulerian models in air pollution modeling*, volume 35, pages 173–178. 2001. URL: https://doi.org/10.1016/S1352-2310(00)00265-X.

[82] Á. Leelőssy, T. Mona, R. Mészáros, I. Lagzi, and Á. Havasi. *Eulerian and Lagrangian approaches for modelling of air Quality*, pages 73–85. Mathematics in Industry. Springer International Publishing. ISBN 978-3-319-40157-7. URL: https://doi.org/10.1007/978-3-319-40157-7_5.

[83] Meissam L. Bahlali, Eric Dupont, and Bertrand Carissimo. *Atmospheric dispersion using a Lagrangian stochastic approach: Application to an idealized urban area under neutral and stable meteorological conditions*, volume 193, pages 103–976. 2019. URL: https://doi.org/10.1016/j.jweia.2019.103976.

[84] B.Pulvirenti R.E.Britter S.Di Sabatino, R.Buccolieri. *Flow and pollutant dispersion in street canyons using FLUENT and ADMS-Urban*, volume 13, pages 369–381. September 2008. URL: https://doi.org/10.1007/s10666-007-9106-6.

[85] W.C.Cheng L.Chun-Ho. *Large-Eddy simulation of flow and pollutant transports in and above two-Dimensional idealized street canyons*, volume 139, pages 411–437. June 2011. URL: https://doi.org/10.1007/s10546-010-9584-y.

[86] L. Soulhac and P. Salizzoni. *Dispersion in a street canyon for a wind direction parallel to the street axis*, volume 98, pages 903–910. 2010. URL: https://doi.org/10.1016/j.jweia.2010.09.004.

[87] L. Soulhac, R. J. Perkins, and P. Salizzoni. *Flow in a street canyon for any external wind direction*, volume 126, pages 365–388. 2008. URL: https://doi.org/10.1007/s10546-007-9238-x.

[88] L. Soulhac, C.V. Nguyen, P. Volta, and P. Salizzoni. *The model SIRANE for atmospheric urban pollutant dispersion. PART III: Validation against NO2 yearly concentration measurements in a large urban agglomeration*, volume 167, pages 377–388. 2017. URL: https://doi.org/10.1016/j.atmosenv.2017.08.034.

[89] V. Garbero, P. Mejan, R. Perkins, P. Salizzoni, and L. Soulhac. *Pollutant dispersion in urban canopy study of the plume behaviour through an obstacle array*. PhD thesis, Ecole Centrale de Lyon, 2008. URL: https://www.witpress.com/Secure/elibrary/papers/AIR06/AIR06061FU1.pdf.

[90] M. Carpentieri, P. Salizzoni, A. Robins, and L. Soulhac. Validation of the neighbourhood scale dispersion model through comparison with wind tunnel data. 2009. URL: https://openresearch.surrey.ac.uk/esploro/outputs/conferencePresentation/Validation-of-a-neighbourhood-scale-dispersion/99515445202346.

[91] M. Carpentieri, P. Salizzoni, A. Robins, and L. Soulhac. *Evaluation of a neighbourhood scale, street network dispersion model through comparison with wind tunnel data*, volume 37, pages 110–124. 2012. URL: https://doi.org/10.1016/j.envsoft.2012.03.009.

[92] P. Salizzoni G. Lamaison L. Soulhac N. Ben Salem, V. Garbero. *Modelling pollutant disper-*

sion in a street network, volume 155, pages 157–187. 2015. URL: https://doi.org/10.1007/s10546-014-9990-7.

[93] L. Soulhac. *Modélisation de la dispersion atmosphérique à l'intérieur de la canopée urbaine*. PhD thesis, Ecole Centrale de Lyon, Ecully, 2000. URL: https://doi.org/10.1007/s10546-014-9990-7.

[94] L. Soulhac, P. Salizzoni, P. Mejean, D. Didier, and I. Rios. *The model SIRANE for atmospheric urban pollutant dispersion; PART II, validation of the model on a real case study*, volume 49, pages 320–337. 2012. URL: https://doi.org/10.1016/j.atmosenv.2011.11.031.

[95] T. Grylls, C. M. A. Le Cornec, P. Salizzoni, L. Soulhac, M. E. J. Stettler, and M. van Reeuwijk. *Evaluation of an operational air quality model using large-eddy simulation*, volume 3. 2019. URL: https://doi.org/10.1016/j.aeaoa.2019.100041.

[96] Diego Nève de Mévergnies. Évaluation de l'effet de la mise en place d'une rue à sens unique sur la concentration en dioxyde d'azote à bruxelles. Master's thesis, Faculté des bioingénieurs, Université catholique de Louvain, 2023. URL http://hdl.handle.net/2078.1/thesis:43410. Prom. : Bogaert, Patrick.

[97] European Commision. Model COPERT - Computer model to calculate emissions from road traffic. . April 2024. URL: https://web.jrc.ec.europa.eu/policy-model-inventory/explore/models/model-copert/.

[98] Emissia. COPERT versions | COPERT. April 2024. URL: https://copert.emisia.com/copert/versions/.

[99] N. Abdull, M. Yoneda, and Y. Shimada. *Traffic characteristics and pollutant emission from road transport in urban area*, volume 13. June 2020. URL: https://doi.org/10.1007/s11869-020-00830-w.

[100] European Commision. Model COPERT - Computer model to calculate emissions from road traffic. . 2024. URL: https://web.jrc.ec.europa.eu/policy-model-inventory/explore/models/model-copert/.

[101] J.C.Chang S.R.Hanna. *Air quality model performance evaluation*, volume 87, pages 167–196. 2004. URL: https://doi.org/10.1007/s00703-003-0070-7.

[102] Bruxelles Environnement. Stratégie de déploiement de l'infrastructure de recharge dans la région de Bruxelles-Capitale. Technical report, Bruxelles Environnement, Novembre 2022. URL: https://environnement.brussels/media/10330/download?inline.

[103] S. Dehouck, A. Gerard, S. Hollander, J. Counet, F. Goor, A. Briffault, C. Ceustermans, F. Couvreur, N. Sergeant, and L. Demuelenaere. Evaluation de la zone à basses emissions, 2022. Rapport 2022.

[104] Guus J.M. Velders and Jan Matthijsen. *Meteorological variability in NO2 and PM10 concen-*

trations in the Netherlands and its relation with EU limit values, volume 43, pages 3858–3866. 2009. URL: https://doi.org/10.1016/j.atmosenv.2009.05.009.

[105] C. Andersson, J. Langner, and R. Bergstroumm. *Interannual Variation and trends in air pollution over Europe due to climate variability during 1958–2001 simulated with a regional CTM coupled to the ERA40 reanalysis*, volume 59, pages 77–98. 2007. doi: 10.1111/j.1600-0889.2006.00231.x. URL: https://doi.org/10.1111/j.1600-0889.2006.00231.x.

[106] Intergovernmental Panel on Climate Change (IPCC). IPCC WGI interactive atlas: regional synthesis, 2022. URL: https://interactive-atlas.ipcc.ch/regional-synthesis#eyJ0eXBlIjoiQ0lEIiwic2VsZWN0ZWRJbmRleCI6WyJoZWF2eV9wcmVjaXBpdGF0aW9uIiwibWVhbl9wcmVjaXBpdGF0aW9uIiwibWVhbl93aW5kX3NwZWVkIiwic2V2ZXJlX3dpbmRfc3Rvcm0iLCJhaXJfcG9sbHV0aW9uX3dlYXRoZXIiXSwic2VsZWN0ZWRWYXJpYWJsZSI6ImNvbmZpZGVuY2UiLCJzZWxlY3RlZENvdW50cnkiOiJHSUMiLCJtb2RlIjoiSEVYIiwiY29tbW9ucyI6eyJsYXQiOjk3NzIsImxuZyI6NDAwNjkyLCJ6b29tIjo0LCJwcm9qIjoiRVBTRzo1NDAzMCIsIm1vZGUiOiJjb21wbGV0ZV9hdGxhcyJ9fQ==.

[107] S.Janssen and P.Thunis. Fairmode guidance document on modelling quality objectives and benchmarking. Technical report, European Commission, 2022. URL : https://fairmode.jrc.ec.europa.eu/document/fairmode/WG1/Guidance_MQO_Bench_vs3.3_20220519.pdf.

[108] P. Thunis, A. Pederzoli, and D. Pernigotti. *Performance criteria to evaluate air quality modeling applications*, volume 59, pages 476–482. 2012. URL: https://doi.org/10.1016/j.atmosenv.2012.05.043.

[109] R.Jaikumar, S.M.Shiva Nagendra, and R.Sivanandan. *Modal analysis of real-time, real world vehicular exhaust emissions under heterogeneous traffic conditions*, volume 54, pages 397–409. July 2017. URL: https://doi.org/10.1016/j.trd.2017.06.015.

[110] R. O'Driscoll, H. M. ApSimon, T. Oxley, N. Molden, M. E. J. Stettler, and A. Thiyagarajah. *A Portable Emissions Measurement System (PEMS) study of NOx and primary NO2 emissions from Euro 6 diesel passenger cars and comparison with COPERT emission factors*, volume 145. September 2016. URL: https://doi.org/10.1016/j.atmosenv.2016.09.021.

[111] International Council on Clean Transportation (ICCT). Euro VI emission standards. Technical report, International Council on Clean Transportation, June 2016. URL: https://theicct.org/sites/default/files/publications/ICCT_Euro6-VI_briefing_jun2016.pdf.

[112] S.Host, C. Honoré, F. Joly, A. Saunal, A. Le Tertre, and S. Medina. *Implementation of various hypothetical low emission zone scenarios in greater Paris: Assessment of fine-scale reduction in exposure and expected health benefits*, volume 185, pages 109–405. 2020. URL: https://doi.org/10.1016/j.envres.2020.109405.

[113] B. Yin, A.O. Diallo, T. Seregina, N. Coulombel, and L. Liu. *Evaluation of Eu-traffic neigh-*

borhoods and scale effects: the Paris case study, volume 2678, pages 88 – 101. 2023. URL: https://api.semanticscholar.org/CorpusID:258736395.

[114] Service Public Régional de Bruxelles - Bruxelles Mobilité. Good network, 2024. URL: https://mobilite-mobiliteit.brussels/fr/good-move/good-network.

[115] *Evaluation of low traffic neighbourhood (LTN) impacts on NO2 and traffic*, volume 113, pages 103–536. 2022. URL: https://doi.org/10.1016/j.trd.2022.103536.

[116] G. Durand and J. Thomas. Pourquoi 'Good Move' rythme autant la fin de campagne bruxelloise, June 2024. URL: https://www.lesoir.be/592106/article/2024-06-02/pourquoi-good-move-rythme-autant-la-fin-de-campagne-bruxelloise.

[117] Ana Claudia Andriolli and Lígia Torres Silva. *Are Low Emission Zones Truly Embraced by the Public?*, volume 11. 2024. URL: https://doi.org/10.3390/environments11060106.

[118] Jiayi Tang, Aonghus McNabola, and Bruce Misstear. *The potential impacts of different traffic management strategies on air pollution and public health for a more sustainable city: A modelling case study from Dublin, Ireland*, volume 60, pages 102–229. 2020. URL: https://doi.org/10.1016/j.scs.2020.102229.

[119] Bruxelles Environnement. Personal communication. Personal communication via email, 2024. Email to the author on April 17, 2024.

[120] Airparif - Surveillance de la Qualité de l'Air en Île-de-France. Évaluation prospective de la qualité de l'air à l'horizon 2020 en Île-de-france, September 2017. URL: https://www.airparif.fr/sites/default/files/document_publication/rapport-ppa_180917.pdf.

[121] H. Klauber, F. Holub, N. Koch, N. Pestel, N. Ritter, and A. Rohlf. Killing prescriptions softly: Low emission zones and child health from birth to school. *American Economic Journal: Economic Policy*, 2024. URL: https://doi.org/10.1257/pol.20210729.

[122] R. Rashid, F. Chong, S. Islam, et al. *Taking a deep breath: a qualitative study exploring acceptability and perceived unintended consequences of charging clean air zones and air quality improvement initiatives amongst low-income, multi-ethnic communities in Bradford, UK*, volume 21, page 1305. 2021. URL: https://doi.org/10.1186/s12889-021-11337-z.

[123] L.Feron. Highest mortality risk due to air pollution exposure in brussels in deprived neighbourhoods. VUB Press, October 2021. URL: https://press.vub.ac.be/highest-mortality-risk-due-to-air-pollution-exposure-in-brussels-in-deprived-neighbourhoods.

[124] F. Lauriks, D. Jacobs, and F. J. R. Meysman. Curieuzenair: Data collection, data analysis and results. Report, University of Antwerp, 2022.

[125] Sang-Hee Woo, Hyungjoon Jang, Seung-Bok Lee, and Seokhwan Lee. *Comparison of total PM emissions emitted from electric and internal combustion engine vehicles: An experimental*

analysis, volume 842, page 156961. 2022. URL: https://doi.org/10.1016/j.scitotenv.2022.156961.

[126] A. Briffault. Personal communication. Oral communication, May 2024. Discussion on Particulate Matter monitoring stations in Brussels.

[127] Institut Scientifique de Service Public (ISSeP). Modèles de la qualité de l'air, 2024. URL: https://www.wallonair.be/fr/en-savoir-plus/modeles.html.

8 Appendices

A Annual NO_2 concentration in 2022 in the measurement stations

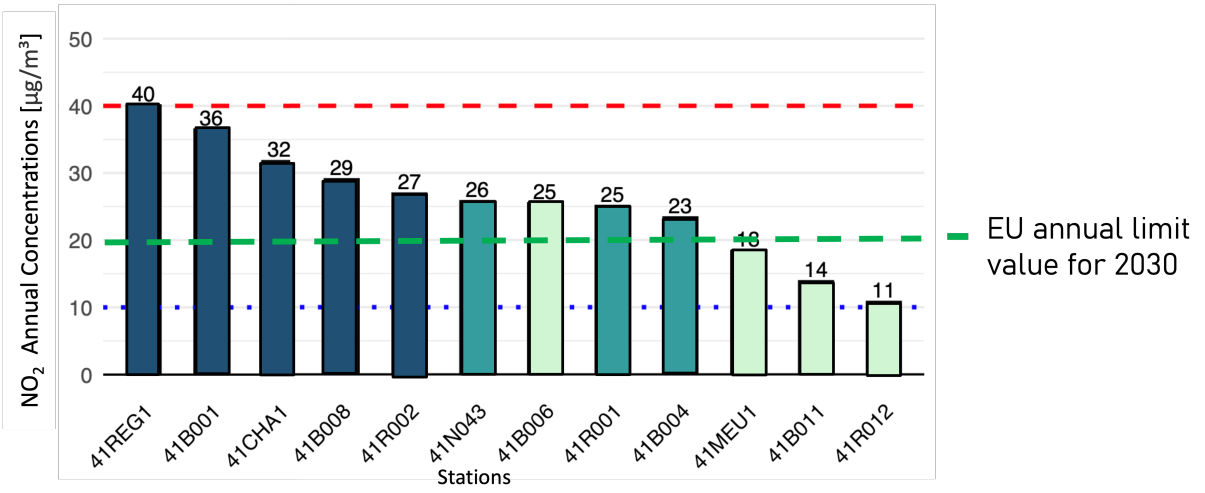

Figure A.1: Average annual NO_2 concentrations at the 12 measurement stations in BCR. The solid red line represents the current EU annual concentration threshold of 40 µg/m³, which must be met universally. The solid green line indicates the EU's 2030 target concentration of 20 µg/m³. The dashed blue line shows the WHO's recommended limit of 10 µg/m³. Source: [1]

B LEZ Calendar

	Fuels	2025	2028	2030	2034	2035	2036
 CAR (M1) & VAN (N1 Class I)	Diesel-Hybrid	Euro 6b,c	Euro 6d	X	X	X	X
	Petrol/Hybrid/ LPG/CNG	Euro 3	Euro 4	Euro 6d	Euro 6d	X	X
 BUS (M3 Class I, II, A)	Diesel-Hybrid	Euro VI	Euro VI	Euro VI	Euro VI	Euro VId	X
	Petrol/Hybrid/ LPG/CNG	Euro III	Euro IV	Euro VI	Euro VI	Euro VId	X
 AUTOCAR (M3 Class III, B)	Diesel-Hybrid	Euro VI	Euro VI	Euro VI	Euro VI	Euro VId	Euro VIe
	Petrol/Hybrid/ LPG/CNG	Euro III	Euro IV	Euro VI	Euro VI	Euro VId	Euro VIe
 MINIBUS (M2) & VAN (N1) (Class II, III)	Diesel-Hybrid	Euro 6	Euro 6d-TEMP	Euro 6d	Euro 6d	X	X
	Petrol/Hybrid/ LPG/CNG	Euro 3	Euro 4	Euro 6d	Euro 6d	X	X
 SCOOTER (L1- L2)	Diesel-Hybrid	X	X	X	X	X	X
	Petrol/Hybrid/ LPG/CNG	< Euro 5	Euro 5	X	X	X	X
 MOTO & SCOOTER (L3-L5)	Diesel-Hybrid	X	X	X	X	X	X
	Petrol/Hybrid/ LPG/CNG	Euro 3	Euro 4	Euro 5	Euro 5	X	X
 MOTO & QUAD (L6-L7)	Diesel-Hybrid	X	X	X	X	X	X
	Petrol/Hybrid/ LPG/CNG	Without Euro norm	Euro 4	Euro 5	Euro 5	X	X
 TRUCK N2 <2610 kg	Diesel-Hybrid	Euro VI	Euro VI	Euro VId	Euro VId	Euro VId	Euro VId
	Petrol/Hybrid/ LPG/CNG	Euro III	Euro IV	Euro VId	Euro VId	Euro VId	Euro VId
 TRUCK N2 >2610 kg & N3	Diesel-Hybrid	Euro VI	Euro VI	Euro VId	Euro VId	Euro VIe	Euro VIe
	Petrol/Hybrid/ LPG/CNG	Euro III	Euro IV	Euro VId	Euro VId	Euro VIe	Euro VIe

Figure B.1: LEZ future years calendar in Brussels, by vehicle type and fuel. The corresponding Euro standard for a given year and vehicle type indicates the oldest Euro standard still permitted; all newer Euro standards are also accepted. A red cross indicates that no vehicles of that fuel type are allowed to operate in the region.

C Pollution dispersion models

C.1 Assessment model

As indicated above, atmospheric dispersion models are used to predict how pollutants spread and interact in the atmosphere after emission. These models simulate the transport, diffusion, and chemical transformation of pollutants, taking into account varying meteorological conditions and terrain. They are critical for forecasting air quality and guiding environmental planning.

Assessment models, on the other hand, are used to evaluate pollution levels based on actual data collected from monitoring stations. They focus on analyzing the distribution of pollutants over time and space, helping to understand exposure levels and inform public health decisions. Unlike dispersion

models, assessment models do not predict future states but provide an analysis of current or past air quality [127].

In Belgium, the entity responsible for disseminating information on outdoor air quality is known as the Interregional Environment Cell (CELINE). A network of automatic measurement stations, dispersed throughout the national territory, is established for tracking the concentrations of various pollutants.

CELINE has developed two evaluation models, the first being an interpolation model named RIO. The purpose of interpolation is to compensate for the lack of data in areas without direct measurements. The RIO interpolation is able to adapt its approach according to the localized or widespread nature of atmospheric pollution. Unlike conventional interpolation methods (inverse distance weighting, ordinary kriging) that assume uniform spatial representativeness for all measurements, the RIO method is specifically designed to address variations in spatial representativeness regarding pollutant concentrations. After performing the interpolation based on measurement points, the local character of each interpolated data is carefully considered. This acknowledgment of local specifics associated with measured concentrations assigns a particular value to each point. Notably, concentrations recorded in rural areas typically provide a more accurate representation for broader regions [127].

The second model, IFDM, combined with the first to form the RIO-IFDM model, assesses the impact of atmospheric pollutant emissions from point and linear sources on air quality in their immediate neighborhood. In contrast to the RIO interpolation method, the IFDM model does not rely on direct measurements but evaluates atmospheric pollutant concentrations based on emission data and meteorological information such as wind speed, wind direction, and temperature. The IFDM model computations cover over 1.3 million points across Belgium, including traffic routes and areas near industrial sources, offering a superior spatial resolution assessment of air quality.

One notable drawback of the model lies in its 'open-street' design, which overlooks the presence of physical barriers (e.q.,trees and buildings alongside roadways) as well as the roadways' topographical features, in its traffic impact assessments. Consequently, in urban environments where narrow passages and heavy traffic predominate, known as "street canyons", there is a propensity for the RIO-IFDM model to deliver lower estimates of pollutant levels.

"To address inaccuracies in modeling 'street canyons,' the OSPM, which accounts for the specific layout of streets, has been integrated into the RIO-IFDM framework—now dubbed ATMO-Street (RIO-IFDM-OSPM). This enhancement allows for more precise calculations by the OSPM for each identified street canyon, taking into account the restricted dispersion of air pollutants in these narrow urban spaces."

C.2 Forecasting model

Forecasting models play a pivotal role in predicting air quality and identifying potential pollution events. These models leverage meteorological data, emissions inventories, and chemical transformation processes to forecast the concentrations of various pollutants across different spatial and temporal scales. In Belgium, the forefront of operational air quality forecasting is marked by the utilization of the CHIMERE model.

CHIMERE, an Eulerian chemistry-transport model is instrumental in operational air quality predictions managed by CELINE, described in Section C.1. Since 2005, CHIMERE has been generating daily forecast maps available on the CELINE website, covering a continuous monitoring array of pollutants such as O3, PM10, NO_2, and SO2. This model is integral to predicting pollution scenarios and, consequently, informs the decision-making process for implementing regional action plans. Described by irCELINE as a deterministic model, CHIMERE simulates the physico-chemical processes in the atmosphere, incorporating meteorological forecasts, ambient air pollutant emissions, and land use data. The model operates with a spatial resolution of approximately 50x50 km^2, a scale that emphasizes the importance of CHIMERE in assessing air quality over large areas, despite the potential for significant local variations near traffic and industrial sources.

D Meteorological and dispersion site parameters used for SIRANE

Table 22: Meteorological and dispersion site parameters used for SIRANE

Parameters	Dispersion site (BCR)	Meteorological measurement site
Aerodynamic roughness [m]	0.9	1.5
Displacement height [m]	13.0	15.0
Albedo [-]	0.275	0.275
Emissivity [-]	0.980	0.980
Priestley-Taylor coefficient [-]	1.00	1.12
Latitude [deg]	50.833	/
Wind measurement height [m]	/	27.0

E SIRANE inputs

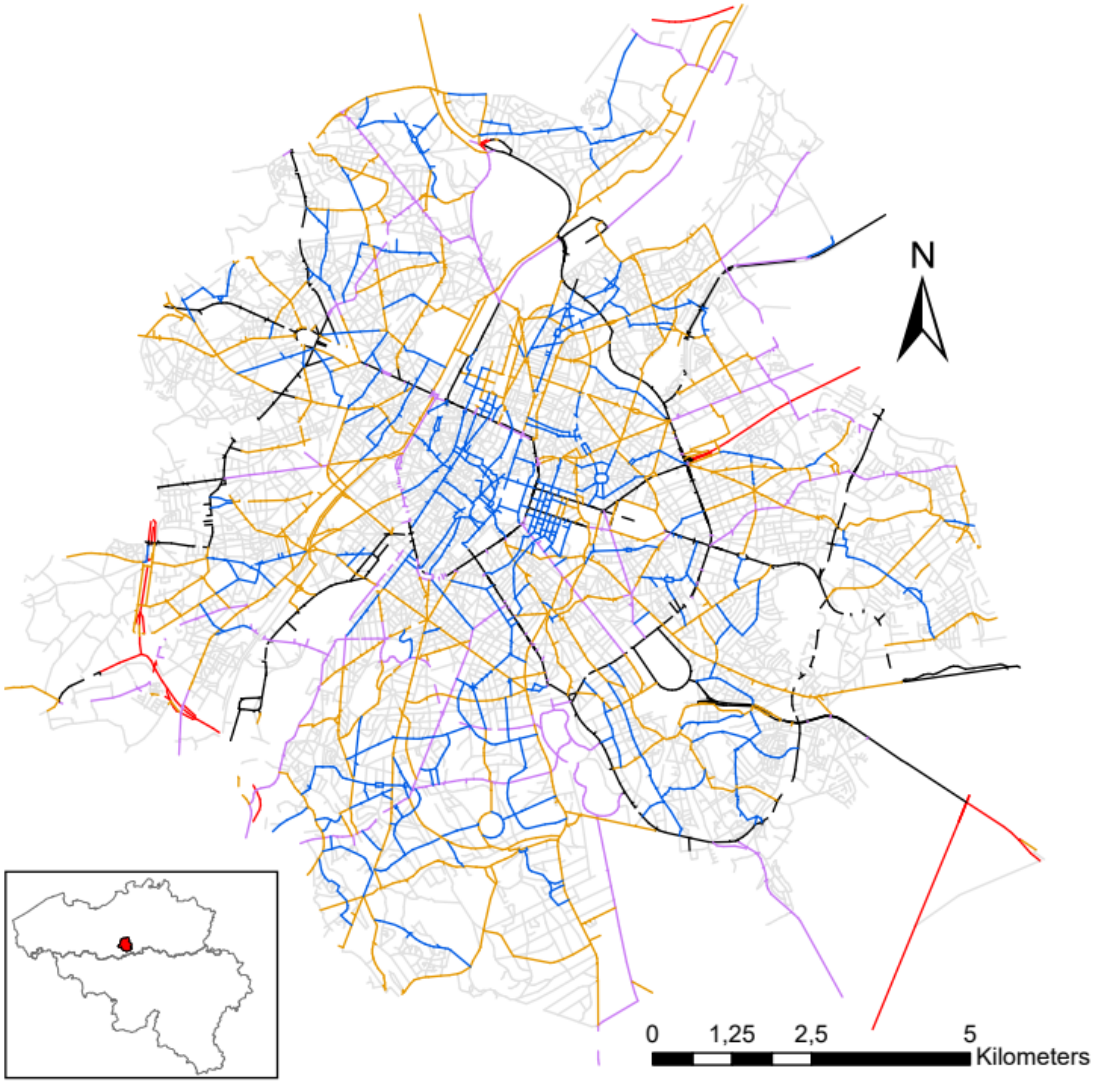

Figure E.1: Representation of the road hierarchies used in MuSti on the street network.
A0: Red A1: Black A2: Purple A3: Orange A4: Blue A5: Grey

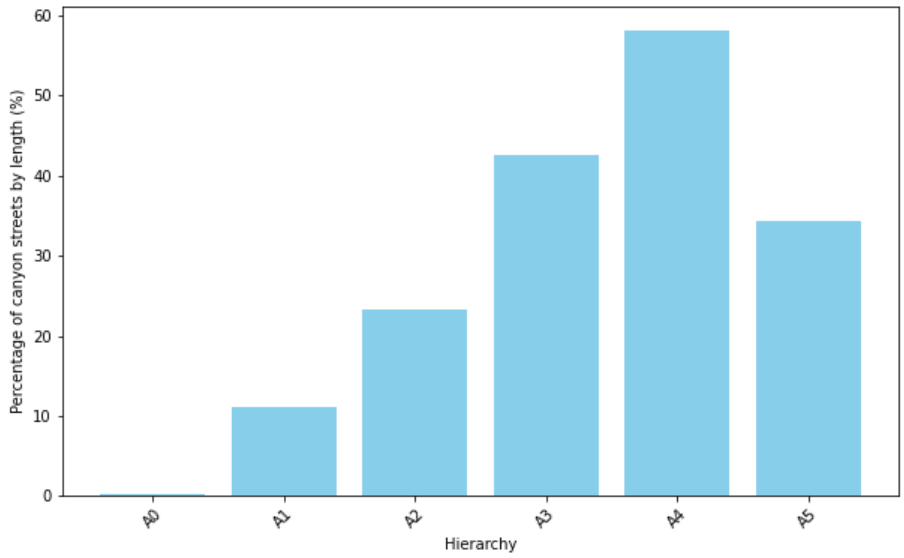

Figure E.2: Percentage of canyon street length compared to the total length within each road hierarchy

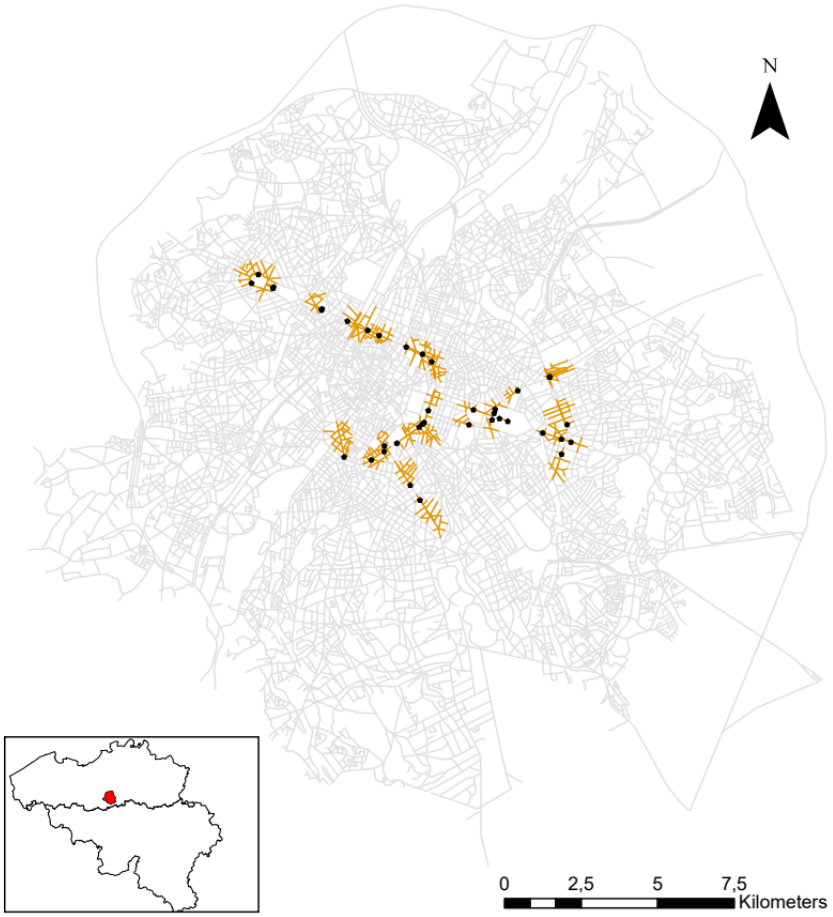

Figure E.3: Representation of tunnels (black dots) used as a point source of emissions by SIRANE. Streets in orange are overestimated by the pollution plume at the tunnel exit.

F MQI$_h$ equations

The Root Mean Squared Error (RMSE) $[\mu g/m^3]$ is calculated as follows (eq. 26):

$$RMSE = \sqrt{\frac{1}{N}\sum_{i=1}^{N}(O_i - M_i)^2} \tag{26}$$

where O_i $[\mu g/m^3]$ and M_i $[\mu g/m^3]$, represent the observed (measured) and modeled concentrations, respectively, at the i-th hour, and N [-] is the total number of hours.

The uncertainty of measurement at each hour, $U(O_i)$ $[\mu g/m^3]$, is calculated as follows (eq. 27):

$$U(O_i) = U_r(RV)\sqrt{(1-\alpha^2)O_i^2 + \alpha^2 RV^2} \tag{27}$$

where $U_r(RV)$ $[-]$ is the relative uncertainty associated with a reference value RV $[\mu g/m^3]$, and α $[-]$ is the fraction of the uncertainty that is independent of the measured concentration O.

The Root Mean Squared Uncertainty (RMS_u) $[\mu g/m^3]$ is given by (eq. 28):

$$RMS_U = \sqrt{\frac{\sum_{i=1}^{N} U(O_i)^2}{N}} \tag{28}$$

The Model Quality Indicator for hourly data (MQI_h) [-] is calculated using the equation (eq. 29):

$$MQI_h = \frac{RMSE}{\beta \cdot RMS_U} \tag{29}$$

Where β is the scaling factor set arbitrarily at 2, implying that the allowed deviation between modeled and measured concentrations is twice the measurement uncertainty.

The 90th percentile of the Model Quality Indicator (MQI$_{90th}$) is calculated as specified in eq. 21, using the same parameters as for MQI$_y$. The Model Quality Objective (MQO) is met when $MQI_{90th} \leq 1$.

G Projection of emissions for all the sectors - WAM scenario

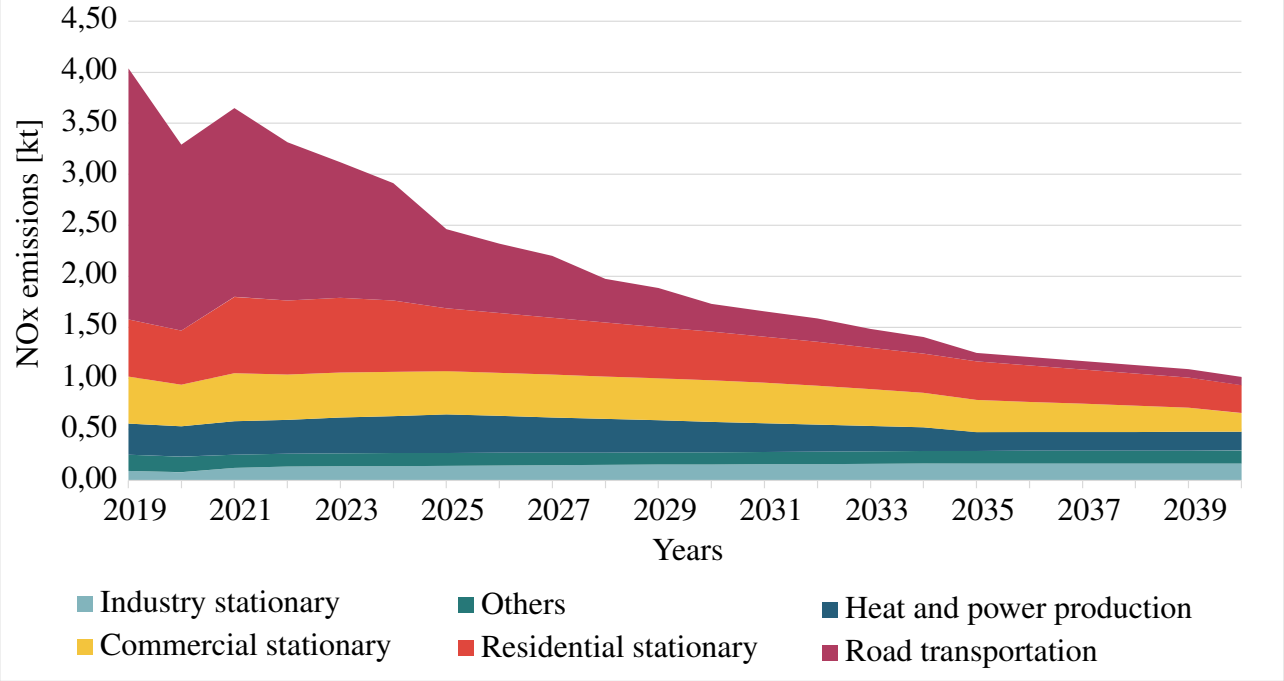

Figure G.1: NOx emissions for the WAM Projection. Data source: [12]

H Fuel Type Projections

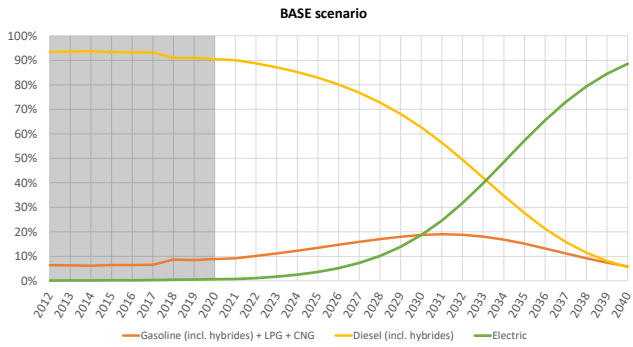

(a) BASE

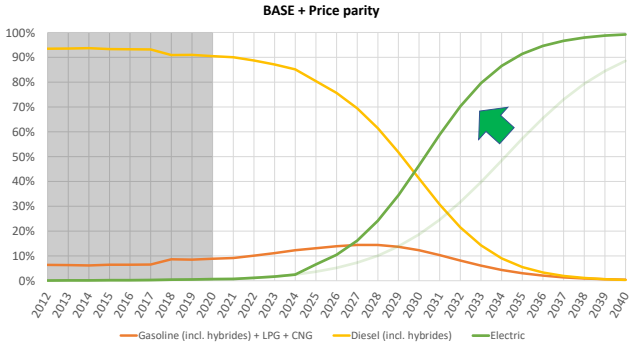

(b) BASE + Price Parity

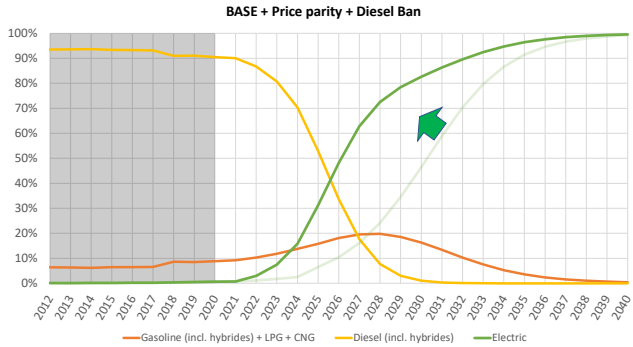

(c) BASE + Price Parity + Diesel Ban

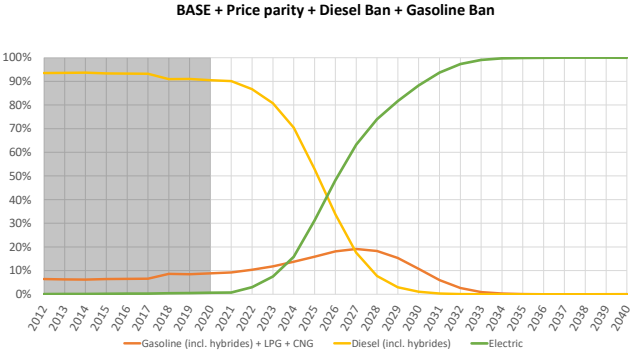

(d) BASE + Price Parity + Diesel Ban + Petrol Ban

Figure H.1: Share of fuels in light and heavy duty vehicles across various scenarios. The light green curve represents outcomes from the preceding scenario, while the green arrow indicates the additional impact introduced by the subsequent scenario. The dark grey area is historical data, and the light grey area represents projections. Source: [13]

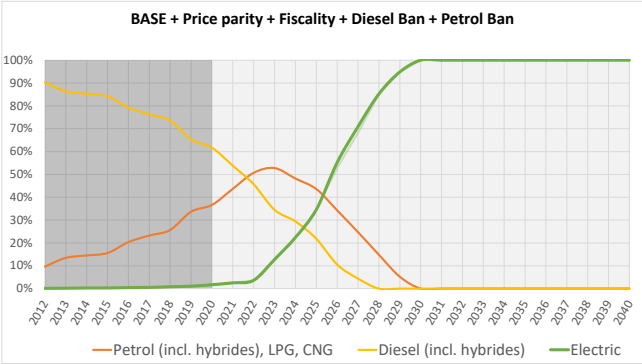

(a) BASE

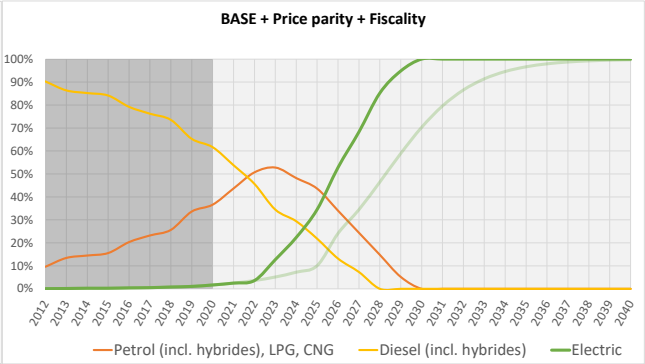

(b) BASE + Price Parity

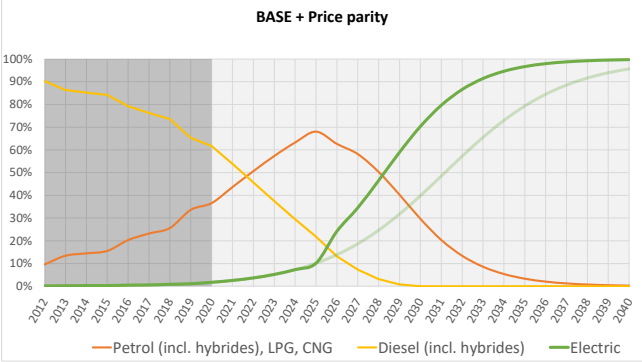

(c) BASE + Price Parity + Diesel Ban

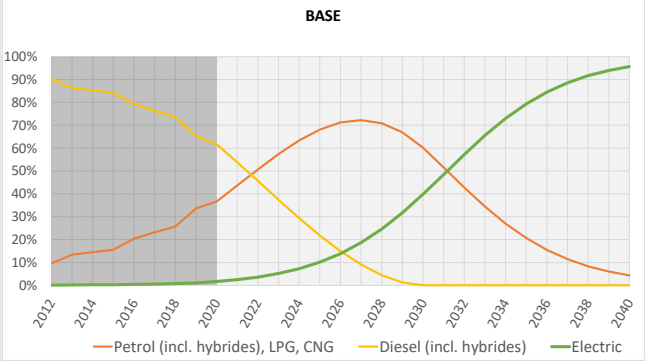

(d) BASE + Price Parity + Diesel Ban + Petrol Ban

Figure H.2: Share of fuels in company vehicles across various scenarios. The light green curve represents outcomes from the preceding scenario, while the green arrow indicates the additional impact introduced by the subsequent scenario. The dark grey area is historical data, and the light grey area represents projections. Source : [13]

I Road refinement

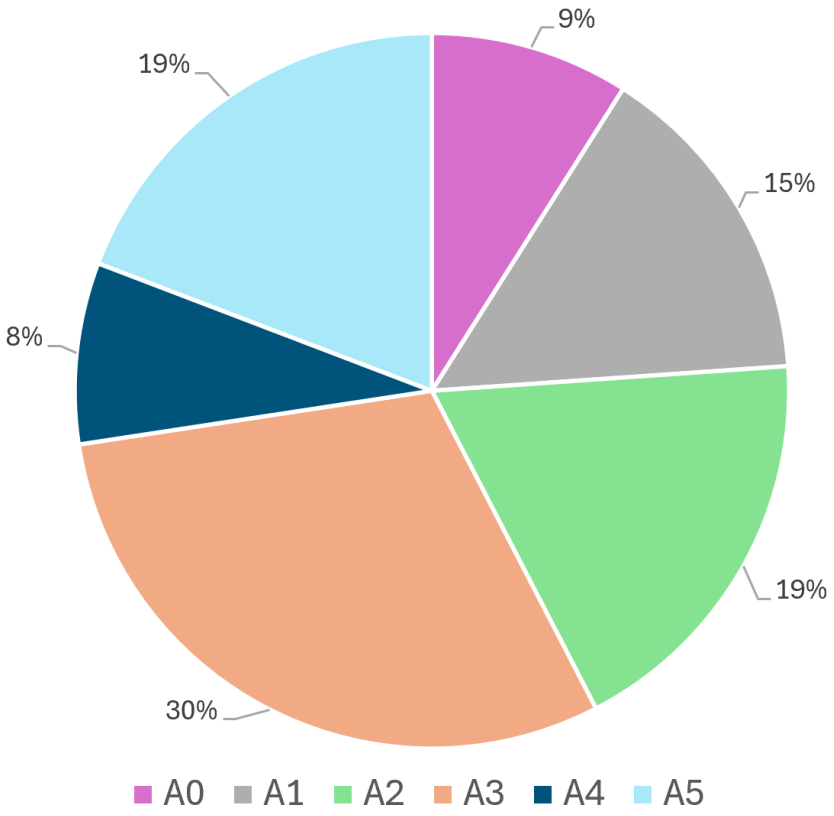

Figure I.1: Distribution of NOx emissions by type of road hierarchy after road refinement in 2022

J Calibration

Figure J.1 displays the density of modeled and measured NO2 concentrations in 2022. The concentration with the highest peak for each station represents the value most frequently recorded (yellow) or modeled by SIRANE (blue) throughout the year. Figure J.2 compares the average concentration modeled by SIRANE for hours when specific concentrations were measured. This does not reflect the density of concentrations; moreover, as the measured concentrations reach up to 100 µg/m³, there are relatively few hours corresponding to this range.

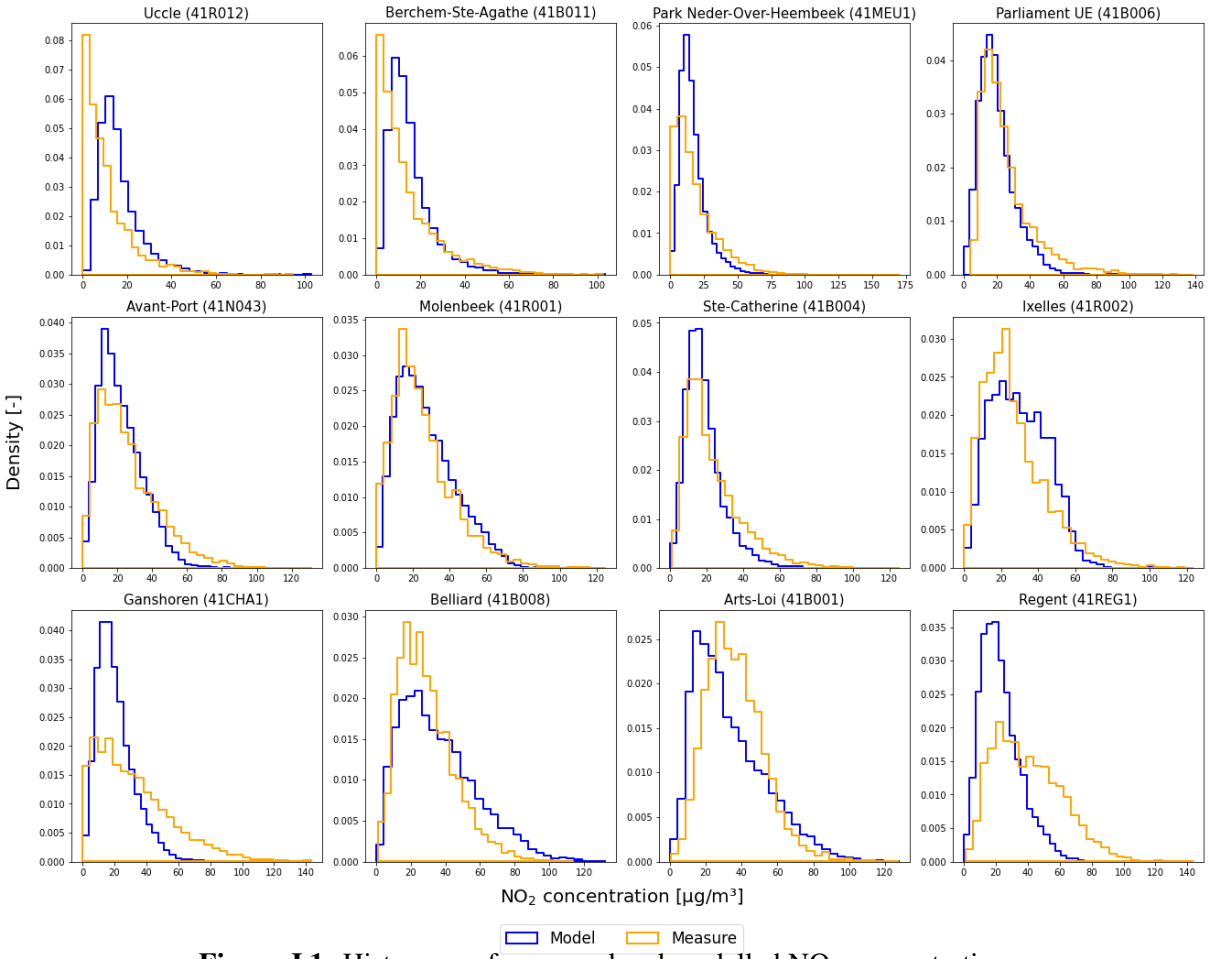

Figure J.1: Histogram of measured and modelled NO_2 concentrations

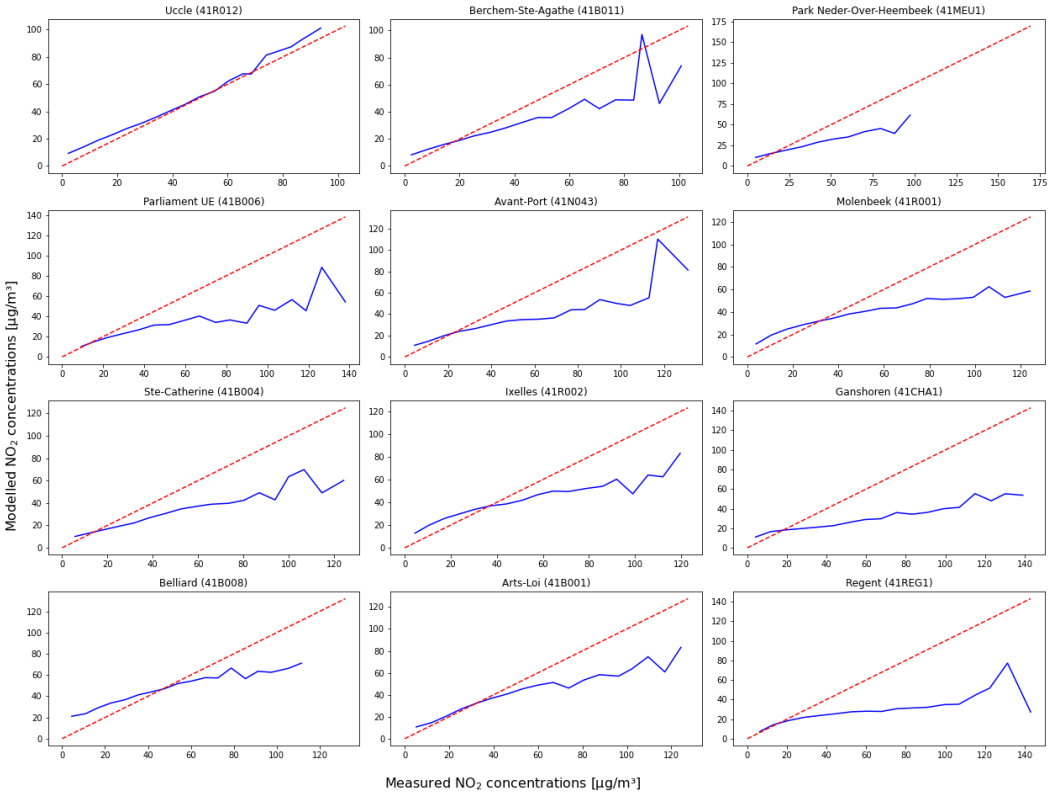

Figure J.2: Comparison of modeled vs. measured NO_2 concentrations in 2022. The dotted red line represents a perfect match between actual measurements and model prediction.

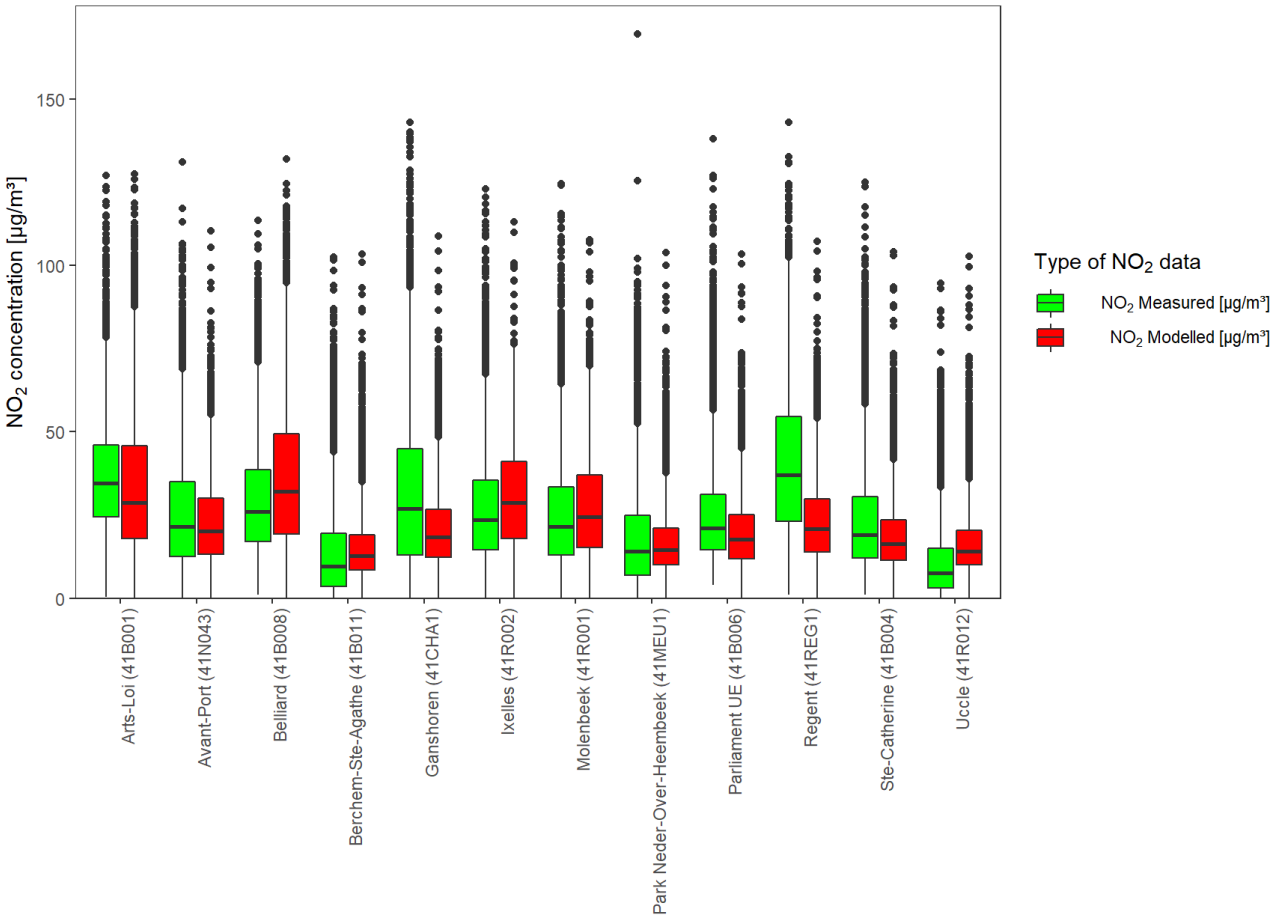

Figure J.3: Distribution of modelled and measured NO_2 concentration values using a box plot at each station in 2022

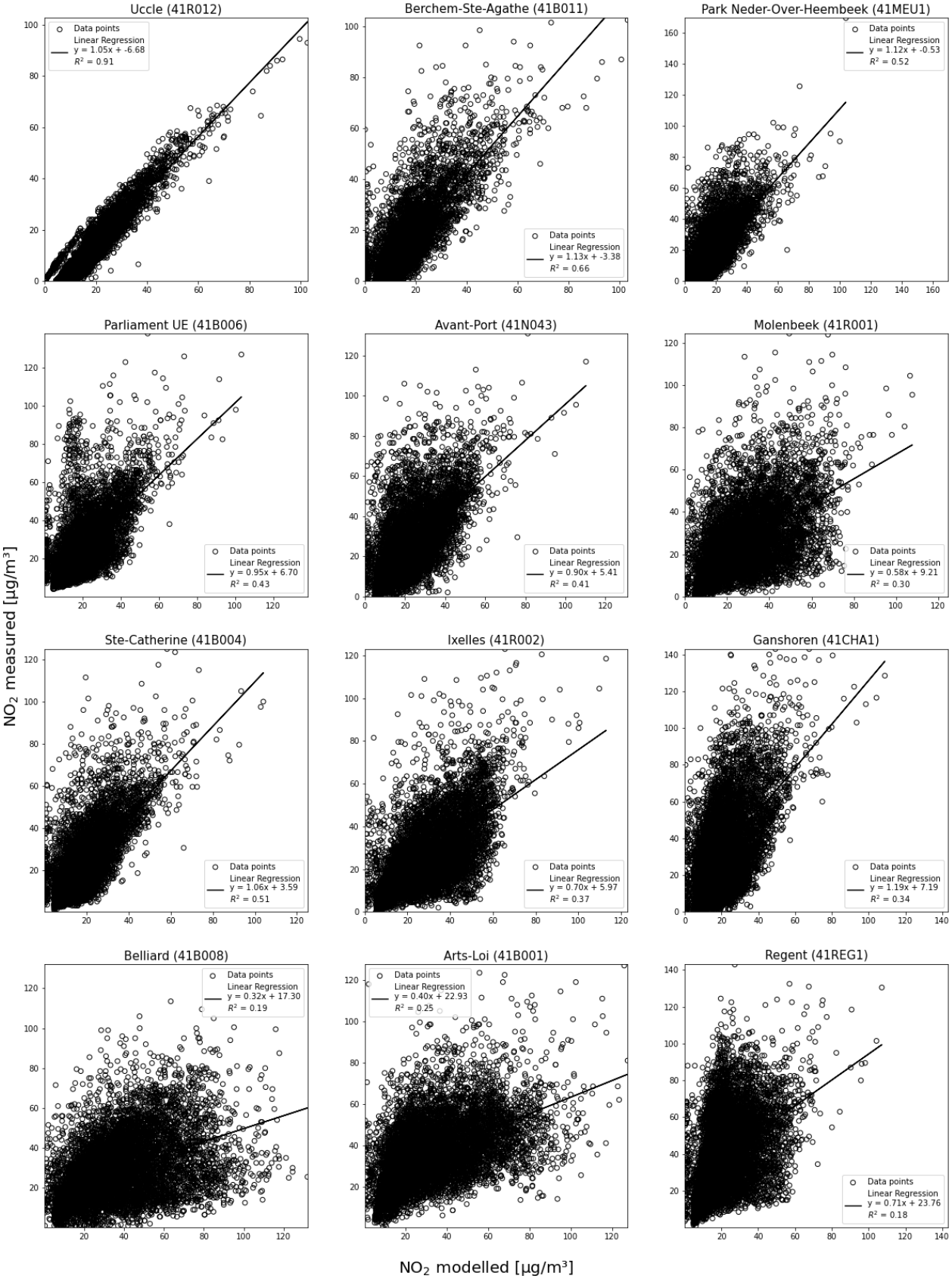

Figure J.4: Comparison of measured vs. modelled concentrations using linear regression for all stations

K Box plot of street segment concentrations for 2022, comparing BASE, WEM, and WAM scenarios with real data

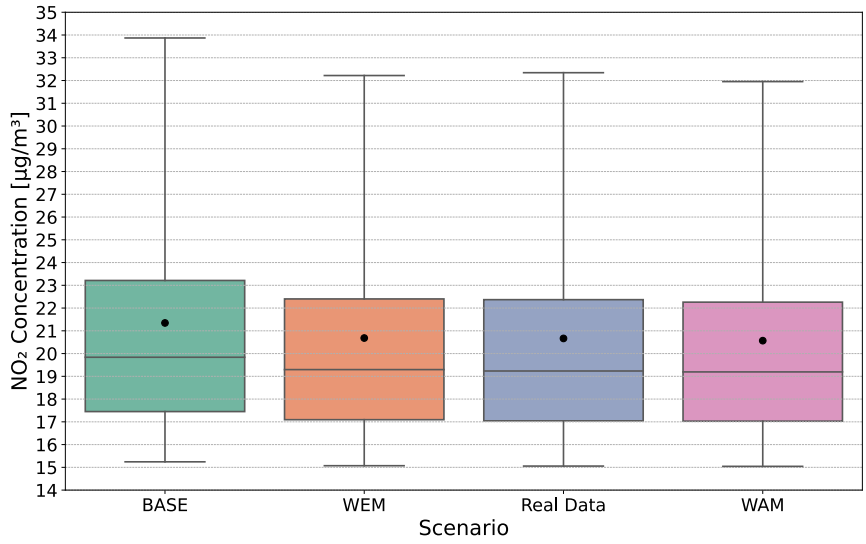

Figure K.1: Box plot of street segment concentrations for 2022, comparing BASE, WEM, and WAM scenarios with real data

Although the plot does not show the actual average concentrations (as the length of the segments varies), it aims to compare the different scenarios with real data. The BASE scenario shows the greatest deviation from the real data, generally overestimating concentrations. The differences between the WEM and WAM scenarios and the real data are minimal.

L Projected emissions of NO and NO_2 and their break down in different categories

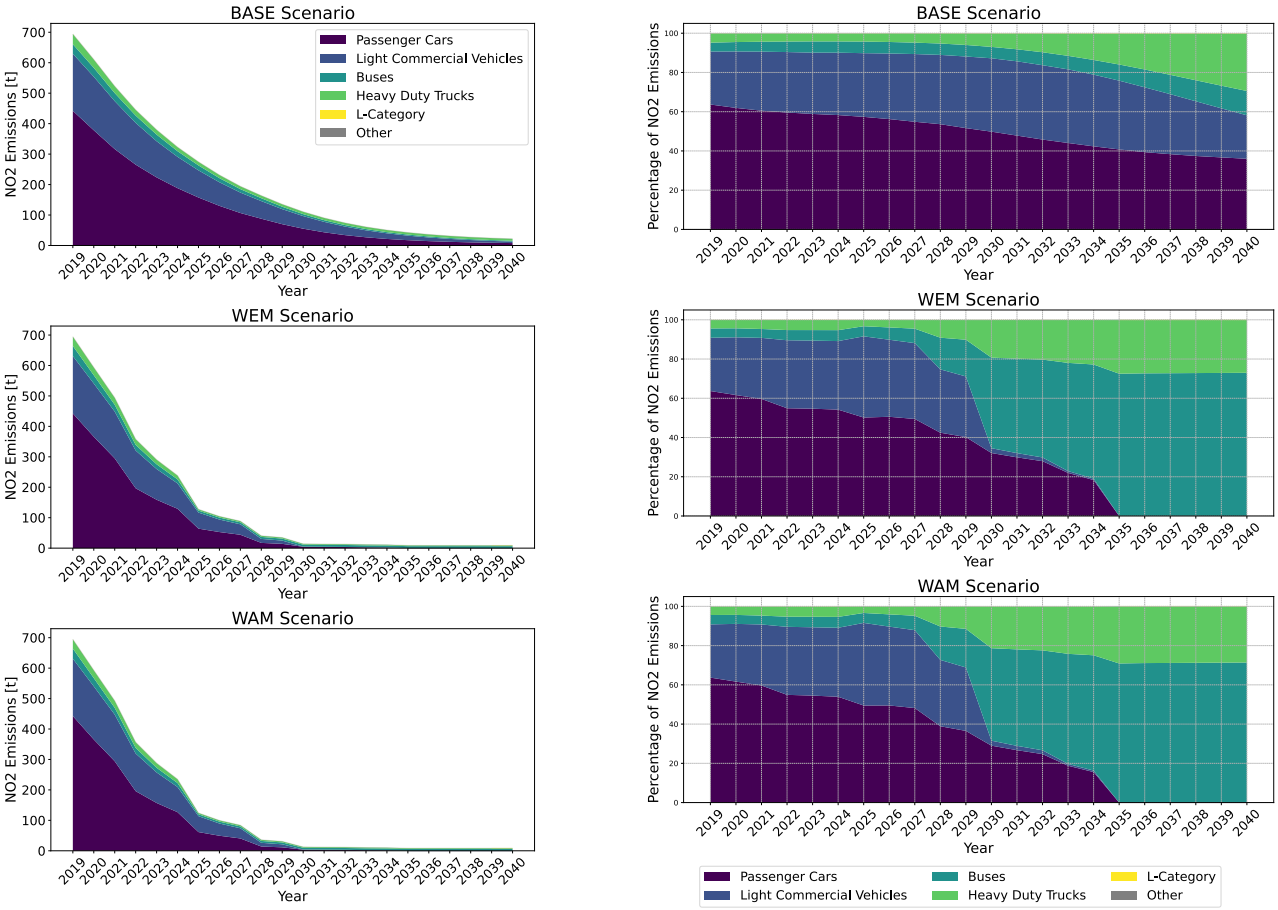

(a) NO_2 evolution

(b) NO_2 share by category

Figure L.1: NO_2 emissions projections in Brussels by vehicle type

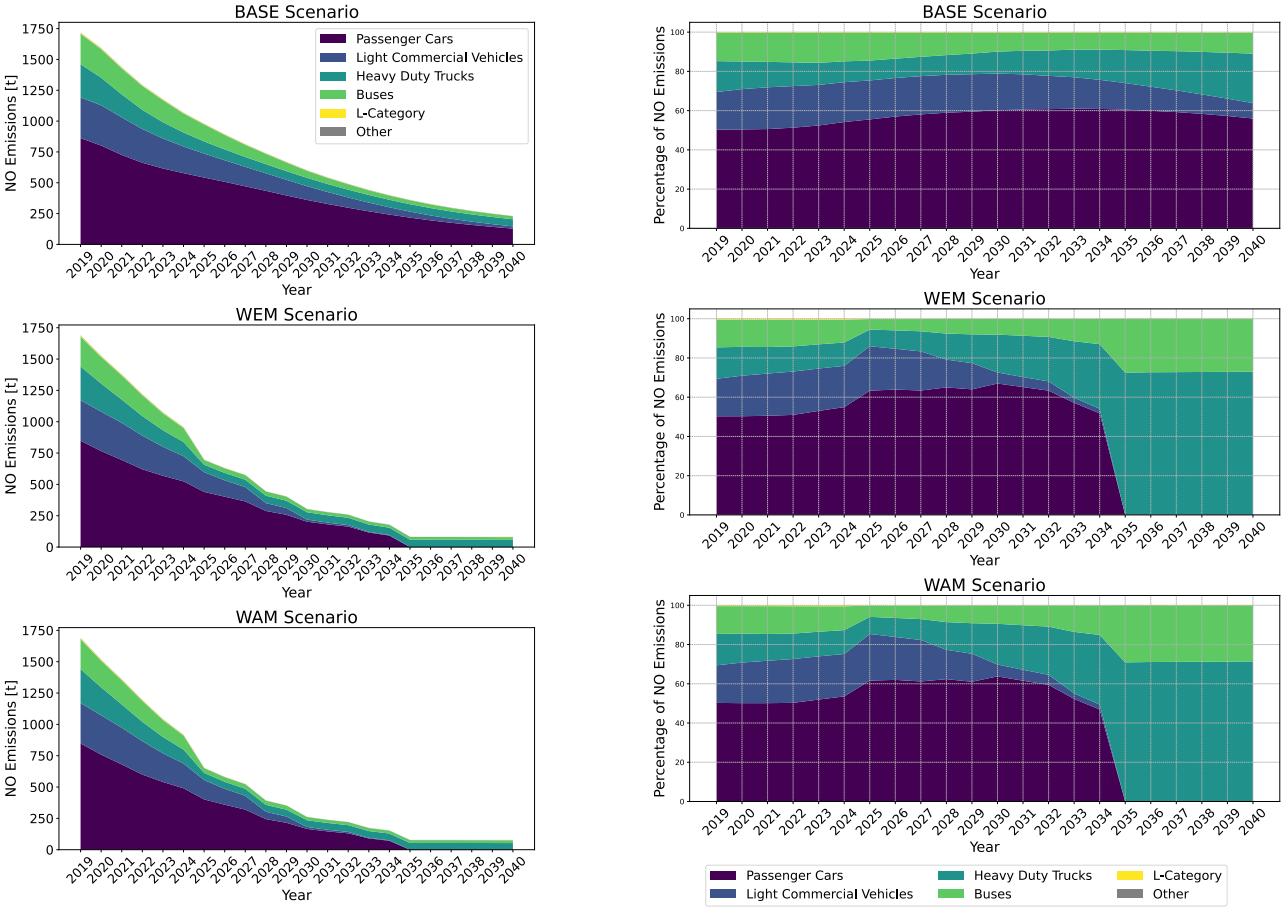

(a) NO evolution

(b) NO share by category

Figure L.2: NO emissions projections in brussels by vehicle type

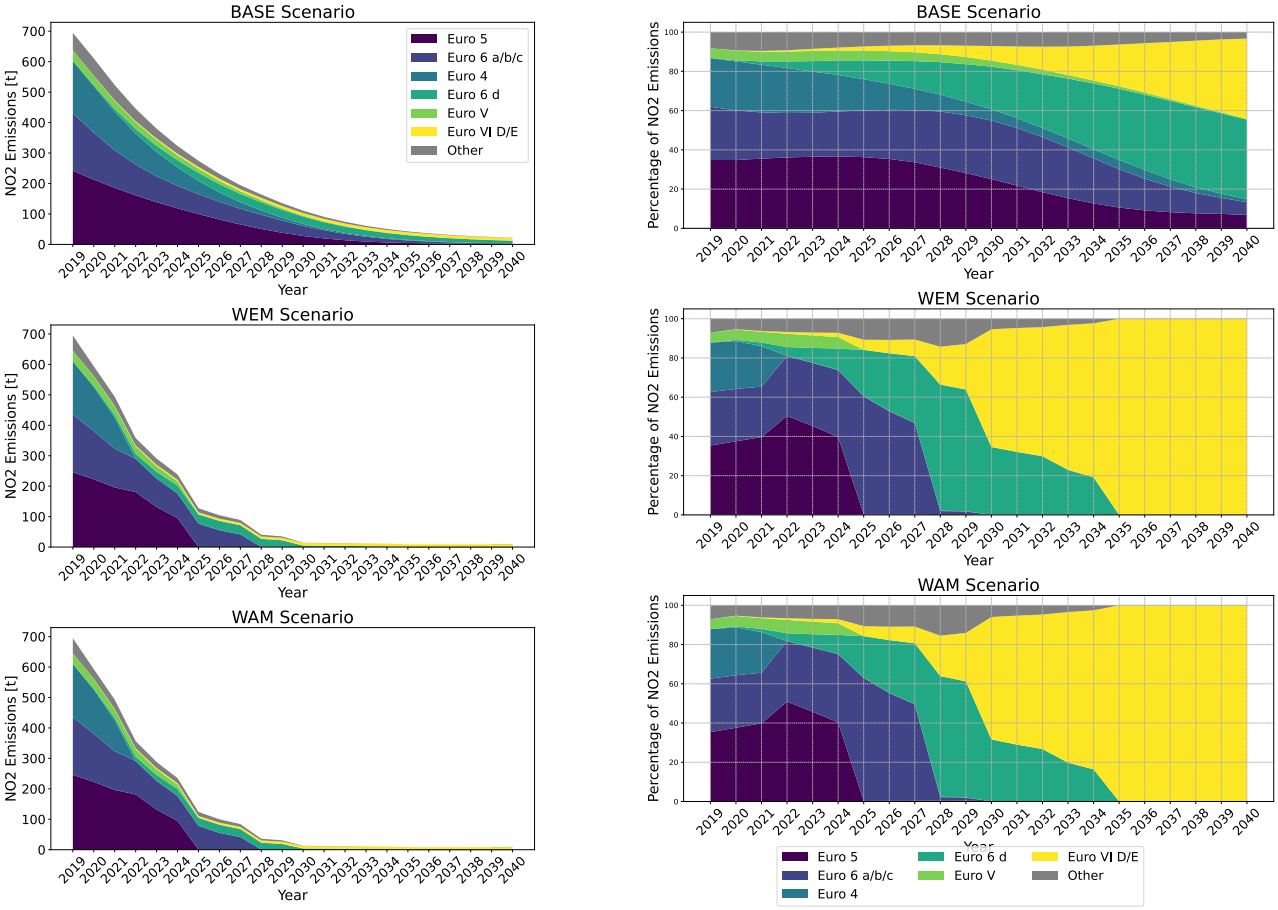

(a) NO_2 evolution

(b) Distribution of NO_2 Emissions by Euro Standard

Figure L.3: NO_2 emissions projections in Brussels by Euro standard

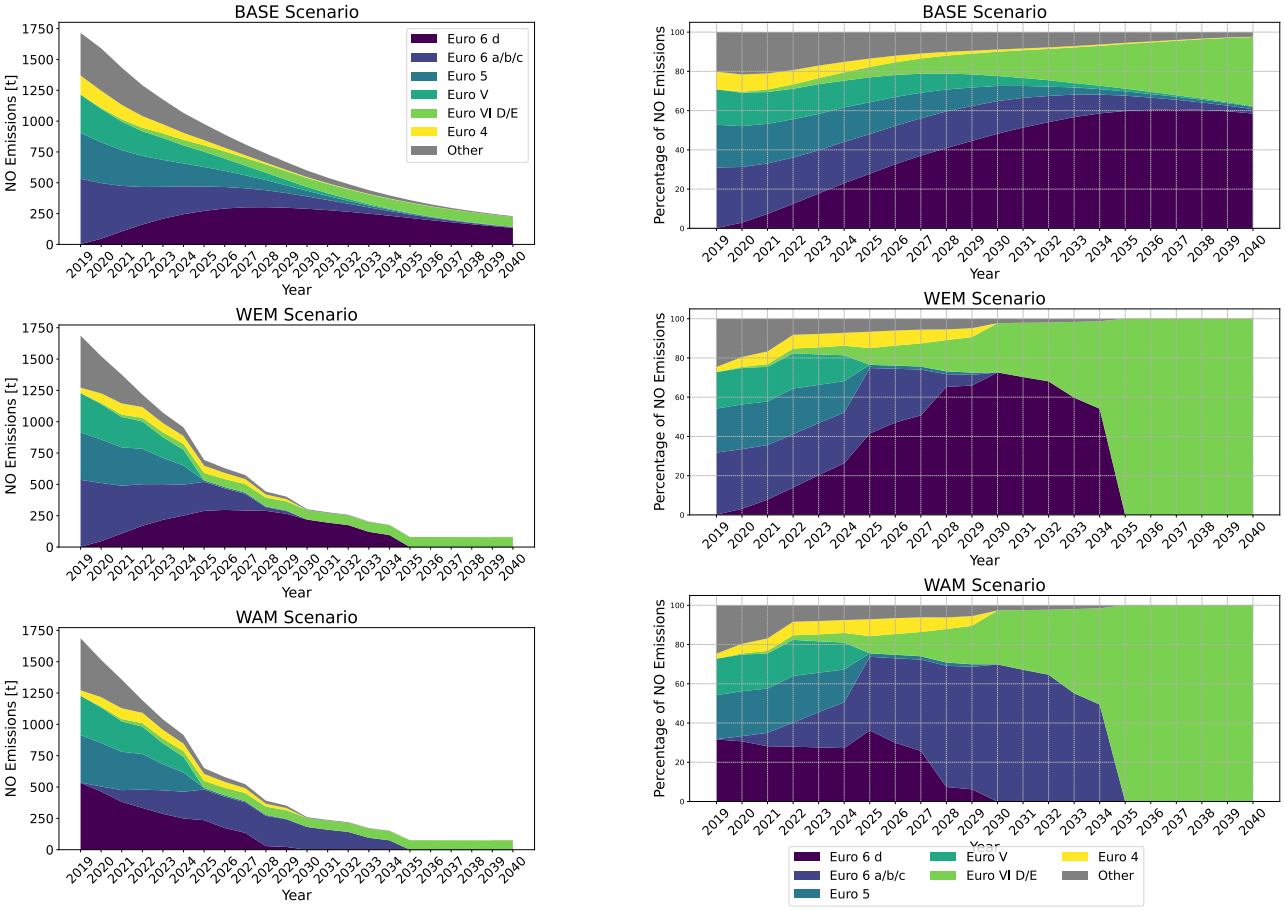

(a) NO evolution

(b) Distribution of NO Emissions by Euro Standard

Figure L.4: NO emissions projections in Brussels by Euro Standard

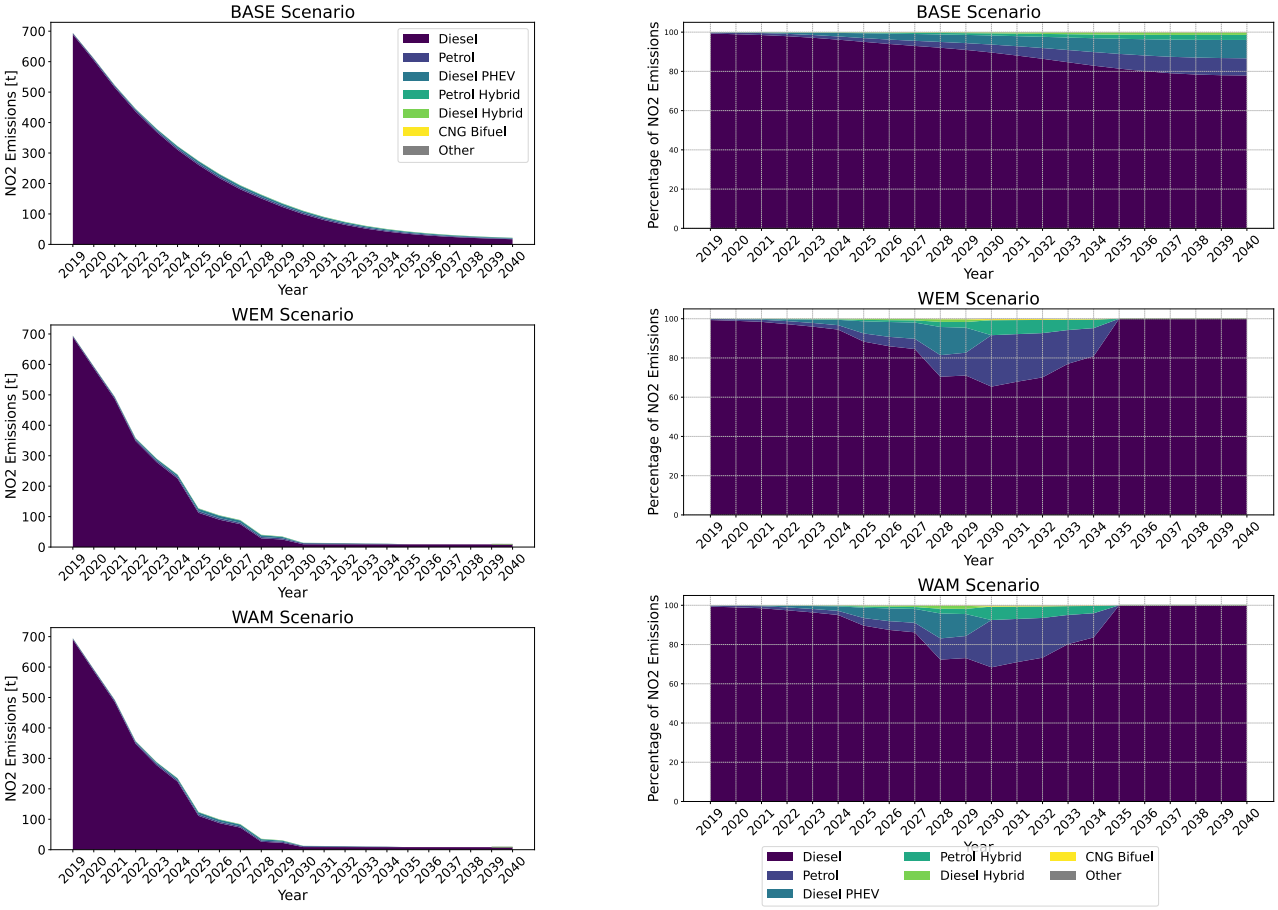

(a) NO_2 evolution

(b) Distribution of NO_2 Emissions by fuel type

Figure L.5: NO_2 emissions projections in Brussels by fuel type

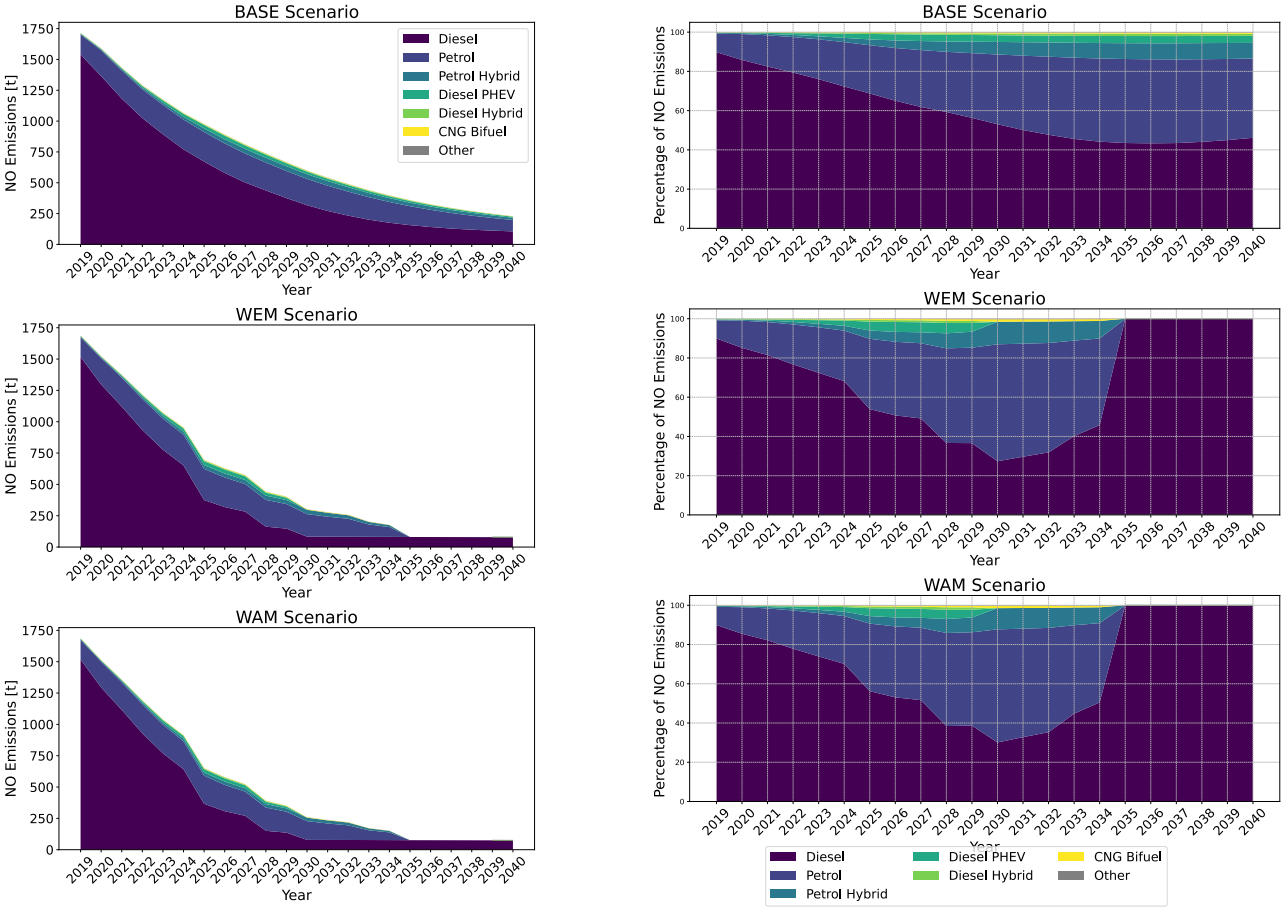

(a) NO evolution

(b) Distribution of NO Emissions by fuel type

Figure L.6: NO emissions projections in Brussels by fuel type

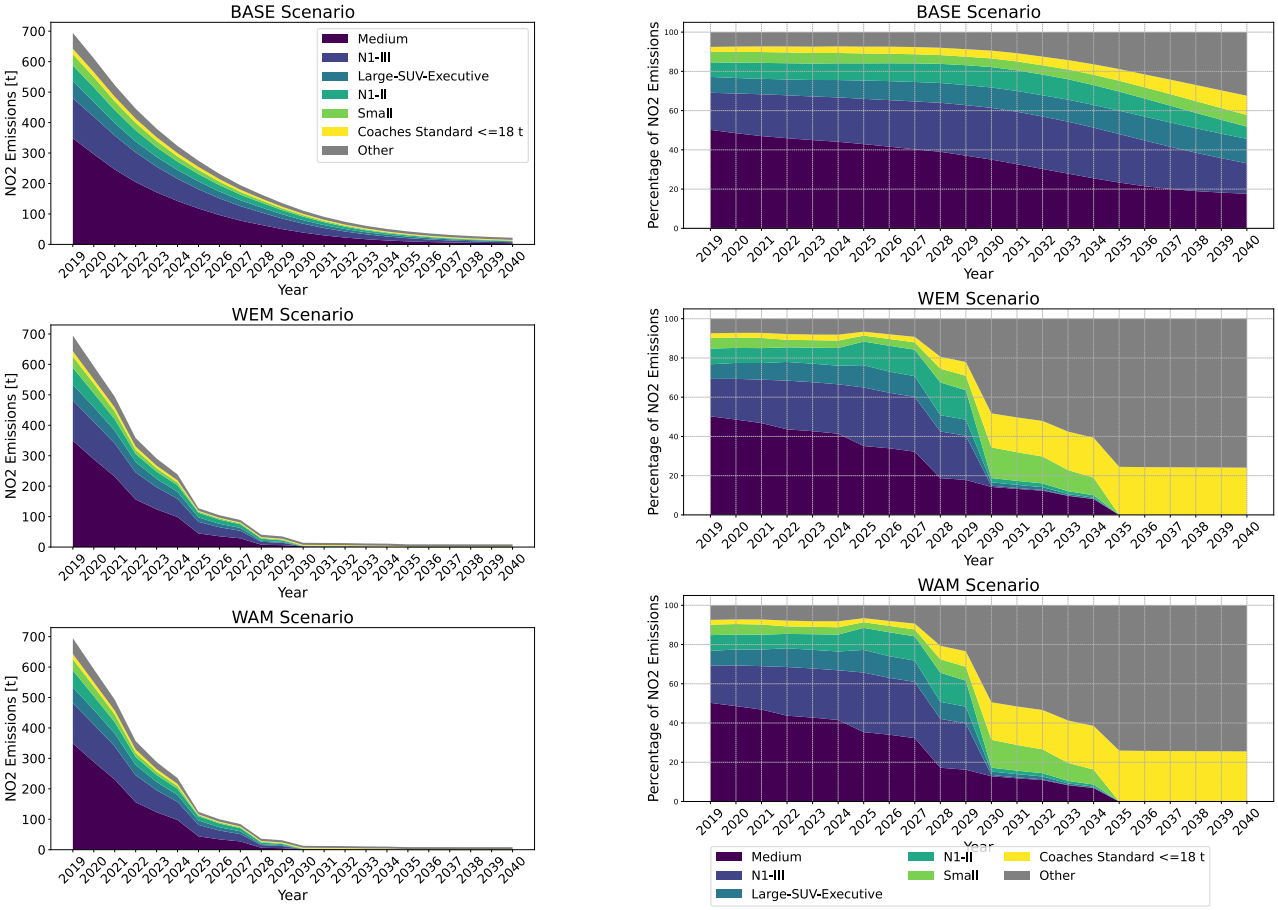

(a) NO_2 evolution

(b) Distribution of NO_2 Emissions by vehicle size

Figure L.7: NO_2 emissions projections in Brussels by vehicle size

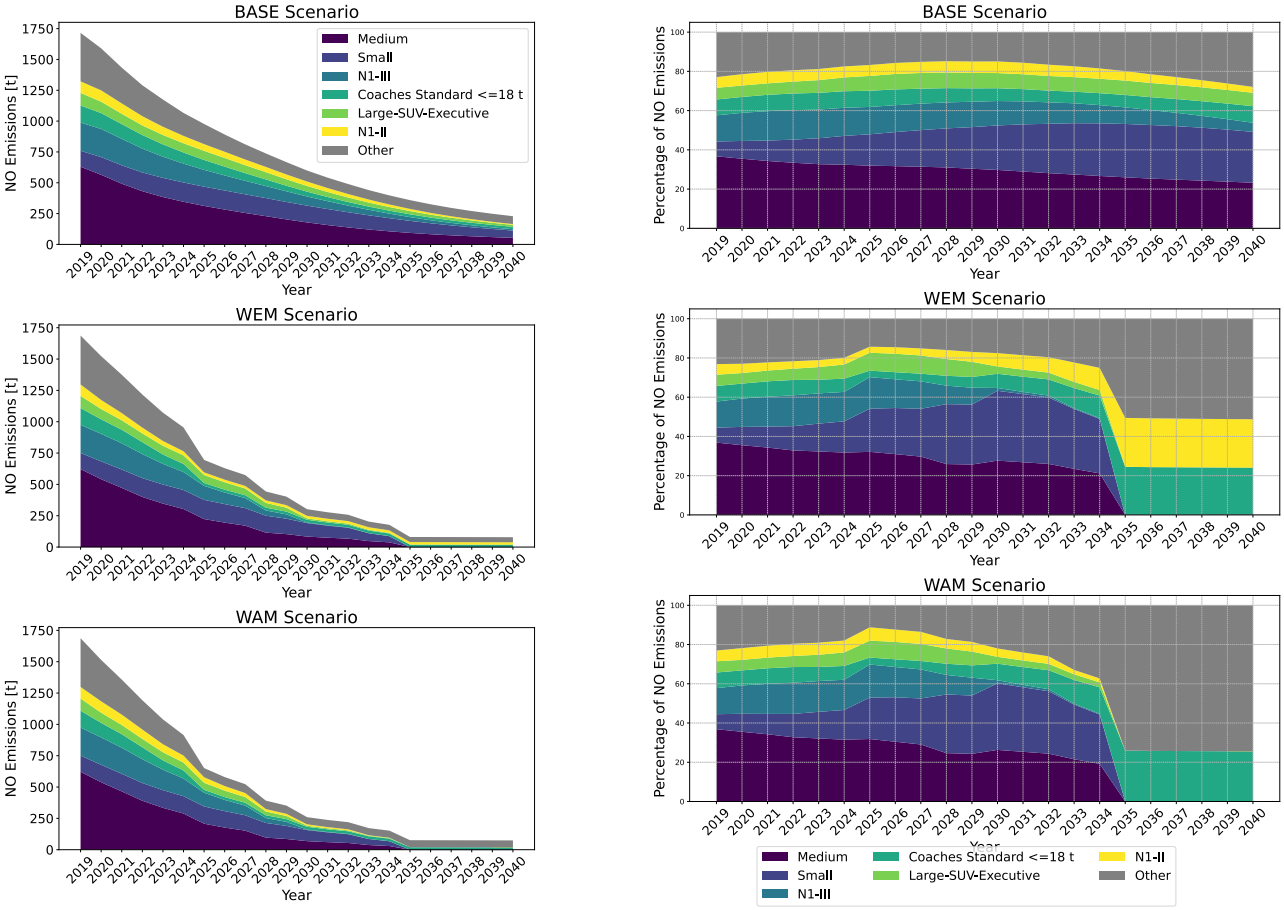

(a) NO evolution

(b) Distribution of NO Emissions by vehicle size

Figure L.8: NO emissions projections in Brussels by vehicle size

M Raw data excel

Click here to access the Excel file

N Comparison of NOx emissions and NO_2 concentrations projections

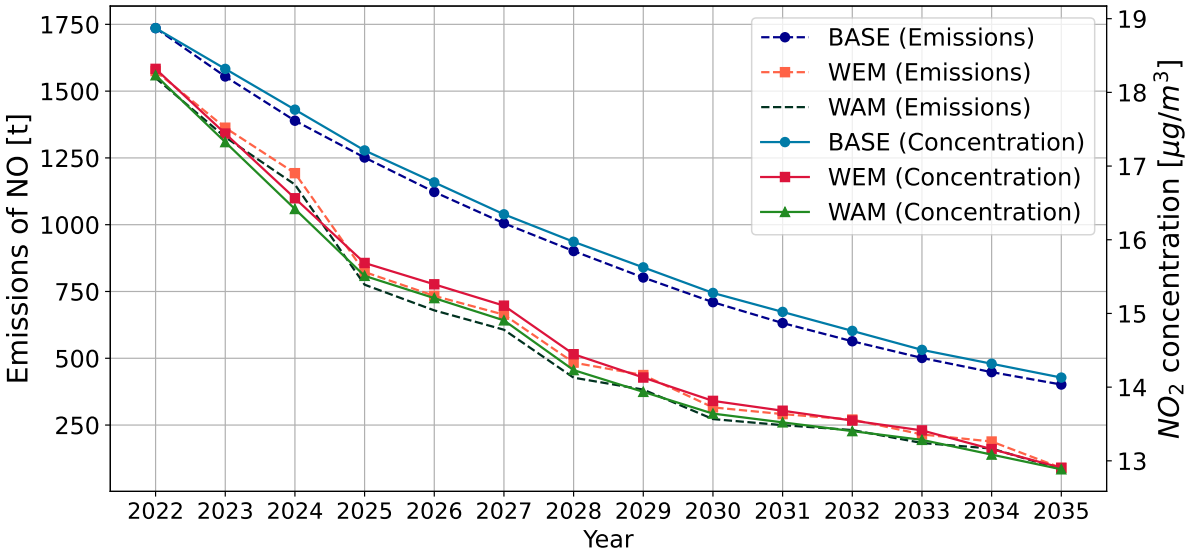

Figure N.1: NOx emissions vs NO_2 concentration comparisons between 2022 and 2035. Data source for NOx emissions: [12]

O Average concentration by road hierarchy

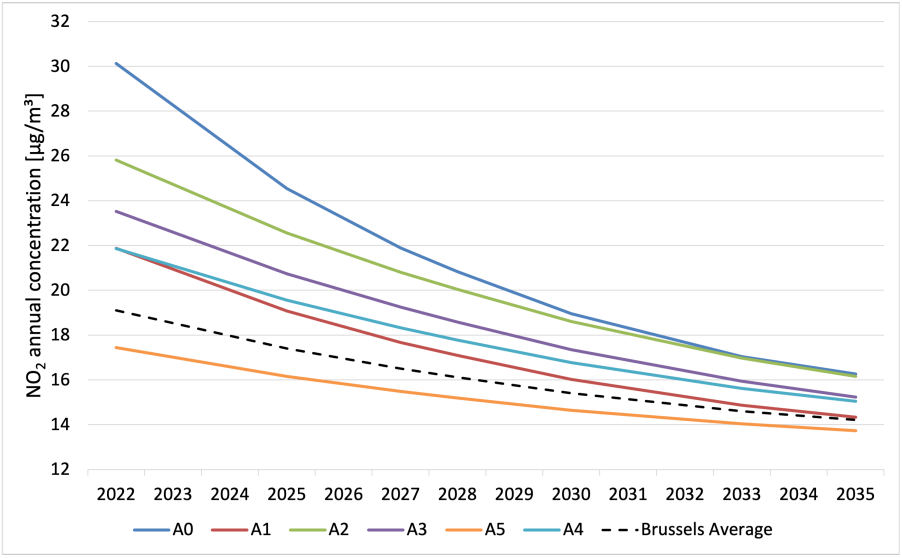

(a) BASE scenario

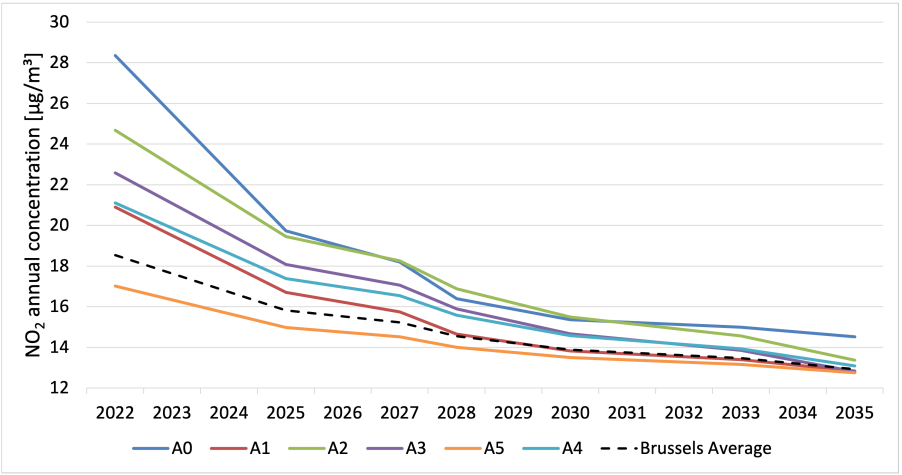

(b) WEM scenario

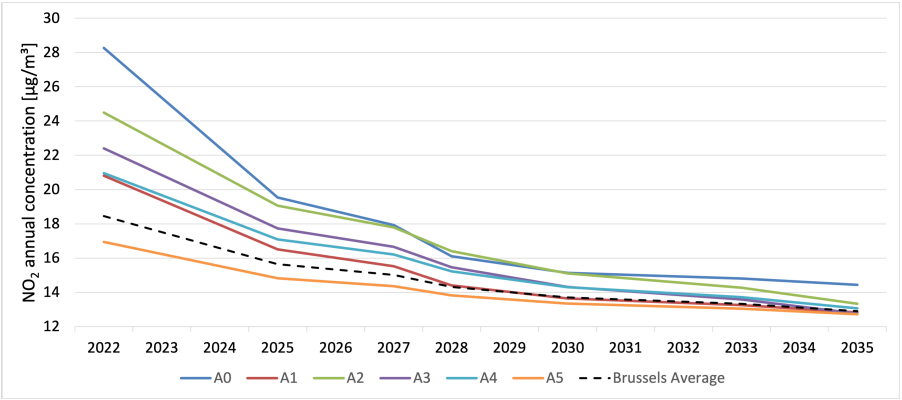

(c) WAM scenario

Figure O.1: Projections of annual NO_2 concentrations in Brussels by road hierarchy under BASE, WEM and WAM scenarios (2022-2035).

P NO_2 concentration trends over time according to different projections

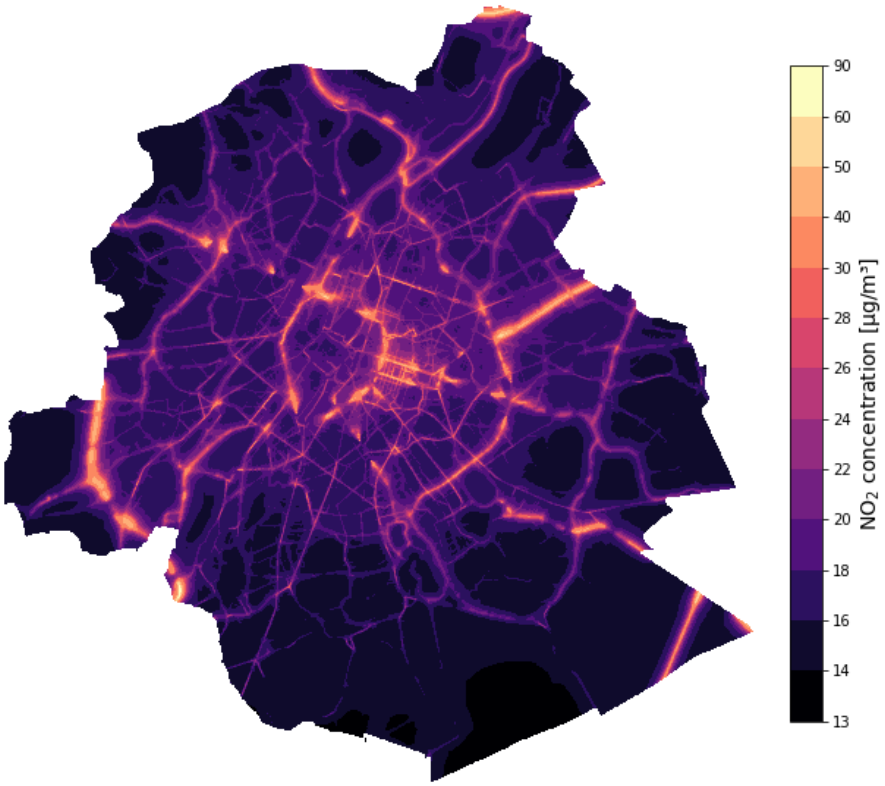

(a) Annual NO_2 concentration with no change in emission distribution between MusTi and Copert

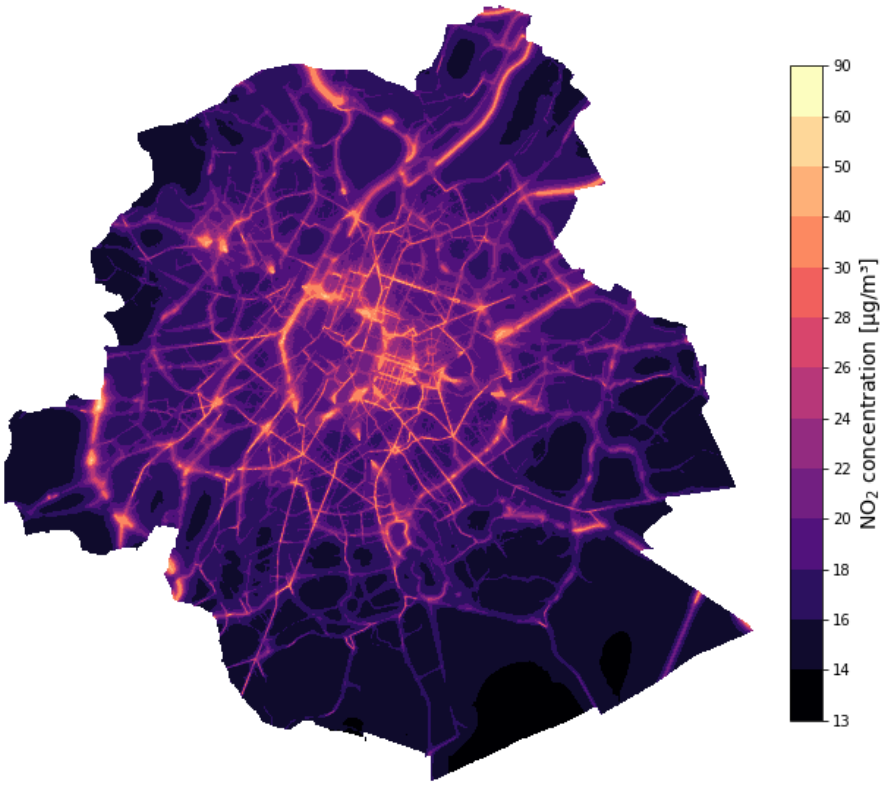

(b) Annual NO_2 concentration with change in emission distribution between MusTi and Copert

Figure P.1: Impact of the change in the distribution of emissions on the average annual NO_2 concentration based on the 2022 emissions inventory for Brussels.

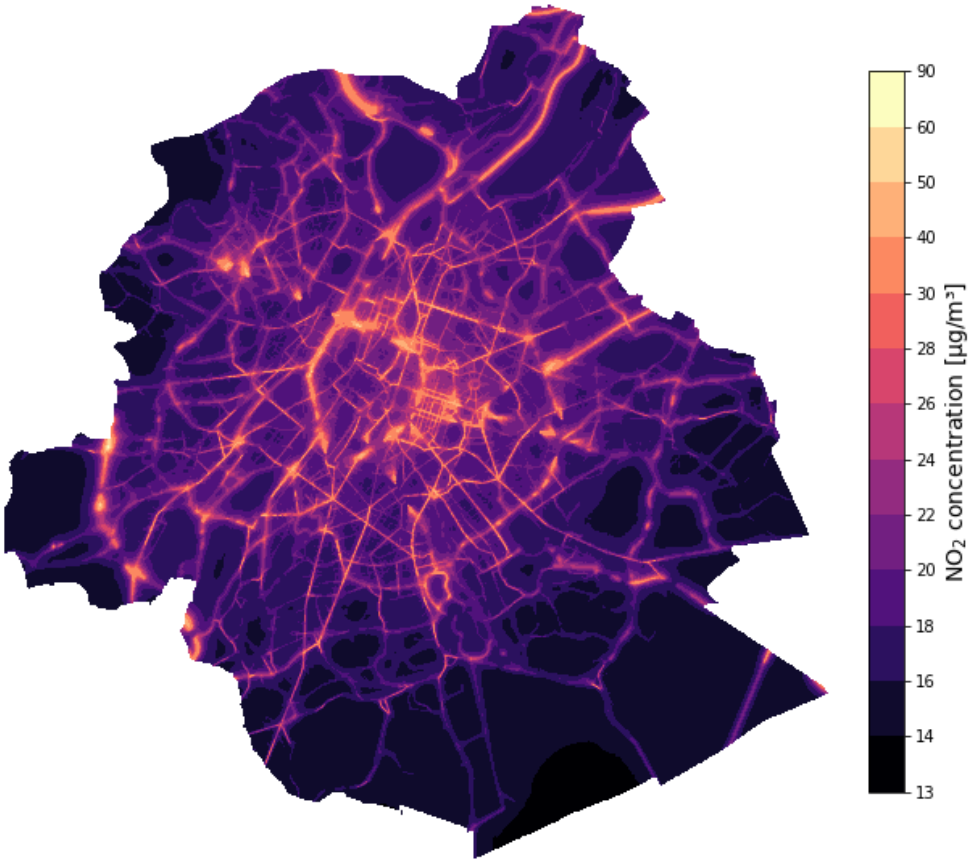

(a) 2022 BASE

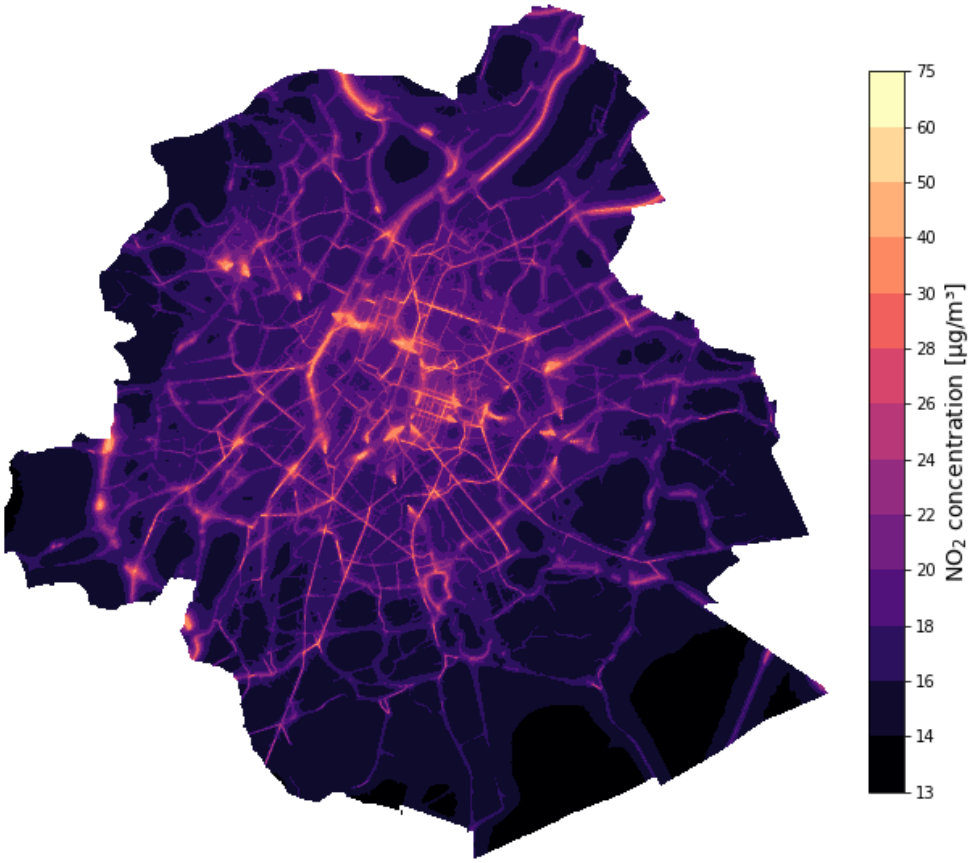

(b) 2025 BASE

Figure P.2: NO_2 concentration trends according to the BASE scenario for 2022, 2025, 2028, 2030, 2033 and 2035

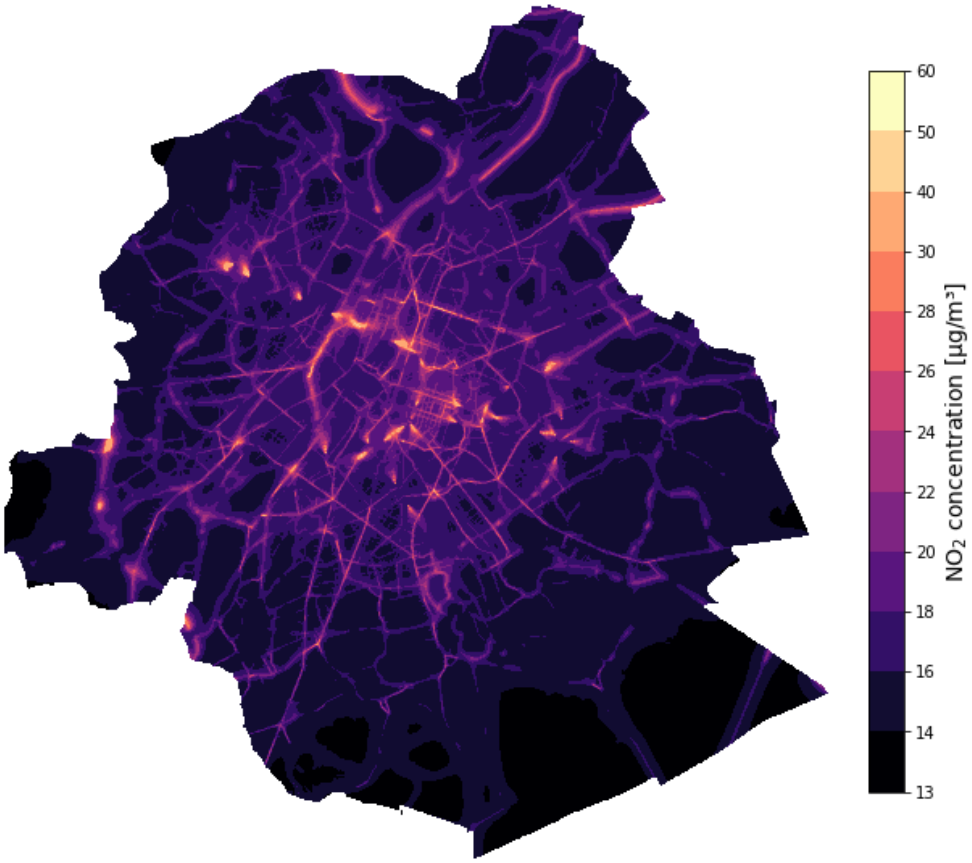

(c) 2028 BASE

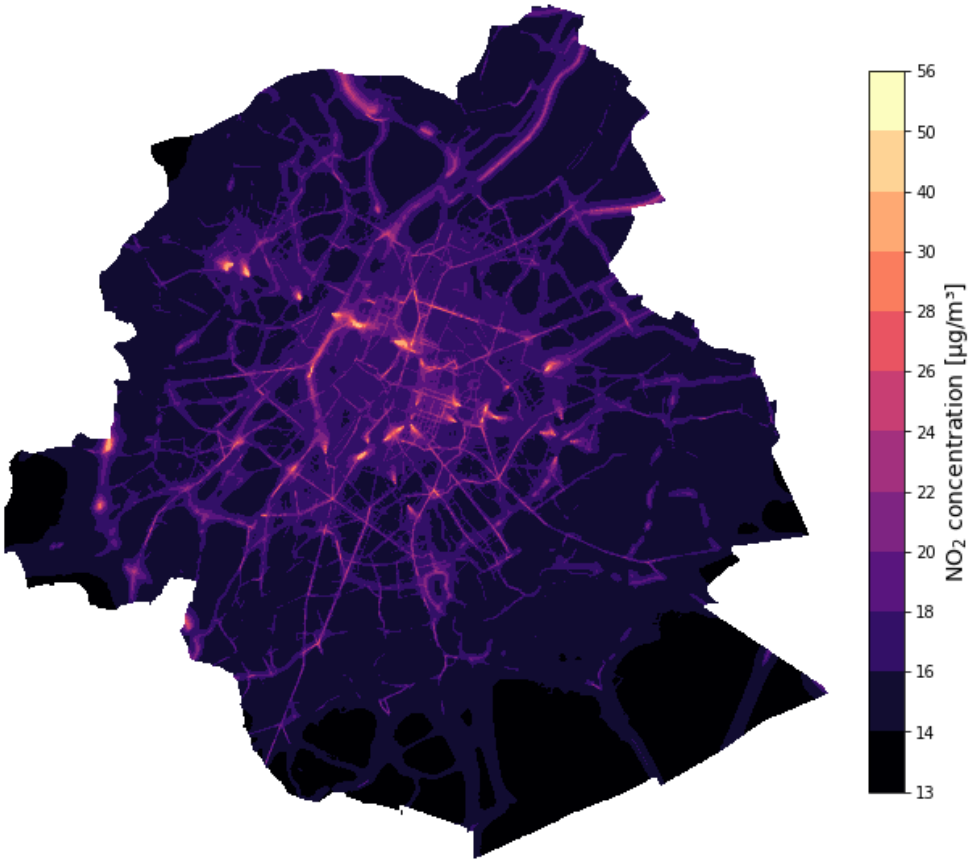

(d) 2030 BASE

Figure P.2: Continued

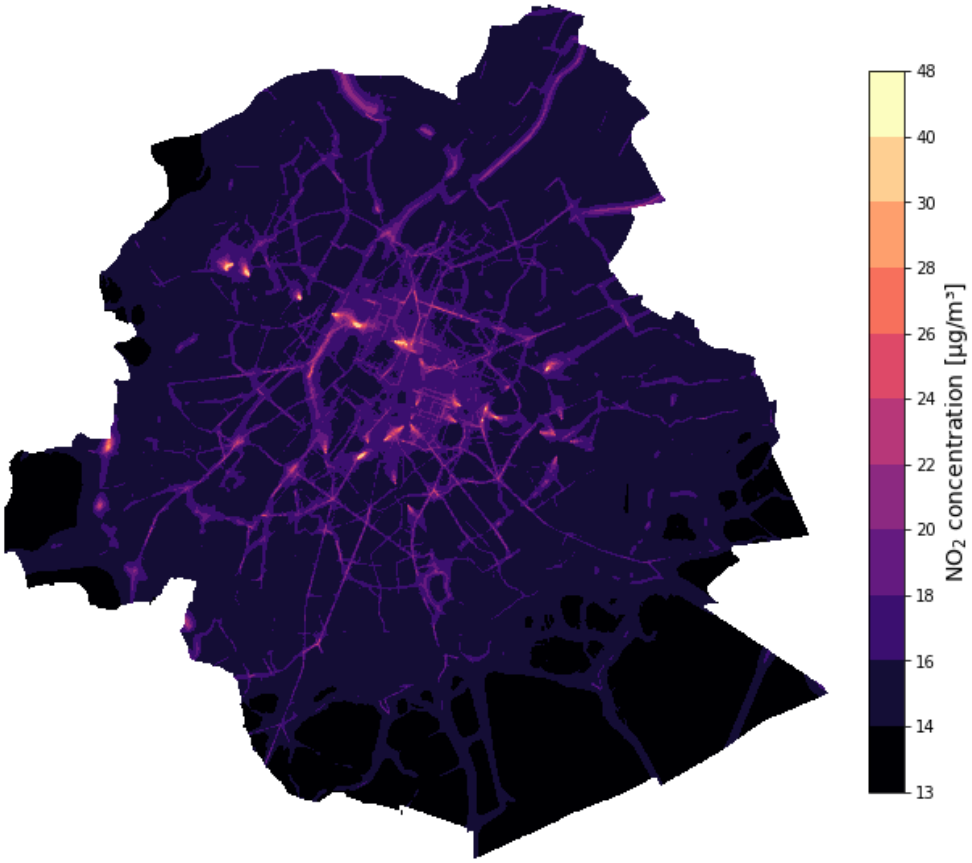

(e) 2033 BASE

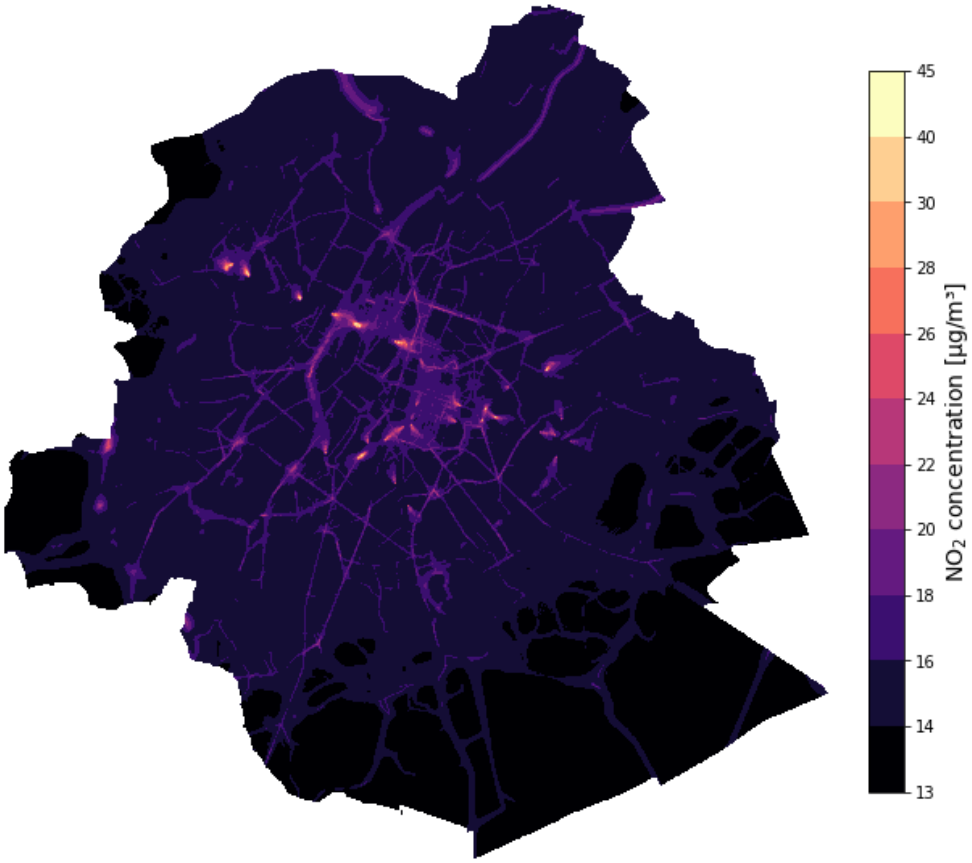

(f) 2035 BASE

Figure P.2: Continued

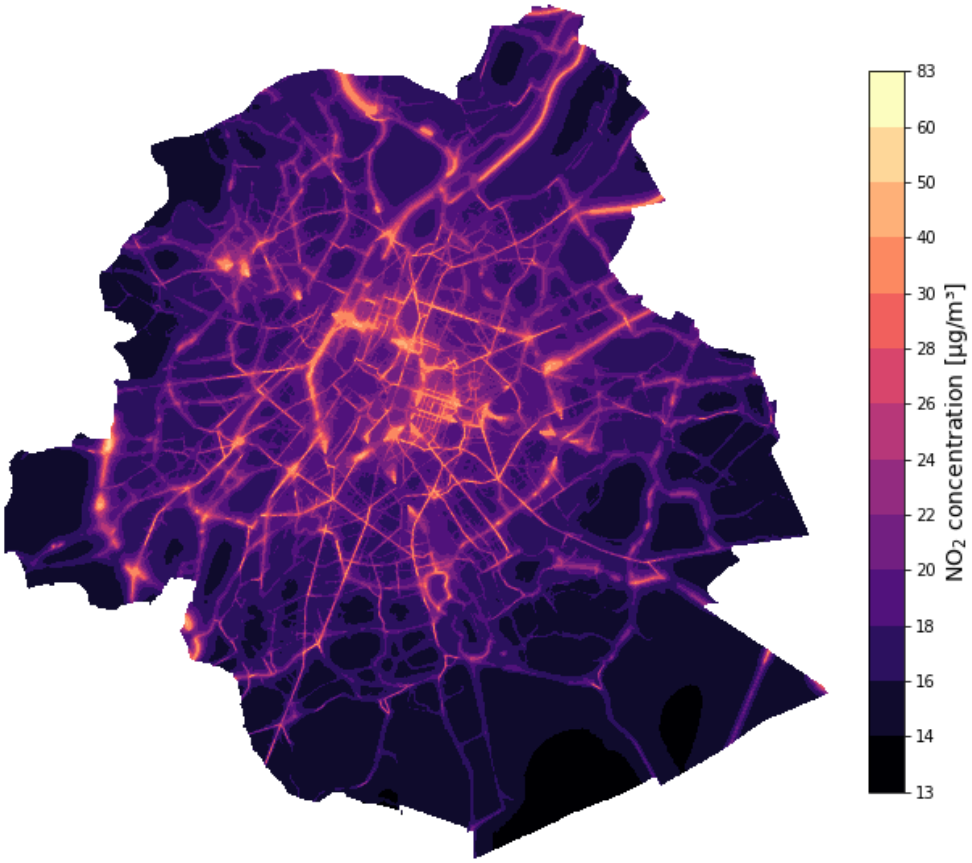

(a) 2022 WEM

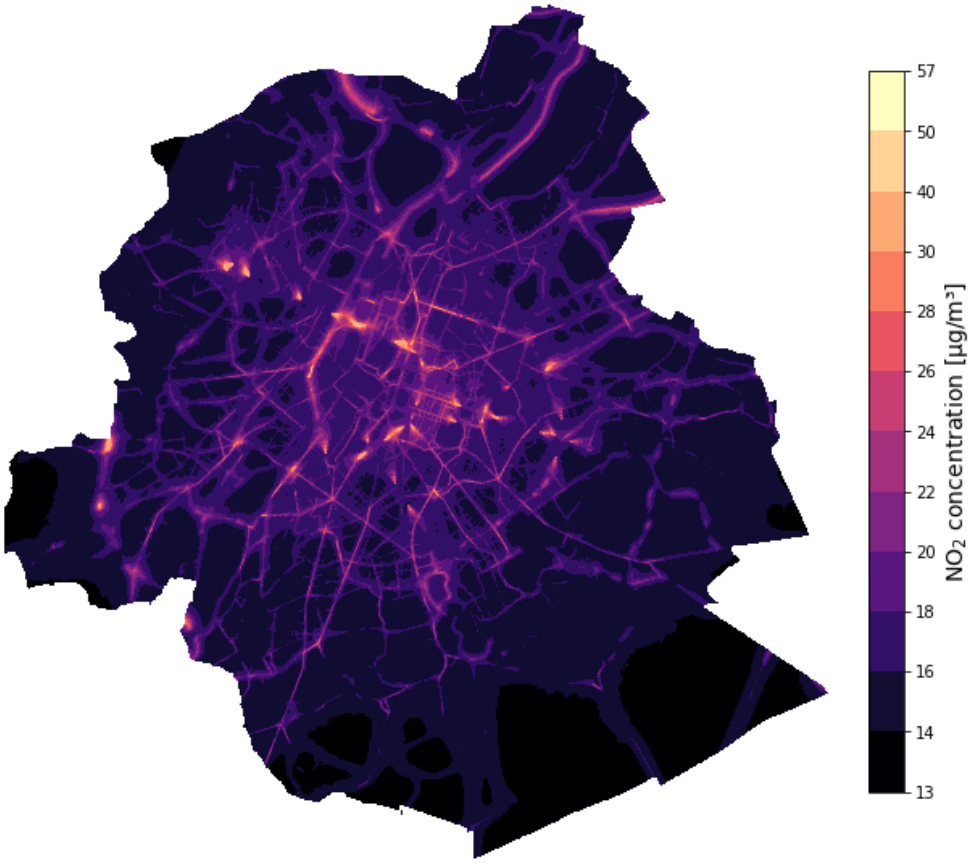

(b) 2025 WEM

Figure P.3: NO_2 concentration trends according to the WEM scenario for 2022, 2025, 2028, 2030, 2033 and 2035

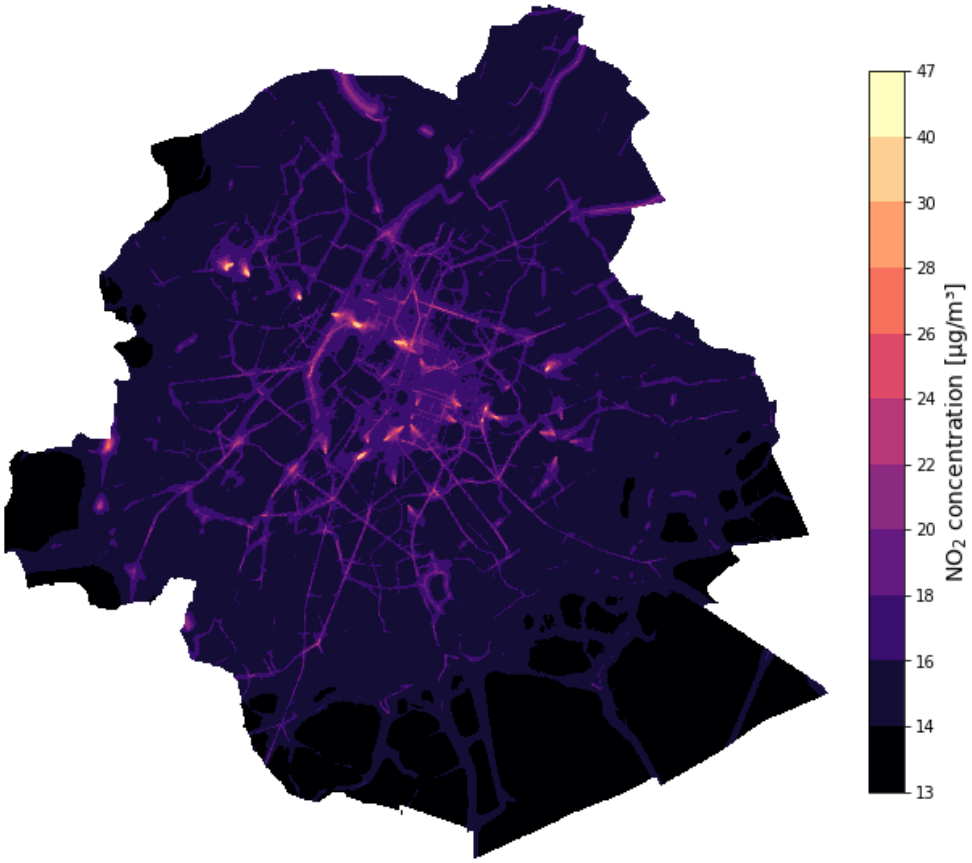

(c) 2028 WEM

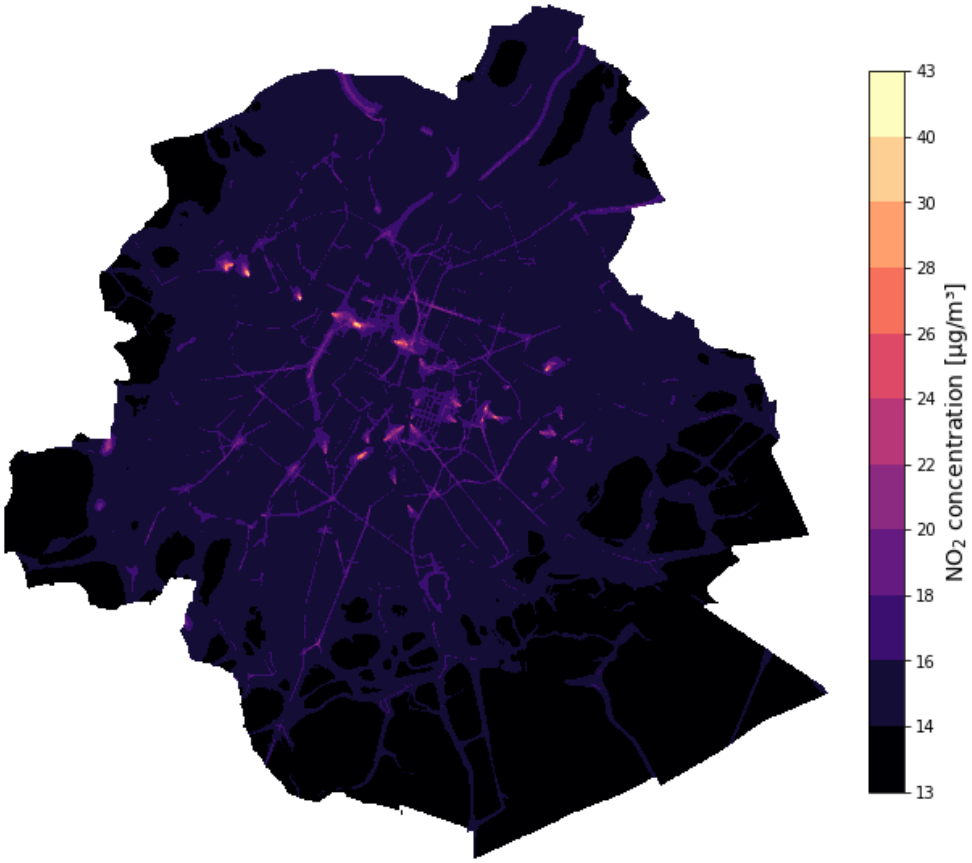

(d) 2030 WEM

Figure P.3: Continued

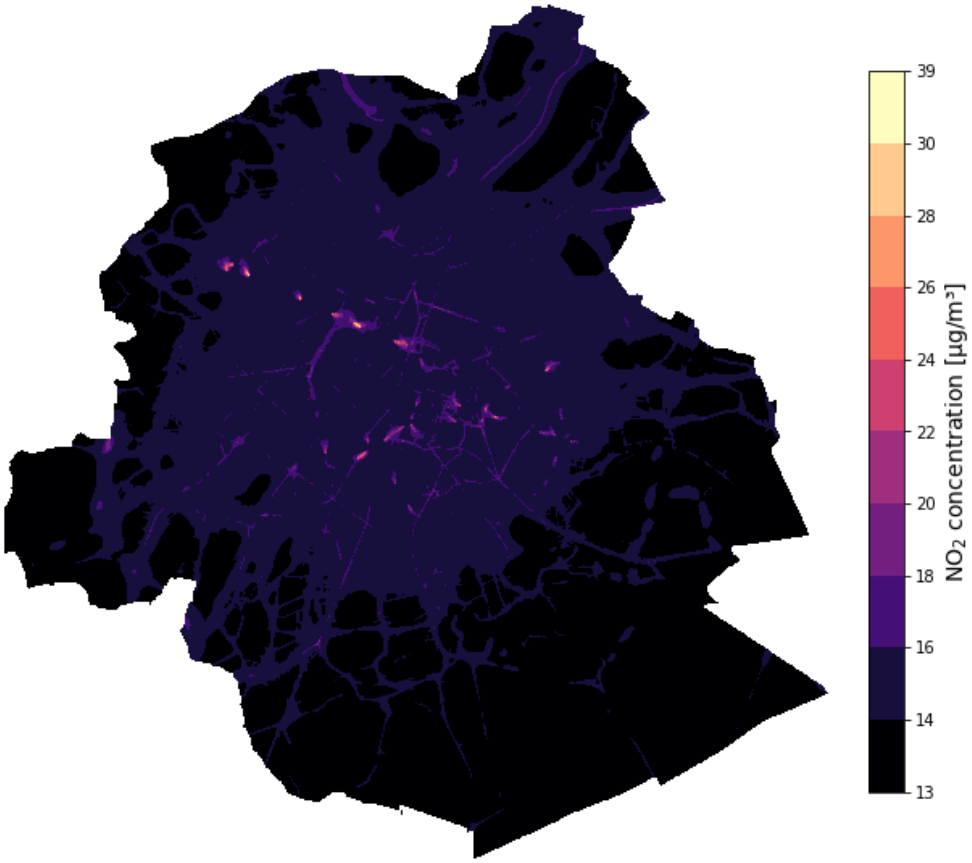

(e) 2033 WEM

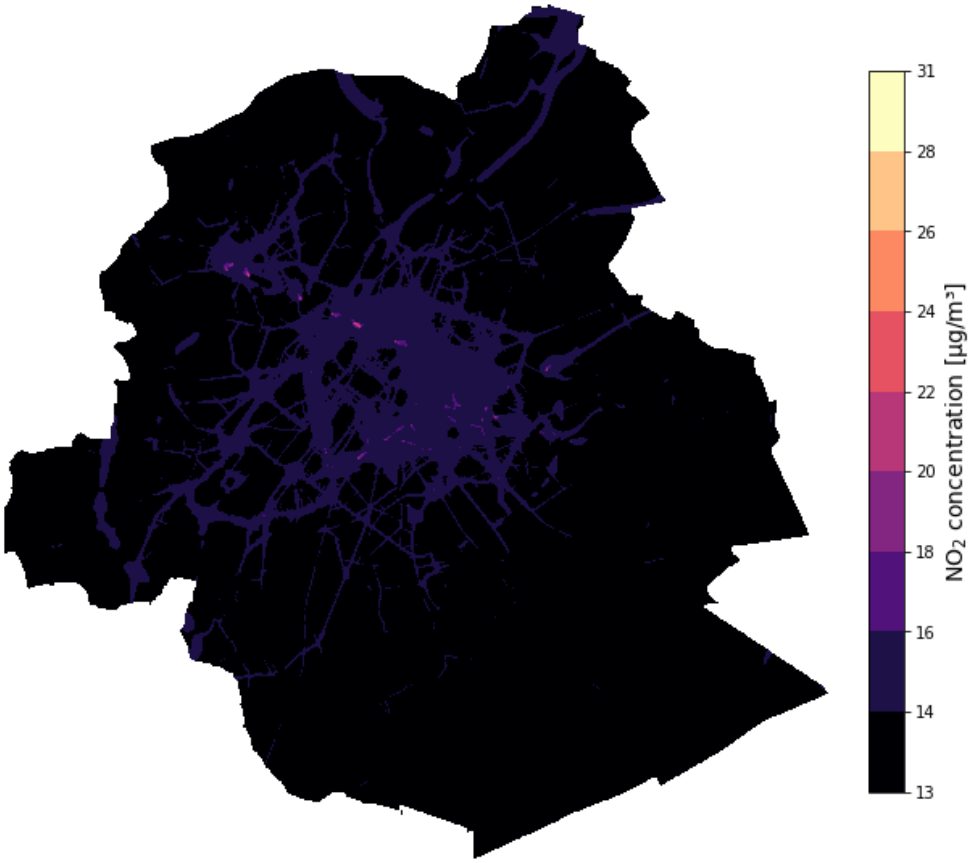

(f) 2035 WEM

Figure P.3: Continued

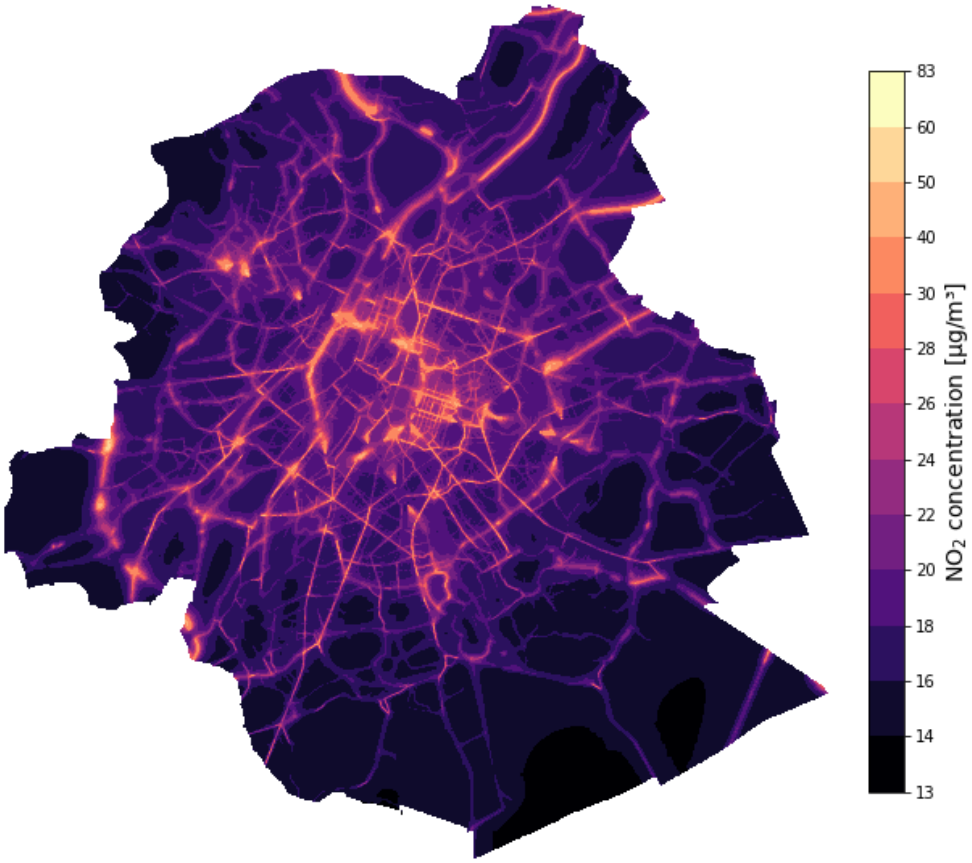

(a) 2022 WAM

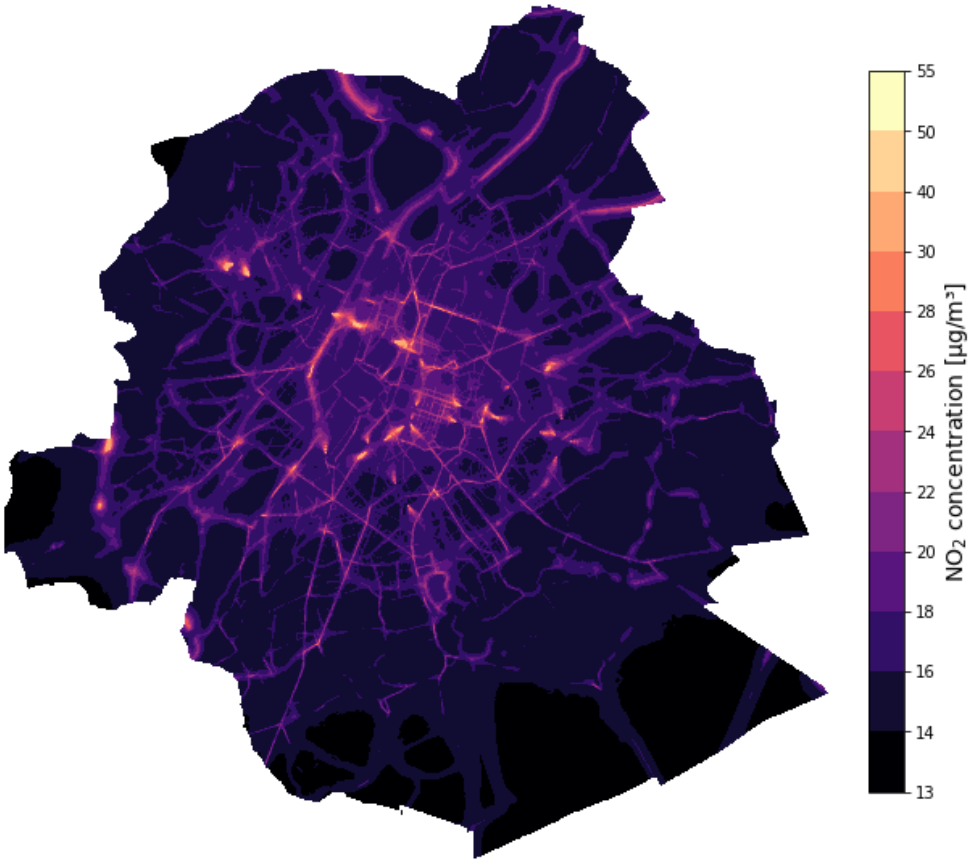

(b) 2025 WAM

Figure P.4: NO_2 concentration trends according to the WAM scenario for 2022, 2025, 2028, 2030, 2033 and 2035

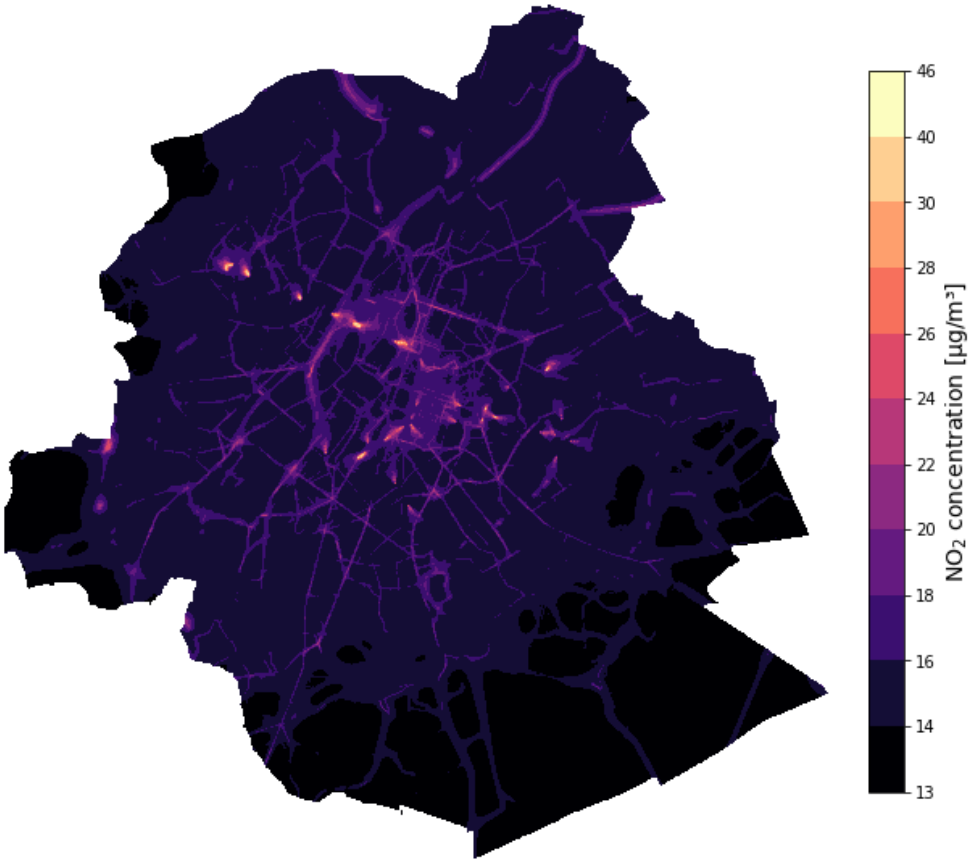

(c) 2028 WAM

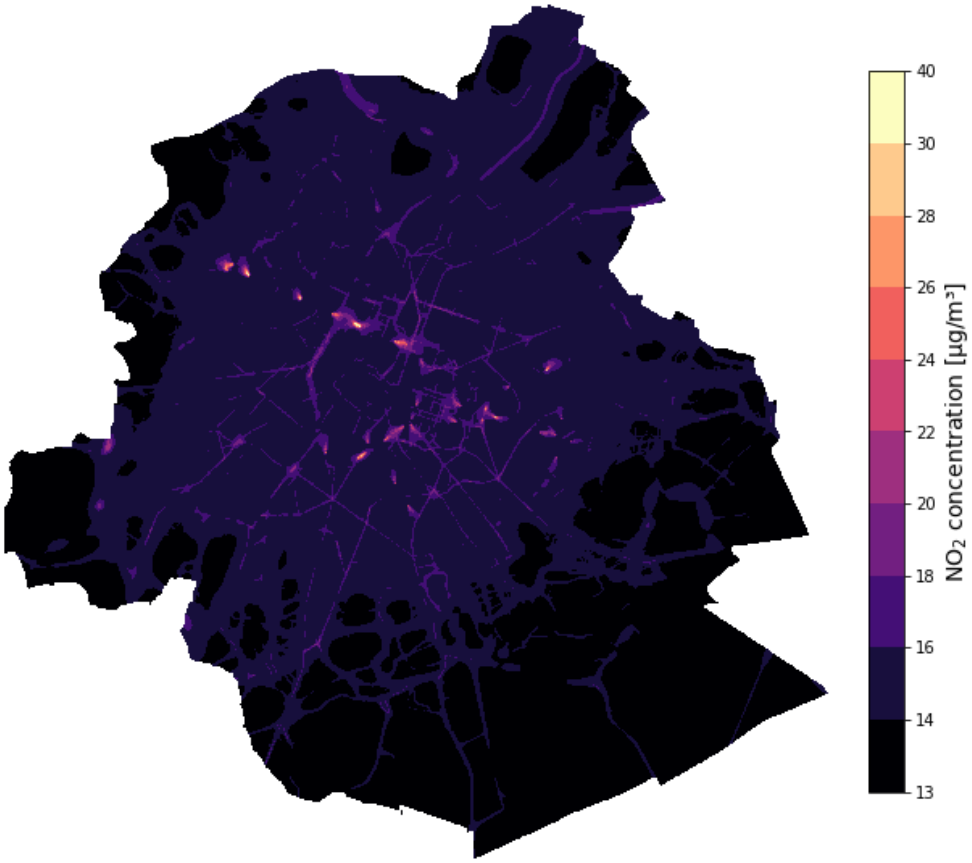

(d) 2030 WAM

Figure P.4: Continued

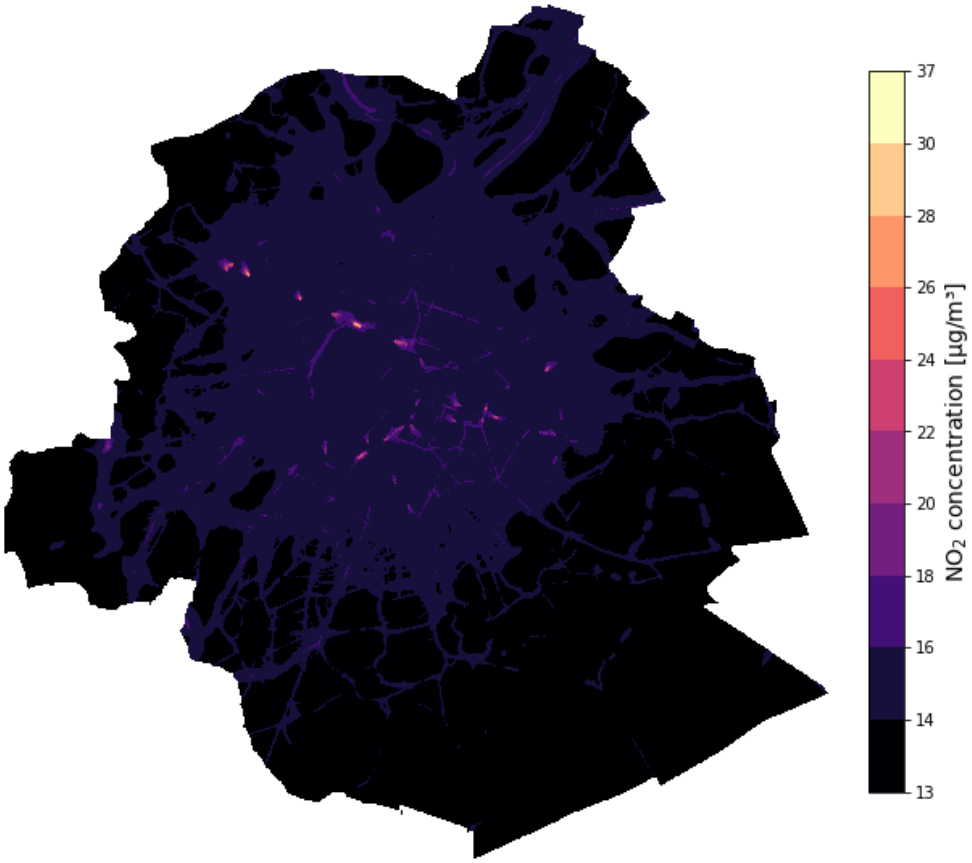

(e) 2033 WAM

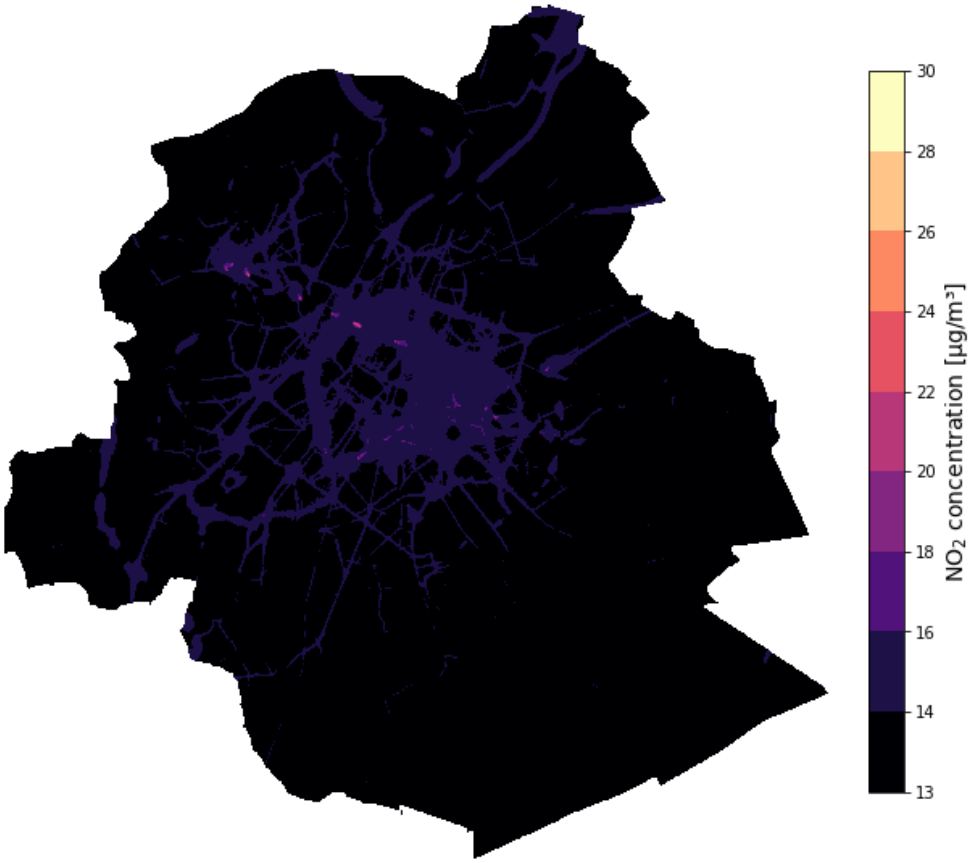

(f) 2035 WAM

Figure P.4: Continued

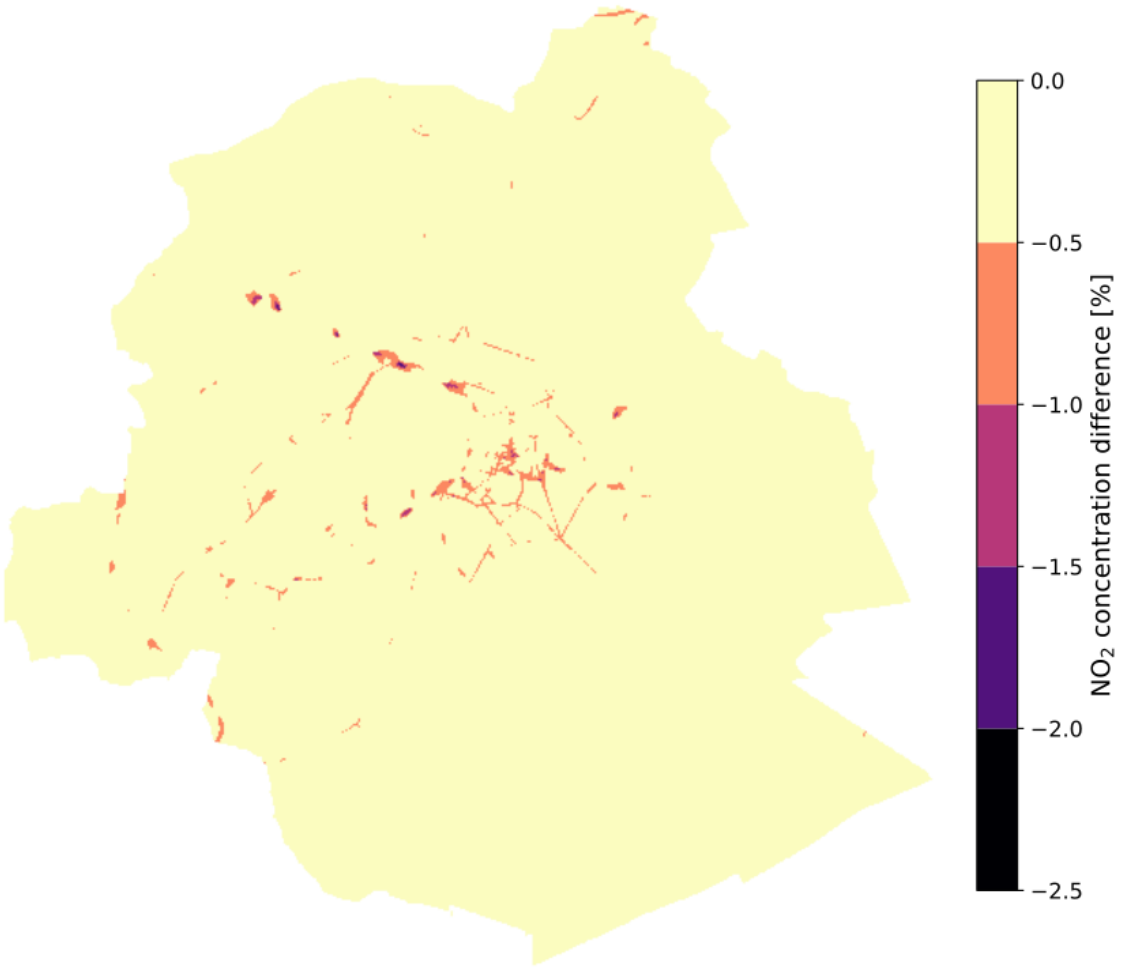

Figure P.5: Difference in percentage between the WAM and WEM scenarios for the year 2035

Evaluating traffic policies on NO_2 pollution in Brussels: Impact of the Low Emission Zone and the Good Move Plan, 2022-2035

Thiry Clément & Mégane Pourtois

Even though air quality has improved over the past two decades in European cities, it remains a significant concern as a primary environmental factor contributing to mortality and morbidity. In Brussels, NO_2 pollution, mainly emitted from thermal vehicles—poses a major threat. Although the current annual EU threshold for NO_2 concentration is set at 40 $\mu g/m^3$ and is being adhered to in Brussels, the EU plans to lower its threshold to 20 $\mu g/m^3$ by 2030, a target not yet met as of 2022.

In this context, Brussels has implemented several policy measures, including a Low Emission Zone (LEZ) that progressively bans the most polluting vehicles. Additionally, the Good Move plan covers many objectives that could have an impact on NO_2 concentration in Brussels. However, this master's thesis focuses specifically on its goal to reduce the kilometers traveled by passenger cars and reroute traffic from local roads to the main arteries.

This master's thesis evaluates the impact of the LEZ and the additional effects of Good Move on annual NO_2 concentrations in Brussels from 2022 to 2035. It also assesses how these policies will help adhere to the forthcoming EU threshold.

The study uses SIRANE, a pollutant dispersion model, to assess spatialized NO_2 concentrations, with traffic NOx emissions projections as input, which has been refined to more accurately map road emissions to corresponding road hierarchies. Then, the model has been calibrated for 2022 to fit the measured concentrations. With these two enhancements, the SIRANE model for 2022 is estimated robust and validated through statistical indicators.

On average, from 2022 to 2035, the LEZ is projected to reduce NO_2 concentrations by 1.18 $\mu g/m^3$ (24% excluding background concentrations), with the most significant impact on high-traffic roads and a peak reduction in 2025 following the ban of Euro 5 diesel light vehicles. Good Move's additional impact is eight times smaller than LEZ's impact, contributing a further average reduction of 0.15 $\mu g/m^3$ (2.9%), primarily affecting urban roads and mostly in 2028. Without any policy measures, the annual EU threshold in 2030 would be exceeded, but it would likely be respected with the LEZ and Good Move. Further research on the health and socio-economic impacts of LEZ and Good Move using the obtained NO_2 concentration maps is advised.

Université Catholique de Louvain

Faculté des bioingénieurs

Croix du Sud, 2bte L7.05.01, 1348 Louvain-La-Neuve, Belgique | www.uclouvain.be/agro